



**HAL**  
open science

# Synthesis of new N-Heterocyclic Carbene (NHC)-based Single Chain Nanoparticles (SCNPs) as catalytically active nanoreactors

Sofiem Garmendia

## ► To cite this version:

Sofiem Garmendia. Synthesis of new N-Heterocyclic Carbene (NHC)-based Single Chain Nanoparticles (SCNPs) as catalytically active nanoreactors. *Polymers*. Université de Bordeaux; University of Warwick (Coventry, Royaume-Uni), 2020. English. NNT : 2020BORD0009 . tel-02872205

**HAL Id: tel-02872205**

**<https://theses.hal.science/tel-02872205>**

Submitted on 17 Jun 2020

**HAL** is a multi-disciplinary open access archive for the deposit and dissemination of scientific research documents, whether they are published or not. The documents may come from teaching and research institutions in France or abroad, or from public or private research centers.

L'archive ouverte pluridisciplinaire **HAL**, est destinée au dépôt et à la diffusion de documents scientifiques de niveau recherche, publiés ou non, émanant des établissements d'enseignement et de recherche français ou étrangers, des laboratoires publics ou privés.

THÈSE PRÉSENTÉE  
POUR OBTENIR LE GRADE DE

**DOCTEUR DE  
L'UNIVERSITÉ DE BORDEAUX ET UNIVERSITY OF  
WARWICK**

École Doctorale des Sciences Chimiques

Spécialité : Polymères

Par **Sofiem GARMENDIA**

**Synthesis of new *N*-Heterocyclic Carbene (NHC)-based Single  
Chain Nanoparticles (SCNPs) as catalytically active nanoreactors**

Synthèse de nouvelles nanoparticules composées de chaînes uniques basé sur de carbènes  
*N*-hétérocycliques comme de nanoréacteurs catalytiquement actifs

Sous la direction de : Pr. Andrew P. DOVE, Pr. Daniel TATON et Pr. Rachel K. O'REILLY

Soutenue le 22/ 01/ 20

Membres du jury :

M. POMPOSO, Jose A.,	Professeur, University of the Basque Country	Rapporteur
M. DROCKENMULLER, Eric,	Professeur, Université de Lyon 1	Rapporteur
M. PERRIER, Sébastien,	Professeur, University of Warwick	Examineur
M. CLOUTET, Eric,	Professeur, Université de Bordeaux	Président du Jury
M. DOVE, Andrew P.,	Professeur, University of Birmingham	Directeur de thèse
M. TATON, Daniel,	Professeur, Université de Bordeaux	Directeur de thèse
M. O'REILLY, Rachel K.,	Professeur, University of Birmingham	Directeur de thèse

# Table of Contents

<b>Acknowledgements</b> .....	6-7
<b>Declaration of Authorship</b> .....	8
<b>List of Publications</b> .....	9-10
<b>Summary</b> .....	11
<b>Abbreviations</b> .....	12-16
<b>List of Figures</b> .....	17-22
<b>List of Schemes</b> .....	23-24
<b>List of Tables</b> .....	25
<b>Chapter I: Introduction to Single Chain Nanoparticles (SCNPs) as nanoreactors</b>	
1.1    Single Chain Nanoparticles (SCNPs) .....	31
1.1.1    Introduction .....	31-32
1.1.2    Synthetic methods towards single-chain nanoparticles.....	32
1.1.2.1    SCNPs <i>via</i> irreversible and reversible bonds.....	32-33
1.1.2.1.1    Covalent bonds.....	33-39
1.1.2.1.2    Organometallic bonds.....	39-44
1.1.2.1.3    Supramolecular chemistry.....	44-50
1.1.2.1.4    Dynamic covalent chemistry.....	50-54
1.1.3    Characterisation of Single Chain Polymer Nanoparticles: analytical techniques.....	54-55
1.1.3.1    Size exclusion chromatography (SEC).....	55-57
1.1.3.2    Spectroscopic characterisation of SCNPs.....	57
1.1.3.2.1    NMR spectroscopy .....	57-59
1.1.3.2.2    IR, UV-VIS, CD and fluorescence spectroscopy.....	59-62

1.1.3.3	Characterisation of Single Chain Nanoparticles morphology.....	62
1.1.3.3.1	Morphological characterisation <i>via</i> TEM.....	62-63
1.1.3.3.2	Morphological characterisation <i>via</i> AFM.....	63-64
1.1.3.3.3	Morphological characterisation <i>via</i> scattering (DLS, SAXS, SANS) .....	65-65
1.1.4	Applications.....	68-69
1.1.4.1	Nanomedicine.....	69
1.1.4.1.1	Drug delivery and imaging.....	69-72
1.1.4.2	Nanoreactors for catalysis.....	73
1.1.4.2.1	Organocatalysis .....	73-77
1.1.4.1.2	Organometallic catalysis.....	77-85
1.1.4.1.3	Enzymatic catalysis .....	85-86
1.1.4.3	Other uses.....	86-89
1.3	Conclusions and aims of the PhD thesis.....	89-91
1.4	References.....	91-97

**Chapter II: Facile Synthesis of Reversibly Crosslinked Poly(ionic liquid)-type Gels: Recyclable Supports for Organocatalysis by *N*-Heterocyclic Carbenes**

2.1.	Abstract.....	101-102
2.2.	Introduction.....	102-104
2.3.	Synthesis, characterisation.....	105-110
2.4.	Manipulation of gel-supported pre-catalyst.....	110-113
2.5.	Organocatalysis from gel-supported NHCs.....	113-116
2.6.	Conclusions.....	116-117
2.7.	References.....	117-119



2.8	Experimental section.....	120-135
-----	---------------------------	---------

**Chapter III: Reversible Ionically-crosslinked Single Chain Nanoparticles as Bioinspired and Recyclable Nanoreactors for *N*-Heterocyclic Carbene Organocatalysis**

3.1.	Abstract.....	139
3.2.	Introduction.....	140-142
3.3.	Synthesis of catalytically active SCNPs.....	143-148
3.4.	Benzoin condensation catalyzed by SCNP 5.....	148-152
3.5.	Conclusions.....	153
3.6.	References.....	153-157
3.7	Experimental section.....	158-169

**Chapter IV: Self-catalysed folding of single chain nanoparticles (SCNPs) by NHC-mediated intramolecular benzoin condensation**

4.1.	Abstract.....	173
4.2.	Introduction.....	174-176
4.3.	Synthesis of catalytically active SCNPs.....	176-182
4.4.	Transesterification reaction catalysed by SCNP 5.....	182-186
4.5	Conclusions.....	186-187
4.6.	References.....	187-189
4.7.	Experimental section.....	190-209

**Chapter V: Catalytically Active *N*-Heterocyclic Carbene Release from Single-Chain Nanoparticles following a Thermolysis-driven Unfolding Strategy**

5.1.	Abstract.....	213
------	---------------	-----

5.2.	Introduction.....	214-215
5.3.	Synthesis of catalytically-active SCNPs.....	216-220
5.4.	NHC-mediated benzoin condensation reaction.....	220-223
5.5.	Conclusions.....	223
5.6	References.....	224-227
5.7.	Experimental Section.....	228-239

## **Chapter VI: Summary, principal conclusions and outlook**

6.1.	Summary.....	243
6.2.	Principal conclusions.....	243
6.2.1.	Importing PILs to SCNPs technology.....	243-244
6.2.2.	Different SCNPs folding techniques.....	244-245
6.2.3	SCNPs as catalytically active nanoreactors.....	245-246
6.3.	Outlook.....	246-247
7.1.	Sommaire.....	248
7.2.	Conclusions principales.....	248
7.2.1.	Importacion de PILs dans la technologie SCNPs.....	248-249
7.2.2.	Différentes techniques de pliage SCNPs.....	249-250
7.2.3	SCNPs en tant que nanoréacteurs catalytiquement actifs.....	250-251
7.3.	Prespectives.....	251-252

# Acknowledgements

Firstly, I would like to give my sincere thanks to my supervisors, Professor Andrew P. Dove, Professor Daniel Taton and Professor Rachel K. O'Reilly for the opportunity to work in their groups in such an amazing field. I am truly grateful for all of your invaluable guidance, advice and continuous support throughout all my research during this PhD. I would also like to thank the three of you for all the comprehension and all the back up you offered regardless the institution I was carrying out my research in, making easier and more comfortable the development of it. Continuous meetings and numerous scientific exchanges have allowed not only to expand my scientific focus but also learning how to perfectly balance to think in and out of the box.

The biggest thanks go to Dove Group, Taton Team and O'Reilly group members, who throughout all my period in one and each of the groups have hardly worked on making my time more enjoyable both socially and scientifically. Making out any simple conversation the perfect time to discuss about scientific suggestions, disagreements or deep conceptual brainstorming. Moreover, without your support it would have been possible to overcome so many challenging situations. It would not be fair to cite only a few numbers of the people who have considerably helped to get throughout this whole research period because I would certainly forget to cite few of these names. However, I could not progress writing these lines without especially thanking in the incredible Taton Team people like Dr. Romain Lambert, Anne-Laure Wirotius, Dr. Leila Mezzasalma or Beste Ohran, Quentin Sobczak and as on-ground-mentor, Dr. Joan Vignolle. My genuine thanks also go to the spectacular people from both Dove and O'Reilly groups like Sètuhn Jimaja, Noe Fanjul, Panos Bexis, Coralie Jehanno, Prof. Mathieu Tschan, Dr. Jeff Foster or Prof. Benoit Couturaud. Especial thank is also dedicated to the people like Dr. Julien Rosselgong, Dr. Joshua Wroch, Dr. Daniele Mantione, Siobhan Kilbride or Dr. Wei Yu, who have rendered the lab a more entertaining place to deploy my research.

I would also dedicate my deepest thank to all those who made the effort and offered the opportunity to jointly work on papers or projects which have not been as successful, especial mention to, Dr. Stefan B. Lawrenson and Dr Maria Chiara Arno and again Dr. Romain Lambert and Anne-Laure Wirocius, because without any of you it would not have been possible to achieve anything developed in this manuscript.

I would also like to acknowledge the European Commission for their support and funding and the University of Bordeaux, University of Warwick and University of Birmingham for enabling the use of their facilities and infrastructure. Equally, I must show my gratitude to all the technical staff from the different departments in all the different universities who have kindly helped me with their assistance, continuous support and valuable pieces of advice.

Finally, there are no words to show all my gratitude to the most important people in my life; my family. You have given me love, energy and support in every single second you noticed I needed it. I am the result of what you have constantly helped to shape, coddled and harvested with all your patience and effort, so this is the result of the “we” who as a team managed to reach so far and has made us invincibles.

# **Declaration of Authorship**

This thesis manuscript is both submitted to the University of Bordeaux and the University of Warwick in support for the double degree of Doctor of Philosophy. I have totally been composed by myself and has not been submitted in any other previous application of any other degree.

All the work presented (the data generated and data analysis) was completely carried out by the author and except from the introduction all the experimental chapters have been published in scientific journals as detailed in Section “List of Publications”

# List of Publications

1. *Facile synthesis of reversibly crosslinked poly(ionic liquid)-type gels: Recyclable supports for organocatalysis by N-heterocyclic carbenes*

Sofiem Garmendia, Romain Lambert, Anne-Laure Wirotius, Joan Vignolle, Andrew P. Dove, Rachel K. O'Reilly, Daniel Taton., *European Polymer Journal*, 2018, **107**, 82-88.

2. *Reversible ionically-crosslinked single chain nanoparticles as bioinspired and recyclable nanoreactors for N-heterocyclic carbene organocatalysis*

Sofiem Garmendia, Andrew P. Dove, Daniel Taton, Rachel K. O'Reilly, *Polym. Chem.*, 2018, **9**, 5286-5294.

3. *Self-catalysed folding of single chain nanoparticles (SCNPs) by NHC-mediated intramolecular benzoin condensation*

Sofiem Garmendia, Andrew P. Dove, Daniel Taton, Rachel K. O'Reilly, *Polym. Chem.*, 2019, **10**, 2282-2289.

4. *Catalytically Active N-Heterocyclic Carbene Release from Single-Chain Nanoparticles Following a Thermolysis-Driven Unfolding Strategy*

Sofiem Garmendia, Stefan B. Lawrenson, Maria C. Arno, Rachel K. O'Reilly, Daniel Taton, Andrew P. Dove, *Macromol. Rapid Commun.*, 2019, **40**, 1900071-1900079

5. *Catalytically Active N-Heterocyclic Carbene Release from Single-Chain Nanoparticles Following a Thermolysis-Driven Unfolding Strategy (Cover Picture)*

Sofiem Garmendia, Stefan B. Lawrenson, Maria C. Arno, Rachel K. O'Reilly, Daniel Taton, Andrew P. Dove, *Macromol. Rapid Commun.*, 2019, **40** (15), 1970033

6. *Pd(II)-NHC coordination-driven formation of water-soluble catalytically active single chain nanoparticles*

Romain Lambert, Anne-Laure Wirocius, Sofiem Garmendia, Pierre Berto, Joan Vignolle, Daniel Taton,  
*Polym.Chem.*, 2018, **9**, 3199-3204

# Summary

**Chapter One** aims at describing existing synthetic methodologies to SCNPs, related characterisation techniques and potential applications reported in the recent literature for these nanoobjects.

**Chapter Two** discusses the use of a PIL-based gel catalytic precursor which show a thermo-responsive behavior. This particularly versatile NHC-based organocatalysts can easily be restored recycled and reused by simply cooling down and no external chemical agent.

**Chapter Three** considers a novel-type of non-covalently bound SCNPs. The nature of PIL parent linear precursors allows and mild anion-metathesis driven intramolecular folding. The resulting SCNPs could be thermally activated for NHC-mediated organocatalysis purpose, showing higher catalytic efficiency compared to molecular/linear polymer models as a result of the confinement effect.

**Chapter Four** reveals a self-catalysed folding strategy to form SCNPs *via* an intramolecular NHC-mediated benzoin condensation, exploiting the thermo-latent NHC-precatalyst supported in the linear parent precursor. Importantly, the thermo-latent NHC retained their catalytic activity and further implemented organocatalysing transesterification reactions.

**Chapter Five** employs Ag(I)-crosslinked SCNPs and demonstrate their application as catalysts. Metalation of the benzimidazolium by Ag(I) was obtained under relatively mild conditions. These Ag-NHC linkages could be subsequently thermally cleaved delivering active NHC moieties organocatalysing a benzoin condensation reaction.

**Chapter Six** summarises the research herein presented, giving general conclusions to the discussion of the potential for future investigations in this research field.



# Abbreviations

3D: three-dimensional

$\delta$ : chemical shift

$\eta$ : dynamic viscosity

$\lambda$ : wavelength

AIBN: Azobis(2-methylpropionitrile)

AFM: atomic force microscopy

Ar: aromatic

ATRP: atom transfer radical polymerisation

BCP: block copolymer

br: broad

Bz: benzyl

*ca.*: circa

Cat: catalyst

CMRP: cobalt-mediated radical polymerisation

coPIL: copoly(ionic liquid)

Cryo: cryogenic

CTA: chain transfer agent

$D_h$ : hydrodynamic diameter

$D_M$ : molar-mass dispersity

DLS: dynamic light scattering

DMF: dimethyl formamide

DMSO: dimethyl sulfoxide

DOSY: diffusion ordered spectroscopy

DP: number average degree of polymerisation

DSC: differential scanning calorimetry

DVB: divinylbenzene

Et<sub>2</sub>O: diethyl ether

Eq.: equivalents

EtOH: ethanol

eV: electron volts

FTIR: Fourier transform infrared

GPC: gel permeation chromatography

I: initiator

IC: ionic conductivity

IL: ionic liquid

kDa: kiloDalton

KHCO<sub>3</sub>: potassium hydrogen carbonate

KHDMS: potassium bis(trimethylsilyl)amide

KPF<sub>6</sub>: potassium hexafluorophosphate

LiTFSI: lithium bis(trifluorosulfonyl)imide

MA: methyl acrylate

MALDI-ToF: matrix-assisted laser desorption ionisation time-of-flight

$M_n$ : number average molar mass

$M_w$ : weight average molar mass

MeOH: methanol

mg: milligram(s)

mL: millilitre(s)

MMA: methyl methacrylate

mol: mole

mmol: milimol

MWCO: molecular weight cut off

NaBF<sub>4</sub>: sodium tetrafluoroborate

NaCl: sodium chloride

NH<sub>4</sub>BF<sub>4</sub>: ammonium tetrafluoroborate

NHC: *N*-heterocyclic carbene

NHC-CO<sub>2</sub>: azolium-2-carboxylate

[NHC(H)][HCO<sub>3</sub>]: azolium hydrogen carbonate

NMP: nitroxide mediated polymerisation

NMR: nuclear magnetic resonance

OAc: acetate

PEDOT: poly(3,4-ethylenedioxythiophene)

PEG: poly(ethylene glycol)

PEO: poly(ethylene oxide)

Ph: phenyl

PILs: poly(ionic liquid)s

PMA: poly(methyl acrylate)

PMMA: poly(methyl methacrylate)

Poly(NHC): poly(*N*-heterocyclic carbene)

Poly(NHC-CO<sub>2</sub>): poly(*N*-heterocyclic carbene-carboxylate) adduct

Poly[NHC(H)][HCO<sub>3</sub>]: poly(*N*-vinyl-3-alkylimidazolium hydrogen carbonate)

ppm: parts per million

PS: poly(styrene)

RAFT: reversible addition-fragmentation chain transfer

R<sub>g</sub>: radius of gyration

RI: refractive index

ROMP: ring-opening metathesis polymerisation

ROP: ring-opening polymerisation

RT/rt: room temperature

SAXS: small-angle X-ray scattering

SCNPs: single chain nanoparticles

Seb: sebacate

SEC: size exclusion chromatography

SEM: scanning electron microscopy

St: styrene

*t*: time

T: temperature

TEM: transmission electron microscopy

TFSI: bis(trifluorosulfonyl) imide

$T_g$ : glass transition temperature

$T_m$ : melting temperature

TGA: thermogravimetric analysis

THF: tetrahydrofuran

TMS: trimethylsilane

TMSCN: trimethylsilyl cyanide

UV: ultraviolet

$v$ : volume

VAc: vinyl acetate

wt.%: weight percent

# List of Figures

<b>Figure 1.1</b> Modes for intramolecular collapse through cross-linking of a single polymer chain, forming SCNPs.....	32
<b>Figure 1.2</b> (A) The introduction of appropriate ligand functionalities in the polymer chain allowing SCNP folding and catalytic functionalisation in one step. (B) Nanoparticle formation <i>via</i> an external trigger and subsequent metal ion loading. <sup>36</sup> .....	39
<b>Figure 1.3.</b> SEC UV detector traces obtained in THF at 40 °C for reaction of styrene functionalized P1 with AIBN to yield NP1-0. <sup>77</sup> .....	56
<b>Figure 1.4</b> <sup>1</sup> H NMR overlay spectrum of polymer (P1) and nanoparticle (NP1) in CDCl <sub>3</sub> .....	58
<b>Figure 1.5</b> DOSY spectra of linear precursor and corresponding SCNP CD <sub>2</sub> Cl <sub>2</sub> . <sup>18</sup> .....	59
<b>Figure 1.6.</b> FTIR spectra of a) linear polymeric precursor and b) corresponding SCNP. <sup>84</sup> .....	60
<b>Figure 1.7</b> (A) UV-vis absorbance of the polymer precursors (smooth lines) and the corresponding SCNPs (dashed lines), (B) Emission spectra of the formed SCNPs and (C) photograph of a solution of SCNPs under a hand-held UV-lamp ( $\lambda = 366$ nm). <sup>85</sup> .....	61
<b>Figure 1.8</b> CD spectra of different particles (P1, P2 and P3) at 20 °C during 120 min of 350 nm UV irradiation. <sup>62</sup> .....	62
<b>Figure 1.9.</b> TEM images of SCNPs at different zooms stained with ammonium molybdate. <sup>87</sup> .....	63
<b>Figure 1.10</b> AFM height imaged of SCNPs capture of two-steps of the molecular folding process (A) before and (B) after UV irradiation. The top right insets show magnifications of the framed areas. <sup>62</sup>	64
<b>Figure 1.11</b> (A) Dynamic light scattering (DLS) data (number distributions) for the folded and unfolded polymer (P6). (B) DLS data for the folded and unfolded polymer P16 in presence of different solvents/salts.....	66
<b>Figure 1.12</b> (A) Form factor from SAXS of precursor (circles) , SCNPs following protocol I (diamonds) and II (crosses) in THF. (B) Form factor from MD simulations of the precursor (circles) and the SCNPs synthesised through protocol I (diamonds) and II (crosses).....	67
<b>Figure 1.13</b> Potential applications of SCNPs.....	69
<b>Figure 1.14</b> (A) Dual-pathway synthetic of SCNPs <i>via</i> Thiol-Michael addition following the organic route (yellow) and aqueous route (blue). (B) Release of Rif from SCNPs by measuring UV-vis absorption at 334 nm. <sup>96</sup> .....	71
<b>Figure 1.15</b> (A) Formation of SCNPs and loading with Gd(III) following a two-step route for their incorporation using CuAAC-based chemistry. (B) Relaxivity values for Gd-SCNPs compared to commercially available reference Magnevist®.....	72

<b>Figure 1.16</b> Chemical structure of L-proline functionalised catalytic polymer and schematic representation of the unfolded polymer and the formation of the compartmentalised catalytic structure in water.....	75
<b>Figure 1.17</b> Schematic illustration of the use of SCNPs as bionpired nanoreactors for the synthesis of polymers through ring-opening polymerisation. <sup>109</sup> .....	77
<b>Figure 1.18</b> Size and size-dependent photoluminescence spectra of CNDs. TEM image and size histogram of big CND ( <b>A</b> ) and small ones ( <b>B</b> ). Photoluminescent spectra of surface oxidised at 340 nm of small CND (green line <b>C</b> ) and big CND (blue line <b>C</b> ) and spectra of reduced surface (green line <b>D</b> and blue line <b>C</b> , respectively). <sup>128</sup> .....	88
<b>Figure 2.1.</b> <sup>1</sup> H NMR (DMSO- <i>d</i> <sub>6</sub> ) showing the insertion of the sebacate forming the physical gel (PS- <i>co</i> -Poly[ViEBIm]Seb) ( <b>5</b> ) from (PS- <i>co</i> -Poly[ViEBIm]Cl) ( <b>3</b> ).....	107
<b>Figure 2.2.</b> Synthesis of ((PS- <i>co</i> -Poly[ViEBIm]Cl)( <b>3</b> )). <sup>13</sup> C NMR spectra in DMSO- <i>d</i> <sub>6</sub> .....	108
<b>Figure 2.3.</b> Synthesis of ((PS- <i>co</i> -Poly[ViEBIm]Seb)( <b>5</b> )). <sup>13</sup> C NMR spectra in DMSO- <i>d</i> <sub>6</sub> .....	108
<b>Figure 2.4.</b> Synthesis of Polystyrene- <i>co</i> -poly(4-vinylbenzylethyl-(benz)imidazolium sebacate) (PS- <i>co</i> -Poly[ViEBIm]Seb) ( <b>5</b> ) overlay with starting materials .FTIR spectra.....	109
<b>Figure 2.5.</b> (PS- <i>co</i> -Poly[ViEBIm]Cl) ( <b>3</b> ), (PS- <i>co</i> -Poly[ViEBIm]Seb) ( <b>5</b> ) and Sebacic Acid plotting with corresponding proposed degradation steps for each case.....	110
<b>Figure 2.6.</b> PS- <i>co</i> -Poly[ViEBIm]Seb ( <b>5</b> ) gelation procedure for heterogeneous supported catalyst synthesis in THF.....	111
<b>Figure 2.7.</b> SEM pictures of polymer <b>5</b> as a heterogeneous catalyst support in organocatalysis showing pore sizes between 100 nm to 10 μm.....	111
<b>Figure 2.8.</b> <sup>1</sup> H NMR spectra overlay (PS- <i>co</i> -Poly[ViEBIm]TFSI)-1 ( <b>4</b> ) and (PS- <i>co</i> -Poly[ViEBIm]TFSI)-2 ( <b>7</b> ) in DMSO- <i>d</i> <sub>6</sub> .....	112
<b>Figure 2.9.</b> SEC traces corresponding (PS- <i>co</i> -Poly[ViEBIm]TFSI)-1 ( <b>4</b> ) (in blue) and (PS- <i>co</i> -Poly[ViEBIm]TFSI)-2 ( <b>7</b> ) in (red) using 10 mM LiTFSI THF as eluent using a RI detector.....	113
<b>Figure 2.10.</b> Synthesis of PS- <i>co</i> -poly(4-vinylbenzyl-NHC-CS <sub>2</sub> ) ( <b>6</b> ) . <sup>13</sup> C NMR spectra in DMSO- <i>d</i> <sub>6</sub> ...	114
<b>Figure 2.11.</b> Different benzoin condensation, transesterification and cyanosilation average conversions obtained after 5 cycles using 10 mol % amount of catalyst in heterogeneous conditions.....	116
<b>Figure S2.1.</b> Synthesis of Polystyrene- <i>co</i> -poly(4-vinylbenzylethyl-(benz)imidazolium chloride) (PS- <i>co</i> -Poly[ViEBIm]Cl) ( <b>3</b> ) . <sup>1</sup> H NMR spectra in DMSO- <i>d</i> <sub>6</sub> .....	125
<b>Figure S2.2.</b> Synthesis of Polystyrene- <i>co</i> -poly(4-vinylbenzylethyl-(benz)imidazolium sebacate) (PS- <i>co</i> -Poly[ViEBIm]Seb)( <b>5</b> ) . <sup>1</sup> H NMR spectra in DMSO- <i>d</i> <sub>6</sub> .....	126
<b>Figure S2.3.</b> TGA plot of (PS- <i>co</i> -Poly[ViEBIm]Cl) ( <b>3</b> ).....	126

<b>Figure S2.4.</b> TGA plot of (PS-co-Poly[ViEBIm]Seb) ( <b>5</b> ).....	127
<b>Figure S2.5.</b> TGA plot of Sebacic Acid.....	128
<b>Figure S2.6.</b> DSC plot of (PS-co-Poly[ViEBIm]Cl) ( <b>3</b> ).....	128
<b>Figure S2.7.</b> DSC plot of (PS-co-Poly[ViEBIm]Seb) ( <b>5</b> ).....	129
<b>Figure S2.8.</b> Synthesis of ((PS-co-Poly[ViEBIm]TFSI)-1 ( <b>4</b> )). <sup>1</sup> H NMR spectra in DMSO- <i>d</i> <sub>6</sub> .....	129
<b>Figure S2.9.</b> Synthesis of ((PS-co-Poly[ViEBIm]TFSI)-2 ( <b>7</b> )). <sup>1</sup> H NMR spectra in DMSO- <i>d</i> <sub>6</sub> .....	130
<b>Figure S2.10.</b> Synthesis of ((PS-co-Poly[ViEBIm]TFSI)-1 ( <b>4</b> )). <sup>19</sup> F NMR spectra in DMSO- <i>d</i> <sub>6</sub> .....	131
<b>Figure S2.11.</b> Synthesis of ((PS-co-Poly[ViEBIm]TFSI)-2 ( <b>7</b> )). <sup>19</sup> F NMR spectra in DMSO- <i>d</i> <sub>6</sub> .....	131
<b>Figure S2.12.</b> Synthesis of ((PS-co-Poly[ViEBIm]TFSI)-1 ( <b>4</b> )). <sup>13</sup> C NMR spectra in DMSO- <i>d</i> <sub>6</sub> .....	132
<b>Figure S2.13.</b> Synthesis of ((PS-co-Poly[ViEBIm]TFSI)-2 ( <b>7</b> )). <sup>13</sup> C NMR spectra in DMSO- <i>d</i> <sub>6</sub> .....	133
<b>Figure S2.14.</b> Benzoin Condensation Conversion. <sup>1</sup> H NMR spectra in DMSO- <i>d</i> <sub>6</sub> .....	134
<b>Figure S2.15.</b> Transesterification Conversion <sup>1</sup> H NMR spectra in DMSO- <i>d</i> <sub>6</sub> .....	134
<b>Figure S2.16.</b> Cyanosilation Conversion <sup>1</sup> H NMR spectra in DMSO- <i>d</i> <sub>6</sub> .....	135
<b>Figure 3.1:</b> <sup>1</sup> H NMR spectrum in DMSO- <i>d</i> <sub>6</sub> of linear precursor <b>4</b> ( <b>A</b> ) and SCNP <b>5</b> ( <b>B</b> ) after folding.....	145
<b>Figure 3.2:</b> Attenuated total reflection Fourier transform infrared (ATR-FTIR) analysis for linear starting copolymeric precursor <b>4</b> (red) and folded SCNP <b>5</b> (blue).....	145
<b>Figure 3.3. A)</b> SEC responses (in DMF in presence of 10 mM NH <sub>4</sub> BF <sub>4</sub> ; RI detector) of SCNP <b>5</b> (red line) obtained <i>via</i> cross-linking of copolymer precursor <b>4</b> (blue line) by anion exchange. <b>B)</b> DLS analysis of SCNP <b>5</b> at rt (solid red line) and at catalysis temperature (solid black line) distributed by volume in THF (conc. = 5 mg/mL). <b>C)</b> TEM images of SCNP <b>5</b> (conc. = 1 mg/mL in methanol) stained with uranyl acetate; scale bar = 50 nm. <b>D)</b> Kratky Log-Log plot from SAXS analysis of precursor <b>4</b> (solid red line) and folded <b>5</b> (solid blue line) in THF (conc. = 1 mg/mL; fitted to compact particle model).....	147
<b>Figure 3.4.</b> Multi-T DLS analysis of SCNP <b>5</b> from 20 to 80 °C in THF with volume (black line) and number (red line) distributions (Conc: 5 mg/mL).....	147
<b>Figure 3.5.</b> <sup>1</sup> H NMR ( <b>A</b> ) <sup>13</sup> C NMR ( <b>B</b> ) spectra of CS <sub>2</sub> post-functionalization reaction in SCNP <b>6</b> in DMSO- <i>d</i> <sub>6</sub> .....	149
<b>Figure S3.1.</b> Original figure of DOSY measurements of the precursor copolymer <b>4</b> and SCNP <b>5</b> , recorded in DMSO- <i>d</i> <sub>6</sub> .....	162
<b>Figure S3.2:</b> <sup>13</sup> C NMR spectrum in DMSO- <i>d</i> <sub>6</sub> of linear precursor <b>4</b> ( <b>A</b> ) and SCNP <b>5</b> ( <b>B</b> ) after folding.....	163
<b>Figure S3.3:</b> <sup>1</sup> H NMR ( <b>A</b> ) <sup>13</sup> C NMR ( <b>B</b> ) spectra of CS <sub>2</sub> post-functionalization reaction in SCNP <b>6</b> in DMSO- <i>d</i> <sub>6</sub> .....	164
<b>Figure S3.4.</b> <sup>1</sup> H NMR spectrum of molecular model catalyst in DMSO- <i>d</i> <sub>6</sub> .....	165
<b>Figure S3.5.</b> <sup>1</sup> H NMR spectrum of catalyst linear copolymer model in DMSO- <i>d</i> <sub>6</sub> .....	166



<b>Figure S3.6.</b> SEC traces of Linear Copolymer model (in Cl <sup>-</sup> anion form) in DMF (10 mM ammonium tetrafluoroborate) with RI detector ( $\ll D= 1.18$ ; Mn = 14.8 kDa: Universal calibration).....	166
<b>Figure S3.7.</b> Reaction of benzoin condensation with benzaldehyde catalyzed by SCNP <b>5</b> and conversion obtained <sup>1</sup> H NMR spectroscopy in DMSO- <i>d</i> <sub>6</sub> .....	167
<b>Figure S3.8.</b> Reaction of benzoin condensation with benzaldehyde catalyzed by molecular model and conversion obtained <sup>1</sup> H NMR spectroscopy in DMSO- <i>d</i> <sub>6</sub> .....	167
<b>Figure S3.9.</b> Reaction of benzoin condensation with benzaldehyde catalyzed by linear copolymer model and conversion obtained <sup>1</sup> H NMR spectroscopy in DMSO- <i>d</i> <sub>6</sub> .....	168
<b>Figure S3.10.</b> <sup>1</sup> H NMR spectra of the SCNP <b>5</b> in D <sub>2</sub> O.....	169
<b>Figure 4.1.</b> <sup>1</sup> H NMR spectrum of copolymer <b>2</b> in DMSO- <i>d</i> <sub>6</sub> .....	179
<b>Figure 4.2.</b> <sup>13</sup> C NMR spectrum of copolymer <b>4</b> in DMSO- <i>d</i> <sub>6</sub> .....	180
<b>Figure 4.3.</b> A) SEC traces (in DMF with 10 mM NH <sub>4</sub> BF <sub>4</sub> ) of SCNP <b>5</b> (blue line) obtained <i>via</i> intramolecular cross-linking of coPIL <b>2</b> (red line) by self-catalysis (UV detector). B) DLS analysis of coPIL <b>2</b> (red line) and SCNP <b>5</b> (blue line) diameters at 20 °C distributed by volume in THF (conc. 1 mg mL <sup>-1</sup> ). C) TEM images of SCNP <b>5</b> (conc. 1 mg mL <sup>-1</sup> in methanol) stained with uranyl acetate. Scale bar = 20 nm.....	181
<b>Figure 4.4.</b> Hydrodynamic diameter-temperature correlation obtained for SCNP <b>5</b> by variable temperature dynamic light scattering (DLS) in THF (Conc.: 1 mg mL <sup>-1</sup> ; 173° back-scattering detector; average value of 4 runs is reported along with the error corresponding to the standard deviation in the measurements; solid red line corresponds to values obtained for the volume distribution, whilst the solid black refers to the number distribution).....	181
<b>Figure 4.5.</b> FTIR spectrum of SCNP <b>5</b> (in red) and NHC-CS <sub>2</sub> functionalised SCNP <b>6</b> (in blue) showing the appearance of the characteristic vibrational signal of CS <sub>2</sub> <sup>-</sup> (at ~1030 cm <sup>-1</sup> ) when forming the betaine	
<b>Figure 4.6.</b> Kinetics for transesterification reaction at 1 mol.% (blue line), 5 mol.% (red line) and 10 mol.% (black line) using A) SCNP <b>5</b> , B) <b>7</b> and C) <b>8</b> as catalysts.....	185
<b>Figure S4.1.</b> <sup>13</sup> C NMR spectrum of copolymer <b>2</b> in DMSO- <i>d</i> <sub>6</sub> .....	193
<b>Figure S4.2.</b> <sup>1</sup> H NMR spectrum of copolymer <b>3</b> in DMSO- <i>d</i> <sub>6</sub> .....	194
<b>Figure S4.3.</b> <sup>13</sup> C NMR spectrum of copolymer <b>3</b> in DMSO- <i>d</i> <sub>6</sub> .....	194
<b>Figure S4.4.</b> <sup>1</sup> H NMR spectrum of SCNP <b>5</b> in DMSO- <i>d</i> <sub>6</sub> .....	195
<b>Figure S4.5.</b> <sup>13</sup> C NMR spectrum of coPIL <b>5</b> in DMSO- <i>d</i> <sub>6</sub> .....	195
<b>Figure S4.6.</b> Representative multiplicity-edited HSQC spectrum of SCNP <b>5</b> in DMSO- <i>d</i> <sub>6</sub> , with tertiary and primary carbons identified in blue, and quaternary and secondary carbons identified in red.....	196
<b>Figure S4.7.</b> Representative FTIR spectrum of SCNP <b>5</b> (in black), linear polymer <b>3</b> (in red) and linear	

polymer <b>2</b> (in blue).....	196
<b>Figure S4.8.</b> DOSY NMR spectroscopy in DMSO- <i>d</i> <sub>6</sub> for linear precursor <b>2</b> ( <b>A</b> ) and folded SCNP <b>5</b> ( <b>B</b> )	197
<b>Figure S4.9.</b> <sup>13</sup> C NMR spectrum of SCNP <b>6</b> in DMSO- <i>d</i> <sub>6</sub> .....	198
<b>Figure S4.10.</b> <sup>1</sup> H NMR spectrum of SCNP <b>6</b> in DMSO- <i>d</i> <sub>6</sub> .....	198
<b>Figure S4.11.</b> <sup>1</sup> H NMR spectrum of linear model <b>7</b> in DMSO- <i>d</i> <sub>6</sub> .....	199
<b>Figure S4.12.</b> SEC trace corresponding to (bis(trifluoromethane)sulfonimide) TFSI-decorated linear model <b>7</b> in DMF (10 mM NH <sub>4</sub> <sup>+</sup> BF <sub>4</sub> <sup>-</sup> ; UV detector; SEC analysis: <i>D</i> <sub>M</sub> = 1.1; <i>M</i> <sub>n</sub> =12.7 kDa).....	199
<b>Figure S4.13.</b> Reaction kinetics for run 1 ( <b>Table 4.1</b> ) monitored by <sup>1</sup> H NMR spectroscopy in DMSO- <i>d</i> <sub>6</sub> .....	200
<b>Figure S4.14.</b> Reaction kinetics for run 2 ( <b>Table 4.1</b> ) monitored by <sup>1</sup> H NMR spectroscopy in DMSO- <i>d</i> <sub>6</sub> .....	200
<b>Figure S4.15.</b> Reaction kinetics for run 3 ( <b>Table 4.1</b> ) monitored by <sup>1</sup> H NMR spectroscopy in DMSO- <i>d</i> <sub>6</sub> .....	201
<b>Figure S4.16.</b> Reaction kinetics for run 4 ( <b>Table 4.1</b> ) monitored by <sup>1</sup> H NMR spectroscopy in DMSO- <i>d</i> <sub>6</sub> .....	202
<b>Figure S4.17.</b> Reaction kinetics for run 5 ( <b>Table 4.1</b> ) monitored by <sup>1</sup> H NMR spectroscopy in DMSO- <i>d</i> <sub>6</sub> .....	203
<b>Figure S4.18.</b> Reaction kinetics for run 6 ( <b>Table 4.1</b> ) monitored by <sup>1</sup> H NMR spectroscopy in DMSO- <i>d</i> <sub>6</sub> .....	204
<b>Figure S4.19.</b> Reaction kinetics for run 7 ( <b>Table 4.1</b> ) monitored by <sup>1</sup> H NMR spectroscopy in DMSO- <i>d</i> <sub>6</sub> .....	205
<b>Figure S4.20.</b> Reaction kinetics for run 8 ( <b>Table 4.1</b> ) monitored by <sup>1</sup> H NMR spectroscopy in DMSO- <i>d</i> <sub>6</sub> .....	206
<b>Figure S4.21.</b> Reaction kinetics for run 9 ( <b>Table 4.1</b> ) monitored by <sup>1</sup> H NMR spectroscopy in DMSO- <i>d</i> <sub>6</sub> .....	206
<b>Figure S4.22.</b> Reaction kinetics for run 11 ( <b>Table 4.1</b> ) monitored by <sup>1</sup> H NMR spectroscopy in DMSO- <i>d</i> <sub>6</sub> .....	207
<b>Figure S4.23.</b> Reaction kinetics for run 12 ( <b>Table 4.1</b> ) monitored by <sup>1</sup> H NMR spectroscopy in DMSO- <i>d</i> <sub>6</sub> .....	208
<b>Figure S4.25.</b> <sup>1</sup> H NMR spectrum of copolymer <b>4</b> in DMSO- <i>d</i> <sub>6</sub> .....	208
<b>Figure 5.1.</b> <b>A</b> ) Ag-NHC complexation reaction monitored by <sup>1</sup> H NMR spectroscopy (400 MHz; 298 K; DMSO- <i>d</i> <sub>6</sub> ) at different time points ( <i>t</i> <sub>0</sub> = blue line, 24 h = red line, 72 h = green line). <b>B</b> ) SEC curves (in DMF with 10 mM NH <sub>4</sub> BF <sub>4</sub> ) of <b>2</b> (red line), <b>3</b> (blue line) and <b>4</b> (black line) using RI detector polystyrene standard. <b>C</b> ) TEM micrograph of SCNPs <b>4</b> (scale bar = 50 nm). <b>D</b> ) Hydrodynamic mean diameter of	

SCNPs <b>4</b> (blue line volume distribution; red line number distribution) using multi-temperature DLS analysis from 20 °C to 80 °C in THF (Conc. 5 mg mL <sup>-1</sup> ).....	219
<b>Figure 5.2.</b> <sup>13</sup> C NMR spectra (100.7 MHz; 298 K; DMSO- <i>d</i> <sub>6</sub> ) of <b>2</b> (blue), SCNP <b>3</b> (red), SCNP <b>4</b> (green), and copolybetaine <b>5</b> (yellow).....	221
<b>Fig. S5.1.</b> <sup>1</sup> H NMR spectrum of linear precursor <b>2</b> (400 MHz; 298 K; DMSO- <i>d</i> <sub>6</sub> ; * <sup>1</sup> methanol; * <sup>2</sup> water and * <sup>3</sup> DMSO) .....	232
<b>Fig.S5.2.</b> <sup>13</sup> C NMR spectrum of linear precursor <b>2</b> (100.7 MHz; 298 K; DMSO- <i>d</i> <sub>6</sub> ; * <sup>1</sup> methanol and * <sup>2</sup> DMSO).....	233
<b>Fig. S5.3.</b> <sup>1</sup> H NMR spectrum of SCNP <b>3</b> (400 MHz; 298 K; DMSO- <i>d</i> <sub>6</sub> ; * <sup>1</sup> dichloromethane; * <sup>2</sup> water and * <sup>3</sup> DMSO).....	233
<b>Fig. S5.4.</b> <sup>13</sup> C NMR spectrum of SCNP <b>3</b> (100.7 MHz; 298 K; DMSO- <i>d</i> <sub>6</sub> ; * <sup>1</sup> dichloromethane and * <sup>2</sup> DMSO).....	234
<b>Fig. S5.5.</b> <sup>1</sup> H NMR spectrum of SCNP <b>4</b> (400 MHz; 298 K; DMSO- <i>d</i> <sub>6</sub> ; * <sup>1</sup> methanol; * <sup>2</sup> water and * <sup>3</sup> DMSO).....	234
<b>Fig. S5.6.</b> <sup>13</sup> C NMR spectrum of SCNP <b>4</b> (100.7 MHz; 298 K; DMSO- <i>d</i> <sub>6</sub> ; * <sup>1</sup> methanol and * <sup>2</sup> DMSO).....	235
<b>Fig. S5.7.</b> <sup>19</sup> F NMR spectrum of SCNP <b>4</b> (376.5 MHz; 298 K; DMSO- <i>d</i> <sub>6</sub> ).....	235
<b>Fig. S5.8.</b> <sup>1</sup> H NMR spectrum of SCNP <b>5</b> (400 MHz; 298 K; DMSO- <i>d</i> <sub>6</sub> ; * <sup>1</sup> tetrahydrofuran; * <sup>2</sup> water and * <sup>3</sup> DMSO).....	236
<b>Fig. S5.9.</b> <sup>13</sup> C NMR spectrum of SCNP <b>5</b> (100.7 MHz; 298 K; DMSO- <i>d</i> <sub>6</sub> ; * <sup>1</sup> tetrahydrofuran and * <sup>2</sup> DMSO).....	236
<b>Fig. S5.10.</b> <sup>1</sup> H NMR spectrum of benzoin condensation catalysis using 10 mol% of catalyst <b>2</b> (400 MHz; 298 K; DMSO- <i>d</i> <sub>6</sub> ; * <sup>1</sup> tetrahydrofuran; * <sup>2</sup> DMSO).....	237
<b>Fig. S5.11.</b> Mean hydrodynamic diameter of SCNP <b>3</b> by volume (black line), number distribution (blue line) and by intensity (red line) obtained by DLS in THF. Concentration 1 mg mL <sup>-1</sup> analysis was performed at room temperature.....	237
<b>Fig. S5.12.</b> Correlation function of SCNP <b>3</b> obtained by DLS in THF. Concentration 1 mg mL <sup>-1</sup> analysis was performed at room temperature.....	238
<b>Fig. S5.13.</b> Mean hydrodynamic diameter of linear precursor <b>2</b> by volume (black line), number distribution (blue line) and by intensity (red line) obtained by DLS in THF. Concentration 1 mg mL <sup>-1</sup> analysis was performed at room temperature.....	238
<b>Fig. S5.14.</b> Correlation function of linear precursor <b>2</b> obtained by DLS in THF. Concentration 1mg mL <sup>-1</sup> analysis was performed at room temperature.....	239

# List of Schemes

<b>Scheme 1.1</b> Different type of nature of cross-linkings of SCNPs.....	33
<b>Scheme 1.2.</b> Synthesis of linear polymer precursor based on poly(MMA)- <i>co</i> -(AEMA) and subsequent cross-linking induced by addition of trimethylolpropane triacrylate (TMPTA). <sup>29</sup> .....	36
<b>Scheme 1.3.</b> Chemical structure of the parent copolymer P1, its photochemically induced folding into SCNP1 and subsequent ligation to SCNP1- <i>co</i> -PEG. <sup>35</sup> .....	38
<b>Scheme 1.4.</b> Synthesis of copolymer P1 <i>via</i> NMP of styrene and 4-(diphenylphosphino)styrene. The subsequent addition of [Pt(cod)Cl <sub>2</sub> ] results in SCNPs formation. <sup>45</sup> .....	42
<b>Scheme 1.5.</b> Schematic illustration of the preparation of the linear poly(COD) by ROMP and subsequent metal complexation (in this particular case iridium is shown as an example). <sup>47</sup> .....	43
<b>Scheme 1.6 a)</b> SCNPs formation based on a triblock copolymer bearing BTA and UPy motifs, <b>b)</b> chemical composition of the employed linear copolymeric precursor, <b>c)</b> helical BTA H-bonding driven self-assembly and <b>d)</b> photoinduced dimerization of UPys via quadrupole H-bonding. <sup>62</sup> .....	48
<b>Scheme 1.7</b> Schematic representation of the SCNP folding of poly(styrene- <i>co</i> -pentafluorostyrene) block copolymer in solution. <sup>66</sup> .....	49
<b>Scheme 1.8</b> Dynamic behaviour of PIL SCNPs by release of radicals after UV-induced homo/heterolytic cleavage for MMA polymerisation initiation. <sup>70</sup> .....	53
<b>Scheme 1.9</b> Overview of the dynamic covalent folding and unfolding of SCNPs using hetero-Diels-Alder (HDA) chemistry. <sup>73</sup> .....	54
<b>Scheme 1.10</b> Design of catalytically active SCNPs for transfer hydrogenation of ketones in water in a BTA-supramolecular interactions based nanoreactors.....	80
<b>Scheme 1.11 (A)</b> Reduction of benzyl benzamide using Ir-SCNPs and <b>(B)</b> biphenyl production catalysed by Rh-SCNPs. <sup>47</sup> .....	83
<b>Scheme 1.12</b> Illustration of a SCNP folding into a Pt-containing nanoreactor employed for the amination of allyl alcohol which can be further recycled. <sup>45</sup> .....	84
<b>Scheme 1.13</b> Preparation of dextran-based SCNPs and subsequent incorporation of the Tn-Antigen. <sup>120</sup>	86
<b>Scheme 1.14</b> Schematic representation of the sensing function of the BiPy-BTA functional polymers. <sup>53</sup>	89
<b>Scheme 2.1.</b> Synthetic route to (PS- <i>co</i> -Poly[ViEBIm]Cl) ( <b>3</b> ) by free radical copolymerization of [ViEBIm]Cl and styrene in methanol, followed by the synthesis of physically crosslinked (PS- <i>co</i> -Poly[ViEBIm]Seb) ( <b>5</b> ) by anion exchange. Synthesis of (PS- <i>co</i> -Poly[ViEBIm]TFSI)-1 ( <b>4</b> ) is also	

displayed.....	106
<b>Scheme 2.2.</b> Two different pathways followed for the synthesis of TFSI anion-containing copolymers ( <b>4</b> , <b>7</b> ) supporting the anion-exchange mediated decrosslinking of the gel.....	112
<b>Scheme 2.3.</b> Benzoin condensation, transesterification and cyanosilylation organocatalyzed by NHC-supported physically crosslinked porous gel under heterogeneous conditions.....	115
<b>Scheme 3.1.</b> Design of catalytically active SCNPs for benzoin condensation reaction.....	142
<b>Scheme 3.2.</b> Synthetic route to the parent linear copolymer <b>4</b> by RAFT copolymerization of <b>2</b> , <b>3</b> , <b>4</b> vinylbenzoic acid and styrene, followed by a folding step caused by anion-metathesis leading to the formation of SCNP <b>5</b> . Unfolded copolymer, <b>6</b> could be obtained by irreversibly post-functionalizing SCNP <b>5</b> with CS <sub>2</sub> .....	143
<b>Scheme S3.1.</b> Synthetic route to prepare molecular catalyst model based on the active monomer and linear catalyst model.....	164
<b>Scheme 4.1.</b> Strategies to conduct SCNP synthesis for use as catalytic nanoreactors. <b>A</b> ) Classic route involving the addition of external reagents to induce chain folding. <b>B</b> ) Self-catalysed SCNPs folding mediated by supported thermally latent NHC precatalysts.....	175
<b>Scheme 4.2.</b> Synthetic route to functional linear copolymer <b>3</b> and subsequent self-catalysed folding step leading to catalytically active SCNP <b>5</b> . The NHC-CS <sub>2</sub> functionalised versions of both linear precursor ( <b>4</b> ) and obtained SCNP ( <b>6</b> ) as well as corresponding active NHC intermediates are also represented.....	178
<b>Scheme 5.1.</b> Folding of a single-chain polymer into a nanoparticle structure <i>via</i> addition of a metal ion source ( <i>i.e.</i> Ag <sub>2</sub> O). These SCNPs are then employed as sources of free NHC upon thermal decomposition of the organometallic Ag-NHC bond in the nanoreactor to form an active catalyst species.....	215
<b>Scheme 5.2.</b> Synthesis of copolymer <b>2</b> <i>via</i> RAFT polymerization of styrene and <b>1</b> in methanol. The subsequent addition of Ag <sub>2</sub> O results in the formation of <b>3</b> as SCNPs. Further anion exchange was performed by inserting a non-coordinating anion (NTf <sub>2</sub> <sup>-</sup> ) into <b>3</b> to confer less dynamic behavior ( <b>4</b> ).216	
<b>Scheme 5.3.</b> Application of SCNPs <b>3</b> as a catalytic platform ( <b>B</b> ) for the benzoin condensation reaction by exposing active NHC upon heating ( <b>C</b> ) Indirect evidence of the formation of active NHC intermediate ( <b>A</b> ).....	220

# List of Tables

<b>Table 1.1.</b> Illustrations of chemical transformations used as well as the structure of the covalent cross-links employed in SCNPs. <sup>5</sup> .....	35
<b>Table 1.2</b> Illustrations of chemical transformations used as well as the structure of the organometallic cross-links employed in SCNPs.....	40
<b>Table 1.3</b> Illustrations of chemical transformations used as well as the structure of the supramolecular cross-links employed in SCNPs.....	45
<b>Table 1.4</b> Illustrations of chemical transformations used as well as the structure of the dynamic covalent cross-links employed in SCNPs.....	50
<b>Table 1.5</b> Summary of reactions catalysed by SCNPs as organocatalysts.....	74
<b>Table 1.6</b> Summary of reactions catalysed by SCNPs as organometallic catalyst.....	77
<b>Table 3.1.</b> Benzoin condensation reactions of benzaldehyde under different conditions using NHC-containing SCNPs and control experiments.....	151
<b>Table 4.1.</b> Transesterification between benzyl alcohol and vinyl acetate under different reaction conditions using masked NHC-containing SCNPs and control experiments.....	183
<b>Table 5.1.</b> Condensation reaction of benzaldehyde under different conditions using Ag-NHC SCNPs and a small molecule model as catalysts .....	222



# **Chapter I: Introduction to Single Chain Nanoparticles (SCNPs) as nanoreactors**





# Table of Contents

## Chapter I: Introduction to Single Chain Nanoparticles (SCNPs) as nanoreactors

1.1	Single Chain Nanoparticles (SCNPs) .....	31
1.1.1	Introduction .....	31-32
1.1.2	Synthetic methods towards single-chain nanoparticles.....	32
1.1.2.1	SCNPs via irreversible and reversible bonds.....	32-33
1.1.2.1.1	Covalent bonds.....	33-39
1.1.2.1.2	Organometallic bonds.....	39-44
1.1.2.1.3	Supramolecular chemistry.....	44-50
1.1.2.1.4	Dynamic covalent chemistry.....	50-54
1.1.3	Characterisation of Single Chain Polymer Nanoparticles: analytical techniques.....	54-55
1.1.3.1	Size exclusion chromatography (SEC).....	55-57
1.1.3.2	Spectroscopic characterisation of SCNPs.....	57
1.1.3.2.1	NMR spectroscopy .....	57-59
1.1.3.2.2	IR, UV-VIS, CD and fluorescence spectroscopy.....	59-62
1.1.3.3	Characterisation of Single Chain Nanoparticles morphology.....	62
1.1.3.3.1	Morphological characterisation via TEM.....	62-63
1.1.3.3.2	Morphological characterisation via AFM.....	63-64
1.1.3.3.3	Morphological characterisation via scattering (DLS, SAXS, SANS) .....	65-67
1.1.4	Applications.....	68-69
1.1.4.1	Nanomedicine.....	69
1.1.4.1.1	Drug delivery and imaging.....	69-72

1.1.4.2 Nanoreactors for catalysis.....	73
1.1.4.2.1 Organocatalysis .....	73-77
1.1.4.1.2 Organometallic catalysis.....	77-85
1.1.4.1.3 Enzymatic catalysis .....	85-86
1.1.4.3 Other uses.....	86-89
1.3 Conclusions and aims of the PhD thesis.....	89-91
1.4 References.....	91-97

## 1.1 Single Chain Nanoparticles (SCNPs)

### 1.1.1 Introduction

Many applications, such as biomedicine or catalysis, require soft matter-based particles that feature sizes in the nanometer range. In nature, precisely defined linear polymers folded into functional nanoarchitectures are recurrent. In this light, it seems reasonable to exploit our understanding of biomolecules to mimic this behavior at the laboratory scale. This is most often achieved using advances in controlled polymerisation techniques in combination with established theories of modern polymer physics.<sup>1-3</sup> The folding of proteins into secondary, tertiary or even quaternary structures is found to dramatically influence their properties and functions.<sup>4</sup> The utility of biomacromolecules mainly derives from their 3D orientation with functionality located either on the surface or in the interior of the structure. For this, tertiary/quaternary structures can occur as a consequence of the precise primary structure, which is unavailable by synthetic methods. Still, in recent years, advances in controlled polymerisation techniques have enabled the precise synthesis of well-defined and -even sequence defined- (co)polymers. With the aim at attaining synthetic globular 3D structures, different polymer structures, such as dendrimers, hyperbranched polymers, foldamers, micelles or star polymers have been considered as a means to synthetically emulate biomacromolecules from nature. However, either their synthesis is tedious and leads to low yields, or they lack of specificity in their structure.<sup>5</sup>

As an alternative to the aforementioned polymer structures mimicking folded biomacromolecules, so-called single chain nanoparticles (SCNPs) have gained an increasing attention. SCNPs consist of a single linear polymer chain precursor that is further intramolecularly collapsed into a folded nanostructure and in a defined manner.<sup>6-10</sup> First examples were reported by Wooley *et al.*<sup>11,12</sup> and Mecerreyes *et al.*<sup>13</sup> two decades ago. Since then, the field has been considerably extended. SCNPs are usually distinguished, as a function of the nature of cross-linking moieties, into three different categories, as depicted in **Fig. 1.1**. Namely, one can differentiate: i) homofunctional crosslinks where motifs are all the same, ii)

heterofunctional crosslinks involving distinct cross-linking motifs and iii) use of an external cross-linker for the folding process.<sup>8</sup>

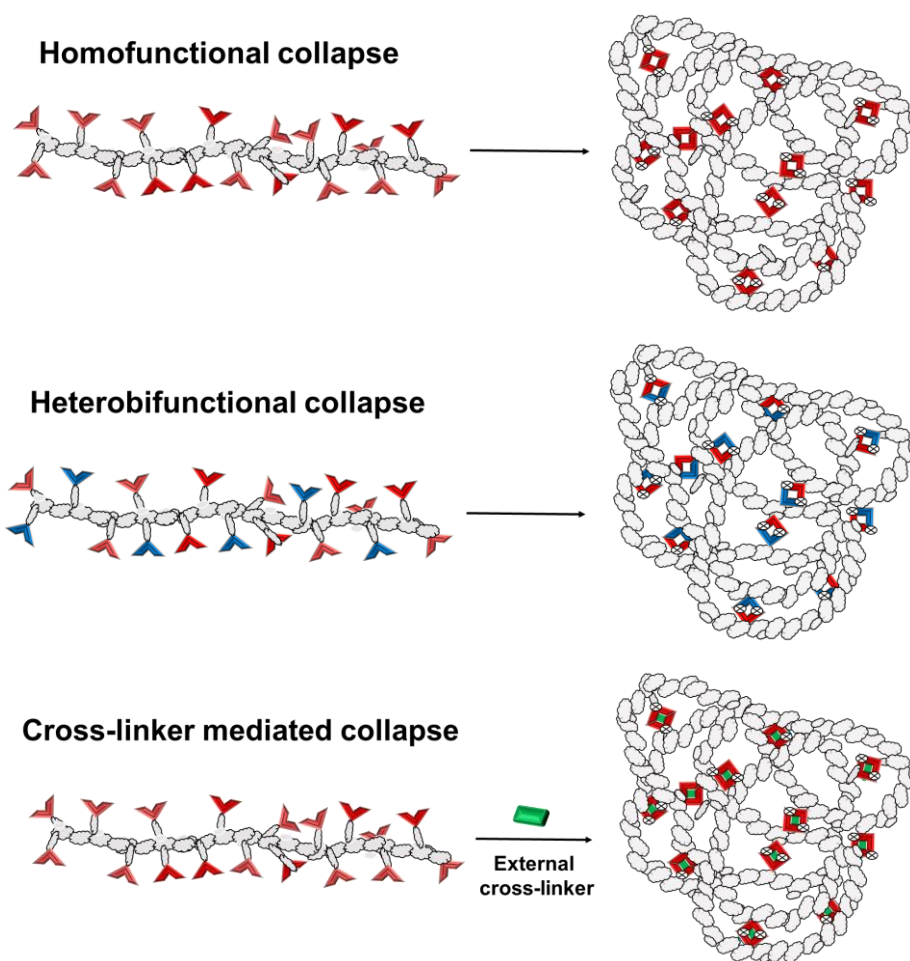


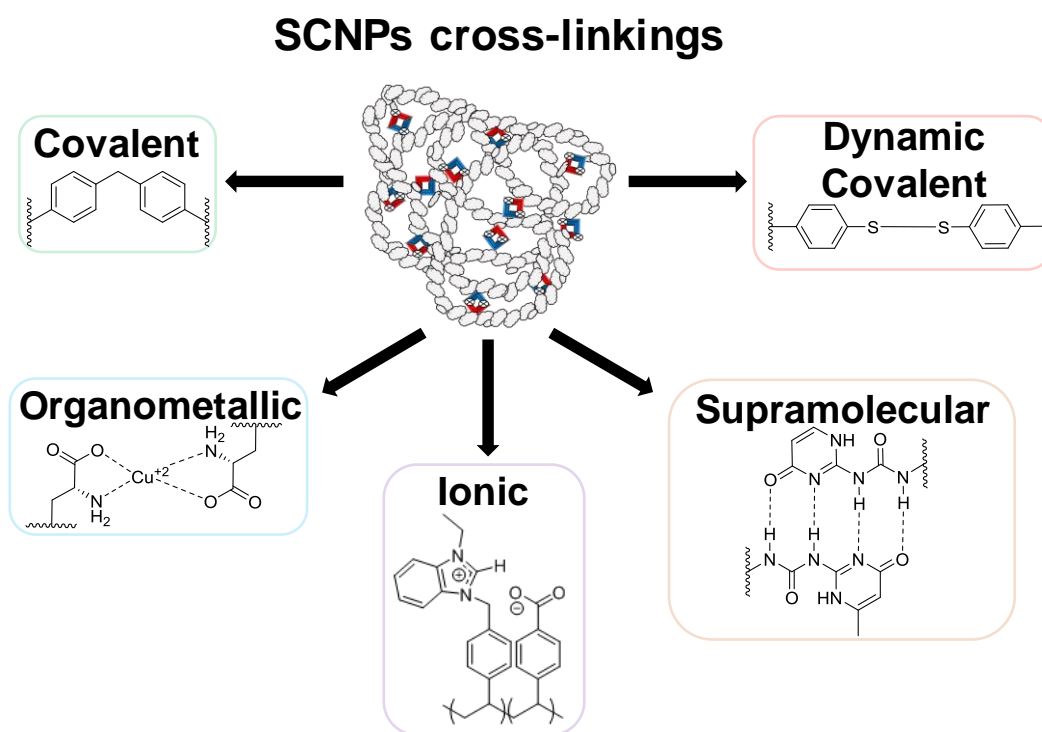
**Figure 1.1** Modes for intramolecular collapse through cross-linking of a single polymer chain, forming SCNPs.

This chapter aims at describing existing synthetic methodologies to SCNPs, related characterisation techniques, and potential applications discussed in the recent literature for these nanoobjects.

## 1.1.2 Synthetic methods towards single-chain nanoparticles

### 1.1.2.1 SCNPs *via* irreversible and reversible bonds

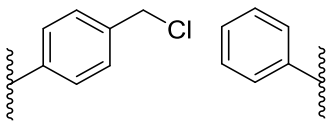
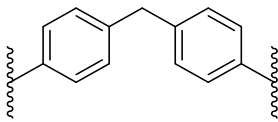
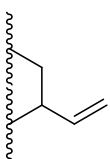
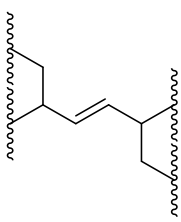
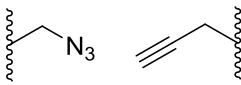
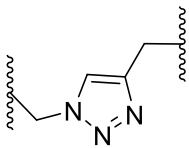
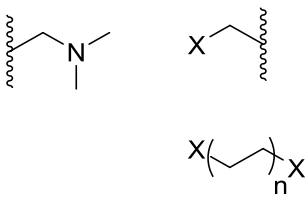
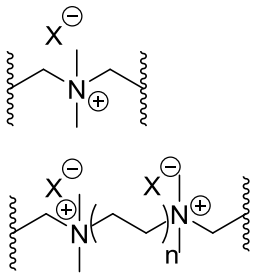
A wide variety of synthetic approaches to SCNPs have been developed. The most common route is based on the post-functionalisation of a linear, generally well-defined (co)polymer precursor, under highly dilute conditions (*ca.*  $< 1 \text{ mg mL}^{-1}$ ). Such conditions indeed promote intra-chain over inter-chain cross-linking.<sup>5</sup> Biomolecules in nature exploit different orthogonal non-covalent interactions (*e.g.* hydrogen bonding or van der Waals interactions), covalent interactions (*e.g.* disulfides) or dynamic covalent interactions (*e.g.* reversible acetal formation). These modus operandi have largely inspired synthetic approaches to SCNPs.<sup>14</sup> The following discussion about the intra-chain cross-linking process will take into account the types of crosslinks generated, namely, covalent, organometallic, ionic, supramolecular and dynamic covalent bonds (**Scheme 1.1**)



**Scheme 1.1** Different type of nature of cross-linkings of SCNPs.

#### 1.1.2.1.1 Covalent bonds

These organic SCNPs could be obtained following different synthetic approaches applying well-known chemistries, as summarised in **Table 1.1**.

Covalent chemistry				
Entry	Before cross-linking	Structure of cross-linking	Type of chemistry	Ref
1			Friedel-Crafts alkylations	15
2			Olefin metathesis	16
3			Azide-alkyne « click » chemistry	17,18
4			Mensuchtkin reactions	19,20

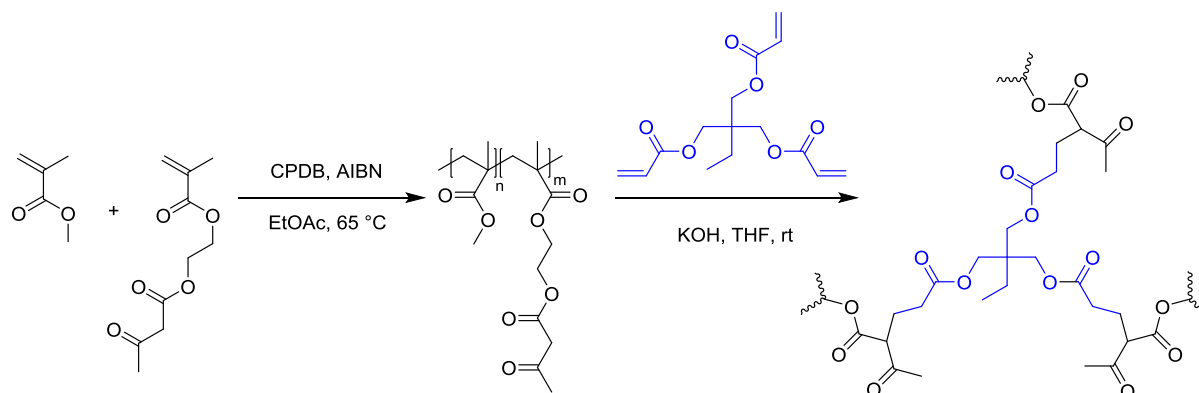
5			Ugi	21
6			Passerini reactions	21,22
7			Thiol-ene « click » chemistry	23
8			Glasser-Hay couplings	24
9			UV-light dimerisations	25– 27

**Table 1.1.** Illustrations of chemical transformations used as well as the structure of the covalent cross-links employed in SCNPs.<sup>5</sup>



Pomposo *et al.* have thoroughly analysed the reported examples of covalently cross-linked SCNPs.<sup>28</sup> Their analysis reveals that, unexpectedly, covalent SCNPs can adopt an open, sparse morphology resembling that of intrinsically disordered proteins (IDPs), rather than a globular architecture like of naturally occurring biomolecules. The covalent nature of cross-links in this type of SCNPs confers them an enhanced robustness and decreasing their probability for further aggregation and/or inter-crosslinking after the critical folding step. This may be crucial for certain applications, particularly where conditions are relatively harsh, such as at high temperatures, extreme pH or concentrated environments.

As representative example of the aforementioned properties regarding covalently cross-linked SCNPs, Diesendruck *et al.* improved the molecular toughness of synthetic polymers by introducing intramolecular covalent cross-links (**Scheme 1.2**). The use of covalent cross-links in the SCNPs was envisaged to study mechanochemical reactions when applying shear (by sonication). Unexpectedly, the collapsed structure of the polymer underwent mechanochemical reactions at accelerated rates, although the scission occurred in sacrificial bonds that did not lead to fragmentation of the chains. This outcome proved that covalently cross-linked SCNPs showed enhanced mechanical properties by maintaining their properties under harsh conditions.<sup>29</sup>



**Scheme 1.2.** Synthesis of linear polymer precursor based on poly(MMA)-*co*-(AEMA) and subsequent cross-linking induced by addition of trimethylolpropane triacrylate (TMPTA).<sup>29</sup>

Inspired by reported reactions at the molecular level, covalently bound SCNPs repeat these reactions all along the polymeric structure leading to multiple covalent linkages in the same nanoparticle. As summarised in **Table 1.1**, elementary reactions implemented to fold the linear polymeric precursors into single (co)polymer chains have been used following different fashions.

One of the earliest examples was reported by Dubrovina *et al.*, who derived linear polystyrene containing 50% and 100% of chloromethylated phenyl residues. Intramolecular cross-links were successfully obtained *via* Friedel-Craft alkylations in presence of SnCl<sub>4</sub> leading to particles with radius *ca.* 17 nm and cross-linking degrees of 60%. This synthesis pathway required however relatively harsh conditions (*i.e.* 80 °C for 100 h in dichloroethane) (**Table 1.1 ; Entry 1**).<sup>15</sup>

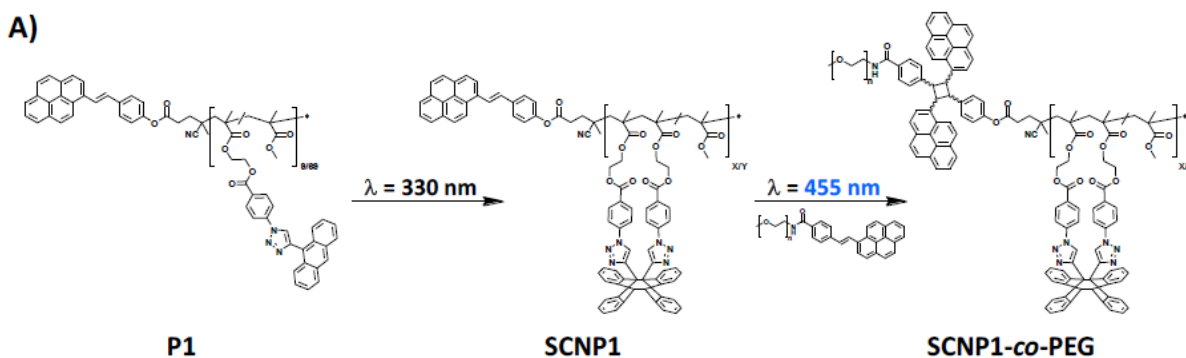
In another example, Coates *et al.* synthesised vinyl-pendant linear polycarbonates using a Zn-derived catalyst (*i.e.* [(BDI)ZnOAc]<sub>2</sub>). Subsequently, intramolecularly cross-linked nanoparticles were obtained by cross-metathesis reaction of pendant vinyl groups using Grubbs 2<sup>nd</sup> generation catalyst. The high catalytic efficiency of the Grubbs catalyst was translated in the fast rate at which cross-links were obtained. In fact, more than 42% of pendant vinyl groups reacted within 15 min, albeit metathesis slowed down as the reaction progressed. However, the use of different metals remains as a potential drawback for biomedical applications or electronics (**Table 1.1 ; Entry 2**).<sup>16</sup>

High efficiency, high functional (group) tolerance, and relatively mild reaction conditions render “click chemistry” reaction an attractive approach for obtaining SCNPs. So far, copper-mediated azide-alkyne cycloaddition (CuAAC) (**Table 1.1 ; Entry 3**),<sup>17,18</sup> Mitsunobu reaction (**Table 1.1 ; Entry 4**),<sup>19,20</sup> multicomponent Ugi (**Table 1.1 ; Entry 5**)<sup>30</sup> and Passerini (**Table 1.1 ; Entry 6**)<sup>22,31</sup> reactions or thiol-ene addition (**Table 1.1 ; Entry 7**)<sup>23,32</sup> (to cite few) have been used as cross-linking “click” methods for SCNP fabrication.

Having the lack of group tolerance as main drawback to circumvent, Pomposo *et al.* directly polymerised terminal alkynes *via* redox-initiated RAFT (reversible addition-fragmentation chain transfer) polymerisation. The obtained functional linear precursor was exposed under diluted conditions to copper-catalysed Glaser-Hay coupling conditions to form SCNPs with no previous deprotection process (**Table 1.1 ; Entry 8**).

Photochemical chemistry is often clean, relatively fast and high yielding and often requires no external catalyst. Therefore, several reactions have been applied in the SCNPs domain such as photoinduced nitrile imine mediated tetrazole-ene cycloaddition<sup>33</sup> or photo-dimerisations of anthracene<sup>27</sup> or coumarin,<sup>34</sup> for instance (**Table 1.1 ; Entry 9**).

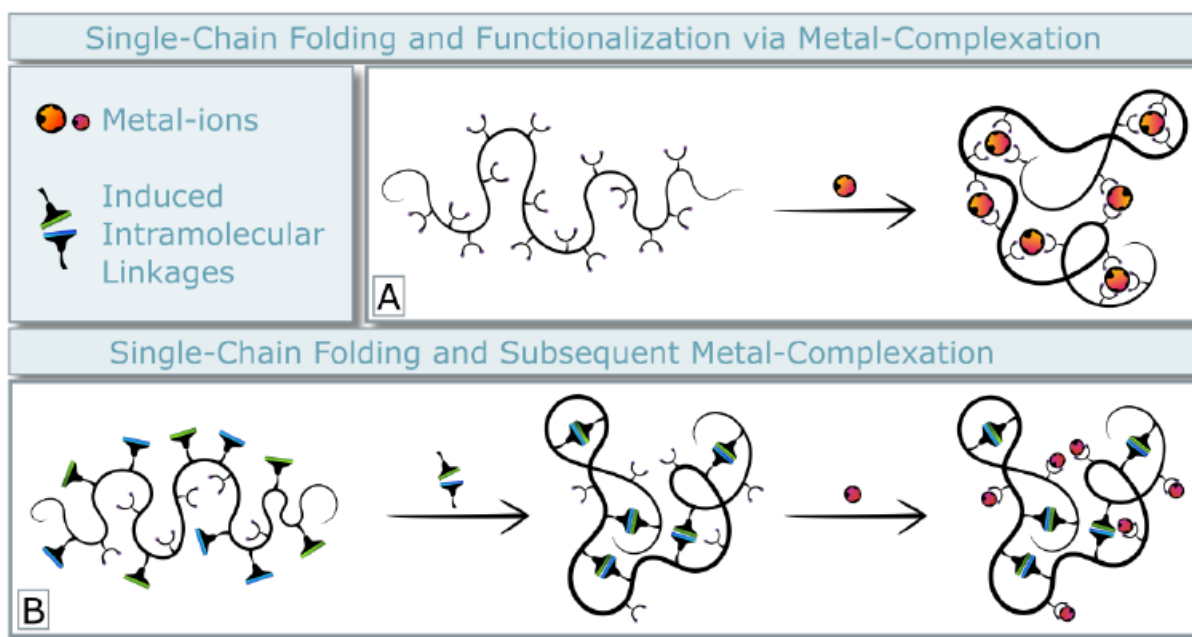
The versatility of employing UV-light was highlighted in a recent study carried out by Barner-Kowollik *et al.* by harnessing different wavelengths for different functionalization purposes.<sup>35</sup> Namely, by synthesising a (co)polymer containing 9-triazolylanthracene units distributed along the polymer chain and a terminal styrylpyrene unit polymer, authors developed amphiphilic SCNPs. By irradiation with UV light at  $\lambda = 330$  nm, P1 was intramolecularly cross-linked. Subsequently, a PEG polymer block was incorporated by irradiating blue light at  $\lambda = 455$  nm (**Scheme 1.3**). The unprecedented selectivity to trigger different dimerisations arised from the unique set of  $\lambda$ -orthogonal photoligations.



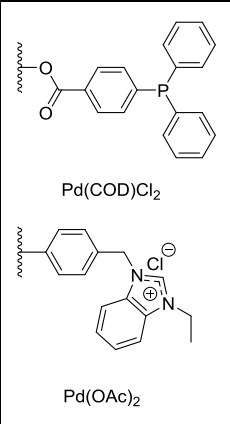
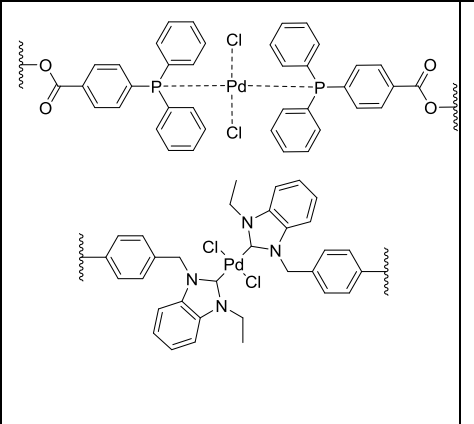
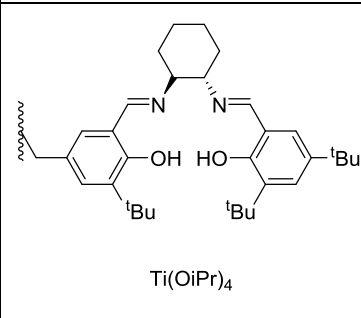
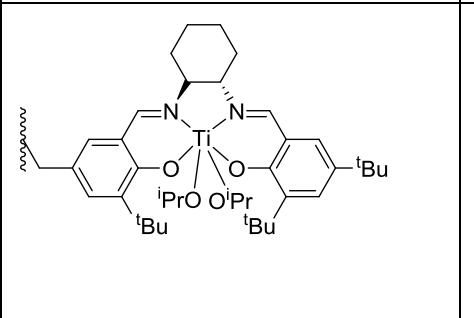
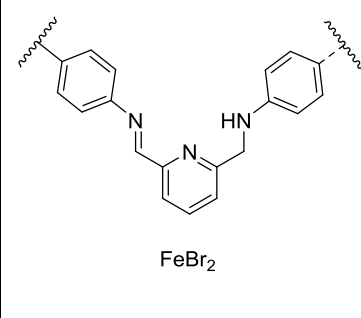
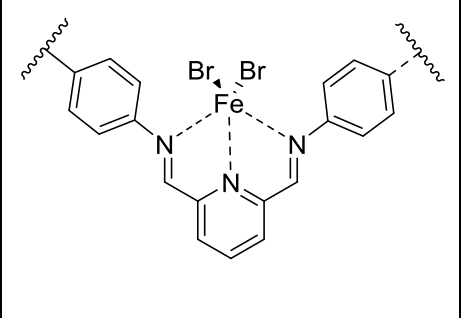
**Scheme 1.3.** Chemical structure of the parent copolymer P1, its photochemically induced folding into SCNP1 and subsequent ligation to SCNP1-*co*-PEG.<sup>35</sup>

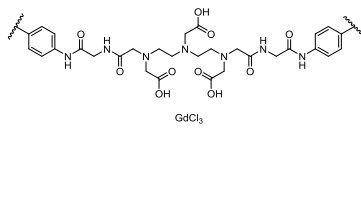
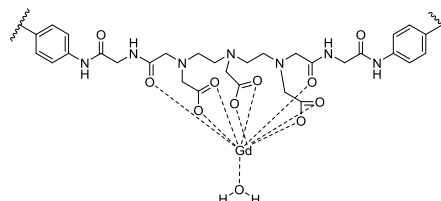
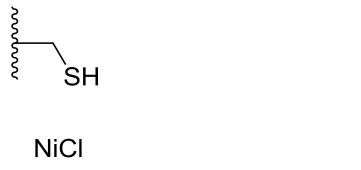
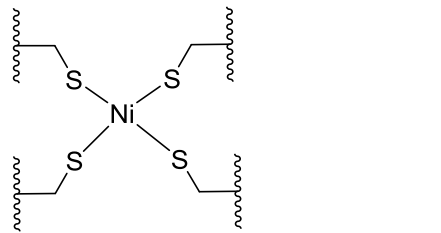
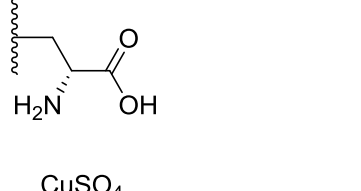
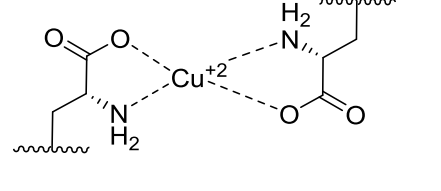
#### 1.1.2.1.2 Organometallic bond

In this part, is discussed the possibility to incorporate metal-ions as a means to intramolecularly crosslink linear chains into SCNPs (summarised in **Table 1.2**). One should distinguish between two types of functionalisation that SCNPs can undergo *via* metal-complexation. Firstly, the externally introduced metal-ions do not only impart the desired catalytic function to the polymeric architecture, but operate instead as structure-forming elements. Alternatively, SCNPs can be previously formed and subsequently loaded with metal ions (**Fig.1.2**).<sup>36</sup> It has to be acknowledged though, that the first case appears the most promising, as related SCNPs may behave as analogous of metallo-enzymes.<sup>36,37</sup>



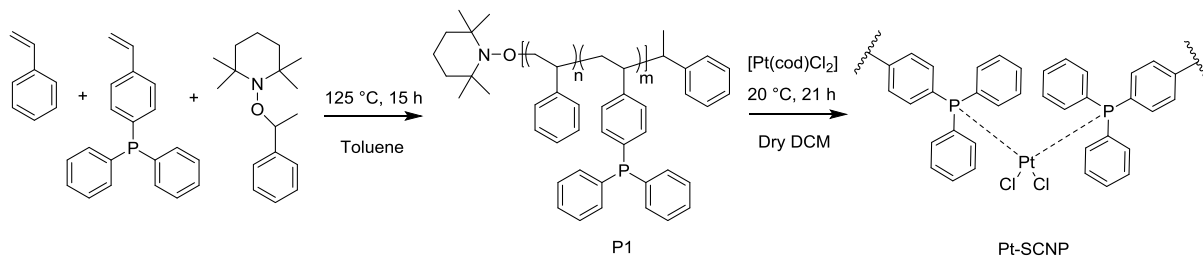
**Figure 1.2** (A) The introduction of appropriate ligand functionalities in the polymer chain allowing SCNP folding and catalytic functionalisation in one step. (B) Nanoparticle formation *via* an external trigger and subsequent metal ion loading.<sup>36</sup>

Organometallic bonds				
Entry	Before cross-linking	Structure of cross-linking	Type of chemistry	Ref
1	 <p>Pd(COD)Cl<sub>2</sub></p> <p>Pd(OAc)<sub>2</sub></p>		Palladium complexation	38,39
2	 <p>Ti(OiPr)<sub>4</sub></p>		Ti complexation	40
3	 <p>FeBr<sub>2</sub></p>		Iron complexation	41

4	 <p style="text-align: center;">GdCl<sub>3</sub></p>		Gadolinium complexati on	42
5	 <p style="text-align: center;">NiCl</p>		Nickel complexati on	43
6	 <p style="text-align: center;">CuSO<sub>4</sub></p>		Copper complexati on	44

**Table 1.2** Illustrations of chemical transformations used as well as the structure of the organometallic cross-links employed in SCNPs.

In order to form organometallic hybrid SCNPs, ligands are generally supported onto the polymeric structure. Specifically, Kowolik *et al.* designed a linear copolymer of styrene and 4-(diphenylphosphino)styrene *via* nitroxide-mediated polymerization.<sup>45</sup> The triarylphosphine ligand moieties along the backbone allowed for the intramolecular cross-linking of SCNPs via the addition of [Pt(1,5-cyclooctadiene)Cl<sub>2</sub>] in diluted conditions. These nanoparticles were developed for catalysis purpose, and interestingly, embedding Pt ions into the SCNPs-structure enabled homogeneous catalytic conditions as well as full recyclability of the SCNPs (**Scheme. 1.4**) (**Table 1.2; Entry 1**).



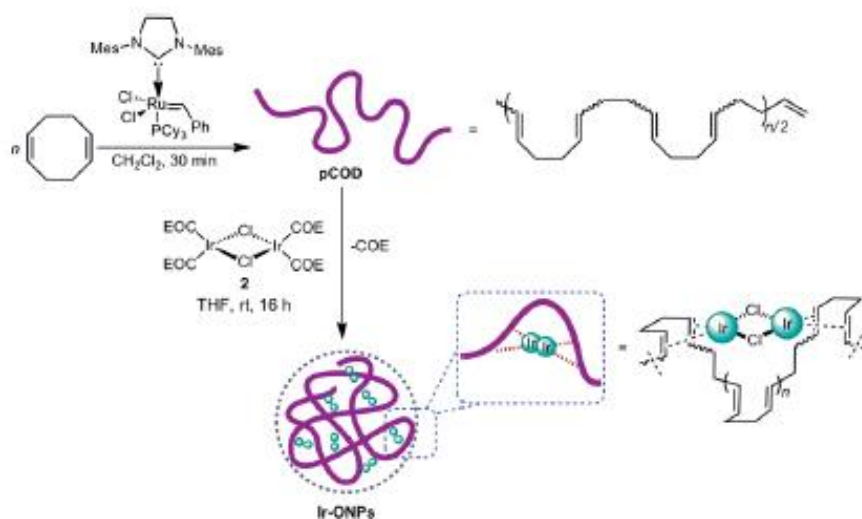
**Scheme 1.4.** Synthesis of copolymer P1 *via* NMP of styrene and 4-(diphenylphosphino)styrene. The subsequent addition of  $[\text{Pt}(\text{cod})\text{Cl}_2]$  results in SCNPs formation.<sup>45</sup>

The ease of preparation of this specific type of ligand-bearing linear polymer precursor has motivated the incorporation of large number of different metal ions. Namely, the same polymer precursor decorated with 4-(diphenylphosphino)styrene served as (poly)ligand for both ruthenium<sup>46</sup> and palladium.<sup>39</sup> Equally to the example represented in **Scheme 1.4**, the latter metal-containing SCNPs were used as nanoreactors for catalysis.

Together with phosphines, several monomers have been derivatized in order to support versatile and highly efficient ligands, such as chiral salen moieties for titanium<sup>40</sup> (**Table 1.2 ; Entry 2**) or NHCs for palladium (**Table 1.2 ; Entry 1**).<sup>38</sup> Of special importance, in the latter example Taton *et al.*,<sup>38</sup> disclosed a synthetic strategy where no active carbenes were employed for the folding step; instead, a benzimidazolium chloride ionic liquid was used as non-sensitive ligand. This achievement critically decreased the complexity of the process enabling an easy handling and storage of both precursors and Pd-SCNPs.

In most cases, the latter backbone is of (meth)acrylic or styrenic-type. Conversely, Lemcoff *et al.* introduced a wide-ranging strategy using the actual polymer backbone for the exploitation of organometallic bonds to induce SCNPs collapse with a diverse system.<sup>47</sup> This was simply achieved by using a pCOD poly(1,5-cyclooctadiene) obtained by ROMP (ring opening metathesis polymerization) as (poly)ligand. This provided a straightforward synthetic route to metal-containing SCNPs without the need

for a specific monomer to act as ligands (**Scheme 1.5**). Moreover, the versatility of COD as ligand was harnessed by serving as support for different metals as rhodium, iridium or nickel.



**Scheme 1.5.** Schematic illustration of the preparation of the linear poly(COD) by ROMP and subsequent metal complexation (in this particular case iridium is shown as an example).<sup>47</sup>

Different to the one-step metal incorporation of metal-ions into polymer supported-ligands, Sawamoto *et al.* created amphiphilic SCNPs bearing iron ions *via* a two-step procedure.<sup>41</sup> Briefly, a linear poly(methyl)methacrylate supported aniline-type motifs was designed. The aniline motifs were post-functionalised to incorporate bifunctional ligand cavities (*i.e.* 2,6-pyridine derivative) and then FeBr<sub>2</sub> was incorporated into the core of already cross-linked SCNPs occupying the previously formed ligand cavities. SCNPs could be recycled after each catalytic cycle thanks to the covalently cross-linked robust structure which enabled to keep catalytic activity and thus efficient recyclability (**Table 1.2; Entry 3**).

Another notorious example of a two-step procedure for incorporating a metallic ion was performed by Odriozola *et al.*<sup>42</sup> In this example, an azide-bearing polyacrylate copolymer was designed and subsequently cross-linked by a Cu(I)-catalyzed click reaction in presence of short dialkyne molecule. This covalently bond cross-linker provided with a DTPA (diethylenetriaminepentaacetic acid) then served as



chelating units for Gd(III) ions. Interestingly, the obtained nanoparticles showed higher relaxivity properties for MRI (magnetic resonance imaging) applications than commercially available analogues, thanks to an enhanced water solubility provided by the polymeric structure, as well as the ease to load multiple Gd(III) ions (**Table 1.2; Entry 4**).

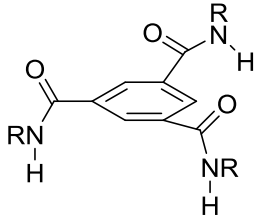
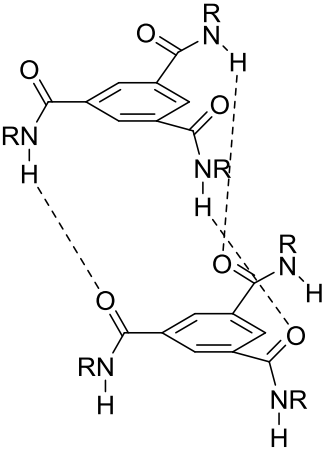
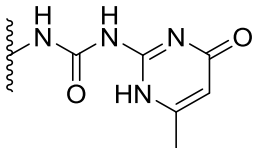
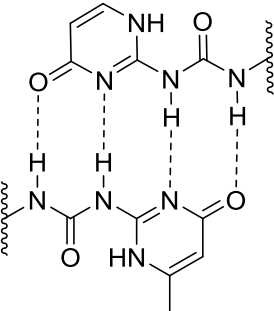
He and coworkers developed SCNPs-based metallofoldamers by intramolecular self-folding through Ni-thiolate coordination within thiol-functionalised linear copolymer.<sup>43</sup> These Ni-thiolate cofactors were employed for catalytic purposes. Interestingly, they were found not only to act as cross-linking bridges but also acted as a secondary coordination environment to promote photocatalytic activity (**Table 1.2; Entry 5**).

Targeting the same mimicry related to metalloenzymes, Pomposo *et al.* developed an efficient vitamin B<sub>9</sub> nanocarriers known as “Michael” nanocarriers, based on Cu(OAc)<sub>2</sub> complexes supported all along SCNPs structure.<sup>44</sup> Helped by computational support, these “Michael nanocarriers” were found to resemble disordered multidomain proteins with semiflexible linkers in solution, whereas they remained collapsed with globular morphology in dry state (**Table 1.2; Entry 6**).

#### 1.1.2.1.3 Supramolecular Chemistry

Supramolecular interactions, such as H-bonding and  $\pi$ - $\pi$  interactions, are the dominant intra-chain linkage in folded biomacromolecules.<sup>5</sup> Monomers employed to this end are typically, functionalized with hydrogen bonding units that are (photo)protected, in an effort to avoid the formation of premature aggregates. As summarised in **Table 1.3; Entry 1**, Palmans, Meijer *et al.* have carried out studies involving 2-ureidopyrimidinone (UPy),<sup>48-50</sup> a motif that is prone to dimerization by hydrogen bondings. The deprotection step, occurring under dilute conditions, favors the formation of intra-chain quadruple hydrogen bonds, promoting the formation of the targeted SCNPs. The authors refer to these SCNPs as metastable particles, as high temperatures and solvent exchange were found to induce polymer

precipitation, as a result of inter-chain interactions. Moreover, Upy dimerization was used to study the effect of several variables in SCNPs formation and its performance for several applications (**Table 1.3; Entry 2**). Briefly, the same group established that the rigidity of the polymer backbone, the placement of additional hydrogen bonding sites in the UPy linker, and the molecular weight of the polymer had little effect on the ability of a polymer to form supramolecular SCNPs. In contrast, solvent was found to play an important role in disrupting or facilitating H-bond formation.<sup>51</sup>

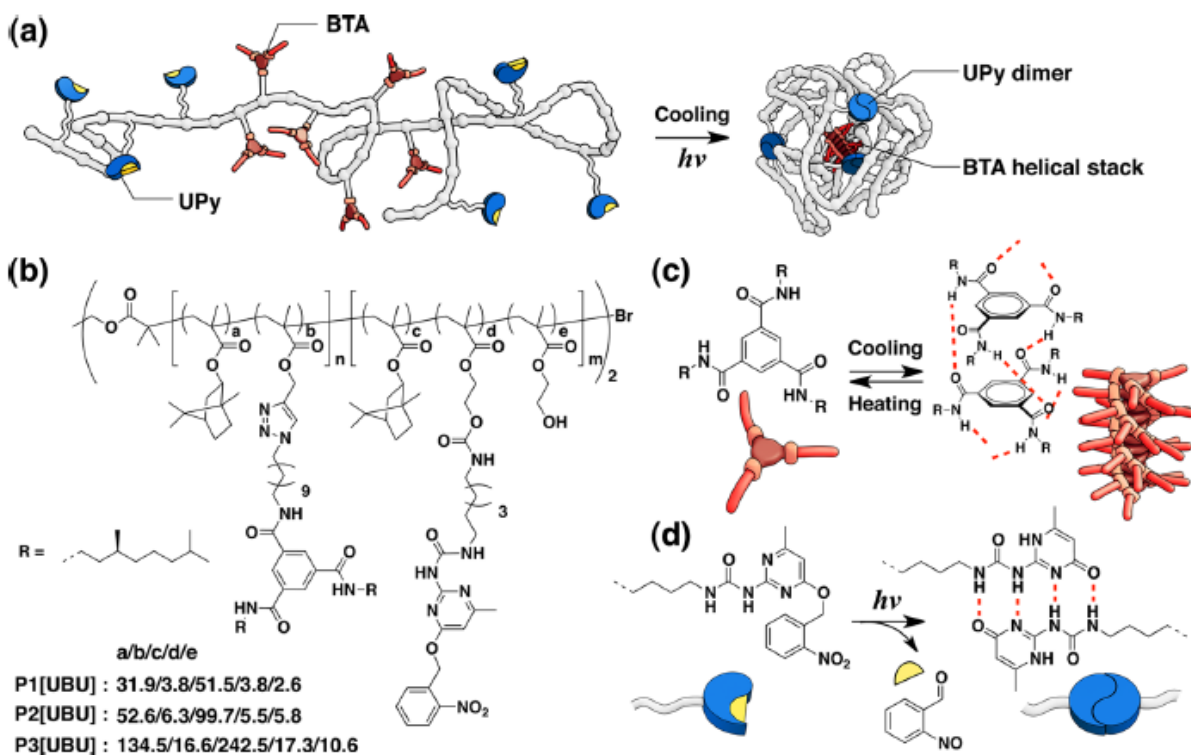
Supramolecular bonds				
Entry	Before cross-linking	Structure of cross-linking	Type of chemistry	Ref.
1			Benzene-1,3,5-tricarboxamide (BTA) hydrogen bonding	6,46,52 -54
2			2-ureido-4[1H]-pyrimidinone (UPy)	48,51

			hydrogen bonding	
3			Thymine, diaminopyridine hydrogen bonding	55,56
4			Hamilton wedge, cyanuric acid hydrogen bonding	55,57
5			Dendritic self-complementary hydrogen bonding	58

**Table 1.3** Illustrations of chemical transformations used as well as the structure of the supramolecular cross-links employed in SCNPs.

In another report, benzene-1,3,5-tricarboxamide (BTA) instead of UPy was used as H-bonding motif causing the single chain folding. This also generated a helical self-assembly along the copolymer

backbone *via* hydrogen bonding.<sup>59</sup> In one instance, a photoprotected BTA containing motif was used to prevent aggregation during polymer synthesis.<sup>54</sup> In more recent publications, this protection strategy was no longer necessary, BTA-based monomers being directly polymerized in a solvent capable of disrupting H-bonds.<sup>46,52,53,60,61</sup> Nevertheless, this group developed, in parallel, a polymer in which BTA units could be attached via azide-alkyne “click” chemistry.<sup>62</sup> In a joint effort to combine both different hydrogen bondings (*i.e.* helical and quadruple hydrogen bondings), Palmans, Meijer *et al.* combined UPy and BTA units in a block copolymer (**Scheme 1.6**).<sup>62</sup> In summary, a polymethacrylate precursor containing BTA and UPy motifs was readily synthesised using a post-functionalisation approach. The resulting copolymer was functionalized using the CuAAC and isocyanate conjugation reactions, affording the final precursor containing distinct self-assembling motifs in a single chain. Interestingly, the obtained linear precursor could thermally fold into SCNPs through intramolecular self-assembly of the BTAs to form internal columnar, helical stacks. Upy deprotection using UV light results in a further collapse of the polymers into more compact conformation *via* intramolecular UPy association. Well-defined SCNPs with orthogonally self-assembling domains mimicking an  $\alpha$ -helix and a  $\beta$ -sheet were herein successfully provided.

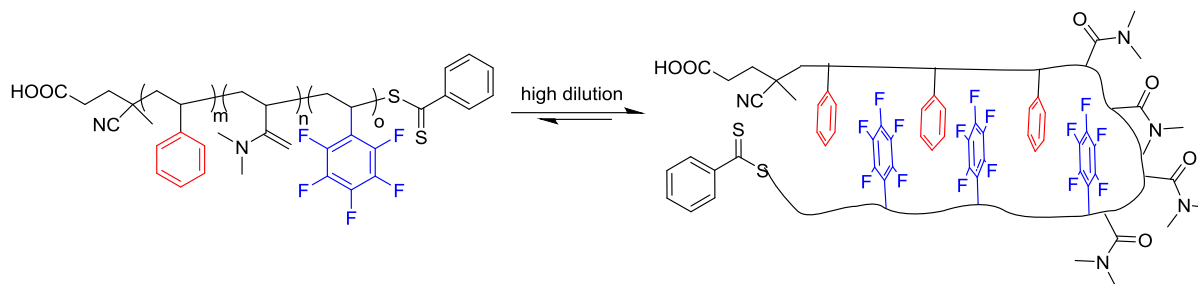


**Scheme 1.6** a) SCNPs formation based on a triblock copolymer bearing BTA and UPy motifs, b) chemical composition of the employed linear copolymeric precursor, c) helical BTA H-bonding driven self-assembly and d) photoinduced dimerization of UPys via quadrupole H-bonding.<sup>62</sup>

Another approach related to supramolecular chemistry and enabling for SCNP synthesis uses cucurbit[n]urils for host-guest complex formation (**Table 1.3; Entry 2**) The Scherman group developed ternary host-guest complex-based SCNPs using methyl viologen and naphthyl-functionalised polymers as building blocks., Important aggregation was however observed therefore studies were therefore conducted at very low concentrations *ca.* 0.1 mg/mL.<sup>63,64</sup>

Weck *et al.* synthesised a triblock copolymer containing styrene and pentafluorostyrene motifs (**Scheme 1.7**). The quadrupole interactions involving the electron-rich and electron-deficient blocks was studied under different concentrations in different solvents. Although SCNP formation was favoured at high dilution (*i.e.* 1 mg/mL), it was found that intramolecular SCNPs folding occurred in chloroform preferably

due to this arene-perfluoroarene quadrupole, whereas in DMF (*N,N*-dimethyl formamide) larger aggregates were observed due to intermolecular interactions (**Scheme 1.8**).<sup>65</sup>



**Scheme 1.7** Schematic representation of the SCNP folding of poly(styrene-*co*-pentafluorostyrene) block copolymer in solution.<sup>66</sup>

In another attempt to make compatible different supramolecular interactions upon the same SCNP structure, Barner-Kowollik *et al.* demonstrated that complex supramolecularly cross-linked SCNPs based on cyanuric acid-Hamilton wedge multiple hydrogen bonding and thymine and diaminopyridine triple hydrogen bonding interactions could be obtained and isolated (**Table 1.3; Entry 3**).<sup>55</sup> Interestingly, it was found that the single chain self/folding was dependent on concentration as well as temperature, with single chain self/folded structures dominating at low temperatures and high dilution regimes.

The effects of solvents and steric hindrance on the self-assembly of the complementary recognition units (*i.e.* thymine and diaminopyridine, (**Table 1.3; Entry 4**)) was studied by Barner-Kowollik *et al.*<sup>56</sup> They established that the sterically less demanding *t*-butyl acetyl group leads to a better assembly process. Moreover, they recognised dichloromethane as the preferred solvent over chloroform, as the nonspecific interactions between the cyanuric acid protons and the solvent were avoided.

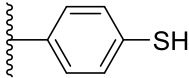

Another important contribution to supramolecular interactions-based SCNPs was brought by S. Kim *et al.* with the use of 2-((3,5-bis(4-carbamoyl-3-(trifluoromethyl)phenoxy)benzyloxy)carbonylamino)ethyl methacrylate units *aka* SHB (**Table 1.3; Entry 5**).<sup>58</sup> At low levels of SHB incorporation (> 1.5%), intermolecular interactions predominated in nonpolar solvents resulting in large-

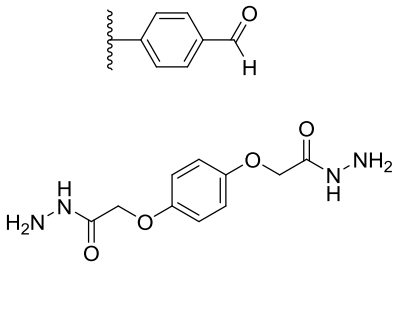
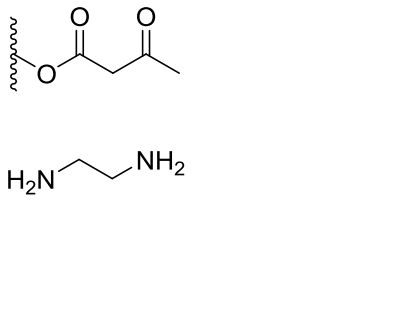
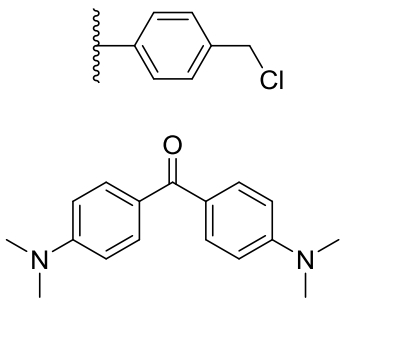
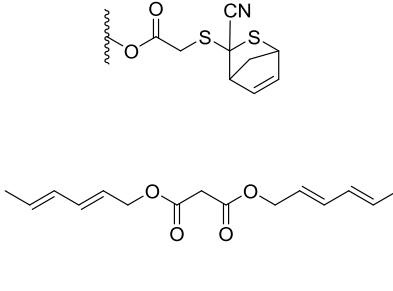
scale aggregation, while for high loading levels (*ca.* 6%), intramolecular hydrogen bonding was favored in toluene leading to the formation of well-defined and stable nanoparticles.

#### 1.1.2.1.4 Dynamic covalent chemistry

As summarised in **Table 4**, SCNP synthesis *via* dynamic covalent bonds proves versatile to achieve adaptable and responsive nanostructures. This indeed creates reversible bonds that can be kinetically cleaved or rearranged after applying a stimulus, such as temperature, pH or radiation.<sup>5</sup> Inspired by analogous occurring redox chemistry in biological systems,<sup>67</sup> the utilisation of disulfides has been an area of interest in the SCNP field.

Specifically, the group of Berda *et al.* developed the synthesis of anhydride functionalized linear polymer precursors, where intramolecular disulfide linkages were incorporated by addition of 4-aminophenyl disulfide, and could be further reversibly cleaved and reformed in dilute solution by treatment with dithiothreitol (reducing) and iron(III) (oxidative) agents, respectively (**Table 1.4; Entry 1**).<sup>67</sup>

Dynamic covalent				
Entry	Before cross-linking	Structure of cross-linking	Type of chemistry	Ref.
1			Disulfide formation	<sup>67</sup>

2		Hydrazon e	69
3		Enamine formation	68
4		Benzophe none	70
5		Diels- Alder	71,7 2

**Table 1.4** Illustrations of chemical transformations used as well as the structure of the dynamic covalent cross-links employed in SCNPs.

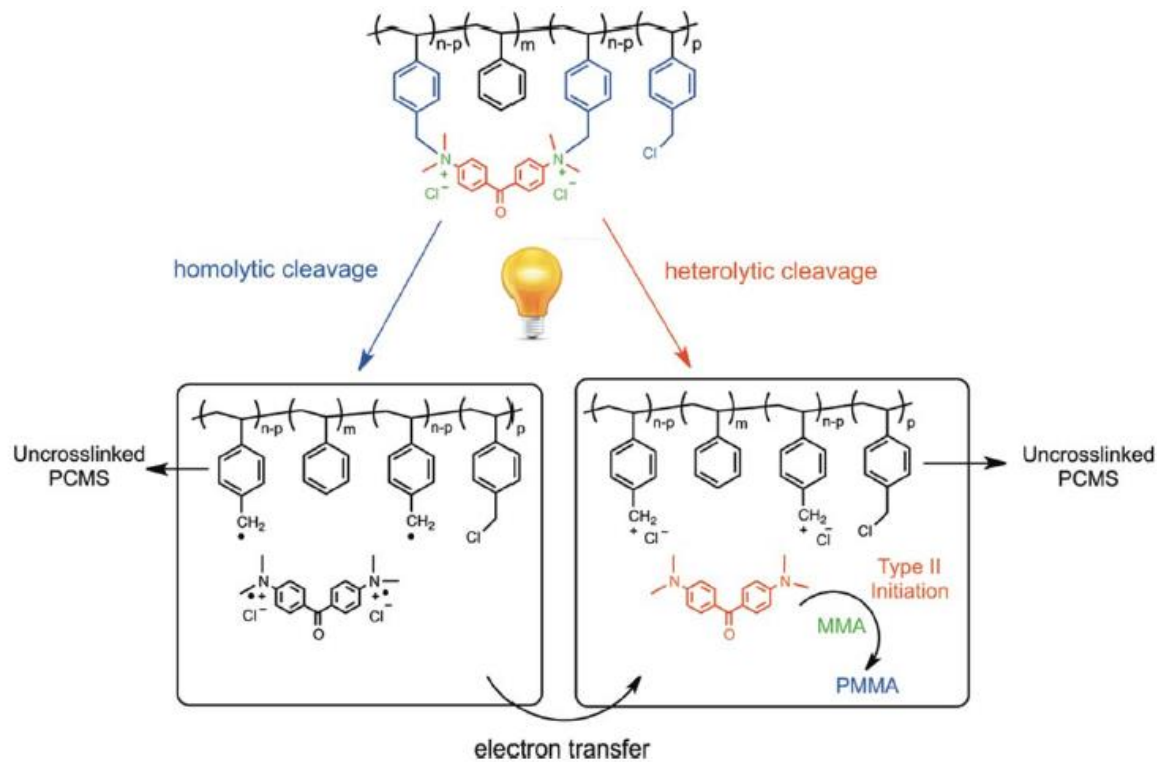
Important contribution to SCNP technology has been brought by the group of Fulton. For instance, acylhydrazone bonds were employed to synthesise SCNPs with a reversible character (**Table 1.4; Entry**



2). Namely, a bis(hydrazide) cross-linker was continuously added to an aldehyde-containing polystyrene in presence of catalytic amounts of trifluoroacetic acid (TFA). In order to isolate the resulting SCNPs, TFA was quenched with triethylamine and hence SCNPs would remain intact upon isolation. Interestingly, no collapse was observed at higher cross-linking densities. The dynamic behavior of the acylhydrazone bond was confirmed by triggering the exchange with a monohydrazide.<sup>69</sup> In a more recent publication by the same group, oligo(ethylene glycol) side chains were incorporated to a similar system, imparting response not only to pH variations, but also to temperature changes. In this manner, at low pH, related SCNPs remained stable in solution, whereas when the system was exposed to acid and heat, the nanoparticles precipitated followed by hydrogel formation. This process could be reversed by simple cooling down.<sup>32</sup>

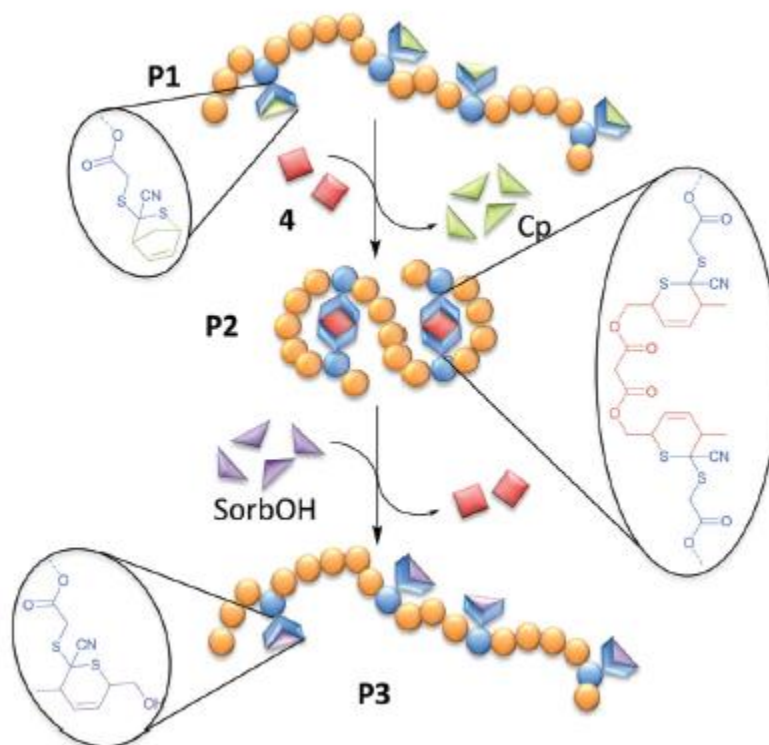
More recently, in a collaboration with the Pomposo group, Fulton *et al.* derived  $\beta$ -ketoester functionalized linear polymers and condensed these precursors with butylamine (**Table 1.4; Entry 3**). SCNPs were then achieved by an enamine exchange reaction with ethylene diamine under dilute conditions. The reversibility of the cross-links was evidenced upon addition of phosphoric acid, and crosslinks could be restored by adding ethylene diamine.<sup>68</sup>

In a contribution brought up by Temel *et al.*, a dynamically covalent photoactive SCNPs were presented. The linear parent precursor was tailored with chloromethyl styrene moieties. The subsequent addition of Michler's ketone by "Menschutkin click chemistry" led to charged SCNPs. Interestingly, the Michler's ketone parts of the nanoparticle proved reactive under photoexcitations to initiate the free-radical polymerization of MMA (**Scheme 1.8**) (**Table 1.4; Entry 4**)..<sup>70</sup>



**Scheme 1.8** Dynamic behaviour of PIL SCNPs by release of radicals after UV-induced homo/heterolytic cleavage for MMA polymerisation initiation.<sup>70</sup>

Dynamic covalent chemistry using Diels-Alder chemistry was harnessed by Kowollik *et al.* Briefly, hetero-Diels-Alder (HDA) chemistry based on cyanodithioester (CDTE), cyclopentadiene (Cp) and sorbic alcohol resulting in reversible chain folding was applied (**Scheme 1.9**) (**Table 1.4; Entry 5**). Cp-protected CDTE moieties were supported in a poly(methacrylate) backbone, and subsequent addition of sorbic derivate bi-linker. Interestingly, the folded structure could return to its linear version by simply adding sorbic alcohol exploiting the reversible nature of HAD chemistry.<sup>73</sup>



**Scheme 1.9** Overview of the dynamic covalent folding and unfolding of SCNPs using hetero-Diels-Alder (HDA) chemistry.<sup>73</sup>

### 1.1.3 Characterisation of Single Chain Polymer Nanoparticles:

#### Analytical Techniques

Corroborating the data provided by a variety of analytical techniques is necessary in order to verify the formation of SCNPs. Most commonly, this approach seeks to identify distinct differences between the linear polymer and the folded SCNPs following cross-linking, such as the disappearance of functional groups or changes in the polymer size/morphology. Probably one limitation is that sensitive techniques have to be used to establish absence of aggregates that can form during the synthesis/purification of SCNPs.<sup>5,74,75</sup>

Although standard polymer analysis techniques, for example, nuclear magnetic resonance (NMR) spectroscopy and size exclusion chromatography (SEC), are often used to analyze the prepared polymers,

much of the work consists on analysing the morphology, size and stability of the obtained particles, in comparison to the parent polymer. Common methods for particle analysis include light scattering techniques and microscopy. However, the combination of different techniques provides a larger and more accurate information of SCNPs in study.<sup>76</sup>

#### 1.1.3.1 Size Exclusion Chromatography (SEC)

SEC has been an invaluable tool for characterising folding processes and better understanding SCNPs. Although the extracted data is based on the hydrodynamic volume of both linear and folded polymers, the SEC measurements not only provide qualitative information, but can also provide quantitative information by applying sensitive detectors, such as MALLS (multi-angle laser light scattering) or a viscosimetric detector.<sup>74,76</sup> SEC analyses have evidenced that polymers will show an increase in retention time and a decrease in apparent molecular weight, following collapse.

As a representative example, Berda *et al.* reported a study where intrachain radical homopolymerisation between stilbene units in a styrenic backbone was performed under dilute conditions. Among different characterisation techniques, one piece of evidence that folding was effective was provided by SEC. As illustrated in **Fig. 1.3**, from the parent polymer to the SCNP, the retention time and molecular weight increased, while the radius decreased which is result of the coil-to-nanoparticle transition.<sup>77</sup>

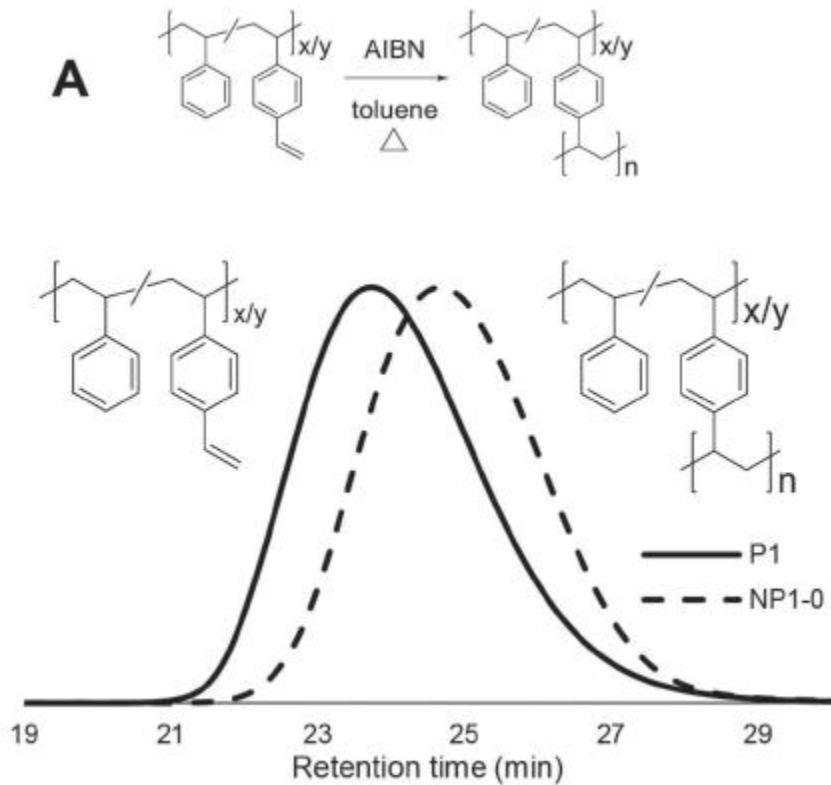


**Figure 1.3.** SEC UV detector traces obtained in THF at 40 °C for reaction of styrene functionalized P1 with AIBN to yield NP1-0.<sup>77</sup>

Additionally, a decrease in the dispersity ( $\mathcal{D}$ ) is often also observed *via* SEC when a folded SCNP is formed from a linear coil. This was studied in more details by Pomposo *et al.* who developed mathematical equations to relate the decrease in hydrodynamic radius to corresponding calibration standards.<sup>78</sup> Nevertheless, they put the attention on the high sensitivity of PDI (polydispersity index) values to the presence of high molecular weight tails arising from minor quantities of byproducts generated by intermolecular secondary reactions.

Related to the diverse nature of polymeric structures, the presence of charged groups, such as those found in polyelectrolytes, *e.g.* in PILs, can result in complications and unreliable characterisation data *via* SEC. Matyjaszewski *et al.* proposed a « universal method » to characterise imidazolium-type PILs, by inserting the non-coordinating anions such as TFSI, tetrafluoroborate ( $\text{BF}_4^-$ ) or hexafluorophosphate ( $\text{PF}_6^-$ ) and use

10 mM LiTFSI in THF as eluent.<sup>79</sup> This technique dramatically decreases the interaction between the PILs and the SEC stationary phase, providing a more accurate and more representative mass and dispersity values for the TFSI-modified PILs.<sup>20</sup>

### 1.1.3.2 Spectroscopic characterisation of SCNPs

Spectroscopic techniques offer convenient ways of characterising SCNPs. Each technique, in tandem with others, provides an elaborate picture of SCNPs features such as structure, morphology or size. NMR spectroscopy has also helped to probe various aspects of macromolecular composition, structure and dynamics.<sup>5-7,76,80</sup>

#### 1.1.3.2.1 NMR spectroscopy

Formation of cross-links can be detected by monitoring characteristic signals in NMR spectra, with the use of 1D <sup>1</sup>H NMR spectroscopy regarded as the quickest way of monitoring the conversion of the linear polymer to cross-linked SCNP.<sup>76</sup>

A clear example was reported by Berda *et al.* in a study where they implemented thermal Diels-Alder chemistry.<sup>72</sup> Random copolymers based on poly(methacrylate) bearing furfuryl and maleimide motifs were employed to achieve internal folding through a thermal Diels-Alder reaction. To prove the efficiency of this approach, <sup>1</sup>H NMR analysis of P1 (**Fig. 1.4** blue traces) and NP1 (**Fig. 1.4** red traces) was carried out to proof Diels Alder adduct formation following the decrease in intensity of key signals.

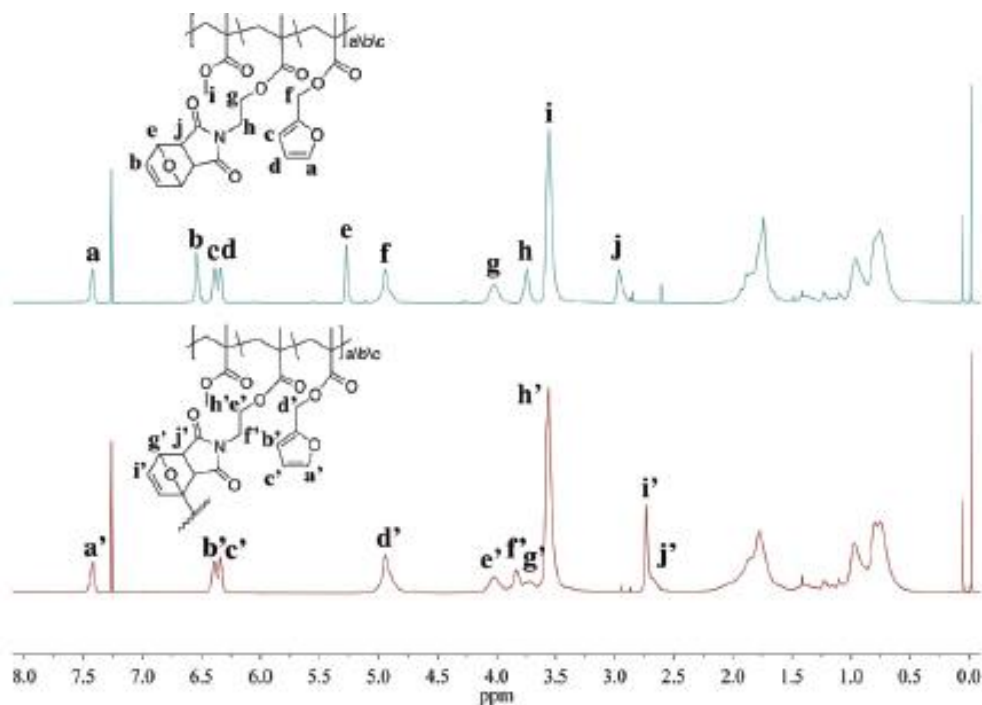


**Figure 1.4**  $^1\text{H}$  NMR overlay spectrum of polymer (P1) and nanoparticle (NP1) in  $\text{CDCl}_3$ .

Fluorine ( $^{19}\text{F}$ ), phosphorous ( $^{31}\text{P}$ ), boron ( $^{11}\text{B}$ ), nitrogen ( $^{15}\text{N}$ ) and carbon  $^{13}\text{C}$  are also very useful in NMR spectroscopy, being sensitive to any environment change induced by polymer folding.<sup>76</sup>

Equally, the use of 1D NMR spectroscopy experiments provides valuable insight for the incorporation of reactive monomer units and the formation of SCNPs. However, it does not provide much information regarding the particle conformation and structure. One common approach to overcome these limitations is by 1D NMR experiments at different temperatures, which can allow for better understanding of the dynamic effects of the polymer, such as ligand exchange.<sup>76</sup> Alternatively, 2D NMR-spectroscopy has emerged as a key tool for probing how SCNPs collapse,<sup>5</sup> techniques such as diffusion-ordered spectroscopy (DOSY) can provide information about  $M_w$  or particle diameter, by using equations based on the polymer/particle diffusion coefficients.<sup>81,82</sup> When applied to SCNPs, the intramolecular collapse of the linear polymer chain leads to an increase in the diffusion coefficient, a complementary evidence of the formation of collapsed SCNPs.<sup>20,83</sup>

As a supplementary evidence of the conformational change from coil linear polymers to intramolecular collapsed NPs, Loinaz *et al.* employed DOSY experiments (**Fig. 1.5**).<sup>18</sup> This enabled to determine the diffusion coefficient of a polymer in solution, a parameter that is reversely proportional to the hydrodynamic volume, hence intramolecular collapse should lead to an increase of the diffusion coefficient, evidencing SCNP formation. For instance, the values of  $D$  for the linear precursor and corresponding SCNP were -8.56 and -8.30, respectively, confirming the reduction of the hydrodynamic radius after collapse, even if in that particular case the amount of cross-linking was only of 3%.

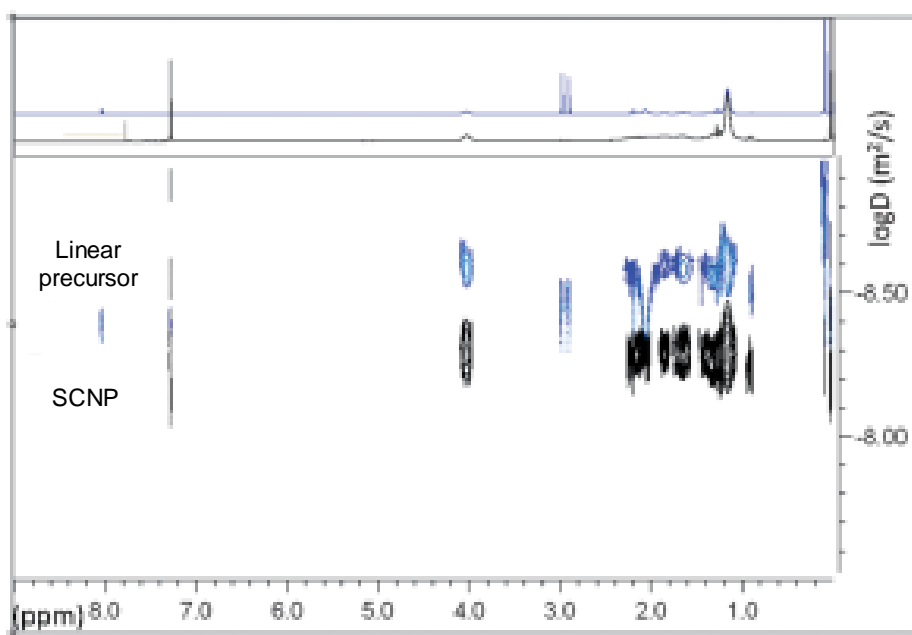


**Figure 1.5** DOSY spectra of linear precursor and corresponding SCNP CD<sub>2</sub>Cl<sub>2</sub>.<sup>18</sup>

#### 1.1.3.2.2 IR, UV-VIS, CD and Fluorescence Spectroscopy

Other spectroscopic techniques, such as infrared (IR), ultraviolet-visible (UV-VIS), fluorescence and circular dichroism (CD) also prove valuable to get an insight into the structure of SCNPs. These methods are typically used in tandem with other techniques to rationalise the characterisation of SCNPs.<sup>76</sup>



IR spectroscopy has been key to characterise the formation of SCNPs following the disappearance or appearance of particular signals depending on the system. As an example, Wang *et al.* resorted to IR spectroscopy to monitor the disappearance of the azide ( $2127\text{ cm}^{-1}$ ) and formation of the C-N ( $1200\text{--}1450\text{ cm}^{-1}$ ) bounds after reacting upon heating. As observed, a new signal corresponding the stretching vibration of groups of C-N appeared at  $1200\text{ cm}^{-1}$ .<sup>84</sup> (**Fig. 1.6**)

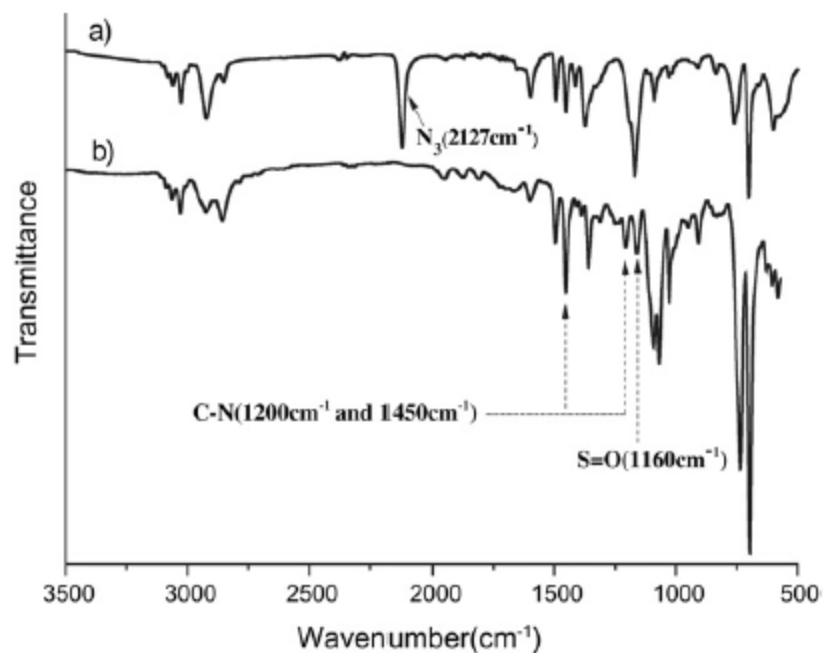


**Figure 1.6.** FTIR spectra of a) linear polymeric precursor and b) corresponding SCNPs.<sup>84</sup>

In a recent study conducted by Kowollik *et al.* a versatile process for the preparation of fluorescent SCNPs *via* two tetrazole chemistry-based mechanism in pure water was introduced.<sup>85</sup> In a polyacrylate-based backbone, tetrazole, alkene and tetraethylene glycol monomethyl ether moieties were incorporated. SCNPs formation was triggered by UV-light and carefully confirmed by various means, among which UV-vis spectroscopy. Namely, as displayed in **Fig. 1.7**, the obtained characteristic pyrazoline absorption band at 415 nm demonstrated that the cross-linking was successfully driven for SCNPs1. On the other hand, SCNPs2 presented a less intense and blue-shifted band corresponding to the carboxylic acid ligation. In

this manner, it was proven SCNPs could present different fluorescence by simply modulating the starting copolymer composition.

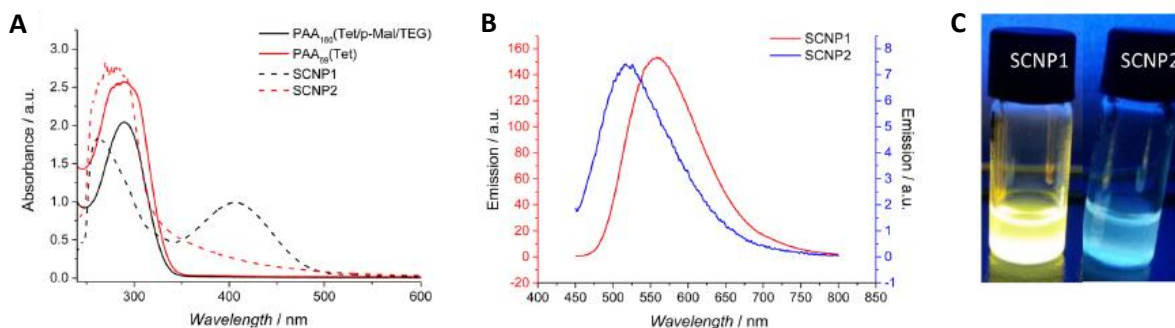


**Figure 1.7** (A) UV-vis absorbance of the polymer precursors (smooth lines) and the corresponding SCNPs (dashed lines), (B) Emission spectra of the formed SCNPs and (C) photograph of a solution of SCNPs under a hand-held UV-lamp ( $\lambda = 366 \text{ nm}$ ).<sup>85</sup>

Meijer *et al.* designed a triblock copolymer with orthogonally self-assembling motifs, BTA and UPy helped to be folded into a SCNP structure.<sup>62</sup> Different SCNPs compositions were studied, where the optically active components were varied, and their behavior upon UV-irradiation in water was studied at 20 °C. CD spectra at 20 °C before and after irradiation were identical (**Fig. 1.8**), confirming that UPy dimer formation did not interfere with BTA self-assembly. This piece of characterisation revealed the enhanced robustness of SCNPs against UV-irradiation on time-scale.

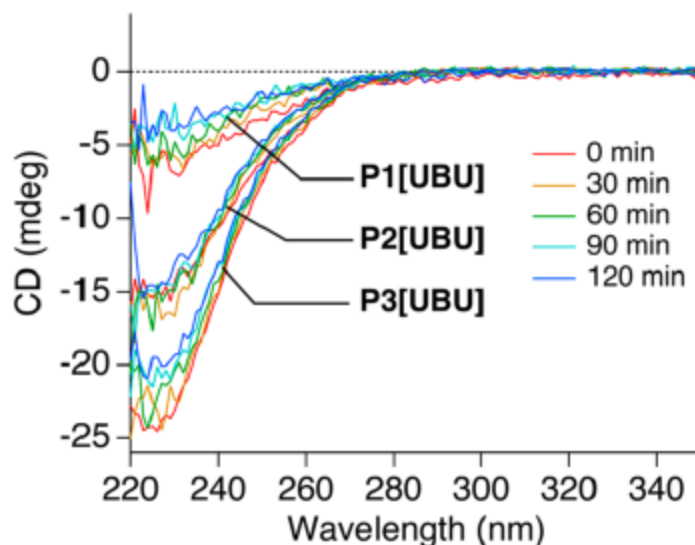


**Figure 1.8** CD spectra of different particles (P1, P2 and P3) at 20 °C during 120 min of 350 nm UV irradiation.<sup>62</sup>

### 1.1.3.3 Characterisation of Single Chain Nanoparticles morphology

One challenging aspect for characterising SCNP is to accurately establish their morphology, which is dependent on the preparation and analysis conditions. The expected spherical morphology of SCNP is not always consistent with experimental findings. This could be due to variability in the morphology itself, which has been found to have a strong dependence on the solvent used, concentration, temperature or pH. Microscopy and scattering techniques have typically been used to determine the size and shape of folded SCNPs.

#### 1.1.3.3.1 Morphological characterisation *via* TEM

With soft SCNPs, contrasting agents, such as ruthenium oxides or uranyl acetate, are applied for TEM to increase the contrast between particles and the surface of the TEM grid. This provides an accurate visual representation of particle size and morphological structure (*e.g.* spherical particles).<sup>5</sup> TEM size measurements are commonly compared with those obtained from light scattering experiments. Although,

the obtained size values remain relatively close, some differences are usually observed, due to differences between the solid and in-solution state of the SCNPs.<sup>61,86</sup>

In a recent example, Zimmerman *et al.* compared sizes obtained in TEM with those observed by DLS for the same SCNPs, *ca.* 8-10 nm and 5.8 nm, respectively (see **Fig. 1.9**). The authors suggested that the polymeric nanoparticles could be flattened when absorbed on the grid surface and that ammonium molybdate negative staining could further increase the diameter.<sup>87</sup>

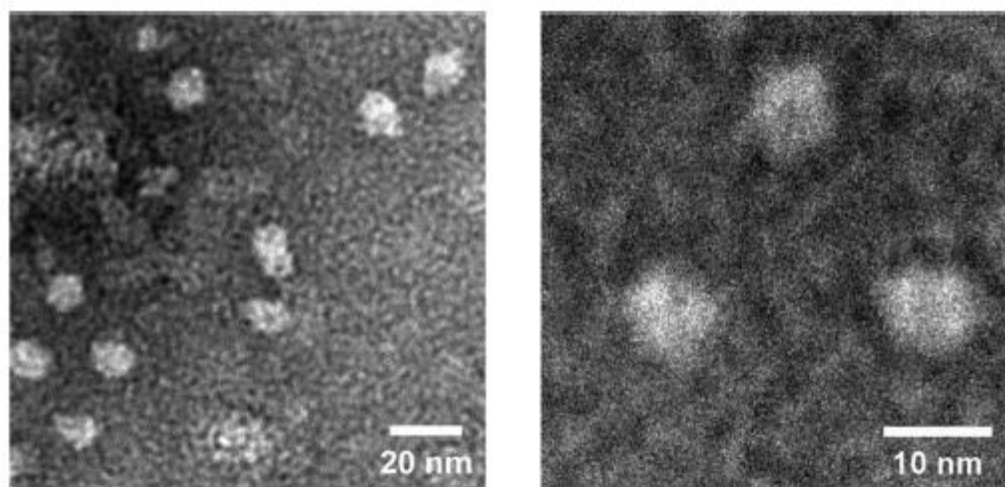


**Figure 1.9.** TEM images of SCNPs at different zooms stained with ammonium molybdate.<sup>87</sup>

Concerning polyelectrolytes, and as mentioned in the section about NMR spectroscopy, their charged nature can cause the retention of solvent among the charges when casting for sample preparation for TEM analysis. This effect can lead to an increase in size, due to the « swollen-state » of SCNPs or possible appearance of aggregated domains in the TEM images.<sup>20,38,83</sup>

#### 1.1.3.3.2 Morphological characterisation *via* AFM

Atomic force microscopy (AFM) is a key technique for the characterisation of SCNPs, as it can provide 3D soft particle images on the nanometer scale. One difference when compared to TEM is that AFM does

not (necessarily) require the addition of contrast agents. Based on the interaction between a scanning cantilever with the particles on a mica or highly oriented pyrolytic graphite (HOPG) surface, AFM enables the observation of either individual SCNPs or their aggregates. The observed SCNPs size has been found to be highly dependent on molecular weight and degree of cross-linking,<sup>49</sup> but also on the concentration used for sample preparation.<sup>50</sup>

Meijer *et al.* used AFM to illustrate a two-step folding process of supramolecularly cross-linked SCNPs.<sup>62</sup> The first folding step involved BTA moieties that self-assembled by decreasing the temperature while the second step involved dimerization of UPy moieties upon UV-irradiation. In this manner, a sample was prepared with the partially folded SCNPs involving BTA interactions by cooling down (**Fig 1.10 A**) and the same sample was irradiated with UV-light to entail UPy dimerisation (**Fig. 1.10 B**). AFM images clearly depict the chain collapse and image the “fully folded” SCNPs. In addition to that, the AFM measurements provided real snapshots of the compartmentalised SCNPs before and after UV irradiation.

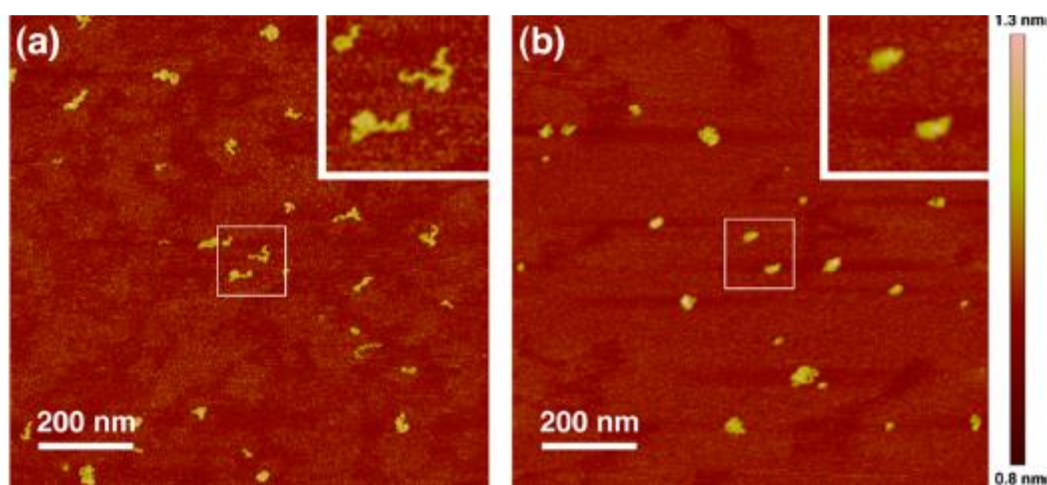


**Figure 1.10** AFM height imaged of SCNPs capture of two-steps of the molecular folding process (**A**) before and (**B**) after UV irradiation. The top right insets show magnifications of the framed areas. <sup>62</sup>

#### 1.1.3.3.3 Morphological characterisation *via* scattering (DLS, SAXS, SANS)

The hydrodynamic diameter of SCNPs is obtained by analysing a sample solution illuminated by a single-wavelength laser. Variations of the Brownian motion detected at a given scattering angle can then be used to extract information about particle size.<sup>76</sup> In DLS measurements, SCNPs are analyzed in solution. SCNP diameter can then be compared with that of the linear parent polymer,<sup>41</sup> or the influence of the SCNPs under different conditions, such as pH<sup>55</sup> or temperature, can be studied.<sup>83</sup> DLS also enables to monitor the folding of the particle over time.<sup>88</sup>

An example was reported by Kowollik *et al.* A dual-gated orthogonal SCNP unfolding system based on benzo-21-crown-7 (B21C7)/secondary ammonium salt (AS) host-guest system was explored in presence of different solvents or salts. DLS analysis revealed the compaction of the unfolded P6 into a more compact structure (P6 folded) in DCM/acetonitrile (9/1 v/v) after folding (**Fig 1.11 A**). Then, a similar particle composition (P16) was studied under different conditions. Namely, when 20  $\mu$ L was added to a solution of SCNPs (P16),  $D_h$  (hydrodynamic diameter) increased by almost 2 nm. When KPF<sub>6</sub> was added,  $D_h$  increased again by almost 2 nm (**Fig. 1.11 B**). Interestingly, inverting the order of the added triggers lead to a similar increase in  $D_h$  based on DLS. This was believed to occur due to the disruption of interactions that kept cross-linked the SCNPs and therefore the addition of different triggers entailed the orthogonal stepwise unfolding.

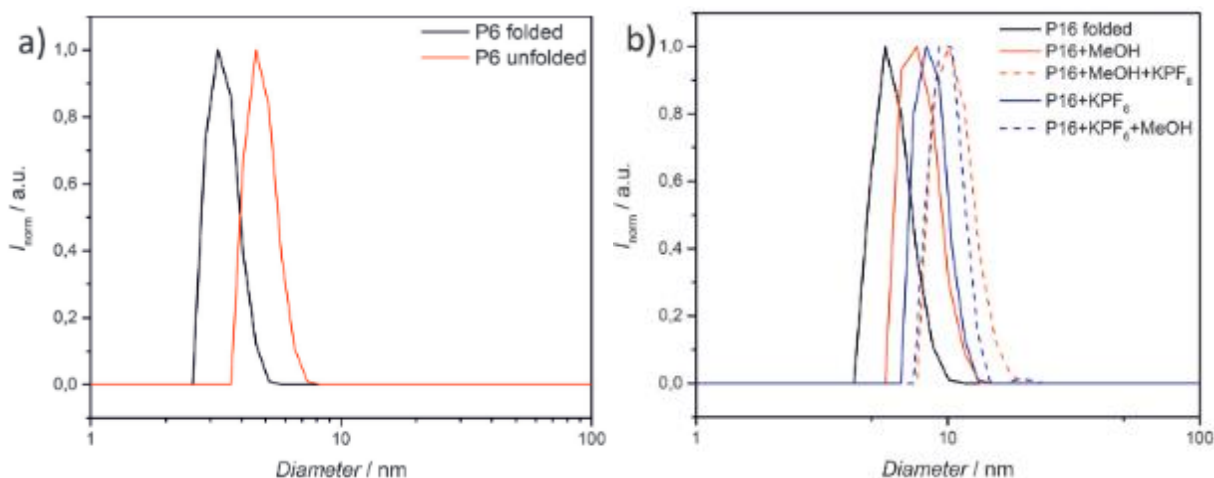


**Figure 1.11** (A) Dynamic light scattering (DLS) data (number distributions) for the folded and unfolded polymer (P6). (B) DLS data for the folded and unfolded polymer P16 in presence of different solvents/salts. X-ray scattering is being increasingly used to track the conformational changes from linear polymer precursors to folded SCNPs based on the change in their diameter. By using this technique, size and morphological aspects can be determined for SCNPs in solution, but with smaller wavelengths used in small-angle X-ray scattering (SAXS) and small-angle neutron scattering (SANS). By SAXS, the hydrodynamic diameter of SCNPs can be obtained in solution by suitable data treatment, by extracting the background solvent and correlating morphologies to theoretical models such as compact, hollow or cylindrical particles.<sup>62,83</sup>

Pomposo *et al.* had performed SAXS measurements to determine the form factor  $w(q)$  of distinct SCNPs obtained by two different synthetic protocols (*i.e.* protocol I and protocol II).<sup>89</sup> This form factor allows calculating the Flory exponent ( $\nu$ ) for a given SCNP in a good solvent (THF in this case). This information provides direct values of degree of chain compaction. Thus, the value obtained of  $\nu = 0.52$  for SCNPs following protocol I only presents a modest degree of chain compaction. But instead, SCNPs obtained by protocol II afford a  $\nu = 0.48$  revealing a sparse morphology (**Fig. 1.12 A**). The obtained values were in good agreement with those obtained from molecular dynamics (MD) simulations in which SCNP synthesis by protocols I and II were simulated (**Fig. 1.12 B**). It is worth noting that, though both protocols

I and II produced sparse SCNPs ( $\nu = 0.5$ ), SCNPs obtained from protocol II were more compact at local sites, as evidenced by the sharper decay of  $w(q)$  after the fractal regime.

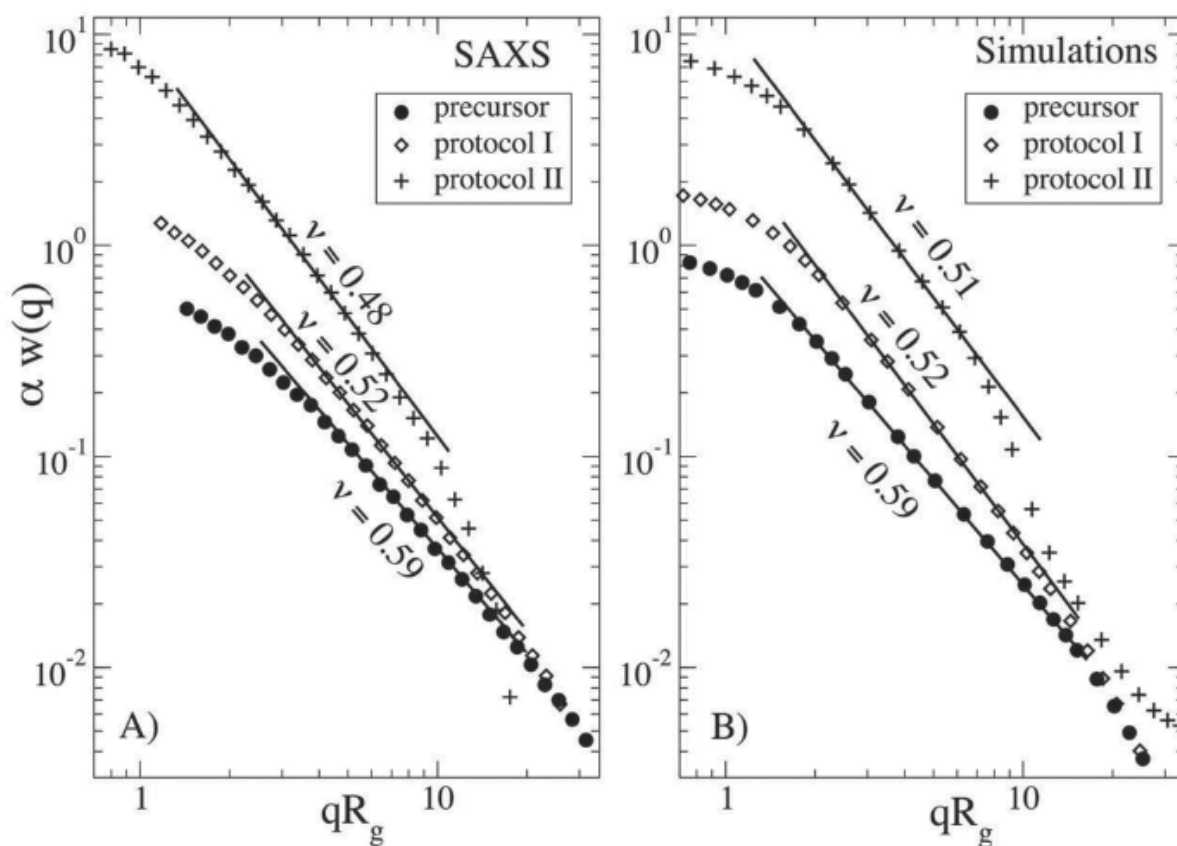


**Figure 1.12** (A) Form factor from SAXS of precursor (circles) , SCNPs following protocol I (diamonds) and II (crosses) in THF. (B) Form factor from MD simulations of the precursor (circles) and the SCNPs synthesised through protocol I (diamonds) and II (crosses).

Conversely, SANS experiments have been used to probe the relationship between the form factor and the concentration for a non-deuterated SCNP system contrasted by a deuterated solvent, allowing for a detailed study of the SCNP morphology.<sup>89,90</sup>

Colmenero *et al.* investigated conformational properties of SCNPs in crowded macromolecular solutions by SANS and MD simulations.<sup>90</sup> Crowding was induced by two means, namely, by adding either linear polymer chains or SCNPs. SCNPs were found to collapse when the total concentration of a diluted SCNPs



solution reaches the value of the overlapping concentration of the pure SCNP solution (23 mg/mL), irrespective of the length of the crowders. Moreover, the analysis of the scaling behavior of the different simulation observables confirmed the trends suggested by the experimental form factors, and suggested that crumpled globular conformations were adopted by SCNPs in crowded macromolecules solutions. Both experimentally obtained conclusions were in agreement with MD simulation outcomes, despite complications arising from the presence of aggregates.

#### 1.1.4 Applications

Due to their size ranging from 5 to 30 nm, the field of SCNPs is part of nanotechnologies, at the interface between polymer and material science, biology, physics and chemistry.<sup>91</sup> The folding of linear polymeric precursors into SCNPs is reminiscent of the folding of proteins in nature. Inspired by this phenomenon, the long-term goal of applications using SCNPs is to construct small soft nano-objects endowed with useful, autonomous and specific functions.<sup>92</sup> Their preparation is expected to affect their subsequent activity and selectivity in important applications, including sensing, drug-delivery or catalysis (**Fig.1.13**). Although promising, SCNPs applicability and viability requires overcoming the synthetic bottleneck of scaling up the synthetic procedures (usually involving highly dilute solutions), for high value-added applications.<sup>93</sup>

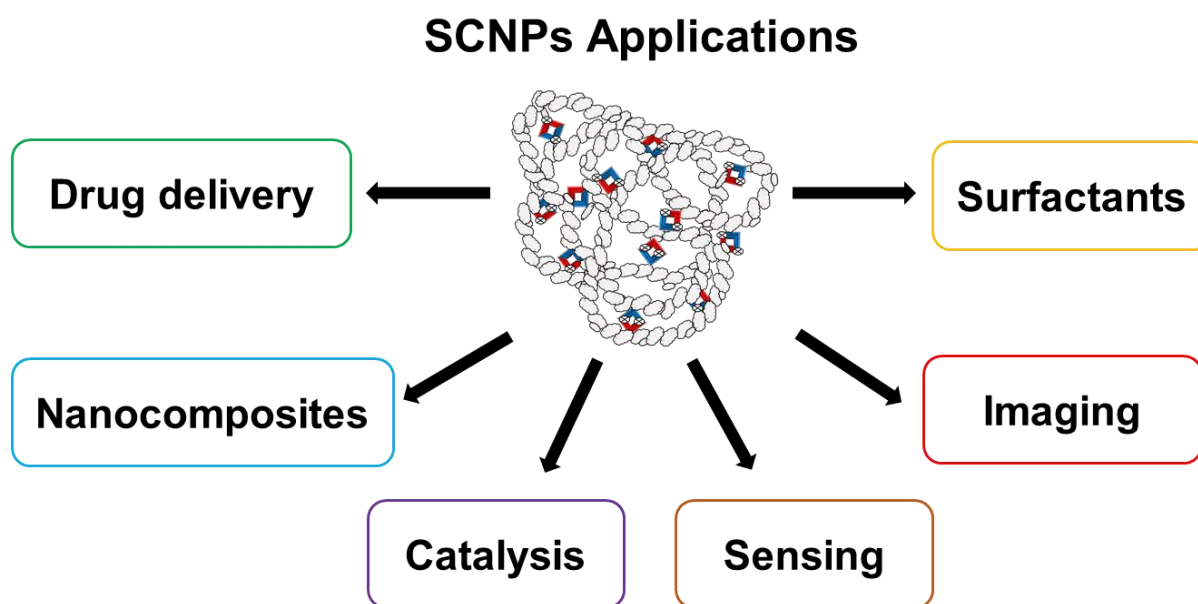


**Figure 1.13** Potential applications of SCNPs.

### 1.1.4.1 Nanomedicine

A promising field where SCNPs could be of practical use is the design and engineering of nano-systems to address disease and human health, for instance, for diagnosis, monitoring of pathological processes, biological systems and therapy.<sup>94</sup>

#### 1.1.4.1 Drug delivery and imaging

Drug delivery is a widespread discipline searching for the optimisation of efficient drug carriers. In this light, several examples have sought to use SCNPs based on a number of macromolecular structures, as controlled drug delivery nanocarriers.<sup>94</sup> Specifically, SCNPs have been used as nanocarriers for small-molecule drugs, *e.g.* vitamins, sacharides, peptides or chiral-amino acids.<sup>91</sup>

Paulusse *et al.* recently reported an innovative study where they intended to replicate naturally occurring glycoconjugates for both efficient targeting and increased cellular uptake of glycoconjugated polymers.<sup>95</sup>

In this work, linear and cyclic glucose moieties were tuned with methacrylates *via* enzymatic synthesis

and further used as building blocks to cross-linked single chain glycopolymer nanoparticles (glyco-SCNPs). C1- and C6-glucose-derived monomers were incorporated in different SCNP structures that were further studied for HeLa cells uptake. SCNPs with glucose moieties conjugated through the C1 and the C6 position in their pyranose and in their partly linear form were compared in terms of the HeLa cellular uptake efficiency by confocal microscopy. The effect of a reducing glucose was less determining in comparison to the position of the conjugations for an efficient cellular uptake.

Two other synthetic routes to SCNPs were reported by the same group, in both organic and aqueous environments (**Fig. 1.14 A**).<sup>96</sup> Importantly, the antibiotic rifampicin (Rif) was encapsulated in an organic medium, and the loaded nanocarriers were rendered water soluble and proceeded to the controlled release of rifampicin, which was tracked by UV-vis spectroscopy. As depicted in **Fig. 1.14 B**, a burst release of Rif was observed in the first 2 h (*ca.* 40%) and more than 60% after 24 h of the original Rif content.

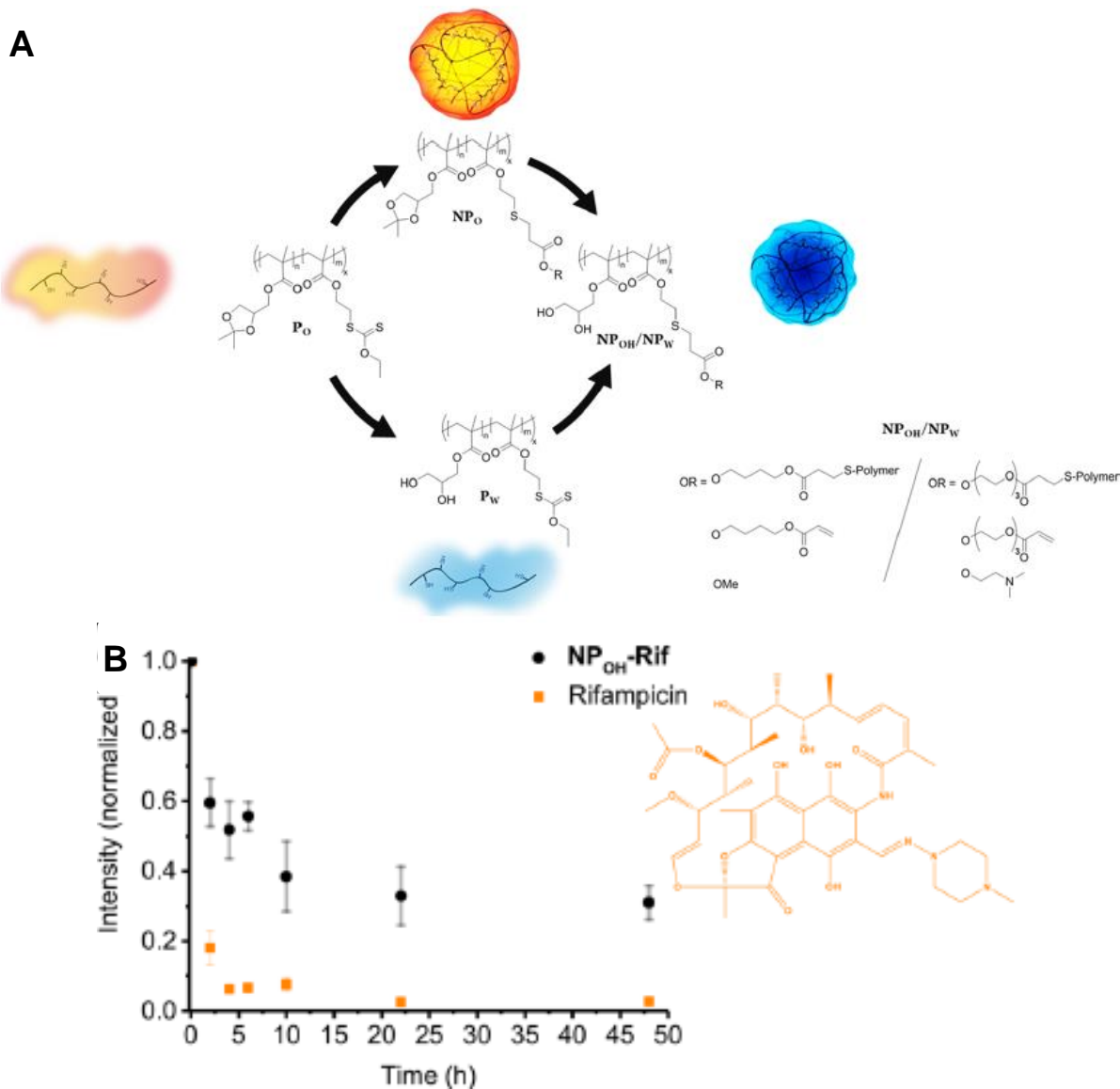


**Figure 1.14** (A) Dual-pathway synthetic of SCNPs *via* Thiol-Michael addition following the organic route (yellow) and aqueous route (blue). (B) Release of Rif from SCNPs by measuring UV-vis absorption at 334 nm.<sup>96</sup>

SCNPs have also been used to increase detection of internal structures within the body using a number of techniques, which can be summarised as follows. Soft-nanodevices have been evaluated as fluorescent probes for confocal laser scanning microscopy (CLSM),<sup>97-99</sup> gamma-emitters for single photon emission computerised tomography (SPECT)<sup>100</sup> or the more commonly used image contrast agents for magnetic resonance imaging (MRI).<sup>42,101</sup>

In an investigation by Odriozola *et al.* a two-step Gd(III) loading procedure based on CuAAC chemistry was presented (**Fig. 1.15 A**).<sup>42</sup> The cross-linked SCNPs possessed Gd(III) ion that is paramagnetic and showing a high relaxivity. However, as these species are not water soluble, they require to be entailed in a hydrophilic macromolecular structure. When the Gd-SCNPs were compared to the commercially used Magnevist® (**Fig. 1.15 B**), the  $r_1$  value of  $6.78 \text{ mM}^{-1} \text{ s}^{-1}$  obtained for the Gd-SCNPs represented already more than a 4-fold increase over its monometallic counterpart on a per Gd basis, and a 2-fold excess over Magnevist®. In addition, the molecular relaxivity for Gd-SCNPs was  $122 \text{ mM}^{-1} \text{ s}^{-1}$ , representing a 38-fold increase over the molecular relaxivity of Magnevist.

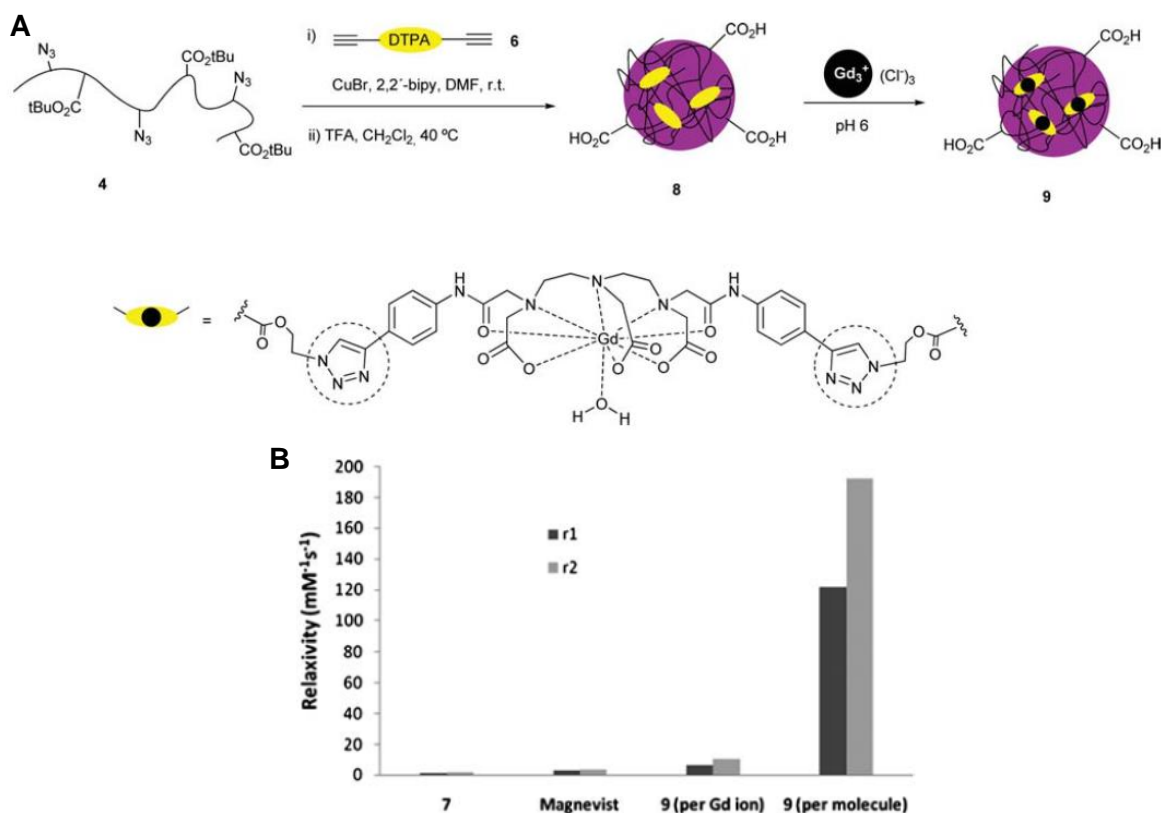


**Figure 1.15** (A) Formation of SCNPs and loading with Gd(III) following a two-step route for their incorporation using CuAAC-based chemistry. (B) Relaxivity values for Gd-SCNPs compared to commercially available reference Magnevist®.

#### 1.1.4.2 Nanoreactors for catalysis

SCNPs also represent versatile platforms as catalytically active nano-objects based on enzyme mimicry. The particular features that SCNPs show compared to other catalytic structures include: large surface-to-volume ratio, the formation of sparse or globular conformations containing localised pockets, size and solubility tunability based on solvent change and the dynamic bonding behaviour of SCNPs.<sup>36,92</sup> Moreover, these nanoreactors could show enhanced catalytic efficiency, due to confinement effects, by increasing the conversion rates or selectivity, or simply affording a polymeric and hence recyclable support.<sup>102–105</sup>

Catalysis mediated by SCNPs as nanoreactors has been classified by the type of enzyme mimicks, *i.e.* reductase, oxidase, aldolase, polymerase or metalloenzyme,<sup>37</sup> by the type of process catalyzed, *i.e.* organic molecular, macromolecular, nanomaterials<sup>92</sup> or by referring to metallo-enzyme mimicry.<sup>36</sup> One can also discriminate different types of catalysts, *i.e.* whether they are organic, organometallic or biological in nature.

##### 1.1.4.2.1 Organocatalysts

Organocatalysis refers to an organic (macro)molecule that does not contain a metal in which substoichiometric amounts accelerates a reaction. However, there are a number of challenges associated with supporting organocatalysts in SCNPs, such as their accessibility within the confined domains, but also the solubility of the catalyst in an aqueous environment. Hydrophilic polymeric stabilisers, *e.g.* polyethyleneglycol (PEG), are generally incorporated within the SCNPs structure to impart a water solubility.<sup>106</sup> It has to be acknowledged that SCNPs, as nanoreactors, are also widely used in organic solvent media. In fact, several studies have used either aqueous, organic or a mixture of both environments for organocatalysis mediated by SCNPs, as summarised in **Table 1.5**.

Entry	Reaction type	Catalytic center	Solvent	t (h)	T(°C)	C(%)	Reference
1	Carbonate hydrolysis	Diphenyl phosphate	H <sub>2</sub> O/MeCN	10	-	-	107
2	Aldol reaction	L-proline	H <sub>2</sub> O	24	r.t.	99	52
3	Benzoin condensation	NHC	THF	24	80	90	20,83
4	Polymerisation of (meth)acrylates	Michler's ketone	THF	2	r.t.	15	70
5	Reduction of $\alpha$ -diketones	B(C <sub>6</sub> F <sub>5</sub> ) <sub>3</sub>	CH <sub>2</sub> Cl <sub>2</sub>	0.1	r.t.	96	109
6	Polymerisation of THF	B(C <sub>6</sub> F <sub>5</sub> ) <sub>3</sub>	CH <sub>2</sub> Cl <sub>2</sub>	0.1	r.t.	99	109

**Table 1.5** Summary of reactions catalysed by SCNPs as organocatalysts.

The first attempt to mimic catalytic active sites of enzymes using SCNPs was carried out by Wull *et al.*<sup>107</sup> Catalytic sites were incorporated following an “imprinted particle” approach, *i.e.* catalytic entities were imprinted during the synthesis of SCNPs *via* a diphenyl phosphate template and subsequently removed from particles. These SCNPs were subsequently used as nanoreactors for carbonate hydrolysis presenting Michaelis-Menten kinetics (**Table 1.5; Entry 1**). The “imprinted particle” route was further

adopted by Nikang *et al.* to prove the enhanced enantioselectivity and binding capacity against chiral amino acid derivatives of imprinted SCNPs, when compared to analogous micelles.<sup>110</sup>

Chirality was harnessed by Meijer *et al.* who developed an approach producing water-soluble organocatalytic SCNPs containing L-proline catalytic centers in the hydrophobic internal pocket (**Fig. 1.16**) (**Table 1.5; Entry 2**).<sup>60</sup>

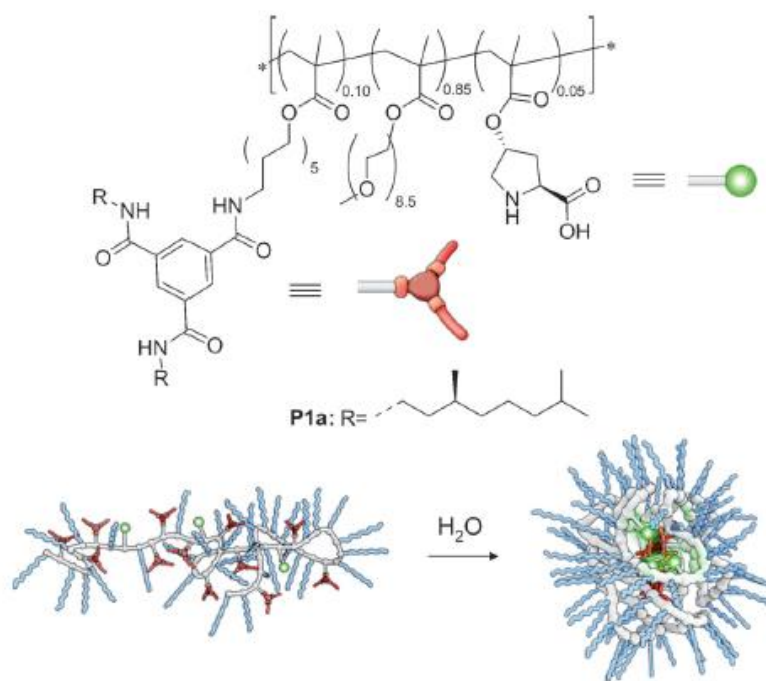


**Figure 1.16** Chemical structure of L-proline functionalised catalytic polymer and schematic representation of the unfolded polymer and the formation of the compartmentalised catalytic structure in water.

These organocatalytic SCNPs served as self-supported catalysts for the aldol reaction of cyclohexanone and p-nitrobenzaldehyde in water, allowing to achieve almost quantitative conversions (99%) and fast rates (TOF of 8 h<sup>-1</sup>), with an enantiomeric excess of 94% and an ee% (enantiomeric excess) of 70%. Conversely, when L-proline decorated BTA moieties were incorporated to a BTA-based SCNPs *via* molecular recognition, a higher stereoselectivity was observed.<sup>111</sup> Further research from the same group revealed that structural and surface hydration features were relatively similar to those found in natural



enzymes, and revealed that retarded surface water diffusivity had a critical impact in SCNPs catalytic activity.

A similar approach was followed by Taton *et al.* for the development of catalytically active SCNPs possessing “hydrophobic cavities” based on NHCs.<sup>20</sup> For this purpose, a statistical copolymer based on styrene, PEG-pendant styrene and antagonist benzimidazole- and chlorobenzyl-based units was synthesised as SCNPs precursor. The intramolecular cross-linking was achieved by quaternization and followed by an anion exchange to afford thermally latent behavior to the entailed “masked-NHC” units. In this manner, active compartmentalised NHCs within SCNPs were generated upon heating (80 °C) in THF thanks to the ability of acetate anions to interact with protons in C<sub>2</sub>-position of benzimidazolium rings. Catalytically active NHC-based SCNPs (10 mol%) were tested for the benzoin condensation obtaining 65% after 24 h (**Table 1.5; Entry 3**).

SCNPs have been used as bioinspired nanoreactors for the synthesis of several polymers. Temel *et al.* used the SCNPs described in **Section 1.2.1.1.5**, which contained Michler’s ketones as cross-linkers that could act as a photoinitiators for MMA polymerisation (**Table 1.5; Entry 4**).<sup>70</sup> Despite the lack of control in the free radical triggered polymerisations ( $\bar{D} = 3.1$ ), PMMA with molecular weights up to 38 kDa were obtained.

To this regard, in a pionnering work by Perez-Baena *et al.*, SCNPs were endowed with enzyme-mimetic activity following a concurrent binding/folding technique (**Fig. 1.17**). Namely, a selection of appropriate polymer precursors allowed concurrent catalyst-assisted intramolecular cross-linking and binding of the catalyst to intramolecular SCNPs sites. Enzyme-mimetic SCNPs were for instance generated from glycidyl-type polymers *via* B(C<sub>6</sub>F<sub>5</sub>)<sub>3</sub>-assisted intramolecular ring-opening polymerization, and B(C<sub>6</sub>F<sub>5</sub>)<sub>3</sub> binding to oxygen-containing functional groups (carbonyl, ether) of the SCNPs through B-O interactions. The catalytic activity resulted from the immobilization of the catalyst used to promote the folding/collapse

in compartmentalized internal nanoparticle sites that were accessible to reagents. Parameters such as size, composition, number and placement of catalytic sites, were found to have an important impact on the reaction kinetics. Namely, these SCNPs organocatalysed the ring-opening polymerization of THF thanks to the presence of small amounts of glycidyl phenyl ether (GPE) (**Table 1.5; Entry 4**). Relatively high molecular weight (55 to 150 kDa) and relatively high dispersities ( $D = 2.2$  to  $3.2$ ) poly(THF-*co*-GPE) with low content of GPE (*ca.* 3%) were thus achieved.

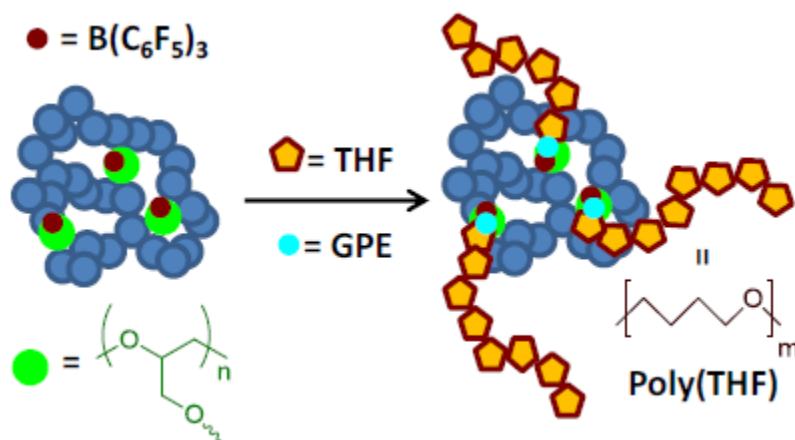


**Figure 1.17** Schematic illustration of the use of SCNPs as bionspired nanoreactors for the synthesis of polymers through ring-opening polymerisation.<sup>109</sup>

#### 1.2.3.1.1 Organometallic catalysts

It is estimated that one-third of known enzymes are metalloproteins,<sup>112</sup> where the presence of metal ions in their structure allows metalloenzymes to perform complex functions (*e.g.* redox reactions) in challenging environments.<sup>37</sup> Synthetically reproducing these types of naturally occurring systems has been intensively investigated in SCNP technology; this is summarized in **Table 6**.

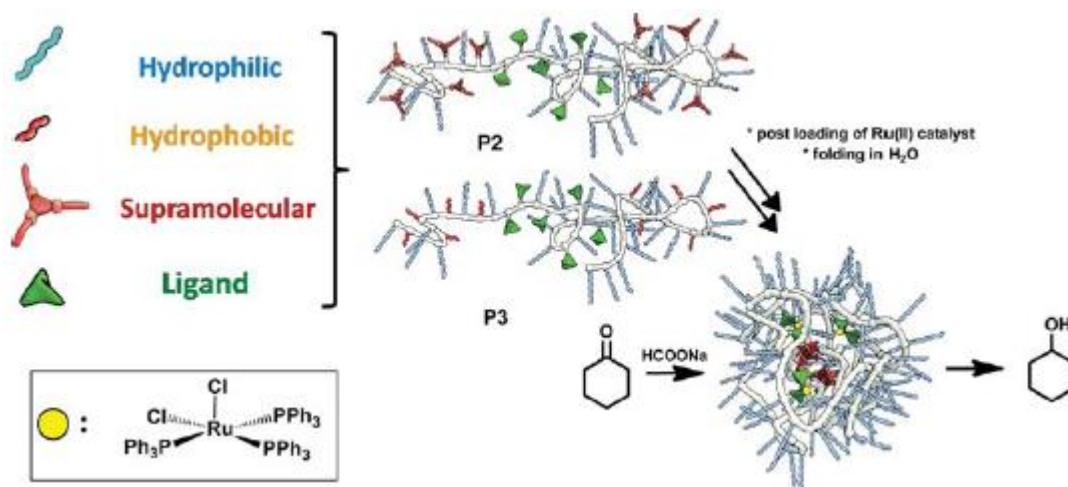
Entry	Reaction type	Catalytic center	Solvent	t (h)	T(°C)	C(%)	Reference

1	Hydrogenation of ketones	Ru(II) (PPh <sub>3</sub> ) <sub>3</sub> Cl <sub>2</sub>	H <sub>2</sub> O	50	40	98	52
2	Oxidation of secondary alcohols	Ru(II) (PPh <sub>3</sub> ) <sub>3</sub> Cl <sub>2</sub>	H <sub>2</sub> O	0.07	r.t.	99	106
3	CuAAC	Cu(I)-Bimpy	PBS	0.2	r.t.	99	113
4	Mono-depropargylation	Pd(II)-Bimpy	PBS	5	r.t.	99	113
5	Bis-depropargylation	Pd(II)-Bimpy	PBS	25	r.t.	99	113
6	CuAAC	Cu(II)-aspartate	H <sub>2</sub> O	24	50	99	116
7	Alkyne dimerisation	Cu(OAc) <sub>2</sub>	Bulk	8	60	98	114
8	Hydrogenation of phenol	RuCl <sub>2</sub> (PPh <sub>3</sub> ) <sub>3</sub>	H <sub>2</sub> O	1	60	28	117
9	Sulfides oxidation	Ti(salen)	H <sub>2</sub> O	1	r.t.	99	40

10	Reduction of secondary amines	$[\text{IrCl}(\text{COE})_2]_2$	THF	16	r.t.	99	<sup>47</sup>
11	Biphenyl formation	$[\text{RhCl}(\text{COE})_2]_2$	THF	16	80	99	<sup>47</sup>
12	Suzuki coupling	Pd-NHC <sub>2</sub>	H <sub>2</sub> O	5	r.t.	99	<sup>38</sup>
13	Sonogashira coupling	Pd(II)-triarylphosphine	HN(C <sub>2</sub> H <sub>5</sub> ) <sub>2</sub>	24	r.t.	99	<sup>115</sup>
14	Amination of allyl alcohol	Pt(II)-triarylphosphine	C <sub>6</sub> D <sub>6</sub>	24	100	99	<sup>45</sup>
15	Photoreduction of CO <sub>2</sub> to CO	Ni-thiolate	DMF, Acetonitrile	1	80	99	<sup>43</sup>
16	Polymerisation of (meth)acrylates	Fe(II)-urea/aniline	Toluene	92	60	90	<sup>41</sup>
17	Polymerisation of PEDOT	Fe(OAc) <sub>2</sub>	H <sub>2</sub> O	5	r.t.	-	<sup>118</sup>

**Table 1.6** Summary of reactions catalysed by SCNPs as organometallic catalyst.

Palmans, Meijer *et al.* also followed in this domain the aforementioned “hydrophobic cavity” strategy with several examples.<sup>46,52</sup> Firstly, catalytically active SCNPs were prepared through self-folding of an amphiphilic random copolymer and post-loading of Ru(II) catalyst *via* ligand exchange with complex.<sup>52</sup> The resulting Ru-based SCNPs were evaluated as catalysts for the transfer hydrogenation of ketones using sodium formate as the hydrogen source, achieving almost quantitative conversion after 2 minutes with a TOF of 20 h<sup>-1</sup> (**Table 1.6; Entry 1**). Interestingly, the same system was found to be active in the oxidation of secondary alcohols with *t*-BuOOH as oxidant, showing quantitative conversions too with TOF values close to 600 h<sup>-1</sup> (**Table 1.6; Entry 2**),<sup>106</sup> probably due to a “confinement effect”/“concentrator effect” in the SCNPs core. This was evidenced as higher selectivity toward more hydrophobic secondary alcohol was observed, due to the more hydrophobic interior of SCNPs. This was further supported by implementing the reverse reaction of transfer hydrogenation with the same hydrophobic selectivity. BTA functional groups that were introduced to produce helical stacked self-assemblies did enable further improvement in the catalytic performance of these SCNPs (**Scheme 1.10**).<sup>46</sup>



**Scheme 1.10** Design of catalytically active SCNPs for transfer hydrogenation of ketones in water in a BTA-supramolecular interactions based nanoreactors.

Similar BTA-based amphiphilic SCNPs were applied for catalysis purpose, this time in phosphate buffer at physiological pH, at low substrate concentrations, and at room temperature.<sup>113</sup> These SCNPs featured different ligands including Bimpy, phenanthroline (Phen), BiPy capable of coordinating to Cu(I) and Pd(II) metallic centers (**Table 1.6; Entry 3-5**). The resulting metal-based SCNPs proved to catalyse azide-alkyne cycloaddition and depropargylation reactions obtaining excellent catalytic performances.

Similarly, Oldfield *et al.* used Cu(I)-containing organometallic SCNPs for azide-alkyne catalysed cycloaddition reactions (**Table 1.6; Entry 6**). The main difference with the previous example comes from the presence of aspartate-containing polyolefins. Remarkably, these SCNPs showed an excellent catalytic performance (TOF 16,667 h<sup>-1</sup>), not only in water, but also in bacteria and mammalian cells environments.<sup>116</sup>

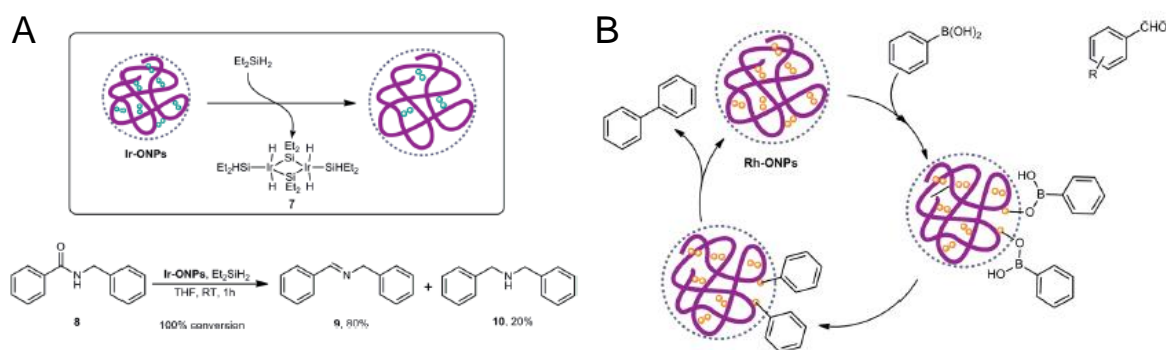
Cu(I) was also the metal ion employed by Pomposo *et al.* for oxidative coupling of mixtures of chemically related terminal alkyne substrates (**Table 1.6; Entry 7**).<sup>28</sup> Interestingly, this type of reactions could be achieved by these SCNPs, but not by more classical catalysts like CuCl<sub>2</sub>, Cu(OAc)<sub>2</sub> or Cu(acac)<sub>2</sub>. This specificity was attributed to the unique compartmentalised local catalytic sites embedded in methacrylate units, permitting an optimum transition state stabilisation for the preferred substrate. The importance of tuning the spatial arrangement of catalytic specific sites in metal-containing SCNPs was investigated using molecular dynamics.<sup>89</sup>

He *et al.* recently reported the synthesis of Cu-bearing SCNPs mimicking metalloenzymes for the hydroxylation of phenols (**Table 1.6; Entry 8**).<sup>117</sup> From a PMMA precursor containing imidazole groups, SCNP folding was triggered by Cu-imidazole binding following the already mentioned “concurrent binding/folding technique”. These Cu-SCNPs exhibited high selectivities (ca. 80%) and quantitative conversions with a TOF of 872 h<sup>-1</sup> converting, phenol to catechol in water using H<sub>2</sub>O<sub>2</sub> as oxidant. Increasing the Cu content did not enhance the catalytic efficiency, which was explained by the difference

in flexibility and adaptability of the folded SCNPs containing less Cu-units, hence less cross-linking points.

Despite not using Cu-centers for their catalysis, Yin *et al.* developed titanium-based SCNPs for waterborne catalysis, exploiting the so-called “hydrophobic cavity” in selective sulfides oxidation reactions (**Table 1.6; Entry 9**).<sup>40</sup> For this purpose, Ti(salen) moieties were supported in a thermoresponsive *N*-isopropyl acrylamide (NIPAm) polymeric platform. It was found that the use of SCNPs enhanced the performance for methyl aryl and alkyl phenyl sulfides (conversions of 85 - 99% and ee of 95%), compared to standard chiral Ti(salen) complex (48% conversion and 65% ee). This was attributed to the site “isolation effect” provided by the shielding of the catalytic sites and the “confinement effect” that effectively concentrated the substrates within the hydrophobic catalytic core, enhancing both the reaction selectivity and rate. More interestingly, the intrinsic thermoresponsive behavior of the NIPAm-based architecture was harnessed by inducing SCNPs recovery upon heating, for recycling into further catalytic runs.

Another rather interesting approach in order to concomit both positive effects of metal catalytic centers and architectural polymer nature was conducted by Lemcoff *et al.* (**Table 1.6; Entry 10**).<sup>47</sup> in which the used polycycloocta-1,5-diene polymer backbone served as actual polyligand. In order to demonstrate the versatility of this polymer platform, different metals were used, namely, Rh(I), Ir (I) and Ni(0) and further studied for distinct catalytic reactions. In the case of Ir(I)-based SCNPs reduction of secondary amines and allylation of benzophenone matched the performance of small-molecule models (**Scheme 1.12 A**) (**Table 1.6; Entry 10**). Cross-coupling reactions between 4-nitrobenzaldehyde and phenyl boronic acid were catalysed by Rh(I)-based SCNPs, unexpectedly showing the first example of selective homo-coupling to cross-coupling which was further optimised by the inclusion of NHC ligands (**Scheme 1.11 B**) (**Table 1.6; Entry 11**).

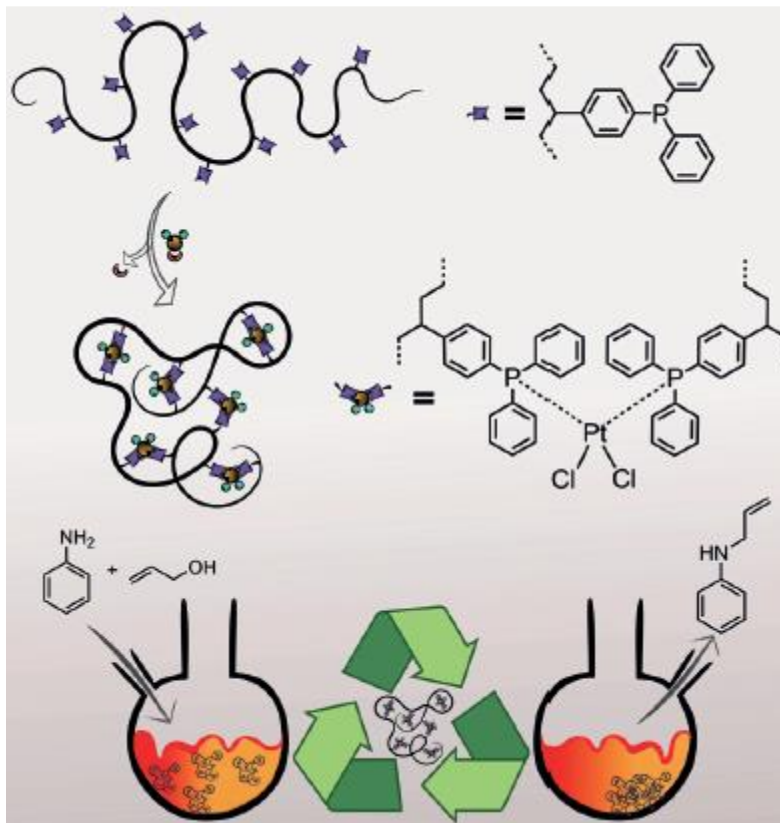


**Scheme 1.11** (A) Reduction of benzyl benzamide using Ir-SCNPs and (B) biphenyl production catalysed by Rh-SCNPs.<sup>47</sup>

Taking into account the novelties disclosed by the previous example, Taton *et al.* developed a water-soluble styrenic precursor bearing NHC-type ligands which could induce SCNPs folding by simple exposure to Pd(II) (**Table 1.6; Entry 12**).<sup>38</sup> Their catalytic potential as nanoreactors was confirmed through the Suzuki coupling reaction, revealing markedly improved catalytic efficacy compared to Pd(OAc)<sub>2</sub>, which was attributed to a favorable microenvironment within SCNPs' pocket.

Pd(II)-based SCNPs were also developed by Kowollik *et al.* using triarylphosphine ligands supported in a styrenic polymer backbone (**Table 1.6; Entry 13**).<sup>115</sup> Distinctly to the latter example, their ability to trigger catalysed reactions was tested in Sonogashira couplings. However, the performance could not reach the one attained by molecular Pd(PPh<sub>3</sub>)<sub>2</sub>Cl<sub>2</sub>. The same group used the same triarylphosphine ligand-based precursors to incorporate Pt(II) catalytic entities (**Table 1.6; Entry 14**).<sup>45</sup> The Pt(II) incorporated as Pt(1,5-cyclooctadiene)Cl<sub>2</sub> to be folded into SCNPs. The resulting organometallic nanoreactors were found to be active in amination of allyl alcohol reactions under homogeneous conditions, obtaining quantitative conversions after only 16 h with only 0.2 mol% catalyst, which could be further recycled with no apparent loss of activity (**Scheme 1.12**).





**Scheme 1.12** Illustration of a SCNP folding into a Pt-containing nanoreactor employed for the amination of allyl alcohol which can be further recycled.<sup>45</sup>

In a more specific enzyme-mimicry attempt, He *et al.* developed Ni(II)-containing SCNPs *via* Ni-thiolate coordination for the photoreduction of CO<sub>2</sub> to CO (**Table 1.6; Entry 15**).<sup>43</sup> The reported conditions included TiO<sub>2</sub> as light absorber support and triethanolamine as electron donor agent. Reactions were conducted at 80 °C leading to TOF values of *ca.* 2500 h<sup>-1</sup> both in DMF and acetonitrile.

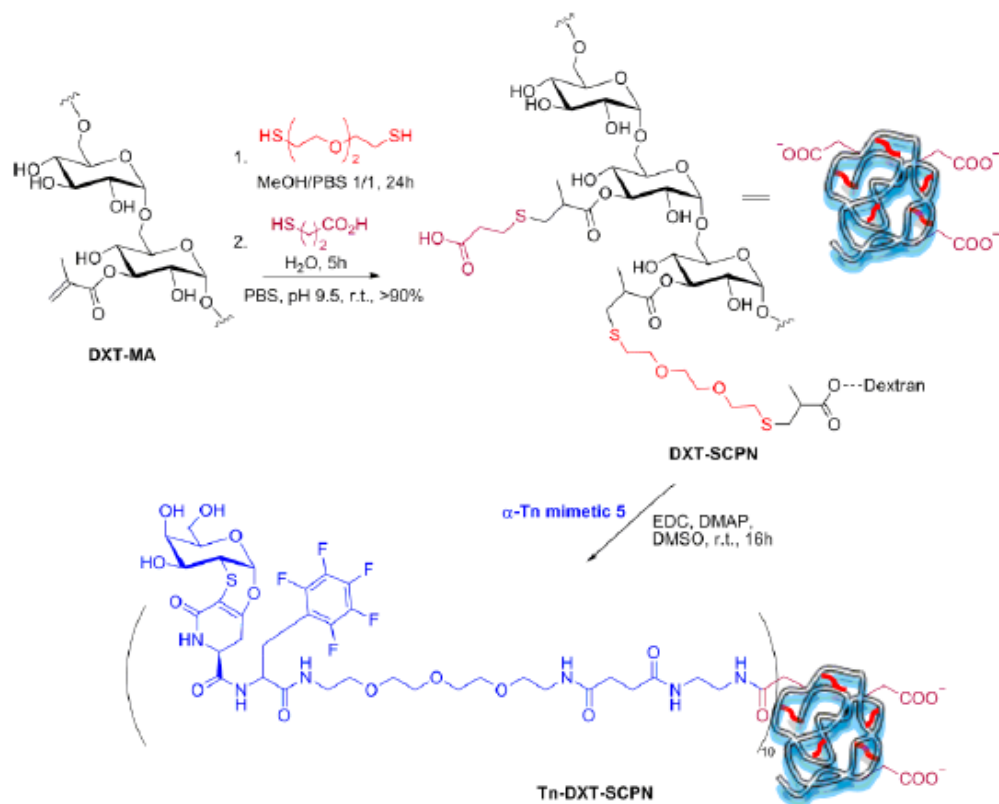
As proof of concept, Sawamoto *et al.* developed a polymerase-like iron-containing SCNPs (**Table 1.6; Entry 16**).<sup>41</sup> After their synthesis was conducted as described in **Section 1.2.1.1.2.**, living radical polymerization of various alkyl methacrylate monomers was efficiently catalysed by these nanoreactors. Well-controlled PMMA's of relatively narrow molecular weight distribution ( $\mathcal{D} = 1.1$ , high conversions 90%) were obtained in toluene. The catalyst recovery and further recycling was achievable thanks to a simple washing with an organic solvent of the aqueous reaction medium.

More recently, Pomposo *et al.* used Fe-SCNPs as enzyme-mimic nanoreactors for the synthesis of polymers (**Table 1.6; Entry 17**).<sup>118</sup> These SCNPs differ from the Sawamoto's ones described above in the fact that supported Fe(OAc)<sub>2</sub> served as catalytic center to trigger the dispersion polymerization of poly(3,4-ethylenedioxythiophene) : polystyrenesulfonate (PEDOT:PSS) in water conditions. Interestingly, the obtained dispersion was casted to form films exhibiting conductivity values ( $\sigma = 1 \times 10^{-4}$  S/cm) similar to those typically obtained with iron-containing proteins.

#### 1.1.4.1.3 Enzymatic catalytic mimics

In nature, different ordered or disordered proteins can be found with functions relating to the binding and transport of various substances. Interestingly, the form factor of sparse SCNPs was found to be very similar to that displayed by intrinsically disordered proteins (IDPs).<sup>37</sup> The main advantage of this particle morphology is their capacity to bind several centers, such as ions, small organic molecules, other proteins and nucleic acids (RNA, DNA). The capacity of SCNPs as enzyme binders has not been widely explored. However, a few studies have started to appear, where either the isolated active site<sup>119</sup> or the protein (antigen)<sup>120</sup> is loaded within the SCNPs structure.

A promising example of this was reported by Loinaz *et al.* The advantageous use of water-dispersible and biocompatible SCNPs based on dextran as naturally occurring polysaccharidic support was reported as a Tn-antigen mimetic (**Scheme 1.13**).<sup>128</sup> The obtained hybrid-SCNPs triggered a series of innate immune responses human peripheral blood mononuclear cells (PBMC) like those elicited by naturally occurring Tn clusters. This could represent an alternative to immune proteins as well as a unique tool to interrogate the role and reactions of Tn-like antigens in cell medium.



**Scheme 1.13** Preparation of dextran-based SCNPs and subsequent incorporation of the Tn-Antigen.<sup>120</sup>

Use of SCNPs as enzyme binders for enzymatic catalysis is still in its infancy and there is still a lot of room for improvement, for instance to address issues such as enzyme compatibility or adaptability in a polymer hybrid structure.

#### 1.1.4.3 Other uses

SCNPs have become a valuable artificial soft nano-objects, which can be efficiently endowed with useful properties in wide array of applications, such as rheology-improving agents for melts of thermoplastics,<sup>121</sup> nanocomposites,<sup>122–124</sup> elastomeric polymers,<sup>29,125,126</sup> paints,<sup>127,128</sup> compartmentalised sensors of metal ions,<sup>53</sup> templates for photoluminescent carbon nanodots(C-NDs)<sup>128</sup> or hydrogels.<sup>32,125</sup>

A diversity of nanomaterials have been synthesised involving the utilization of SCNPs, not only in catalysis, but for many other applications. In a pionnering work by Qian *et al.* SCNPs obtained by Bergman cyclization intramolecular folding were employed to encapsulate quantum dots (QDs) in a one-pot reaction.<sup>97</sup> As a proof of concept, photoluminescent (PL) zinc sulfide (ZnS) quantum dots (QD) were fabricated and encapsulated in SCNPs of different sizes. The smallest nanoreactors produced a single QD of 4 nm in diameter and giving a quantum yield (QY) of 17% at 310 nm excitation wavelength, while bigger nanoreactors trapping multiple QDs presented QY of only 2%. The versatility of SCNPs as QDs platform, cadmium sulfide (CdS) QDs of 4.7 nm were obtained with QY = 45%.

The same group also developed bright photoluminescent C-NDs with low toxicity as suitable candidates for *in vivo* imaging. SCNPs were obtained following the same Bergman cyclization chemistry, but water solubility was improved by inserting PEG chains.<sup>128</sup> In this manner, the optimal emission wavelength of the C-NDs was found to red-shifted upon decreasing the size of the studied C-NDs probably, due to the amorphous core architecture (**Fig. 1.18**), as further evidenced by computational calculations.<sup>130</sup> Interestingly, the surface chemistry of the C-NDs was found to affect the QY through aggregate-induced energy/charge transfer processes, leading to lower QYs.

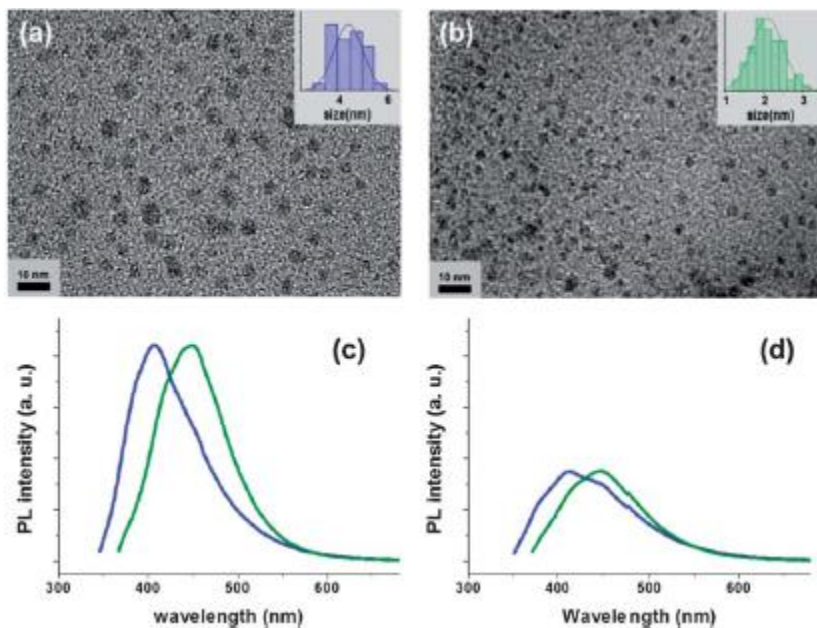
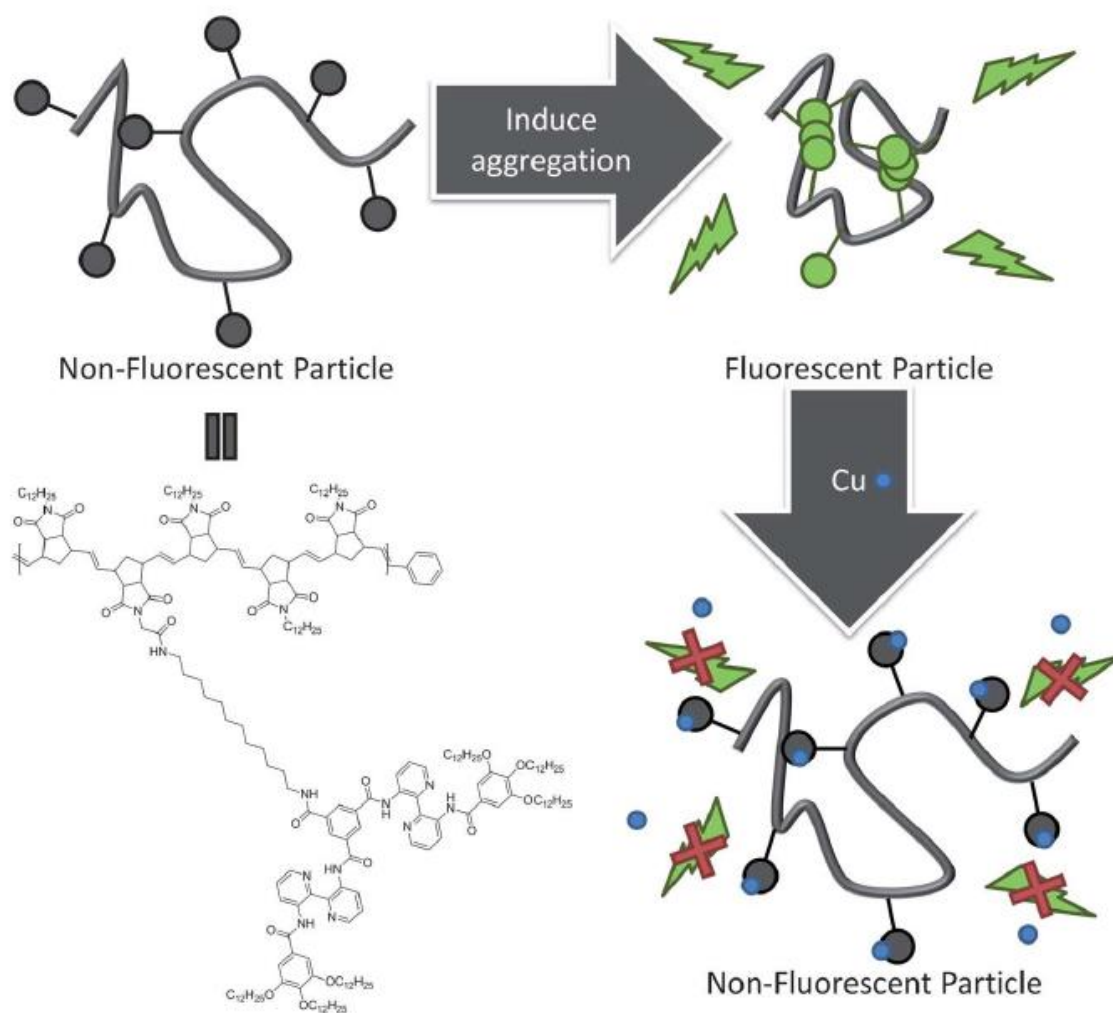


**Figure 1.18** Size and size-dependent photoluminescence spectra of CNDs. TEM image and size histogram of big CND (A) and small ones (B). Photoluminescent spectra of surface oxidised at 340 nm of small CND (green line C) and big CND (blue line C) and spectra of reduced surface (green line D and blue line C, respectively).<sup>128</sup>

Palmans *et al.* reported the synthesis of BiPy-BTA pendant polymers by ROMP chemistry.<sup>53</sup> Corresponding SCNPs were intramolecularly self-assembled by supramolecular interactions between BiPy-BTA motifs. Addition of copper to solutions led to binding of the added Cu(II) BiPy units (**Scheme 1.14**). This binding was probed by fluorescence and UV-vis spectroscopy. Outcome from this study contrasted with other reported examples utilising other polymers by showing enhanced fluorescence, presumably due to the absence of interpolymer interactions and compartmentalization of the sensor units.



**Scheme 1.14** Schematic representation of the sensing function of the BiPy-BTA functional polymers.<sup>53</sup>

## 1.5 Conclusions and aims of this PhD thesis

Although far from reaching the structural complexity of proteins, SCNP have yet allowed the creation of functional macromolecular compounds featuring globular, stimuli-responsive structures and, in some cases, with some compartmentalized functions, such as site isolated catalysts, like in enzymes. Interest in SCNPs is thus growing due to the different folding strategies available for generating organic-, metallic-

or enzyme-polymer hybrid structures.

The success of these structures requires first for the accurate characterisation, to provide the whole picture of the system to better understanding their ultimate performance in their respective applications. Associated to the SCNPs synthetic challenges, their characterisation is also a tricky, which in most of the cases requires the combination of different analytical techniques for better depicting their structure, morphology or stability. Moreover, the difficulties come often from the need of sensitive characterisation techniques to detect, even at small concentrations, the presence of the targeted single molecule structure and discard intermolecularly cross-linked aggregates that may occur during synthesis.

SCNPs technology is advantageous in several areas (*e.g.* catalysis, sensors or nanomedicine) due in large part to the small size of the nanoparticles and the ease in which they can specifically tailored. While the research involving SCNPs has been primarily inspired by nature (*i.e.* enzymes), other new applications related to their intrinsic performance have been found (*e.g.* nanocomposite materials) due to their unique properties and large variety of opportunities to incorporate selective functions, afford functional chemical compartmentalised environments or easily modulate their solubility.

In relation to the state-of-the art described in this chapter, the four following chapters presenting the work of this PhD thesis will deal with the synthesis and the manipulation of new polymer-based structures for specific catalysis. More specifically, random copolymers based on poly(ionic liquids) will be developed under different architectures such as single chain nanoparticles (SCNPs) or as (macro)gels. Those different systems will be employed as *N*-heterocyclic carbenes (NHCs) precursors to be used as organocatalysts. The incorporation of relatively basic counteranions in PIL units derived from imidazolium moieties allows the *in situ* generation of active NHC species for catalysis. Firstly, a reactive PIL based (macro)gel will represent the preliminary study to better understand and analyse the catalytic performance in the macroscale. This study will then permit the identification of suitable model reactions

as well as conditions and standards, becoming a reference system all along this thesis. Moreover, this (macro)gel will also serve as a base for the further development of more sophisticated nanogels known as single chain nanoparticles (*aka* SCNPs). These SCNPs will specially be designed based on their PIL tunability and synthesised by reversible additions fragmentation chain transfer (RAFT) polymerisation. In first place, the ionic nature of the NHC precatalyst will be exploited by triggering the interaction between imidazolium derivatives and basic anions supported in the polymer leading to a ionically cross-linked SCNPs. Secondly, the thermolatent properties of NHC precursors will be harnessed by proving the compatibility of both substrates and precatalyst supported on the same polymer chain and triggering the folding by condensing the substrates by the simple application of heat. Finally, the intrinsic capacity of poly(NHC)s to act as poly-ligands will innovatively be demonstrated by forming SCNPs after organometallic complexation using a silver salt.

## 1.6 References

- 1 M. Danial, C. My-Nhi Tran, P. G. Young, S. Perrier and K. A. Jolliffe, *Nat. Commun.*, , DOI:10.1038/ncomms3780.
- 2 N. G. Engelis, A. Anastasaki, G. Nurumbetov, N. P. Truong, V. Nikolaou, A. Shegiwal, M. R. Whittaker, T. P. Davis and D. M. Haddleton, *Nat. Chem.*, 2017, **9**, 171–178.
- 3 J.-F. Lutz, M. Ouchi, D. R. Liu and M. Sawamoto, *Polym. Process.*, 2013, **341**, 10.
- 4 Jeremy M. Berg, J. L. Tymoczko and L. Stryer, *Biochemistry*, W. H. Freeman, New York, 5th edn., 2002.
- 5 C. K. Lyon, A. Prasher, A. M. Hanlon, B. T. Tuten, C. A. Tooley, P. G. Frank and E. B. Berda, *Polym. Chem.*, 2015, **6**, 181–197.
- 6 M. Ouchi, N. Badi, J.-F. Lutz and M. Sawamoto, *Nat. Chem.*, 2011, **3**, 917–924.
- 7 A. M. Hanlon, C. K. Lyon and E. B. Berda, *Macromolecules*, 2016, **49**, 2–14.
- 8 S. Mavila, O. Eivgi, I. Berkovich and N. G. Lemcoff, *Chem. Rev.*, 2016, **116**, 878–961.
- 9 O. Altintas and C. Barner-Kowollik, *Macromol. Rapid Commun.*, 2016, **37**, 29–46.
- 10 M. Gonzalez-Burgos, A. Latorre-Sanchez and J. A. Pomposo, *Chem Soc Rev*, 2015, **44**, 6122–6142.
- 11 K. B. Thurmond, T. Kowalewski and K. L. Wooley, *J. Am. Chem. Soc.*, 1997, **119**, 6656–6665.
- 12 Q. Zhang, E. E. Remsen and K. L. Wooley, *J. Am. Chem. Soc.*, 2000, **122**, 3642–3651.



- 13 D. Mecerreyes, V. Lee, C. J. Hawker, J. L. Hedrick, A. Wursch, W. Volksen, T. Magbitang, E. Huang and R. D. Miller, *Adv. Mater.*, 2001, **13**, 204–208.
- 14 A. Sanchez-Sanchez, I. Pérez-Baena and J. Pomposo, *Molecules*, 2013, **18**, 3339–3355.
- 15 V. A. Davankov, M. M. Ilyin, M. P. Tsyurupa, G. I. Timofeeva and L. V. Dubrovina, *Macromolecules*, 1996, **29**, 8398–8403.
- 16 A. E. Cherian, F. C. Sun, S. S. Sheiko and G. W. Coates, *J. Am. Chem. Soc.*, 2007, **129**, 11350–11351.
- 17 A. R. de Luzuriaga, N. Ormategui, H. J. Grande, I. Odriozola, J. A. Pomposo and I. Loinaz, *Macromol. Rapid Commun.*, 2008, **29**, 1156–1160.
- 18 N. Ormategui, I. García, D. Padro, G. Cabañero, H. J. Grande and I. Loinaz, *Soft Matter*, 2012, **8**, 734–740.
- 19 J. Wen, L. Yuan, Y. Yang, L. Liu and H. Zhao, *ACS Macro Lett.*, 2013, **2**, 100–106.
- 20 R. Lambert, A.-L. Wirotius and D. Taton, *ACS Macro Lett.*, 2017, **6**, 489–494.
- 21 J. P. Cole, J. J. Lessard, K. J. Rodriguez, A. M. Hanlon, E. K. Reville, J. P. Mancinelli and E. B. Berda, *Polym. Chem.*, 2017, **8**, 5829–5835.
- 22 J. Steinkoenig, T. Nitsche, B. T. Tuten and C. Barner-Kowollik, *Macromolecules*, 2018, **51**, 3967–3974.
- 23 D. M. Stevens, S. Tempelaar, A. P. Dove and E. Harth, *ACS Macro Lett.*, 2012, **1**, 915–918.
- 24 A. Sanchez-Sanchez, I. Asenjo-Sanz, L. Buruaga and J. A. Pomposo, *Macromol. Rapid Commun.*, 2012, **33**, 1262–1267.
- 25 H. Frisch, F. R. Bloesser and C. Barner-Kowollik, *Angew. Chem.*, , DOI:10.1002/ange.201811541.
- 26 C. Heiler, S. Bastian, P. Lederhose, J. P. Blinco, E. Blasco and C. Barner-Kowollik, *Chem. Commun.*, 2018, **54**, 3476–3479.
- 27 P. G. Frank, B. T. Tuten, A. Prasher, D. Chao and E. B. Berda, *Macromol. Rapid Commun.*, 2014, **35**, 249–253.
- 28 J. A. Pomposo, I. Perez-Baena, F. Lo Verso, A. J. Moreno, A. Arbe and J. Colmenero, *ACS Macro Lett.*, 2014, **3**, 767–772.
- 29 A. Levy, F. Wang, A. Lang, O. Galant and C. E. Diesendruck, *Angew. Chem. Int. Ed.*, 2017, **56**, 6431–6434.
- 30 J. P. Cole, J. J. Lessard, K. J. Rodriguez, A. M. Hanlon, E. K. Reville, J. P. Mancinelli and E. B. Berda, *Polym Chem.*, , DOI:10.1039/C7PY01133D.
- 31 J. P. Cole, A. M. Hanlon, K. J. Rodriguez and E. B. Berda, *J. Polym. Sci. Part Polym. Chem.*, 2017, **55**, 191–206.
- 32 D. E. Whitaker, C. S. Mahon and D. A. Fulton, *Angew. Chem. Int. Ed.*, 2013, **52**, 956–959.

- 33 J. Willenbacher, K. N. R. Wuest, J. O. Mueller, M. Kaupp, H.-A. Wagenknecht and C. Barner-Kowollik, *ACS Macro Lett.*, 2014, **3**, 574–579.
- 34 J. He, L. Tremblay, S. Lacelle and Y. Zhao, *Soft Matter*, 2011, **7**, 2380.
- 35 H. Frisch, F. R. Bloesser and C. Barner-Kowollik, *Angew. Chem. Int. Ed.*, 2019, **58**, 3604–3609.
- 36 H. Rothfuss, N. D. Knöfel, P. W. Roesky and C. Barner-Kowollik, *J. Am. Chem. Soc.*, 2018, **140**, 5875–5881.
- 37 A. Latorre-Sánchez and J. A. Pomposo, *Polym. Int.*, 2016, **65**, 855–860.
- 38 R. Lambert, A.-L. Wirotius, S. Garmendia, P. Berto, J. Vignolle and D. Taton, *Polym. Chem.*, 2018, **9**, 3199–3204.
- 39 J. Willenbacher, O. Altintas, V. Trouillet, N. Knöfel, M. J. Monteiro, P. W. Roesky and C. Barner-Kowollik, *Polym Chem*, 2015, **6**, 4358–4365.
- 40 Y. Zhang, R. Tan, M. Gao, P. Hao and D. Yin, *Green Chem*, 2017, **19**, 1182–1193.
- 41 Y. Azuma, T. Terashima and M. Sawamoto, *ACS Macro Lett.*, 2017, **6**, 830–835.
- 42 I. Perez-Baena, I. Loinaz, D. Padro, I. García, H. J. Grande and I. Odriozola, *J. Mater. Chem.*, 2010, **20**, 6916.
- 43 S. Thanneeru, J. K. Nganga, A. S. Amin, B. Liu, L. Jin, A. M. Angeles-Boza and J. He, *ChemCatChem*, 2017, **9**, 1157–1162.
- 44 A. Sanchez-Sanchez, S. Akbari, A. Etxeberria, A. Arbe, U. Gasser, A. J. Moreno, J. Colmenero and J. A. Pomposo, *ACS Macro Lett.*, 2013, **2**, 491–495.
- 45 N. D. Knöfel, H. Rothfuss, J. Willenbacher, C. Barner-Kowollik and P. W. Roesky, *Angew. Chem. Int. Ed.*, 2017, **56**, 4950–4954.
- 46 M. Artar, T. Terashima, M. Sawamoto, E. W. Meijer and A. R. A. Palmans, *J. Polym. Sci. Part Polym. Chem.*, 2014, **52**, 12–20.
- 47 S. Mavila, I. Rozenberg and N. G. Lemcoff, *Chem. Sci.*, 2014, **5**, 4196–4203.
- 48 E. J. Foster, E. B. Berda and E. W. Meijer, *J. Am. Chem. Soc.*, 2009, **131**, 6964–6966.
- 49 E. B. Berda, E. J. Foster and E. W. Meijer, *Macromolecules*, 2010, **43**, 1430–1437.
- 50 E. J. Foster, E. B. Berda and E. W. Meijer, *J. Polym. Sci. Part Polym. Chem.*, 2011, **49**, 118–126.
- 51 P. J. M. Stals, M. A. J. Gillissen, R. Nicola?, A. R. A. Palmans and E. W. Meijer, *Polym. Chem.*, 2013, **4**, 2584.
- 52 T. Terashima, T. Mes, T. F. A. De Greef, M. A. J. Gillissen, P. Besenius, A. R. A. Palmans and E. W. Meijer, *J. Am. Chem. Soc.*, 2011, **133**, 4742–4745.
- 53 M. A. J. Gillissen, I. K. Voets, E. W. Meijer and Anja. R. A. Palmans, *Polym. Chem.*, 2012, **3**, 3166.

- 54 T. Mes, R. van der Weegen, A. R. A. Palmans and E. W. Meijer, *Angew. Chem. Int. Ed.*, 2011, **50**, 5085–5089.
- 55 O. Altintas, E. Lejeune, P. Gerstel and C. Barner-Kowollik, *Polym Chem*, 2012, **3**, 640–651.
- 56 O. Altintas, T. Rudolph and C. Barner-Kowollik, *J. Polym. Sci. Part Polym. Chem.*, 2011, **49**, 2566–2576.
- 57 O. Altintas, P. Gerstel, N. Dingenouts and C. Barner-Kowollik, *Chem. Commun.*, 2010, **46**, 6291.
- 58 M. Seo, B. J. Beck, J. M. J. Paulusse, C. J. Hawker and S. Y. Kim, *Macromolecules*, 2008, **41**, 6413–6418.
- 59 S. Cantekin, T. F. A. de Greef and A. R. A. Palmans, *Chem. Soc. Rev.*, 2012, **41**, 6125.
- 60 E. Huerta, P. J. M. Stals, E. W. Meijer and A. R. A. Palmans, *Angew. Chem. Int. Ed.*, 2013, **52**, 2906–2910.
- 61 P. J. M. Stals, M. A. J. Gillissen, T. F. E. Paffen, T. F. A. de Greef, P. Lindner, E. W. Meijer, A. R. A. Palmans and I. K. Voets, *Macromolecules*, 2014, **47**, 2947–2954.
- 62 N. Hosono, M. A. J. Gillissen, Y. Li, S. S. Sheiko, A. R. A. Palmans and E. W. Meijer, *J. Am. Chem. Soc.*, 2013, **135**, 501–510.
- 63 E. A. Appel, J. Dyson, J. del Barrio, Z. Walsh and O. A. Scherman, *Angew. Chem. Int. Ed.*, 2012, **51**, 4185–4189.
- 64 E. A. Appel, J. del Barrio, J. Dyson, L. Isaacs and O. A. Scherman, *Chem. Sci.*, 2012, **3**, 2278.
- 65 J. Lu, N. ten Brummelhuis and M. Weck, *Chem. Commun.*, 2014, **50**, 6225.
- 66 J. Lu, N. ten Brummelhuis and M. Weck, *Chem. Commun.*, 2014, **50**, 6225.
- 67 B. T. Tuten, D. Chao, C. K. Lyon and E. B. Berda, *Polym. Chem.*, 2012, **3**, 3068.
- 68 B. S. Murray and D. A. Fulton, *Macromolecules*, 2011, **44**, 7242–7252.
- 69 A. Sanchez-Sanchez, D. A. Fulton and J. A. Pomposo, *Chem. Commun.*, 2014, **50**, 1871–1874.
- 70 S. Babaoglu, D. Karaca Balta and G. Temel, *J. Polym. Sci. Part Polym. Chem.*, 2017, **55**, 1998–2003.
- 71 N. Wedler-Jasinski, T. Lueckerath, H. Mutlu, A. S. Goldmann, A. Walther, M. H. Stenzel and C. Barner-Kowollik, *Chem Commun*, 2017, **53**, 157–160.
- 72 A. M. Hanlon, I. Martin, E. R. Bright, J. Chouinard, K. J. Rodriguez, G. E. Patenotte and E. B. Berda, *Polym. Chem.*, 2017, **8**, 5120–5128.
- 73 N. Wedler-Jasinski, T. Lueckerath, H. Mutlu, A. S. Goldmann, A. Walther, M. H. Stenzel and C. Barner-Kowollik, *Chem Commun*, 2017, **53**, 157–160.
- 74 E. Blasco, B. T. Tuten, H. Frisch, A. Lederer and C. Barner-Kowollik, *Polym Chem*, , DOI:10.1039/C7PY01278K.

- 75 J. Steinkoenig, H. Rothfuss, A. Lauer, B. T. Tuten and C. Barner-Kowollik, *J. Am. Chem. Soc.*, 2017, **139**, 51–54.
- 76 K. J. Rodriguez, R. Chen, E. R. Bright and E. B. Berda, in *Single-Chain Polymer Nanoparticles*, ed. A. M. Hanlon, Wiley-VCH Verlag GmbH & Co. KGaA, Weinheim, Germany, 2017, pp. 91–128.
- 77 C. K. Lyon, E. O. Hill and E. B. Berda, *Macromol. Chem. Phys.*, 2016, **217**, 501–508.
- 78 J. A. Pomposo, I. Perez-Baena, L. Buruaga, A. Alegría, A. J. Moreno and J. Colmenero, *Macromolecules*, 2011, **44**, 8644–8649.
- 79 H. He, M. Zhong, B. Adzima, D. Luebke, H. Nulwala and K. Matyjaszewski, *J. Am. Chem. Soc.*, 2013, **135**, 4227–4230.
- 80 E. Blasco, B. T. Tuten, H. Frisch, A. Lederer and C. Barner-Kowollik, *Polym. Chem.*, 2017, **8**, 5845–5851.
- 81 C. S. Johnson, *Prog. Nucl. Magn. Reson. Spectrosc.*, 1999, **34**, 203–256.
- 82 Peter. Stilbs, *Anal. Chem.*, 1981, **53**, 2135–2137.
- 83 S. Garmendia, A. P. Dove, D. Taton and R. K. O'Reilly, *Polym. Chem.*, 2018, **9**, 5286–5294.
- 84 X. Jiang, H. Pu and P. Wang, *Polymer*, 2011, **52**, 3597–3602.
- 85 C. Heiler, J. T. Offenloch, E. Blasco and C. Barner-Kowollik, *ACS Macro Lett.*, 2017, **6**, 56–61.
- 86 M. A. J. Gillissen, T. Terashima, E. W. Meijer, A. R. A. Palmans and I. K. Voets, *Macromolecules*, 2013, **46**, 4120–4125.
- 87 J. Chen, J. Wang, Y. Bai, K. Li, E. S. Garcia, A. L. Ferguson and S. C. Zimmerman, *J. Am. Chem. Soc.*, 2018, **140**, 13695–13702.
- 88 O. Altintas, J. Willenbacher, K. N. R. Wuest, K. K. Oehlenschlaeger, P. Krolla-Sidenstein, H. Gliemann and C. Barner-Kowollik, *Macromolecules*, 2013, **46**, 8092–8101.
- 89 S. Basasoro, M. Gonzalez-Burgos, A. J. Moreno, F. L. Verso, A. Arbe, J. Colmenero and J. A. Pomposo, *Macromol. Rapid Commun.*, 2016, **37**, 1060–1065.
- 90 M. González-Burgos, A. Arbe, A. J. Moreno, J. A. Pomposo, A. Radulescu and J. Colmenero, *Macromolecules*, 2018, **51**, 1573–1585.
- 91 J. Rubio-Cervilla, E. González and J. A. Pomposo, in *Single-Chain Polymer Nanoparticles*, ed. J. A. Pomposo, Wiley-VCH Verlag GmbH & Co. KGaA, Weinheim, Germany, 2017, pp. 341–388.
- 92 J. Rubio-Cervilla, E. González and J. Pomposo, *Nanomaterials*, 2017, **7**, 341.
- 93 A. M. Hanlon, R. Chen, K. J. Rodriguez, C. Willis, J. G. Dickinson, M. Cashman and E. B. Berda, *Macromolecules*, 2017, **50**, 2996–3003.
- 94 A. P. P. Kröger and J. M. J. Paulusse, *J. Controlled Release*, 2018, **286**, 326–347.

- 95 A. P. P. Kröger, M. I. Komil, N. M. Hamelmann, A. Juan, M. H. Stenzel and J. M. J. Paulusse, *ACS Macro Lett.*, 2019, **8**, 95–101.
- 96 A. P. P. Kröger, N. M. Hamelmann, A. Juan, S. Lindhoud and J. M. J. Paulusse, *ACS Appl. Mater. Interfaces*, 2018, **10**, 30946–30951.
- 97 G. Qian, B. Zhu, Y. Wang, S. Deng and A. Hu, *Macromol. Rapid Commun.*, 2012, **33**, 1393–1398.
- 98 Y. Bai, H. Xing, G. A. Vincil, J. Lee, E. J. Henderson, Y. Lu, N. G. Lemcoff and S. C. Zimmerman, *Chem Sci*, 2014, **5**, 2862–2868.
- 99 C. Song, L. Li, L. Dai and S. Thayumanavan, *Polym. Chem.*, 2015, **6**, 4828–4834.
- 100 A. B. Benito, M. K. Aiertza, M. Marradi, L. Gil-Iceta, T. Shekhter Zahavi, B. Szczupak, M. Jiménez-González, T. Reese, E. Scanziani, L. Passoni, M. Matteoli, M. De Maglie, A. Orenstein, M. Oron-Herman, G. Kostenich, L. Buzhansky, E. Gazit, H.-J. Grande, V. Gómez-Vallejo, J. Llop and I. Loinaz, *Biomacromolecules*, 2016, **17**, 3213–3221.
- 101 C. T. Adkins, J. N. Dobish, S. Brown and E. Harth, *ACS Macro Lett.*, 2013, **2**, 710–714.
- 102 R. K. O'Reilly, C. J. Hawker and K. L. Wooley, *Chem. Soc. Rev.*, 2006, **35**, 1068.
- 103 P. Cotanda, N. Petzetakis and R. K. O'Reilly, *MRS Commun.*, 2012, **2**, 119–126.
- 104 A. Lu, D. Moatsou, D. A. Longbottom and R. K. O'Reilly, *Chem Sci*, 2013, **4**, 965–969.
- 105 A. Lu, P. Cotanda, J. P. Patterson, D. A. Longbottom and R. K. O'Reilly, *Chem. Commun.*, 2012, **48**, 9699.
- 106 M. Artar, E. R. J. Souren, T. Terashima, E. W. Meijer and A. R. A. Palmans, *ACS Macro Lett.*, 2015, **4**, 1099–1103.
- 107 G. Wulff, B.-O. Chong and U. Kolb, *Angew. Chem. Int. Ed.*, 2006, **45**, 2955–2958.
- 108 I. Perez-Baena, F. Barroso-Bujans, U. Gasser, A. Arbe, A. J. Moreno, J. Colmenero and J. A. Pomposo, *ACS Macro Lett.*, 2013, **2**, 775–779.
- 109 G. Njikang, G. Liu and L. Hong, *Langmuir*, 2011, **27**, 7176–7184.
- 110 E. Huerta, B. van Genabeek, P. J. M. Stals, E. W. Meijer and A. R. A. Palmans, *Macromol. Rapid Commun.*, 2014, **35**, 1320–1325.
- 111 R. H. Holm, P. Kennepohl and E. I. Solomon, *Chem. Rev.*, 1996, **96**, 2239–2314.
- 112 Y. Liu, T. Pauloehrl, S. I. Presolski, L. Albertazzi, A. R. A. Palmans and E. W. Meijer, *J. Am. Chem. Soc.*, 2015, **137**, 13096–13105.
- 113 Y. Bai, X. Feng, H. Xing, Y. Xu, B. K. Kim, N. Baig, T. Zhou, A. A. Gewirth, Y. Lu, E. Oldfield and S. C. Zimmerman, *J. Am. Chem. Soc.*, 2016, **138**, 11077–11080.
- 114 A. Sanchez-Sanchez, A. Arbe, J. Colmenero and J. A. Pomposo, *ACS Macro Lett.*, 2014, **3**, 439–443.

- 115 S. Thanneeru, S. S. Duay, L. Jin, Y. Fu, A. M. Angeles-Boza and J. He, *ACS Macro Lett.*, 2017, **6**, 652–656.
- 116 J. Willenbacher, O. Altintas, V. Trouillet, N. Knöfel, M. J. Monteiro, P. W. Roesky and C. Barner-Kowollik, *Polym. Chem.*, 2015, **6**, 4358–4365.
- 117 J. De-La-Cuesta, I. Asenjo-Sanz, A. Latorre-Sánchez, E. González, D. E. Martínez-Tong and J. A. Pomposo, *Eur. Polym. J.*, 2018, **109**, 447–452.
- 118 Y. Liu, S. Pujals, P. J. M. Stals, T. Paulöhr, S. I. Presolski, E. W. Meijer, L. Albertazzi and A. R. A. Palmans, *J. Am. Chem. Soc.*, 2018, **140**, 3423–3433.
- 119 R. Gracia, M. Marradi, G. Salerno, R. Pérez-Nicado, A. Pérez-San Vicente, D. Dupin, J. Rodriguez, I. Loinaz, F. Chiodo and C. Nativi, *ACS Macro Lett.*, 2018, **7**, 196–200.
- 120 M. E. Mackay, T. T. Dao, A. Tuteja, D. L. Ho, B. Van Horn, H.-C. Kim and C. J. Hawker, *Nat. Mater.*, 2003, 762–766.
- 121 A. Tuteja, P. M. Duxbury and M. E. Mackay, *Macromolecules*, 2007, **40**, 9427–9434.
- 122 B. Robles-Hernández, M. González-Burgos, J. Pomposo, J. Colmenero and Á. Alegría, *Polymers*, 2019, **11**, 533.
- 123 M. J. A. Hore, *Soft Matter*, 2019, **15**, 1120–1134.
- 124 M. González-Burgos, E. González and J. A. Pomposo, *Macromol. Rapid Commun.*, 2018, **39**, 1700675.
- 125 M. Formanek and A. J. Moreno, *Macromolecules*, 2019, **52**, 1821–1831.
- 126 H. Cengiz, B. Aydogan, S. Ates, E. Acikalin and Y. Yagci, *Des. Monomers Polym.*, 2011, **14**, 69–78.
- 127 J. B. Beck, K. L. Killops, T. Kang, K. Sivanandan, A. Bayles, M. E. Mackay, K. L. Wooley and C. J. Hawker, *Macromolecules*, 2009, **42**, 5629–5635.
- 128 B. Zhu, S. Sun, Y. Wang, S. Deng, G. Qian, M. Wang and A. Hu, *J Mater Chem C*, 2013, **1**, 580–586.
- 129 W. Kwon and S.-W. Rhee, *Chem. Commun.*, 2012, **48**, 5256.

## **Chapter II: Facile Synthesis of Reversibly Crosslinked Poly(ionic liquid)-type Gels: Recyclable Supports for Organocatalysis by *N*-Heterocyclic Carbenes**





# Table of Contents

## Chapter II: Facile Synthesis of Reversibly Crosslinked Poly(ionic liquid)-type Gels: Recyclable

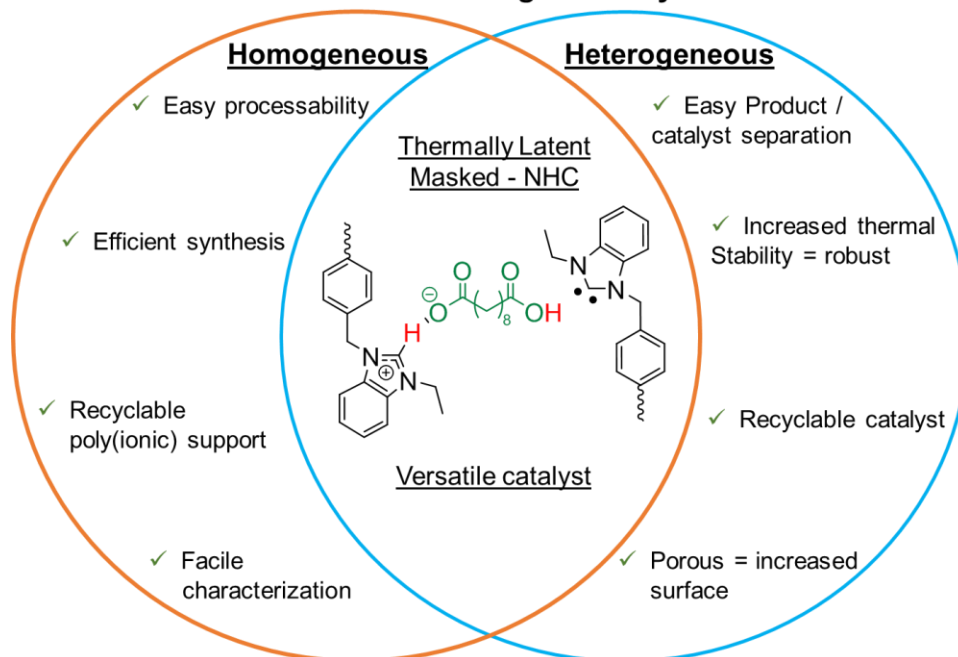
### Supports for Organocatalysis by *N*-Heterocyclic Carbenes

2.1.	Abstract.....	101-102
2.2.	Introduction.....	102-104
2.3.	Synthesis, characterisation.....	105-110
2.4.	Manipulation of gel-supported pre-catalyst.....	110-113
2.5.	Organocatalysis from gel-supported NHCs.....	113-116
2.6.	Conclusions.....	116-117
2.7.	References.....	117-119
2.8	Experimental section.....	120-135

## 2.1 Abstract

Owing to their broad modularity, polymeric versions of ionic liquids, referred to as poly(ionic liquids) (PILs), have attracted increasing attention as recyclable polymer-supported (pre)catalysts for various chemical transformations. Herein, an imidazolium-based statistical copolymer based on PIL (= coPIL) is specifically designed by free-radical copolymerization of styrene and 4-vinylbenzylethyl(benz)imidazolium chloride. A selective ion-exchange reaction can be subsequently achieved to incorporate bio-sourced difunctional sebacate-type counter-anions, causing the physical crosslinking of the coPIL precursor via electrostatic interactions between pendant imidazolium moieties and sebacate dianions. The as-obtained gel-type precursor exhibits a thermally latent behavior in THF, proving advantageous for a facile manipulation and practical use for organocatalysis. Upon heating, typically at 80 °C, interaction between the sebacate dianion and the proton in C2-position of the imidazolium moieties generates polymer-supported *N*-heterocyclic carbene units that act as catalytic active species towards NHC-organocatalyzed reactions, namely, benzoin condensation, transesterification and cyanosilylation. The PIL-based gel precursors can be restored, recycled and reused by simply cooling down, *i.e.* with no need of an external chemical reagent, due to the shift of the intramolecular equilibrium towards the formation of imidazolium sebacate-type units. Overall, this novel gel-type copolymeric platform shows a thermo-responsive behaviour, and proves particularly versatile for heterogeneous organocatalysis.

## NHC-mediated Organocatalysis



## 2.2 Introduction

Polymeric versions of molecular ionic liquids (ILs), namely, poly(ionic liquids) or polymerized ionic liquids, abbreviated as PILs, have attracted a great deal of attention as a new class of polyelectrolytes in the past two decades.<sup>1-5</sup> In PILs, cationically or anionically charged monomer units are covalently tethered to the polymer backbone, while counter-ions generally show high mobility. Typical organic cations of PILs include imidazolium, pyridinium and phosphonium groups, which can be associated to anions, such as  $\text{Cl}^-$ ,  $\text{Br}^-$ ,  $\text{BF}_4^-$ ,  $\text{CH}_3\text{SO}_3^-$ ,  $(\text{CF}_3\text{SO}_2)_2\text{N}^-$ ,  $\text{CH}_3\text{CO}_2^-$ , etc.<sup>6,7</sup> A very broad range of PILs with a large number of functionalities have been designed, either following a chain-growth or a step-growth polymerization pathway, sometimes involving a post-chemical modification step of a polymer precursor.<sup>3</sup> Subsequent exchange of the counter-ion, referred to as ion metathesis, provides another means to tune PIL properties.<sup>1</sup> PILs thus combine essential features of ILs, including a high  $\text{CO}_2$  solubility and a high ionic conductivity, with inherent qualities of polymers. These combined properties make PILs highly attractive in various

applications, for instance, in analytical chemistry,<sup>8</sup> gas separation,<sup>9</sup> precursors of porous structures and nanostructured carbon-based materials,<sup>10</sup> as solid ionic conductors for energy storage,<sup>11</sup> and for catalysis as well,<sup>3,12</sup> which is the topic of the present contribution.

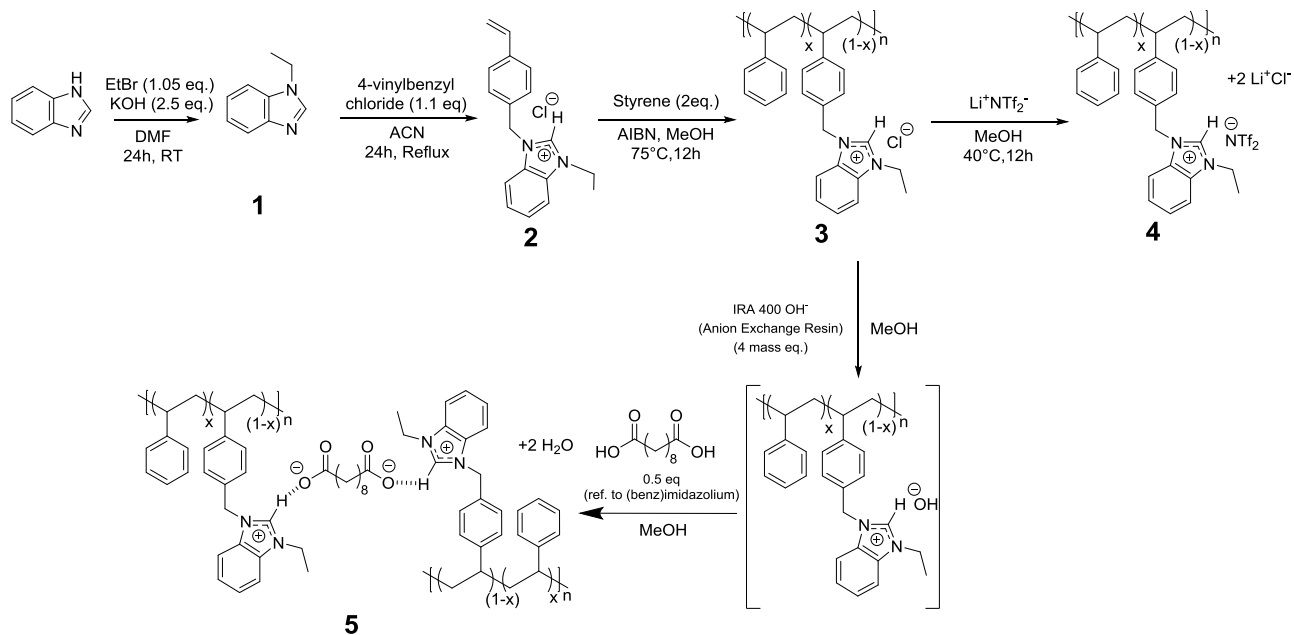
In the latter case, PILs eventually play two distinct roles. On the one hand, they can serve as efficient polymeric stabilizers of metal nanoparticles (NP), forming PILs@NP nanohybrids<sup>13</sup> in which the presence of PIL chains allows minimization of metal coalescence, providing efficient electrostatic + steric (= electrosteric) stabilization.<sup>14</sup> On the other hand, PILs can also operate as versatile polymeric supports of various types of catalysts.<sup>15,16</sup> For the general purpose of organocatalysis, PILs featuring sulfonic acid or proline moieties can for instance be employed as polymer-supported Brønsted acids and Lewis bases, respectively.<sup>3</sup> Furthermore, imidazolium-based PILs are handy precursors of polymer-supported *N*-heterocyclic carbenes (= polyNHCs).<sup>17-22</sup> Such polyNHCs can either be employed for reference organocatalyzed reactions of molecular chemistry, or serve as polymer-supported ligands for transition metals, *i.e.* forming polyNHC-metal derivatives,<sup>19</sup> by analogy with molecular NHC counterparts.<sup>23</sup> The latter polymer-supported metallic complexes have been advantageously employed to catalyze various organometallic reactions. In many of these catalysis applications, “task specific PILs” have been found to greatly facilitate separation, recovery and reuse, *i.e.* recycling of the polymer-supported (pre)catalysts – most often by simple filtration– and/or to improve stabilization of PILs@NP nanohybrids.<sup>13,24</sup>

In this context, imidazolium-based PILs featuring anions such as hydrogen carbonate,  $\text{HCO}_3^-$ ,<sup>20</sup> or acetate,  $\text{CH}_3\text{COO}^-$ ,<sup>21,22</sup> have been shown to serve as efficient air-stable progenitors of polyNHCs. This relates to the weakly basic character of both counter-anions interacting with the proton in C2-position of pendant imidazolium rings. Specifically, the imidazolium acetate-containing PILs exhibit a thermally latent behavior when employed in organocatalyzed reactions, and their catalytic activity can be turned on and off by a simple temperature increase and decrease.<sup>21,25</sup> Furthermore, such precursors can be readily recycled and reused, with no need of an exogenous chemical reagent, owing to the aforementioned

intramolecular and temperature-dependent interaction between the acetate and the imidazolium moiety.<sup>21</sup> This convenient way of masking and manipulating polymer-supported NHCs can be further exploited, as discussed in the present contribution. By incorporating a commercially available and bio-sourced dicarboxylic acid, namely, sebacic acid, imidazolium-based physically crosslinked PIL gels can be achieved, and be readily manipulated and recycled for various NHC-organocatalyzed reactions. Here we describe for the first time the design of gel-supported NHC precursors from imidazolium-based PILs that are physically crosslinked, *i.e.* the crosslinking process is reversible, through the formation of a bis-carboxylate-type reagent. In addition, such gel-supported NHC precursors exhibit a thermally latent behavior when used in selected organocatalyzed reactions, namely, benzoin condensation, transesterification and cyanosilylation, which enables the manipulation of the catalytic activity by a simple temperature change. Overall, this novel polymeric platform is proven to be particularly flexible for heterogeneous organocatalysis.

### 2.3 Synthesis, characterisation

A statistical copoly(ionic liquid) (coPIL), namely, polystyrene-*co*-poly(4-vinylbenzylethyl-(benz)imidazolium chloride), denoted as PS-*co*-Poly[ViEBIm]Cl (**3**), was prepared by free-radical copolymerization of 4-vinylbenzylethylbenzimidazolium chloride (**2**) and styrene, using AIBN as a radical source (**Scheme 2.1**). Benzimidazolium- rather than imidazolium-type units as reported in previous works<sup>22</sup> were introduced here, owing to their slightly higher proton-acidity in the C<sub>2</sub> position. It was thus expected that the equilibrium could be better shifted towards the formation of the NHC active species. After 12 h of reaction achieving 50% monomer conversion, the resulting copolymer was chemically modified into the coPIL **4** possessing non-coordinating anions, namely, bis(trifluoromethane)sulfonylimide (TFSI) = (CF<sub>3</sub>SO<sub>2</sub>)<sub>2</sub>N<sup>-</sup>, prior to characterisation by size exclusion chromatography (SEC) in THF containing 10 mM LiTFSI. This was readily achieved by anion exchange, as previously reported.<sup>26</sup> The as-obtained TFSI-containing coPIL **4** exhibited a unimodal distribution of molar masses with a dispersity ( $D_M$ ) of 1.35. Copolymer **3** then served as precursor for the synthesis of a physically crosslinked gel *via* anion metathesis converting **3** into PS-*co*-Poly[ViEBIm]Seb (**5**). The commercially available Amberlite® IRA-400 hydroxy resin was employed for this purpose, providing an entirely metal-free synthetic route to the imidazolium-based physically crosslinked gel (**Scheme 2.1**).<sup>30</sup> The anion exchange reaction indeed allowed substituting OH<sup>-</sup> counter-anions for Cl<sup>-</sup> ones and further introduction of sebacic acid yielded copolymer **5** and water as side product.<sup>31</sup>



**Scheme 2.2.** Synthetic route to (PS-*co*-Poly[ViEBIm]Cl) (**3**) by free radical copolymerization of [ViEBIm]Cl and styrene in methanol, followed by the synthesis of physically crosslinked (PS-*co*-Poly[ViEBIm]Seb) (**5**) by anion exchange. Synthesis of (PS-*co*-Poly[ViEBIm]TFSI)-1 (**4**) is also displayed.

In addition to being a non-fossil bio-based resource, sebacic acid contains two carboxylic acid groups with a similar  $pK_a \sim 4.6$  to that of acetic acid, *i.e.* the conjugated acid of acetate counter-anion that has been found to efficiently generate polymer-supported NHCs from imidazolium acetate-containing PILs.[20-21] Interestingly, copolymer **5** could be solubilized in DMSO, facilitating its structural characterization by NMR spectroscopy, whereas it was not soluble at all in solvents such as THF or acetonitrile. Near quantitative anion exchange reaction ( $\sim 95\%$ ) was achieved as determined by <sup>1</sup>H NMR spectroscopic analysis (**Figs. 2.1 & S2.1, S2.2**). Importantly, the characteristic proton of the C2-position of benzimidazolium units appearing at  $\delta = 10.5$  ppm in **3** was shifted downfield to  $\delta = 11.5$  ppm, as a consequence of the insertion of *bis*-carboxylate anions, while the signal at  $\delta \sim 12$  ppm that resulted from the resonance of the carboxylic acid protons of sebacic acid disappeared. This attested to the formation

of hydrogen bond-type interactions between C2-protons of the imidazolium moieties and the carboxylate anions.

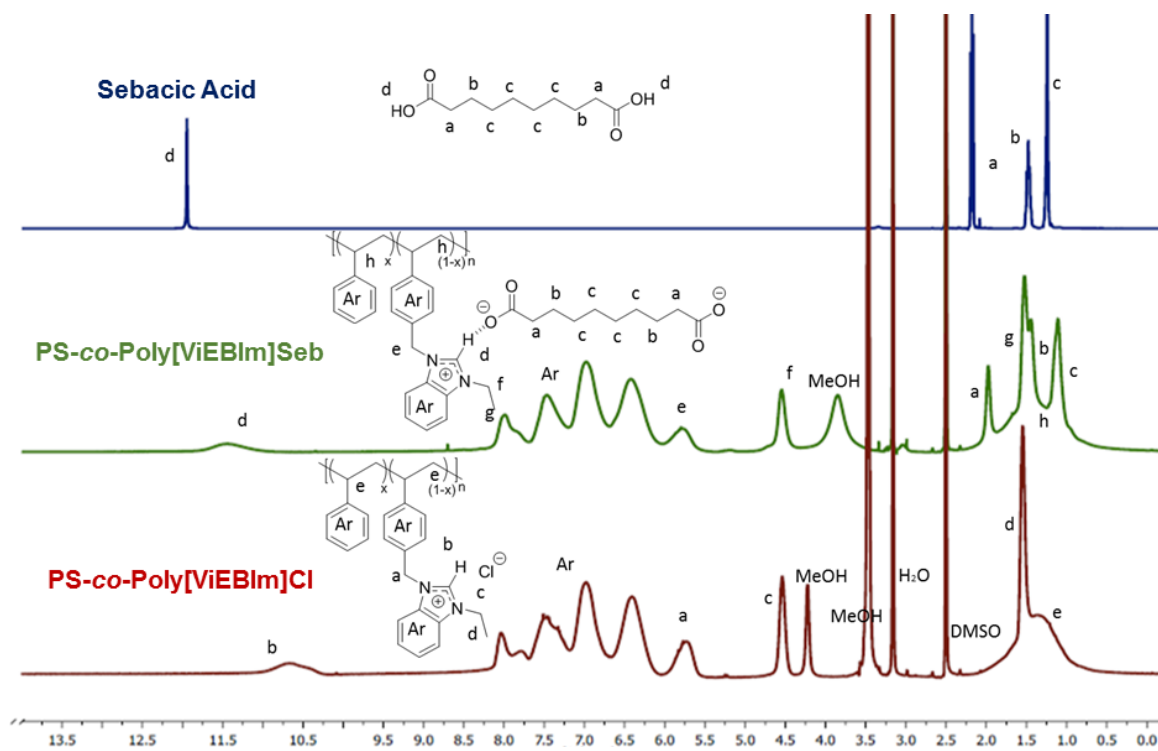


**Figure 2.1.**  $^1\text{H}$  NMR ( $\text{DMSO-}d_6$ ) showing the insertion of the sebacate forming the physical gel (PS-co-Poly[ViEBIm]Seb) (**5**) from (PS-co-Poly[ViEBIm]Cl) (**3**).

Characterization of the two copolymers by  $^{13}\text{C}$  NMR spectroscopy (**Fig. 2.2, 2.3**) confirmed the selective incorporation of sebacate anions, as evidenced by the presence of sebacate carboxylate single signal at  $\delta \sim 168$  ppm.



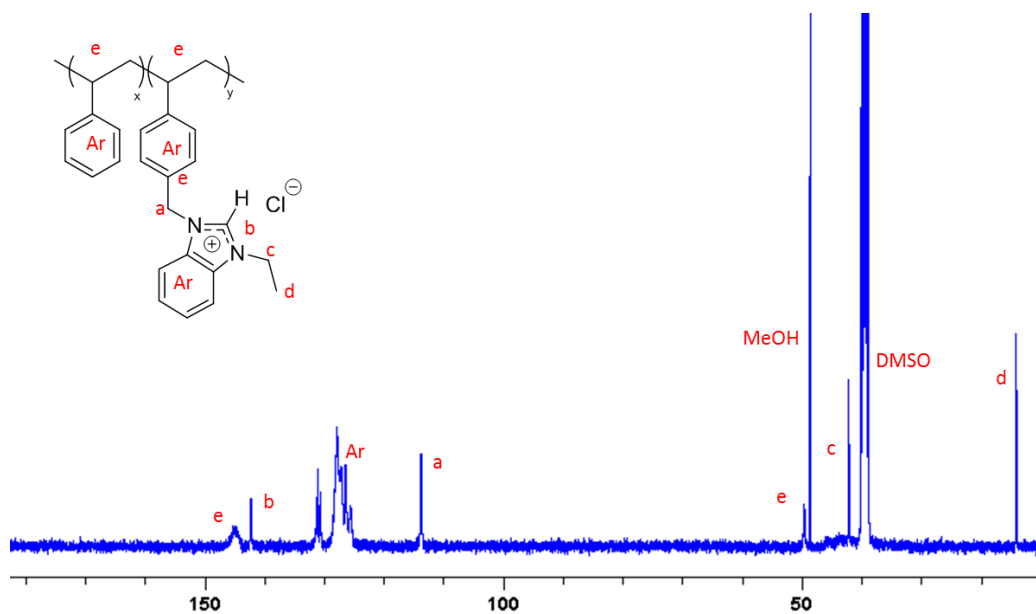


**Figure 2.2.** Synthesis of ((PS-co-Poly[ViEBIm]Cl)(3).  $^{13}\text{C}$  NMR spectra in  $\text{DMSO-}d_6$ .

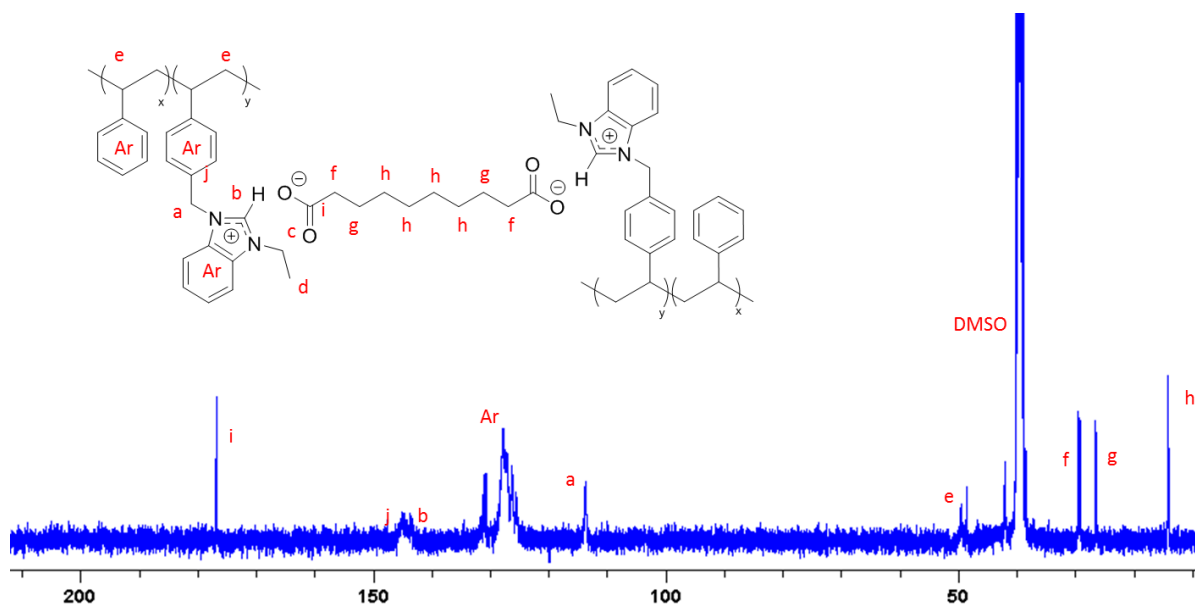


**Figure 2.3.** Synthesis of ((PS-co-Poly[ViEBIm]Seb)(5).  $^{13}\text{C}$  NMR spectra in  $\text{DMSO-}d_6$ .

This was also confirmed by FTIR spectroscopic analysis of copolymer **5**. The presence of a strong band at  $1640\text{ cm}^{-1}$  (**Fig. 2.4**) can be assigned to the C=O stretching of carboxylates. Thermogravimetric analysis also evidenced a significant change in the degradation profile, before and after anion exchange, the stability of the resulting imidazolium sebacate-containing coPIL **5** (**Fig. 2.5**) being lower than that of its parent copolymer **3** (5 wt.% loss observed at 200 and at 300 °C, respectively; see **Fig. S2.3-5**). This result is consistent with previous observations concerning imidazolium-type coPILs featuring acetate counter-anions.<sup>21</sup> This was also reflected in the  $T_g$  values, a  $T_g$  of 23 °C being determined for the chloride-containing precursor **3** (**Fig. S2.6, 7**), while coPIL **5** did not exhibit any clearly detectable  $T_g$ , likely due to its gel-like behavior.

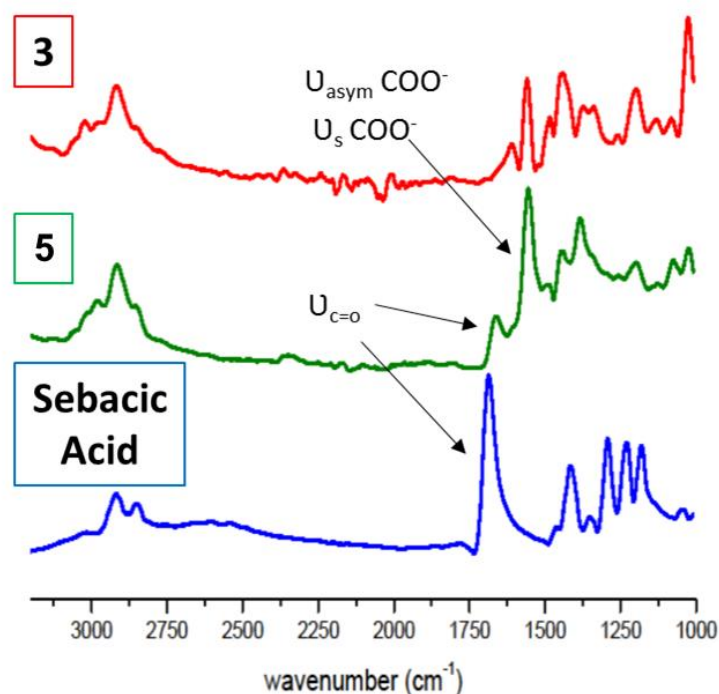


**Figure 2.4.** Synthesis of Polystyrene-co-poly(4-vinylbenzylethyl-(benz)imidazolium sebacate) (PS-co-Poly[ViEBIm]Seb) (**5**) overlay with starting materials .FTIR spectra.

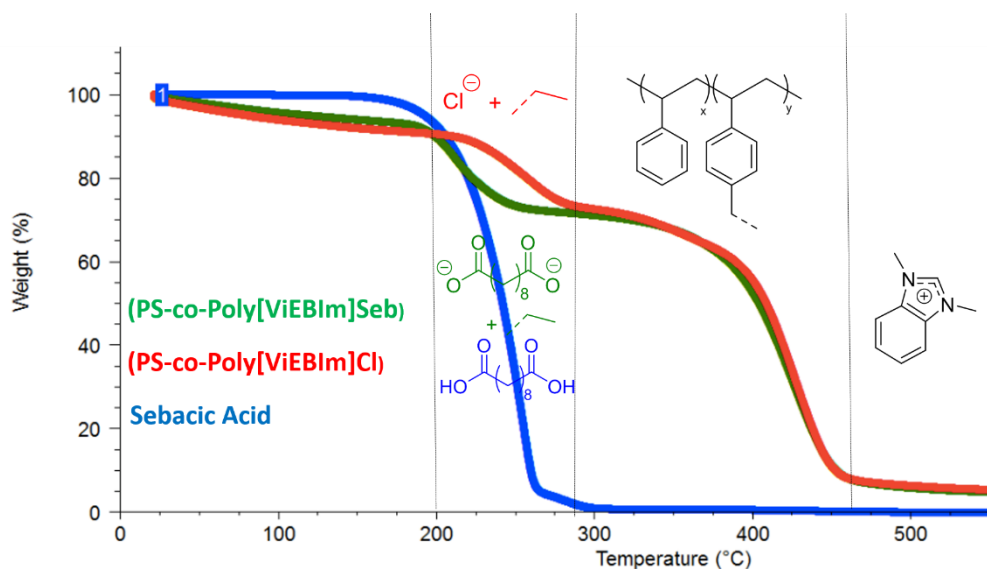


**Figure 2.5.** (PS-co-Poly[ViEBIm]Cl) (**3**), (PS-co-Poly[ViEBIm]Seb) (**5**) and Sebacic Acid plotting with corresponding proposed degradation steps for each case.

## 2.4 Manipulation of gel-supported pre-catalysts

Heating coPIL **5** at 80 °C in THF for 4 h led to an orange swollen gel (see **Fig. 2.6**). This bathochromic effect could be due to an increase in electron donating ability from C2-benzimidazolium as a consequence of basic carboxylate insertion, leading to higher-energy associated HOMO as similarly found in some carbene metal ligands.<sup>32</sup> After drying, this physically crosslinked copolymer exhibited a porous monolith structure featuring open pores with pore sizes in the range 100 nm-10 μm, as revealed by scanning electron microscopy (SEM; **Fig. 2.7**). Such porosity was expected to enhance the interfacial mass and energy exchange and be beneficial for catalytic performance of the monolith. Unfortunately, this hypothesis could not be confirmed by analysis of the surface area by Brunauer–Emmett–Teller (BET), owing to the high heterogeneous porosity.<sup>33</sup>

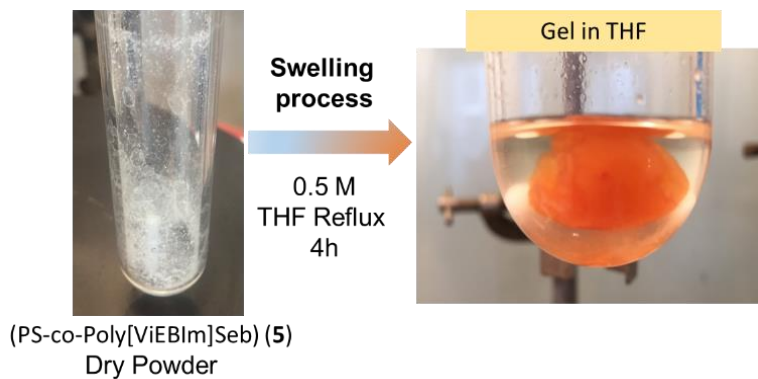


**Figure 2.6.** PS-*co*-Poly[ViEBIm]Seb (**5**) gelation procedure for heterogeneous supported catalyst synthesis in THF.

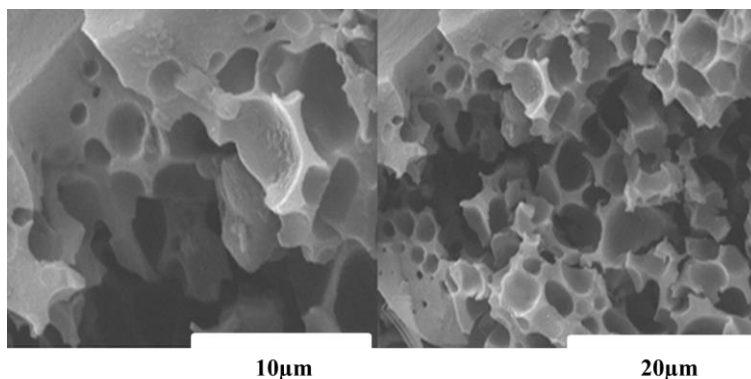
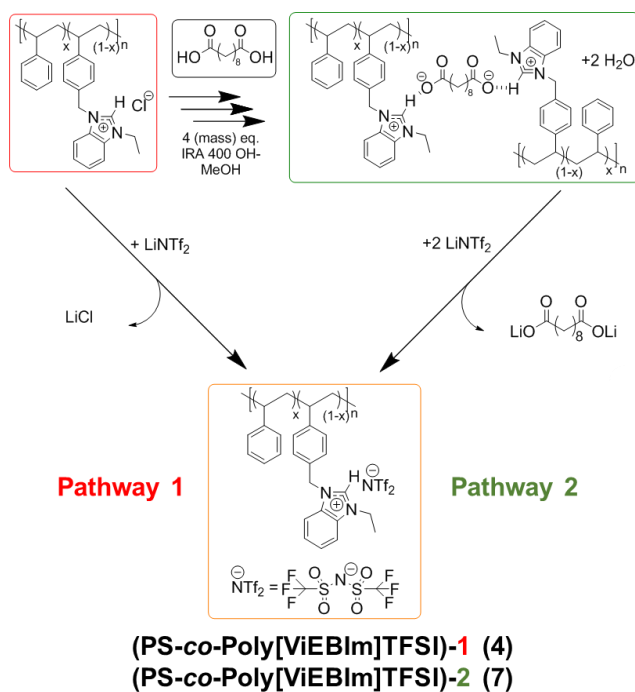


**Figure 2.7.** SEM pictures of polymer **5** as a heterogeneous catalyst support in organocatalysis showing pore sizes between 100 nm to 10  $\mu\text{m}$ .

Owing to the absence of covalent bonds in the gel deriving from copolymer **5**, *i.e.* to the formation of physical crosslinking points, this gel could be easily manipulated by further anion exchange, for instance, by using the non-coordinating TFSI anion.<sup>3,4</sup> In this way, the gel could be readily de-crosslinked, restoring a linear and eventually soluble copolymer (**7**; see **Scheme 2.2**). Addition of LiTFSI onto a methanol solution of gel **5** thus caused its gradual disruption, ultimately yielding a fully dissolved compound after 12 h of stirring. The corresponding  $^1\text{H}$  NMR spectra of both TFSI-containing copolymers **4** and **7**,

emanating from the same parent copolymer **3** proved to be identical (**Fig. S2.8**), validating the decrosslinking method by anion exchange.



**Scheme 2.2.** Two different pathways followed for the synthesis of TFSI anion-containing copolymers (**4**, **7**) supporting the anion-exchange mediated decrosslinking of the gel.

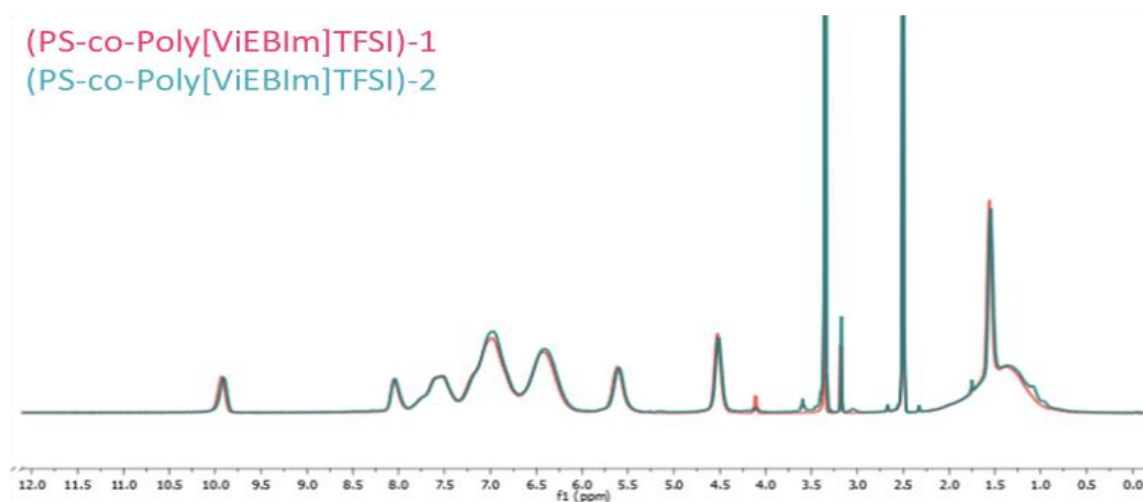


**Figure 2.8.**  $^1\text{H}$  NMR spectra overlay (PS-co-Poly[ViEBIm]TFSI)-1 (**4**) and (PS-co-Poly[ViEBIm]TFSI)-2 (**7**) in  $\text{DMSO-}d_6$ .

This was also evidenced by analysis by  $^{13}\text{C}$  and  $^{19}\text{F}$  NMR spectroscopy of compounds obtained after anion exchange (see **Fig. S2.8-13**). In addition, SEC analysis of copolymers **4** and **7** showed chromatograms that were almost superimposable (**Fig. 2.9**). In other words, these results did not show any evidence of degradation or side reactions or aggregation phenomena occurring during the post-chemical modification of coPIL derivatives.

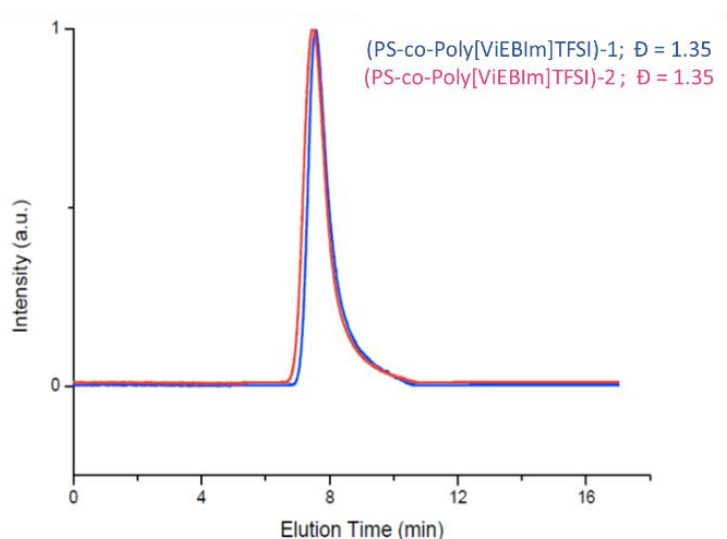


**Figure 2.9.** SEC traces corresponding (PS-co-Poly[ViEBIm]TFSI)-1 (**4**) (in blue) and (PS-co-Poly[ViEBIm]TFSI)-2 (**7**) (in red) using 10 mM LiTFSI THF as eluent using a RI detector.

## 2.5 Organocatalysis from gel-supported NHCs

The ability for coPIL-type gel **5** to *in situ* generate self-supported NHC units was first demonstrated by adding a large excess of  $\text{CS}_2$  as electrophilic reagent.<sup>21,34,35</sup> This chemical post-modification step led to copolymer **6** consisting of polymer-supported NHC- $\text{CS}_2$  betaine-type adducts. The  $^{13}\text{C}$  NMR spectrum of the as-obtained red solid compound showed the characteristic signal at  $\delta = 231$  ppm due to the dithiolate group ( $\text{CS}_2^-$ ; **Fig. 2.10**). Although this chemical transformation was not quantitative, as observed by signals corresponding to residual bis-carboxylate in  $^{13}\text{C}$  NMR analysis, it provided an indirect proof for

the *in situ* formation of polymer-supported NHCs. NHC-CS<sub>2</sub> adduct formation also allowed disrupting the physically crosslinked copolymer gel, leading to a copolymer-supported betaines soluble in methanol and corresponding free sebacic acid as by-product.

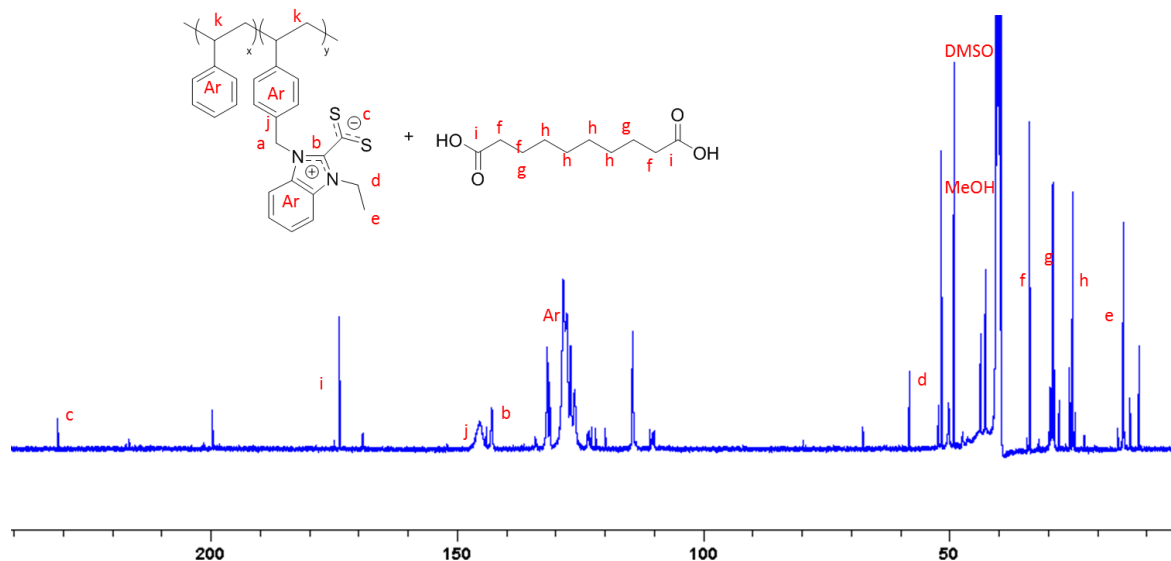
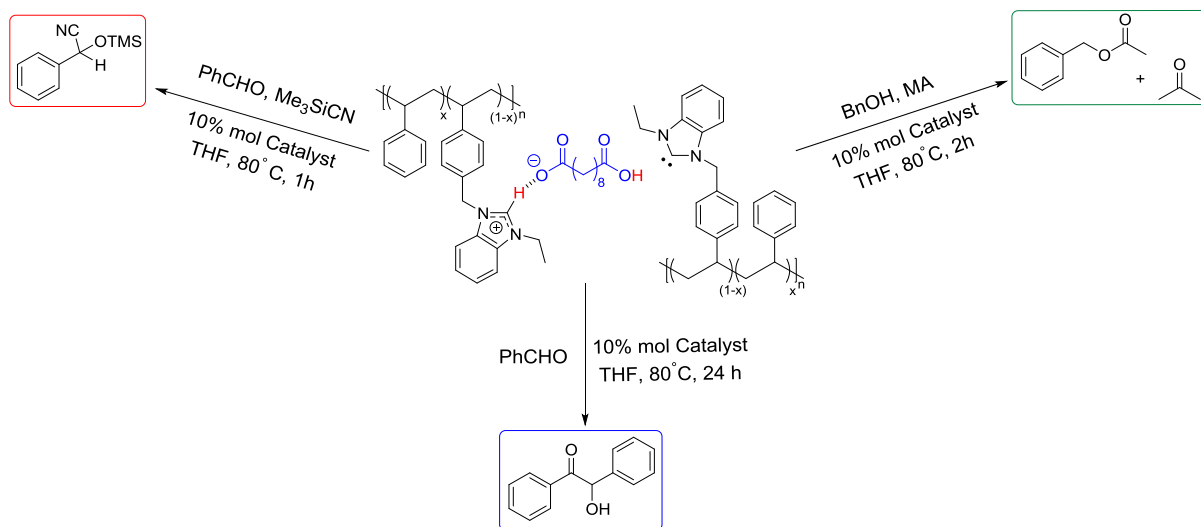


**Figure 2.10.** Synthesis of PS- co -poly(4-vinylbenzyl-NHC-CS<sub>2</sub>) (**6**) . <sup>13</sup>C NMR spectra in DMSO-*d*<sub>6</sub>.

Copolymer **5** was then employed as a gel-support of masked NHCs in three distinct benchmark NHC-organocatalyzed reactions, including benzoin condensation,<sup>36</sup> transesterification and cyanosilylation (**Scheme 2.3**). Of particular interest, NHC-type active species could be thermally activated with no need of an exogenous reagent, owing to the dynamic equilibrium between sebacate anions and protons of imidazolium units, enabling to switch the catalytic activity on and off upon heating and cooling, respectively. The temperature change also allowed us to easily recycle copolymer **5** and reuse it for subsequent catalytic cycles.



**Scheme 2.3.** Benzoin condensation, transesterification and cyanosilylation organocatalyzed by NHC-supported physically crosslinked porous gel under heterogeneous conditions.

Benzoin condensation was first implemented in THF using benzaldehyde as the substrate and 10% mol. of copolymer **5** referred to imidazolium moieties. For sake of comparison, the TFSI- and chlorine-containing copolymers, **4** and **3**, were also tested under the same conditions. However, no benzoin product was obtained with the two latter precursors, corroborating the non-innocent role of carboxylate counteranions to *in situ* generate catalytic polymer-supported NHCs. In contrast, conversions were in the range 65-70% after 24 h in five consecutive catalytic cycles when gel **5** was applied (**Fig. 2.11**). As discussed, the benzoin product was formed only upon heating at 80 °C, *i.e.* no catalytic activity was noted at RT, presumably owing to the shift of the equilibrium to the formation of inactive imidazolium units. With the benzoin product being soluble in THF, the coPIL-type gel precursor **5** could be simply recovered by filtration due to its insoluble character. It could further be stored and handled in air for several weeks, without apparent degradation. It could also be implemented both in the NHC-organocatalyzed transesterification and cyanosilylation reactions under heterogeneous conditions in THF (**Scheme 2.3**). The former reaction was performed using benzyl alcohol and vinyl acetate as substrates, which in presence of 10 mol % of **5** as gel-supported pre-catalyst, yielded benzyl acetate with conversions in the range 72-



90% during 5 different catalytic cycles (**Fig. 2.4**). Finally, when treating benzaldehyde with trimethylsilyl cyanide (TMSCN) in presence of gel **5**,  $\alpha$ -trimethylsilyloxy-phenylacetonitrile was obtained in near quantitative yields after 1h (**Fig. 2.4**). This series of results thus verified that **5** could be readily applied to a range of organocatalytic reactions and could be readily recycled, without any significant loss of catalytic activity (see Experimental for details). Overall, catalytic performances of coPIL gel **5** were found similar to those obtained with the different linear polymer-supported NHCs previously reported.<sup>19,21,22,24</sup>

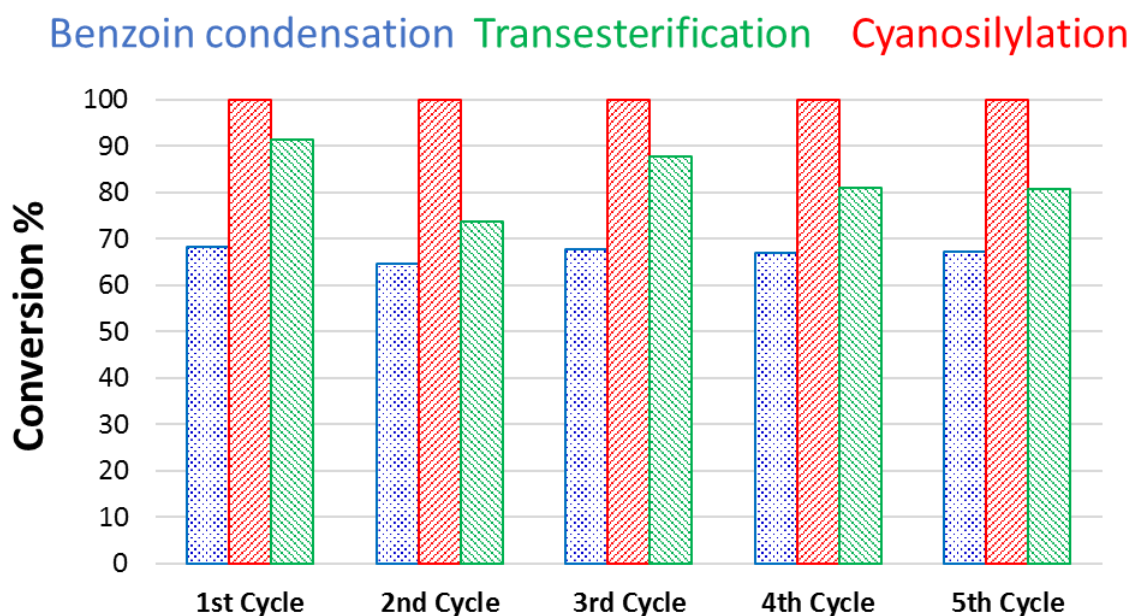


**Figure 2.11.** Different benzoin condensation, transesterification and cyanosilylation average conversions obtained after 5 cycles using 10 mol % amount of catalyst in heterogeneous conditions.

## 2.6 Conclusion

Air-stable physically crosslinked porous gels swollen in THF were designed for the purpose of organocatalysis under heterogeneous conditions. This was achieved by free-radical copolymerisation to obtain a statistical benzimidazolium-based styrenic-type copoly(ionic liquid), followed by a metal-free anion exchange reaction to incorporate dicarboxylate functions deriving from a biosourced dicarboxylic

acid, namely, sebacic acid. Difunctional sebacate anions eventually played a dual role of i) ionic crosslinker and ii) slightly basic internal counter-anion to *in situ* deliver catalytically active NHC species upon heating. The as-obtained gels could be reversibly manipulated to regenerate a linear coPIL by anion exchange using a monofunctional anion. These distinctive advantages allowed performing standard molecular heterogeneous NHC-organocatalysed reactions, leading to relatively high conversions in reaction products. The gel-like catalysts could be readily recycled up to 5 times, without any significant loss of catalytic activity or leaching. The catalytic performance could be tuned by thermal activation/deactivation, shifting the equilibrium either towards NHC active species, or to inactive imidazolium sebacate.

## 2.7 References

- 1 W. Qian, J. Texter and F. Yan, *Chemical Society Reviews*, 2017, **46**, 1124–1159.
- 2 D. Mecerreyes, *Progress in Polymer Science*, 2011, **36**, 1629–1648.
- 3 J. Yuan, D. Mecerreyes and M. Antonietti, *Progress in Polymer Science*, 2013, **38**, 1009–1036.
- 4 J. Yuan and M. Antonietti, *Polymer*, 2011, **52**, 1469–1482.
- 5 D. Mecerreyes, Ed., *Applications of Ionic Liquids in Polymer Science and Technology*, Springer Berlin Heidelberg, Berlin, Heidelberg, 2015.
- 6 A. Eftekhari and T. Saito, *European Polymer Journal*, 2017, **90**, 245–272.
- 7 A. S. Shaplov, D. O. Ponkratov and Y. S. Vygodskii, *Polymer Science Series B*, 2016, **58**, 73–142.
- 8 S. V. Muginova, D. A. Myasnikova, S. G. Kazarian and T. N. Shekhovtsova, *Analytical Sciences*, 2017, 261–274.
- 9 L. C. Tomé and I. M. Marrucho, *Chemical Society Reviews*, 2016, **45**, 2785–2824.

- 10 T.-P. Fellingner, A. Thomas, J. Yuan and M. Antonietti, *Advanced Materials*, 2013, **25**, 5838–5855.
- 11 F. N. Ajjan, M. Ambrogi, G. A. Tiruye, D. Cordella, A. M. Fernandes, K. Grygiel, M. Isik, N. Patil, L. Porcarelli, G. Rocasalbas, G. Vendramiento, E. Zeglio, M. Antonietti, C. Detrembleur, O. Inganäs, C. Jérôme, R. Marcilla, D. Mecerreyes, M. Moreno, D. Taton, N. Solin and J. Yuan, *Polymer International*, 2017, **66**, 1119–1128.
- 12 W. Qian, J. Texter, F. Yan, A. Sivaramakrishna, D. Mecerreyes, B. Sreedhar, N. R. Choudhury, C. B. Williams, T. E. Long, J. P. Tan, F. Winnik, S. Zauscher, I. Luzinov and S. Minko, *Chem. Soc. Rev.*, 2017, **46**, 1124–1159.
- 13 K. Manojkumar, A. Sivaramakrishna and K. Vijayakrishna, *Journal of Nanoparticle Research*, , DOI:10.1007/s11051-016-3409-y.
- 14 M.-R. Gao, J. Yuan and M. Antonietti, *Chemistry - A European Journal*, 2017, **23**, 5391–5403.
- 15 D. Enders, O. Niemeier and A. Henseler, *Chemical Reviews*, 2007, **107**, 5606–5655.
- 16 S. Ghazali-Esfahani, H. Song, E. Păunescu, F. D. Bobbink, H. Liu, Z. Fei, G. Laurenczy, M. Bagherzadeh, N. Yan and P. J. Dyson, *Green Chemistry*, 2013, **15**, 1584.
- 17 S. Naumann and M. R. Buchmeiser, *Catalysis Science & Technology*, 2014, **4**, 2466.
- 18 M. Fevre, J. Pinaud, Y. Gnanou, J. Vignolle and D. Taton, *Chemical Society Reviews*, 2013, **42**, 2142.
- 19 P. Coupillaud, J. Vignolle, D. Mecerreyes and D. Taton, *Polymer*, 2014, **55**, 3404–3414.
- 20 P. Coupillaud, J. Pinaud, N. Guidolin, J. Vignolle, M. Fevre, E. Veaudecenne, D. Mecerreyes and D. Taton, *Journal of Polymer Science Part A: Polymer Chemistry*, 2013, n/a-n/a.
- 21 R. Lambert, P. Coupillaud, A.-L. Wirotius, J. Vignolle and D. Taton, *Macromolecular Rapid Communications*, 2016, **37**, 1143–1149.
- 22 R. Lambert, A.-L. Wirotius and D. Taton, *ACS Macro Letters*, 2017, **6**, 489–494.
- 23 S. Díez-González, N. Marion and S. P. Nolan, *Chemical Reviews*, 2009, **109**, 3612–3676.

- 24 D. Kuzmich, P. Coupillaud, Y. Men, J. Vignolle, G. Vendramineto, M. Ambrogi, D. Taton and J. Yuan, *Polymer*, 2014, **55**, 3423–3430.
- 25 O. Holloczki, D. Gerhard, K. Massone, L. Szarvas, B. Nimeth, T. Veszprimi and L. Nyulaszi, *New Journal of Chemistry*, 2010, **34**, 3004.
- 26 H. He, M. Zhong, B. Adzima, D. Luebke, H. Nulwala and K. Matyjaszewski, *Journal of the American Chemical Society*, 2013, **135**, 4227–4230.
- 27 H. Long and B. Pivovar, *The Journal of Physical Chemistry C*, 2014, **118**, 9880–9888.
- 28 A. G. Wright, T. Weissbach and S. Holdcroft, *Angewandte Chemie International Edition*, 2016, **55**, 4818–4821.
- 29 O. Holloczki, P. Terleczyk, D. Szieberth, G. Mourgas, D. Gudat and L. Nyulaszi, *Journal of the American Chemical Society*, 2011, **133**, 780–789.
- 30 P. Barbaro and F. Liguori, *Chemical Reviews*, 2009, **109**, 515–529.
- 31 N. Pothanagandhi, A. Sivaramakrishna and K. Vijayakrishna, *Polym. Chem.*, 2017, **8**, 918–925.
- 32 V. A. Krylova, P. I. Djurovich, B. L. Conley, R. Haiges, M. T. Whited, T. J. Williams and M. E. Thompson, *Chem. Commun.*, 2014, **50**, 7176–7179.
- 33 Y. Zhang, B. Wang, E. H. M. Elageed, L. Qin, B. Ni, X. Liu and G. Gao, *ACS Macro Letters*, 2016, **5**, 435–438.
- 34 L. Delaude, *European Journal of Inorganic Chemistry*, 2009, **2009**, 1681–1699.
- 35 L. Delaude, X. Sauvage, A. Demonceau and J. Wouters, *Organometallics*, 2009, **28**, 4056–4064.
- 36 R. S. Menon, A. T. Biju and V. Nair, *Beilstein Journal of Organic Chemistry*, 2016, **12**, 444–461.

## 2.8 Experimental section

### Instrumentation

$^1\text{H}$  NMR,  $^{13}\text{C}$  NMR and  $^{19}\text{F}$  NMR spectra were recorded on a Bruker AC-400 spectrometer in appropriate deuterated solvents. All  $^{13}\text{C}$  NMR measurements were carried out at 298 K on a Bruker Avance III 400 spectrometer operating at 100.7 MHz and obtained over 6144 scan with a  $30^\circ$  flip angle ( $90^\circ$  pulse =  $9\mu\text{s}$ ), an acquisition time of 1.3s, a relaxation delay of 3 s and 65 k data points. All HSQC (heteronuclear single quantum correlation) measurements were also performed at 298 K on a Bruker Avance III HD 400 spectrometer operating at 400,33 MHz. THF soluble polymers were previously modified inserting TFSI as counter-anion and their molar masses were determined by size exclusion chromatography (SEC) in THF in presence of 10mM LiTFSI as eluent (1 mL / min ) at  $40^\circ\text{C}$  using both refractometric (RI) and UV detectors (Varian).<sup>26</sup> Analyses were performed using a three-column set of TSK gel TOSOH (G4000, G3000, G2000 with pore sizes 20, 75, 200 Å respectively, connected in series). A Bruker spectrometer was used for ATR-FTIR analysis. Differential scanning calorimetry (DSC) measurements were carried out with a Q1000 apparatus from TA Instruments. DSC experiments were performed with aluminum sealed pans. A constant heating/cooling rate of  $10^\circ\text{C}/\text{min}$  and gas purging ( $\text{N}_2$ ) at a flow rate of 100mL/min was used for all experiments. Thermogravimetric analyses (TGA) were performed using a TA instrument Q50 under a nitrogen atmosphere, from temperature ( $10^\circ\text{C} / \text{min}$ ) to  $800^\circ\text{C}$ . The weight loss was recorded as a function of temperature. The macroporous gel was examined using scanning electron microscopy (SEM) in a JEOL JSM-6360 microscope operating at an accelerating voltage of 20kV and 5000/10000 magnification.

### Materials

Benzimidazole ( $\geq 95\%$ ), ethyl bromide (99%), 4-vinylbenzyl chloride (90%), lithium bis(trifluoromethane)sulfonylimide and Amberlite® IRA400 (hydroxide form) were obtained from

Aldrich and cleaned by passing a mixture of water/methanol prior to use. Azobis(2-methylpropionitrile) (AIBN, 99%) was received from Aldrich and was recrystallized from methanol. Styrene and 4-vinylbenzylchloride (90%) were dried over CaH<sub>2</sub> and distilled prior to use. Sebacic acid (98%) and potassium hydroxide (KOH) were obtained from Alfa Aesar and benzimidazole (99%) was obtained from TCI and used as received. Tetrahydrofuran (THF) was distilled over Na/benzophenone. Ethyl acetate, acetonitrile and methanol (99.7%, Aldrich) were used without further purification. Pre-wetted dialysis tubing with a cut-off of 10 kDa (Spectra/Por® 6 Standard RC) was obtained from Spectrumlabs.

## General Procedures

**Synthesis of *N*-ethylbenzimidazole (1).** Benzimidazole (8 g, 67.72 mmol) was dissolved in DMF (45 mL) and (7.6 g, 135 mmol) of potassium hydroxide were added. The solution was stirred for 1 hour and 5.5 mL (74.5 mmol) of ethyl bromide were added dropwise. After stirring at RT for 24 h, the solution was diluted in 100 mL of water and extracted with chloroform (3x25 mL). Organic phases were combined, dried over MgSO<sub>4</sub> and evaporated, yielding a yellow viscous oil (yield: 80%; 7.9 g). <sup>1</sup>H NMR (DMSO-*d*<sub>6</sub>):  $\delta$  = 8.25 (s, 1H, N-CH-N), 7.69-7.20 (m, 4H, aromatics), 4.12 (t, 2H, N-CH<sub>2</sub>-CH<sub>3</sub>), 1.32 (t, 3H, -CH<sub>3</sub>). <sup>13</sup>C NMR (DMSO-*d*<sub>6</sub>):  $\delta$  = 144.5, 143.7, 123, 119.8, 110, 43.1, 14.8.

### ***Synthesis of 4-vinylbenzylethyl(benz)imidazolium chloride ([ViEBIm]Cl) by quaternization (2).***

1-vinyl-4-chloromethylstyrene (8.37 mL, 59.4 mmol) and (7.9 g, 54 mmol) of **1** was dissolved in acetonitrile (20 mL) and heated to 80 °C for 24 h. The solvent was evaporated and the resulting powder was washed with diethyl ether. The product was dried for 8h under vacuum, yielding a white powder (yield 77%, 12.41 g). <sup>1</sup>H NMR (DMSO-*d*<sub>6</sub>):  $\delta$  = 9.68 (s, 1H, N-CH-N), 8.12-7.14 (m, 8H, aromatics), 6.72 (dd, 1H, Ph-CH-CH<sub>2</sub>), 5.95 (s, 2H, Ph-CH<sub>2</sub>-N), 5.76 (d, 1H, CH=CH<sub>2</sub>), 5.25 (d, 1H, CH=CH<sub>2</sub>), 4.15 (dd, 2H, N-CH<sub>2</sub>-CH<sub>3</sub>), 1.31 (t, 3H, -CH<sub>2</sub>-CH<sub>3</sub>). <sup>13</sup>C NMR (DMSO-*d*<sub>6</sub>):  $\delta$  = 142, 136.2, 135, 133.8, 131.5, 128.8, 128.7, 126.5, 126.3, 114.1, 113.5, 58.6, 44.5, 14.9.

**Synthesis of polystyrene-co-poly(4-vinylbenzylethyl-(benz)imidazolium chloride) (PS-co-Poly[ViEBIm]Cl) (3) by free-radical copolymerization.** 5 g (0.167 mmol) of **2**, 3.84 mL (0.335 mmol) of styrene, 41 mg of AIBN and 20 mL of dry methanol were added in a Schlenk tube. Five freeze-thaw pump cycles were performed and the solution was stirred at 75 °C for 12h. The resulting compound was purified by two dialyses against methanol (10kDa MWCO). (Yield: 38%; final composition: 63% styrene / 37% of **2**). <sup>1</sup>H NMR (DMSO-*d*<sub>6</sub>): δ=10.5 (br, 1H, N-CH-N), 8.22-5.68 (br, 16.5, aromatics), 5.9-5.5 (br, 2H, Ph-CH<sub>2</sub>-N), 4.6-4.4 (br, 2H, -CH<sub>2</sub>-CH<sub>3</sub>), 2.1-0.9 (br, 12.7H, CH-CH<sub>2</sub> backbone, CH<sub>3</sub> ethyl chain).

**Synthesis of Polystyrene-co-poly(4-vinylbenzylethyl-(benz)imidazolium sebacate) (PS-co-Poly[ViEBIm]Seb)(5) by anion metathesis using Amberlite resin.** 4 g of Amberlite® IRA 400 OH<sup>-</sup> were taken in a round bottom flask and agitated for 12 h in a 50:50 MeOH:H<sub>2</sub>O solution. Finally, the resin was filtered and air-dried. The resin was suspended in 15mL of MeOH and 1g of polymer **3** was added to the solution and stirred for 10 minutes. Sequential addition of 0.215 g (0.106 mmol) of sebacic acid were added to the solution and stirred for 15 minutes. Note that addition in sequence was preferred owing to the instability known to OH<sup>-</sup> anions in imidazolium derivatives that can lead to hydrolysis.<sup>27-29</sup> The solution was filtered and dried under vacuum to yield a yellowish powder (yield 94%). <sup>1</sup>H NMR (DMSO-*d*<sub>6</sub>): δ=11.4 (br, 1H, N-CH-N), 8.22-5.68 (br, 16.5, aromatics), 6-5.5 (br, 2H, Ph-CH<sub>2</sub>-N), 4.6-4.4 (br, 2H, -CH<sub>2</sub>-CH<sub>3</sub>), 2.2-0.9 (br, 12.7H, CH-CH<sub>2</sub> backbone, CH<sub>3</sub> ethyl chain, CH<sub>2</sub>-CH<sub>2</sub> sebacate, CH<sub>2</sub>-CH<sub>3</sub> sebacate).

**Synthesis of gel-supported precatalysts.** 0.251 g of **5** were dried by azeotropic distillation in dry THF (3x5 mL) in a Schlenk tube. After, polymer **5** powder was suspended in THF (0.5 M) and heated at 80 °C for 4 hours, yielding a physically-crosslinked insoluble orange gel (yield 99%).

**Synthesis of PS-co-poly(4-vinylbenzyl-NHC-CS<sub>2</sub>) (6).** In a Schlenk tube, 41 mg of gelled **5** were suspended in 5 mL of dry MeOH. 0.5 mL (8.3mmol) of CS<sub>2</sub> were then added and the mixture was stirred

at 80 °C for 48h when the formed **6** became soluble in the solvent (MeOH) dissolving the gel. The solvent and the excess of CS<sub>2</sub> were evaporated, forming a reddish powder (PS-*co*-Poly[ViEBIm]CS<sub>2</sub>). <sup>1</sup>H NMR (DMSO-*d*<sub>6</sub>): δ= 12.3-11.8 (br, 1H, -COOH) 8.22-5.98 (br, 16.5, aromatics), 6-5.5 (br, 2H, Ph-CH<sub>2</sub>-N), 4.6-4.4 (br, 2H, -CH<sub>2</sub>-CH<sub>3</sub>), 3-0.8 (br, 12.7H, CH-CH<sub>2</sub> backbone, CH<sub>3</sub> ethyl chain, CH<sub>2</sub>-CH<sub>2</sub> sebacic acid, CH<sub>2</sub>-CH<sub>3</sub> sebacic acid) <sup>21</sup>

**Benzoin Condensation.** In a typical experiment, 0.251 g (0.446 mmol) of gelled **5**, a portion of 4 mL of THF was added and 0.455 mL (4.46 mmol) of benzaldehyde was added in a Schlenk tube. The reaction mixture was stirred for 24 h at 80 °C. The mixture was allowed to cool down to room temperature, and the liquid phase removed and analysed. This phase was analysed by <sup>1</sup>H NMR in DMSO-*d*<sub>6</sub>. Benzoin conversion was determined by <sup>1</sup>H NMR in DMSO-*d*<sub>6</sub> by comparing the integral value of the aldehyde signal of benzaldehyde (d, 10ppm) with the one of the -CH- benzoin signal (d, 6 ppm) (**Fig. S14**). The swollen gel was dried and cleaned with dry THF at 40 °C twice. Finally, the same quantity of dry THF was added enabling the next run of catalysis. Note that every cycle the polymer-supported catalyst was weight and no loss of catalyst was observed.

**Transesterification.** In a typical experiment, 0.170 g (0.3 mmol) of **5** were previously gelled and a portion of 4 mL of THF was added. Then 0.32 mL (3 mmol) of benzyl alcohol and 0.30 mL (3.27 mmol) vinyl acetate were added. The mixture was stirred for 2 h at 80 °C. After cooling down to room temperature, the liquid phase was retired and analyzed by <sup>1</sup>H NMR in DMSO-*d*<sub>6</sub> and conversion calculated comparing the integral value of the -CH<sub>2</sub>- benzyl alcohol signal (4.5 ppm) to that of the -CH<sub>2</sub>- benzyl acetate signal (d, 5ppm) (**Fig. S2.15**). The swollen gel was dried and cleaned with dry THF at 40 °C two times. Finally, the same quantity of dry THF was added to perform next catalytic run using the same catalyst.

**Cyanosilylation.** In a typical experiment, 0.1 g (0.176 mmol) of **5** were previously gelled in THF as explained in **Fig. 2.2.**, a portion of 4mL THF was included and then 0.18 mL (1.76 mmol) of benzaldehyde



and 0.24 mL (1.9 mmol) trimethylsilyl cyanide (TMSCN) were added. The mixture was stirred for 1 h at 80 °C. After cooling down to room temperature, the liquid phase was retired and analyzed by <sup>1</sup>H NMR in DMSO-*d*<sub>6</sub> and conversion of α-trimethylsilyloxy-phenylacetonitrile calculated comparing the integral value of aldehyde signal (10 ppm) to that of the –CH– cyanide product (d, 5.5 ppm). The swollen gel was dried and cleaned with dry THF at 40 °C twice. The same amount of dry THF was added to proceed to next catalytic run. (See **Fig. S2.16**).

*Procedure for reversibility of gels.* 0.1g (0.176mmol) of **5** previously gelled in THF was dried under vacuum. Gel **5** was suspended in methanol afterwards and heated at 40 °C. Then, 0.505 g (1.76 mmol) of LiTFSI were added and let stir overnight. The polymer ((PS-*co*-Poly[ViEBIm]TFSI)-2 (**7**)) became insoluble after the anion metathesis. The excess of methanol and LiTFSI was removed and the precipitated polymer washed with water and ((PS-*co*-Poly[ViEBIm]TFSI)-2 (**7**)) recovered (yield 71%). The same procedure was applied to (PS-*co*-Poly[ViEBIm]Cl) (**3**) in order to obtain the (PS-*co*-Poly[ViEBIm]TFSI)-1 (**4**) as well (yield 80%).

## Related spectra

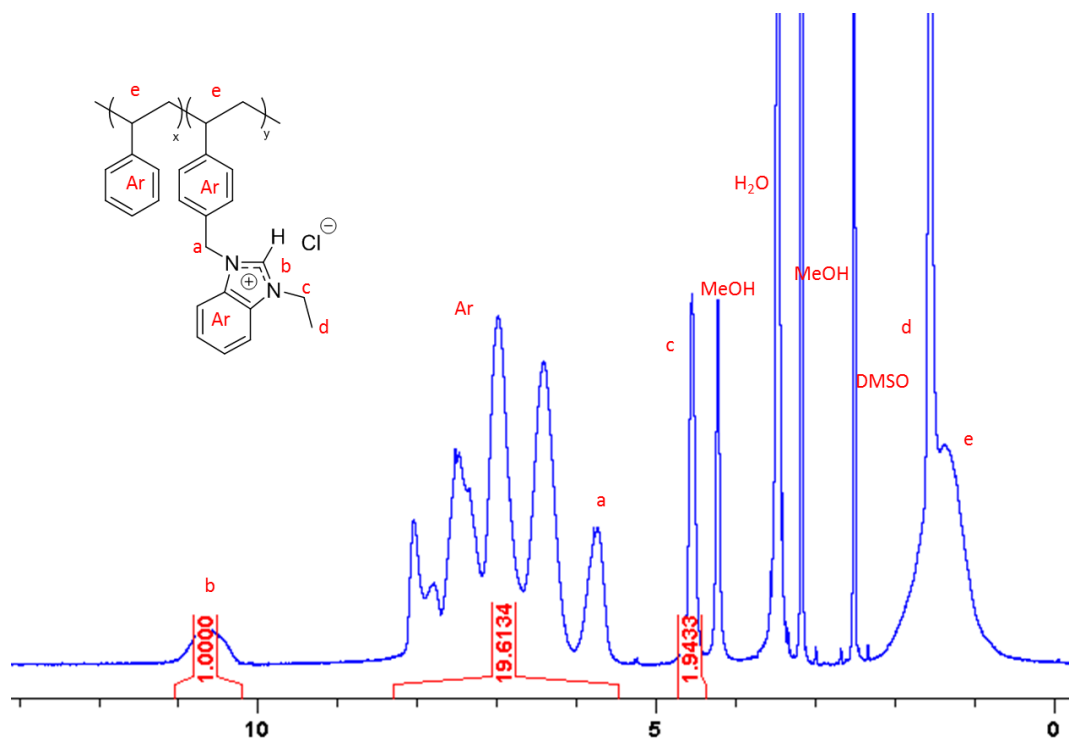


**Figure S2.1.** Synthesis of Polystyrene-co-poly(4-vinylbenzylethyl-(benz)imidazolium chloride) (PS-co-Poly[ViEBIm]Cl) (3).  $^1\text{H}$  NMR spectra in  $\text{DMSO-}d_6$ .

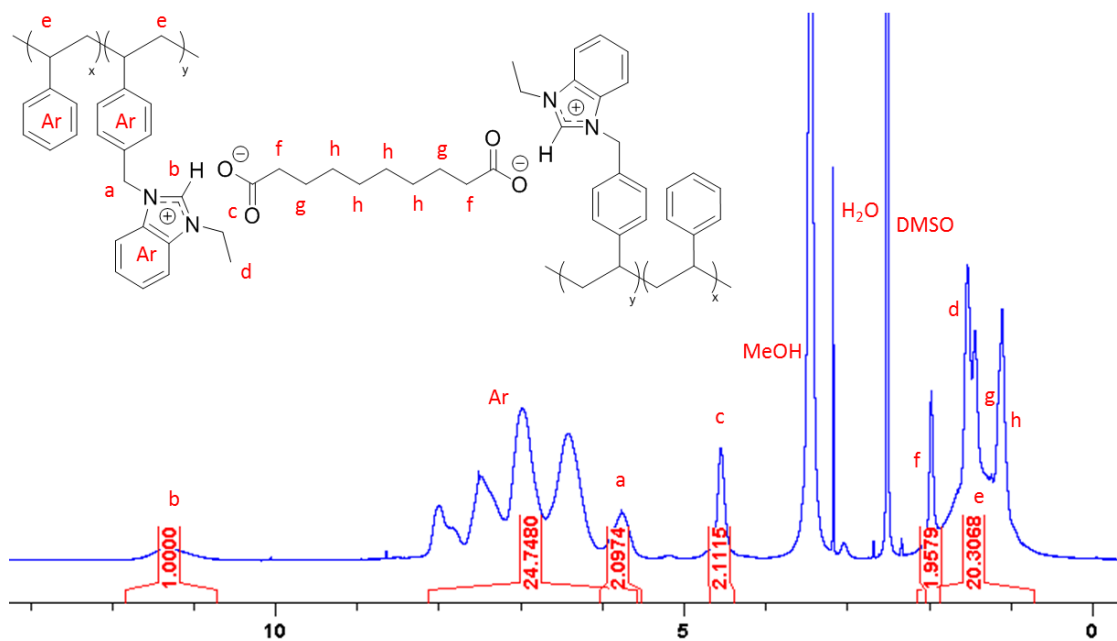


**Figure S2.2.** Synthesis of Polystyrene-co-poly(4-vinylbenzylethyl-(benz)imidazolium sebacate) (PS-co-Poly[ViEBIm]Seb)(5) .  $^1\text{H}$  NMR spectra in  $\text{DMSO-}d_6$ .

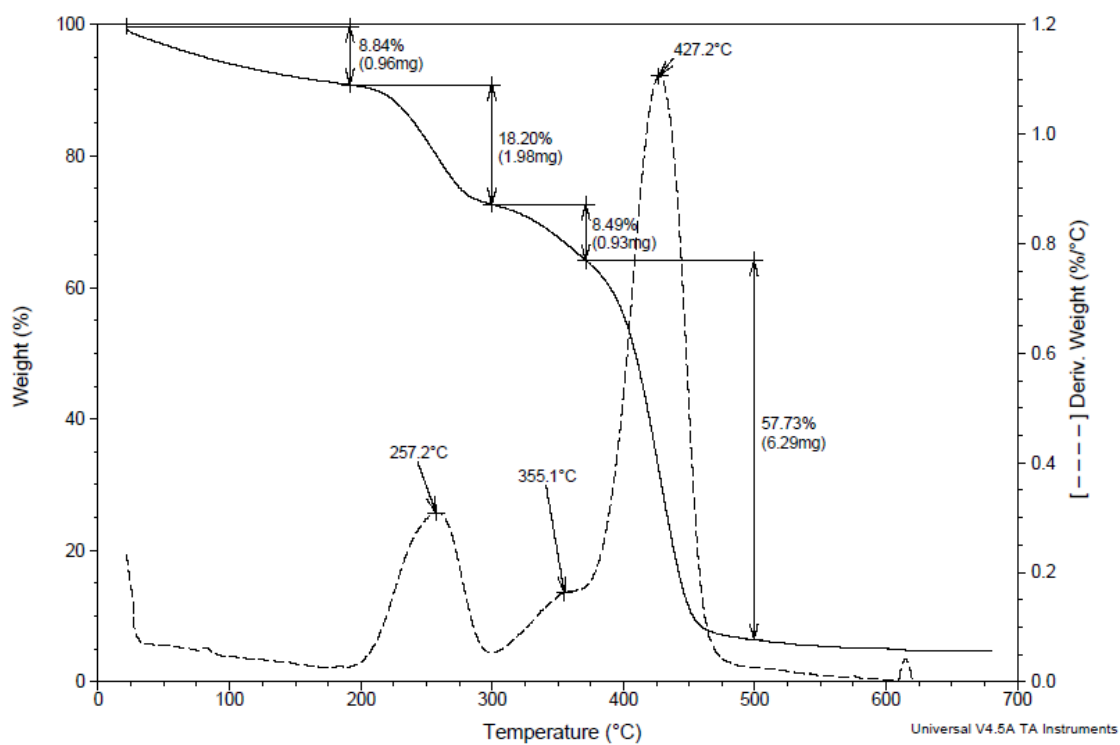


**Figure S2.3.** TGA plot of (PS-co-Poly[ViEBIm]Cl) (3).

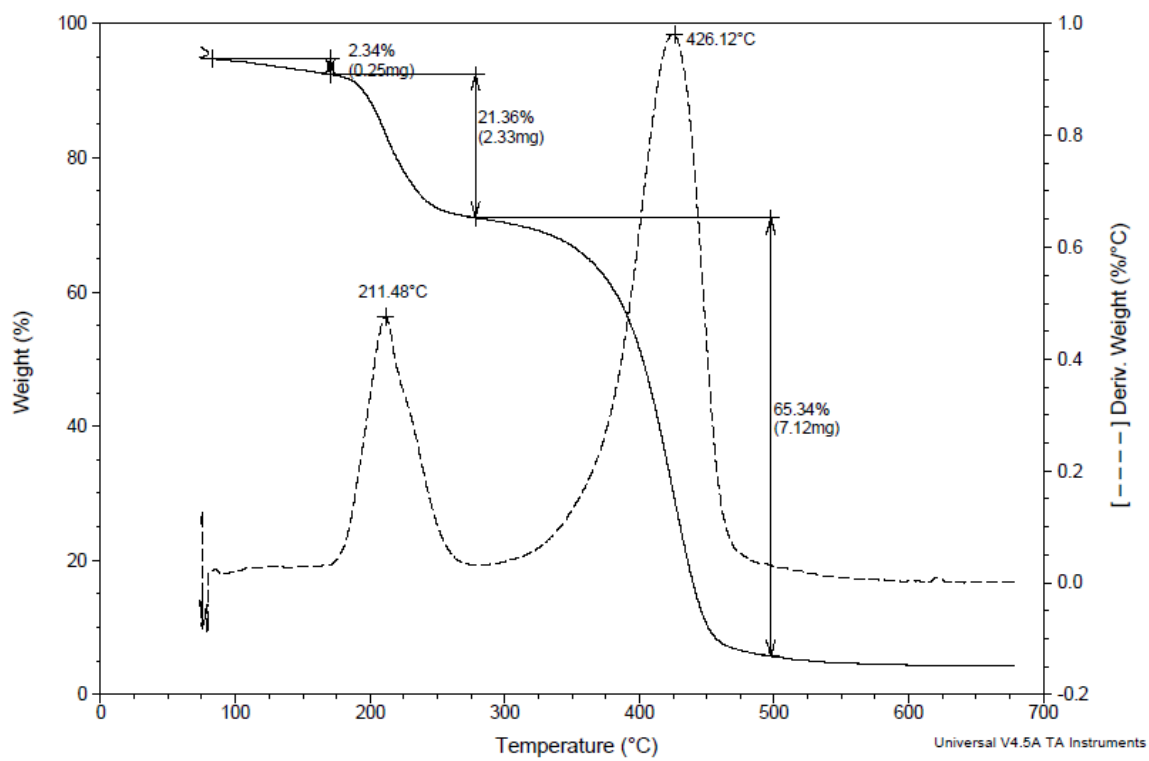


**Figure S2.4.** TGA plot of (PS-co-Poly[ViEBIm]Seb) (5).

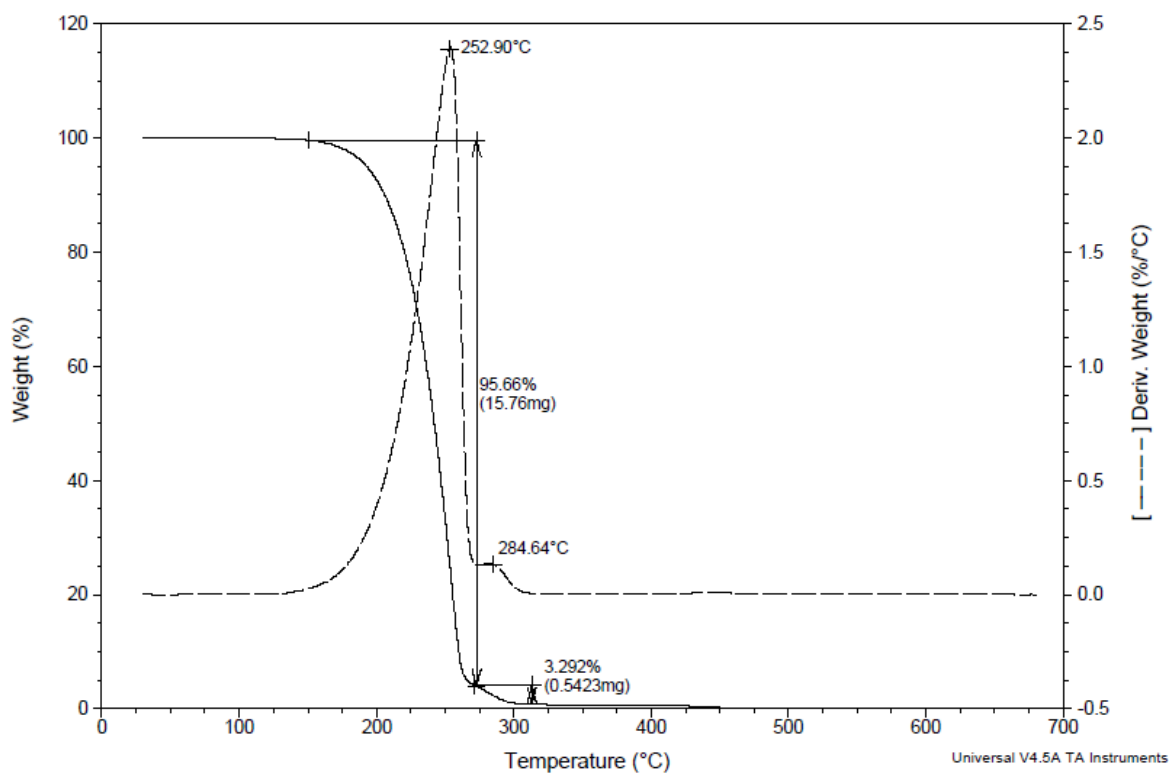


**Figure S2.5.** TGA plot of Sebacic Acid.

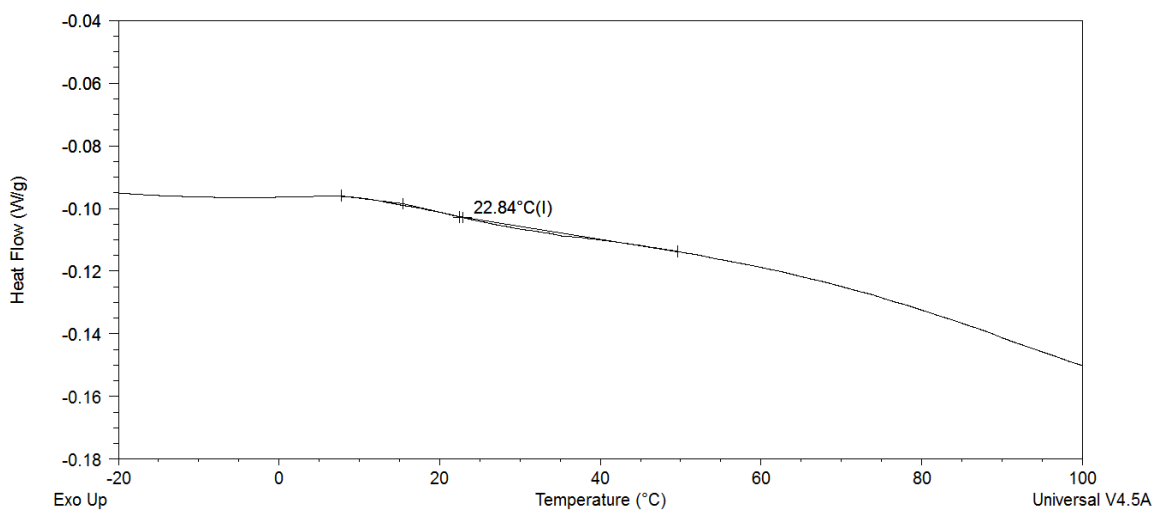


**Figure S2.6.** DSC plot of (PS-co-Poly[ViEBIm]Cl) (3).

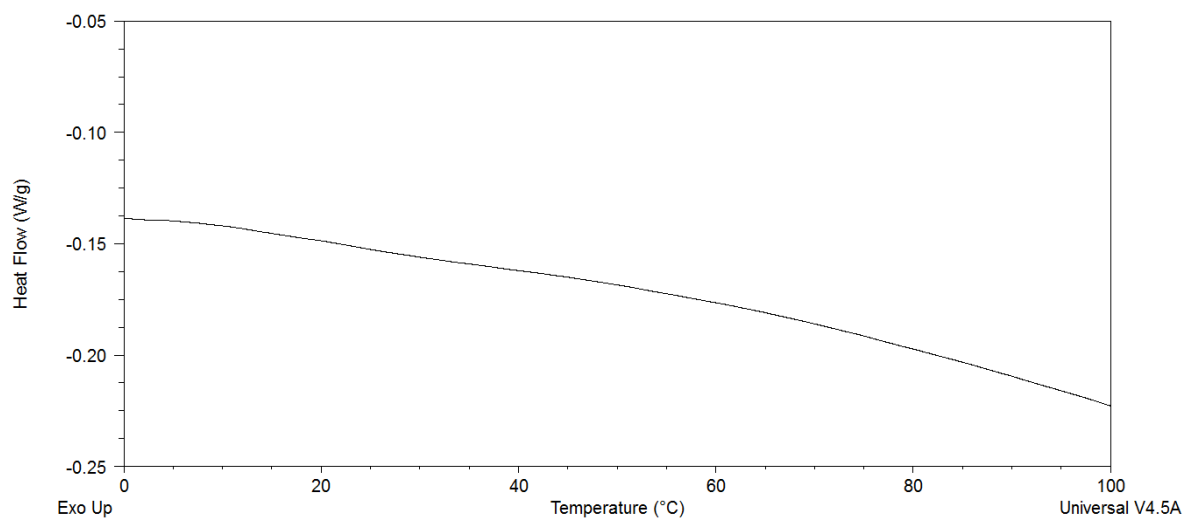


**Figure S2.7.** DSC plot of (PS-co-Poly[ViEBIm]Seb) (**5**)

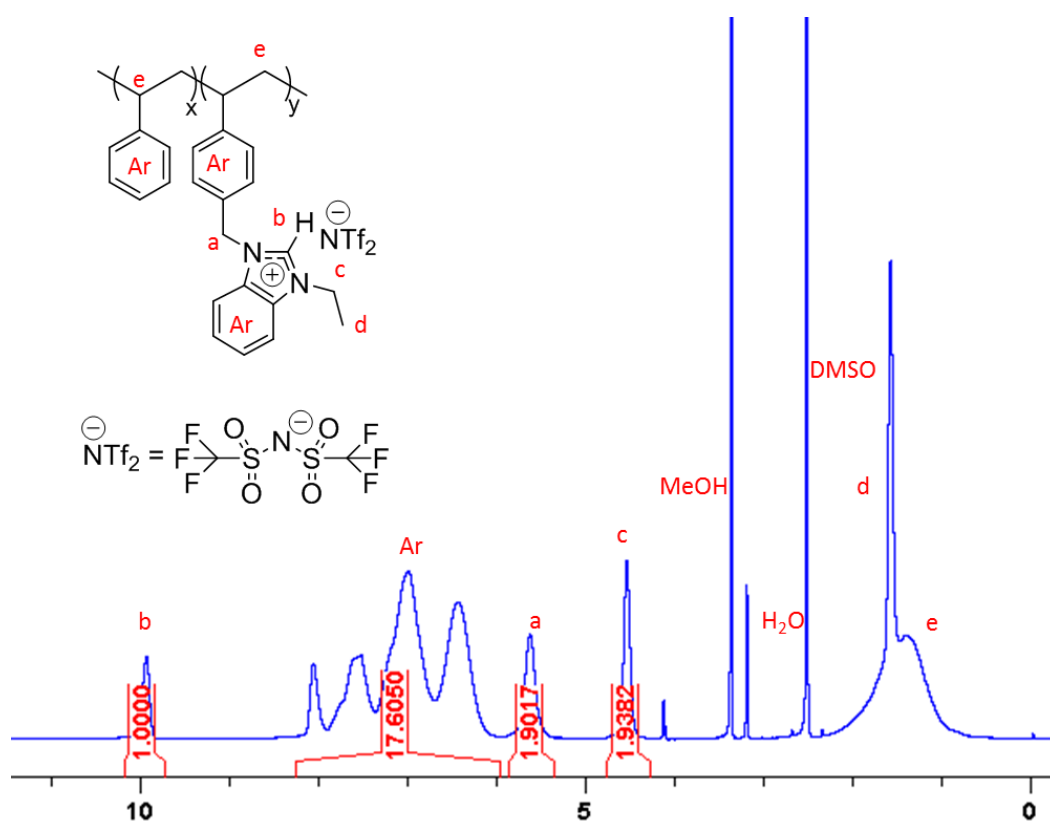


**Figure S2.8.** Synthesis of ((PS-co-Poly[ViEBIm]TFSI)-1 (**4**).  $^1\text{H}$  NMR spectra in  $\text{DMSO-}d_6$

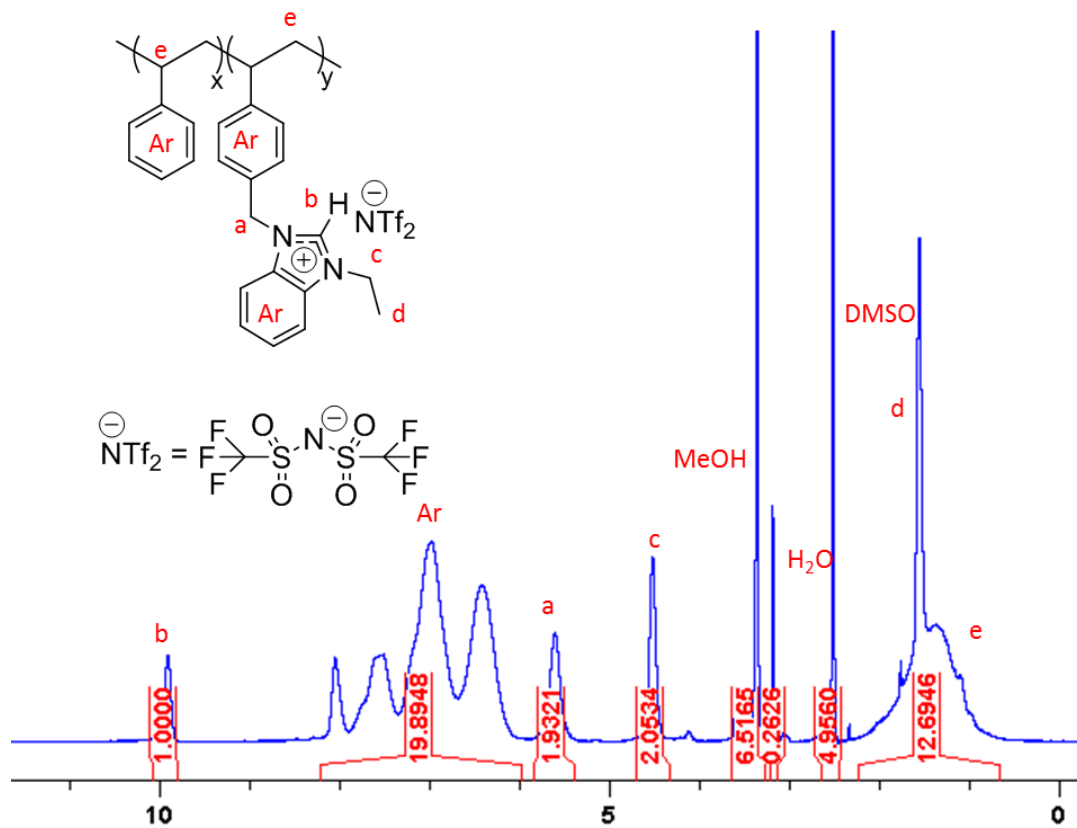


**Figure S2.9.** Synthesis of ((PS-co-Poly[ViEBIm]TFSI)-2 (**7**).  $^1\text{H}$  NMR spectra in  $\text{DMSO-}d_6$ .

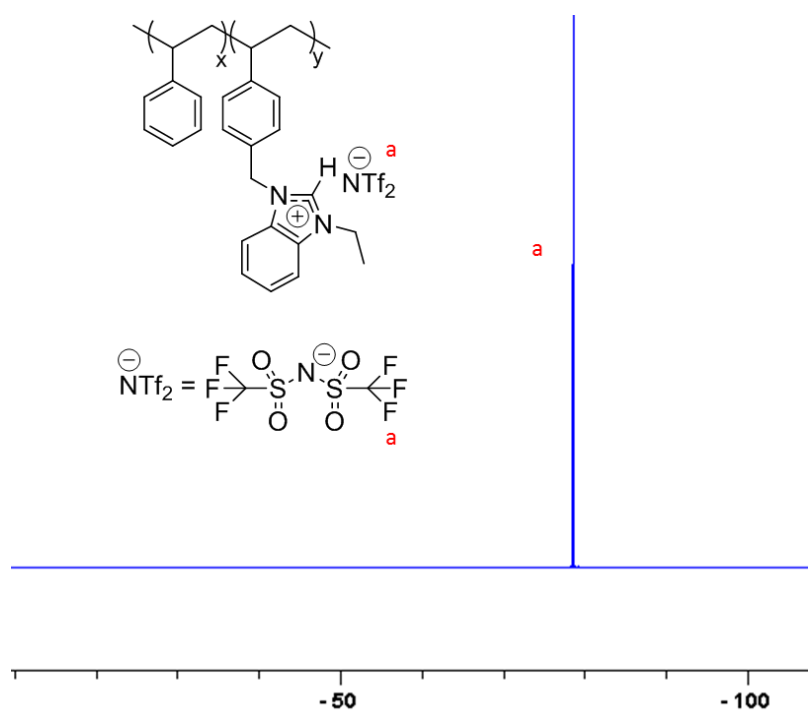


**Figure S2.10.** Synthesis of ((PS-co-Poly[ViEBIm]TFSI)-1 (4).  $^{19}\text{F}$  NMR spectra in  $\text{DMSO-}d_6$ .

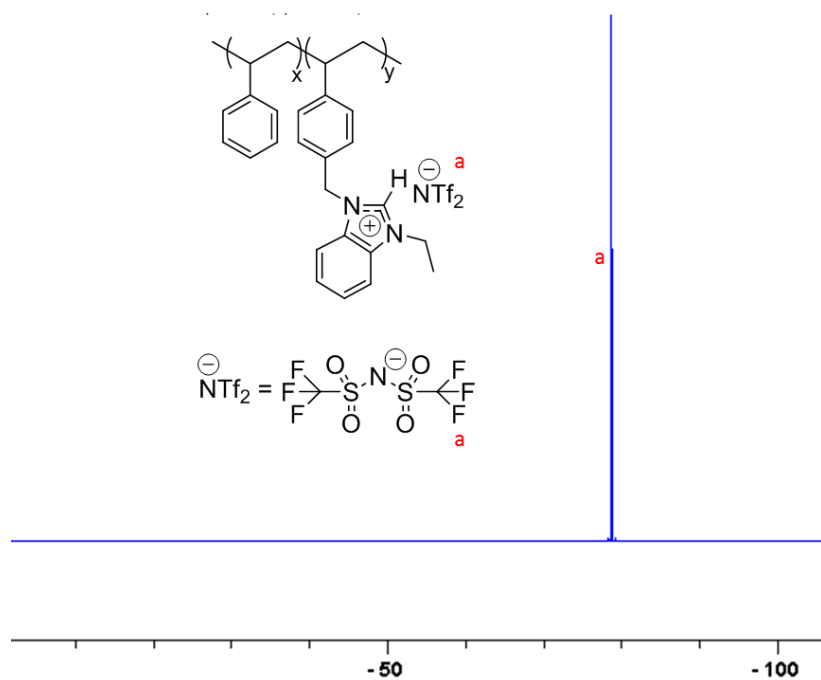


**Figure S2.11.** Synthesis of ((PS-co-Poly[ViEBIm]TFSI)-2 (7).  $^{19}\text{F}$  NMR spectra in  $\text{DMSO-}d_6$ .



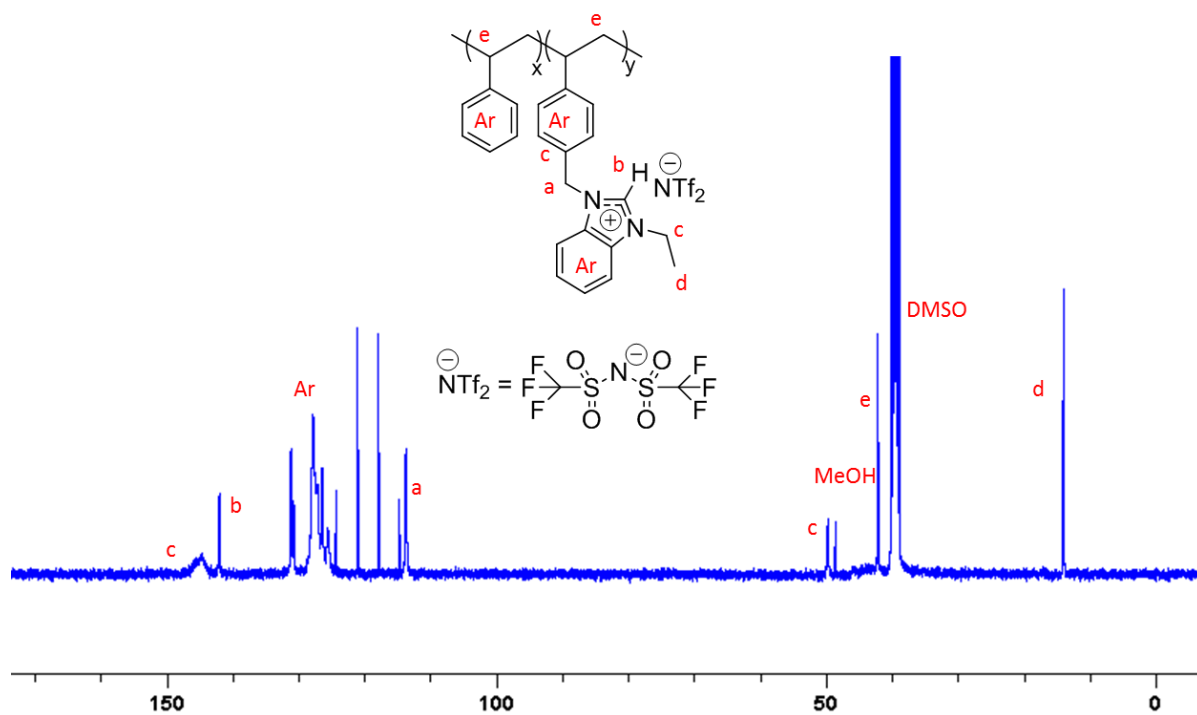


**Figure S2.12.** Synthesis of ((PS-co-Poly[ViEBIm]TFSI)-1 (4).  $^{13}\text{C}$  NMR spectra in  $\text{DMSO-}d_6$ .

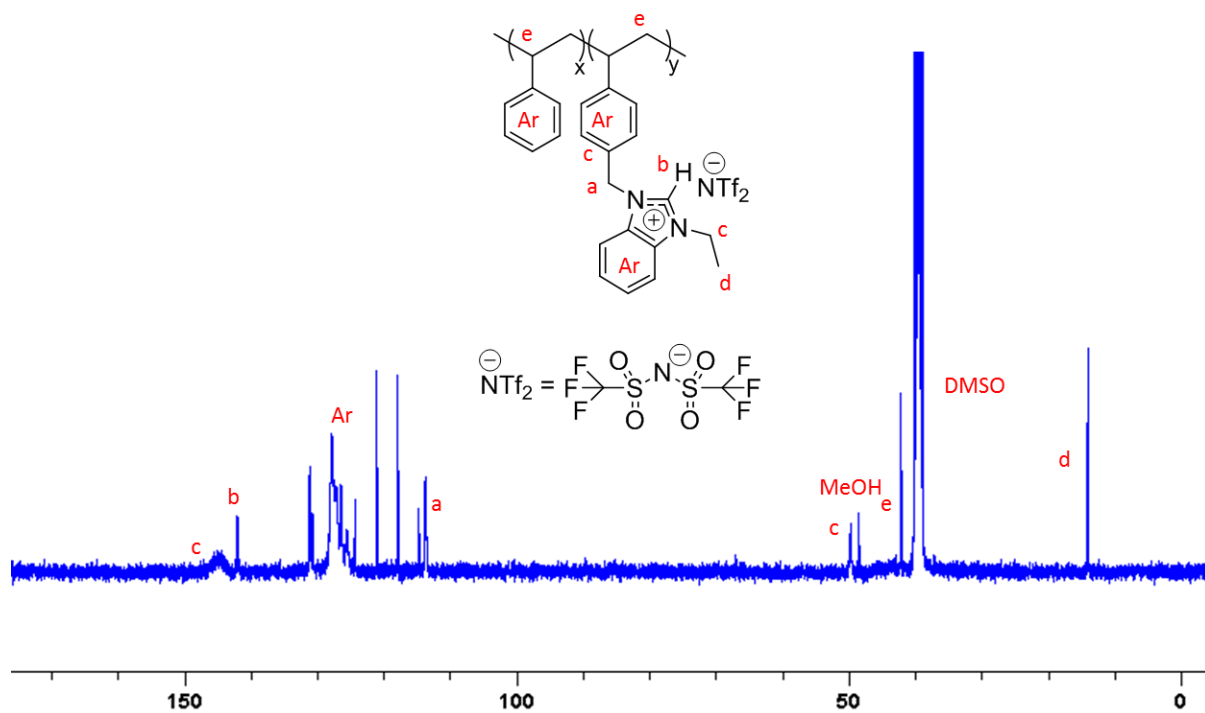


**Figure S2.13.** Synthesis of ((PS-co-Poly[ViEBIm]TFSI)-2 (7).  $^{13}\text{C}$  NMR spectra in  $\text{DMSO-}d_6$ .

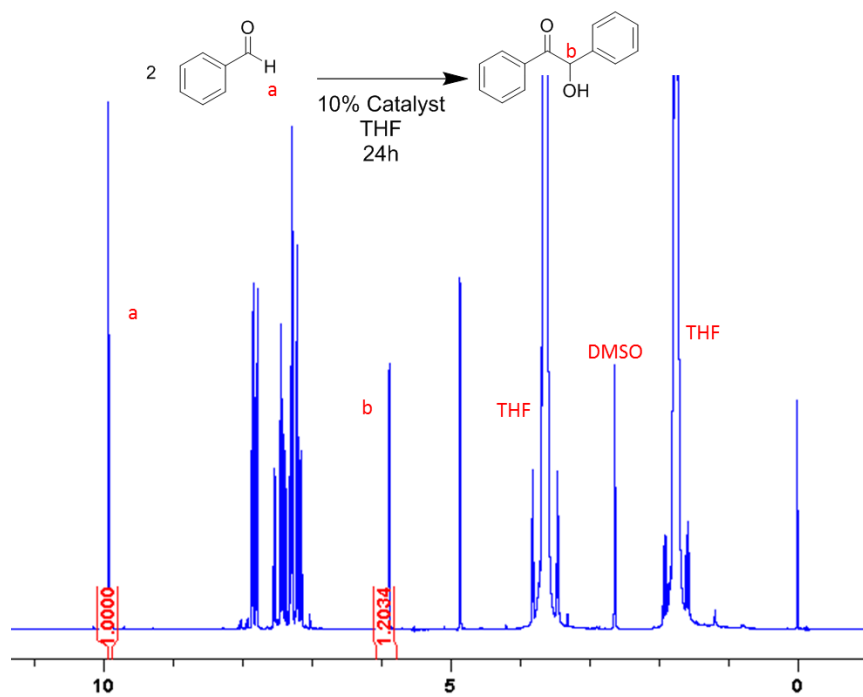


**Figure S2.14.** Benzoin Condensation Conversion. <sup>1</sup>H NMR spectra in DMSO-d<sub>6</sub>.

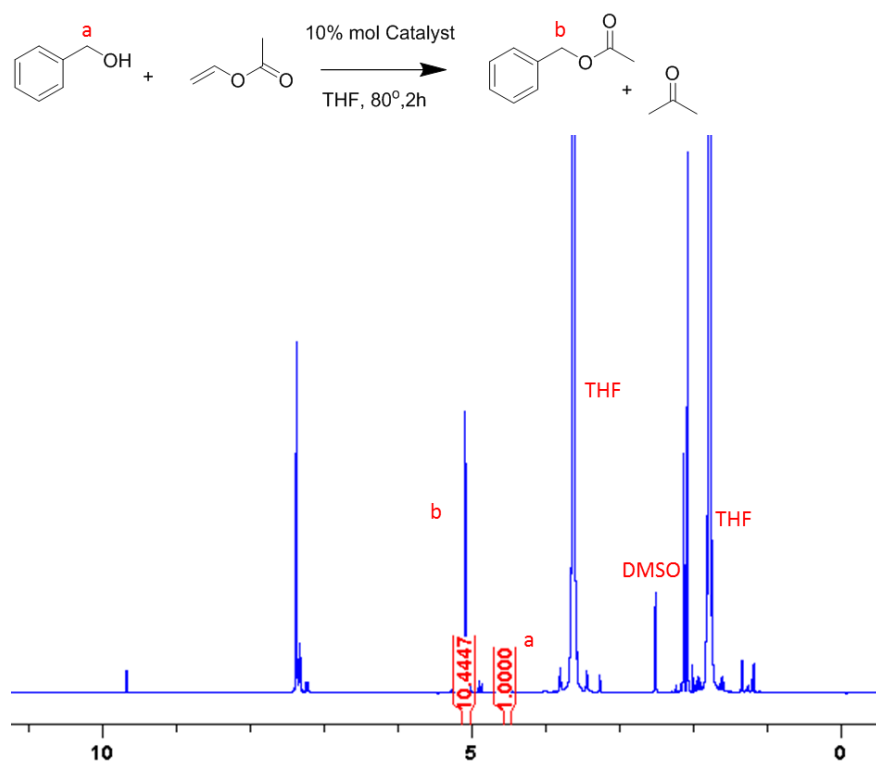


**Figure S2.15.** Transesterification Conversion  $^1\text{H}$  NMR spectra in  $\text{DMSO-}d_6$ .

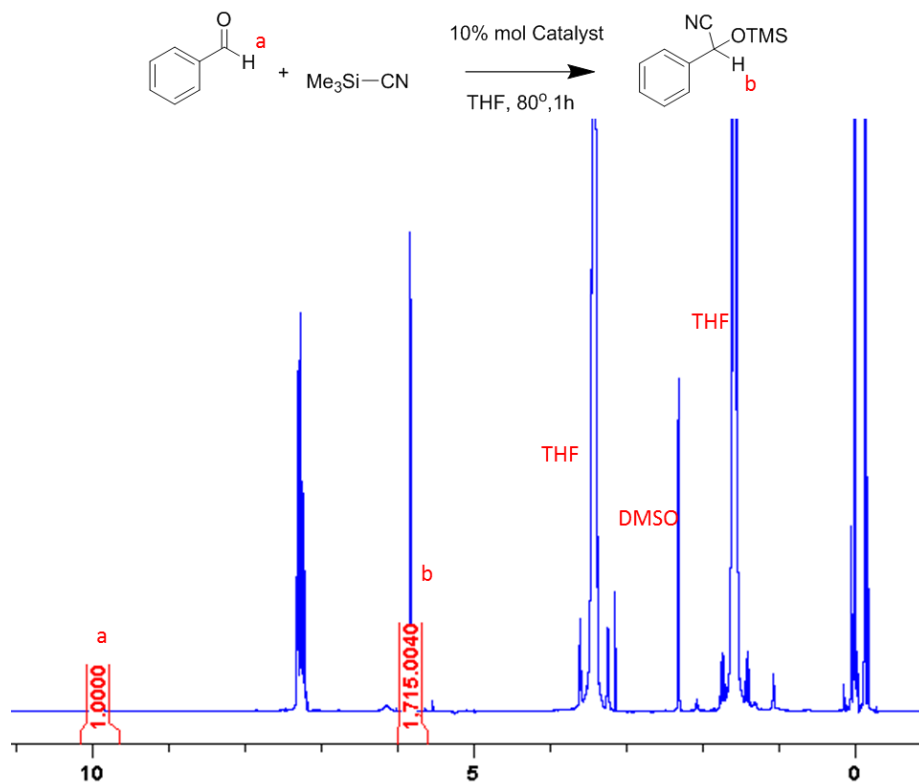


**Figure S2.16.** Cyanosilation Conversion  $^1\text{H}$  NMR spectra in  $\text{DMSO-}d_6$ .

**Chapter III: Reversible Ionically-crosslinked Single  
Chain Nanoparticles as Bioinspired and Recyclable  
Nanoreactors for *N*-Heterocyclic Carbene  
Organocatalysis**



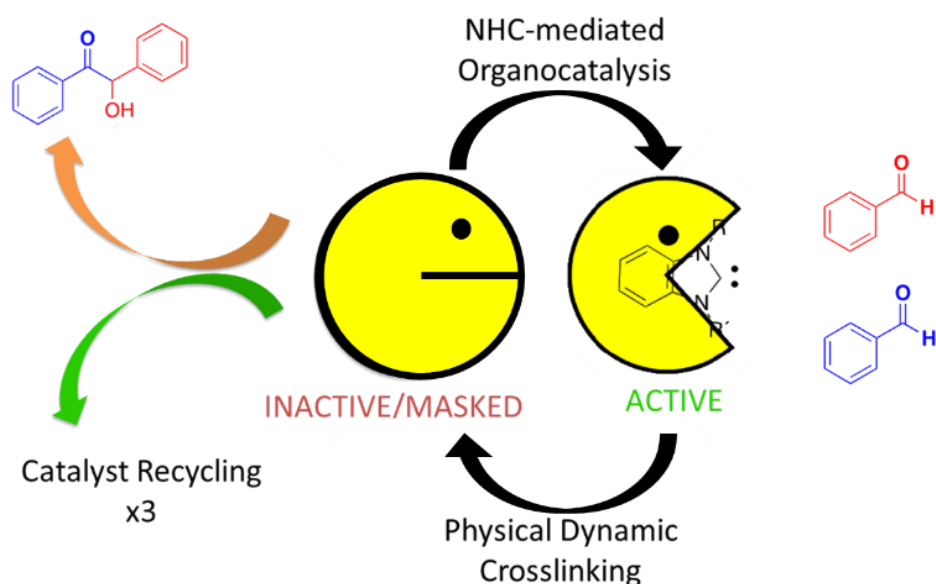
# Table of Contents

## **Chapter III: Reversible Ionically-crosslinked Single Chain Nanoparticles as Bioinspired and Recyclable Nanoreactors for *N*-Heterocyclic Carbene Organocatalysis**

3.1. Abstract.....	139
3.2. Introduction.....	140-142
3.3. Synthesis of catalytically active SCNPs.....	143-148
3.4. Benzoin condensation catalyzed by SCNP 5.....	148-152
3.5. Conclusions.....	153
3.6. References.....	153-157
3.7 Experimental section.....	158-169

### 3.1 Abstract

The intrinsic advantages of poly(ionic liquid)s (PILs), based on their high chemical activity and flexible structure, have been harnessed by exploring their applicability as catalytic single chain nanoparticles (SCNPs). A non-covalent bioinspired approach has been established to ionically crosslink an imidazolium-based poly(ionic liquid) to form a folded SCNPs. An amphiphilic styrenic-type coPIL was synthesized by reversible addition fragmentation chain transfer (RAFT) to include hydrophilic stabilizers units, hydrophobic spacers and two antagonist functionalities randomly distributed through the polymer backbone. The antagonist functionalities were then intramolecularly and ionically-crosslinked using a simple anion metathesis reaction, which resulted in folding to form the SCNPs under mild conditions. The folding process enabled the protection of the N-heterocyclic carbene (NHC) functionality, through the benzoate-imidazolium interaction between antagonist monomer units. Upon the application of heat, free NHCs could be generated within the confined SCNPs, which could be further utilized in benzoin catalysis. Most importantly, the reversible nature of the crosslinking and reversible generation of the active functionality allowed for utilization of the SCNPs as a recyclable catalytic support.



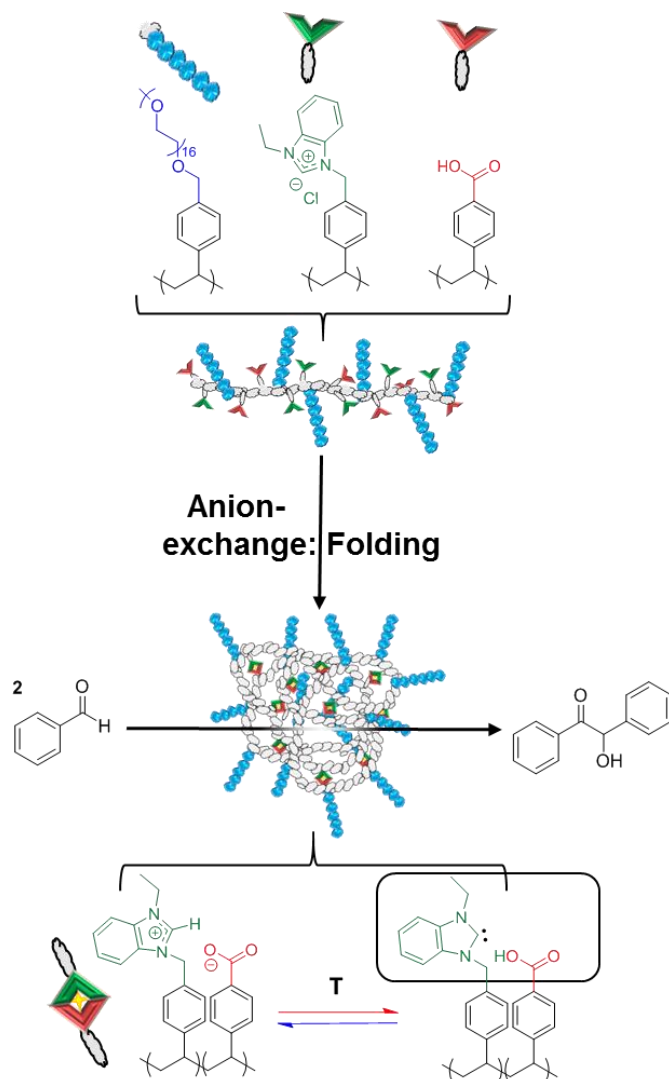


### 3.2 Introduction

Single-chain polymer nanoparticles (SCNPs) have recently attracted increasing interest due to their exceptional and unique properties in an array of applications in nanomedicine, catalysis and information storage.<sup>1-6</sup> SCNPs are based on self-collapsed individual chains that mimic the structure of folded biomacromolecules, such as (poly)peptides or enzymes.<sup>7</sup> Particularly in catalysis, these biomacromolecules serve as source of inspiration for the construction of artificial nano-objects (*i.e.* nanoreactors) trying to emulate such precision pathways towards functionality, specificity and efficiency.<sup>7,8</sup> The strategy followed is based on folding individual synthetic polymer chains through intramolecular crosslinking to obtain SCNPs containing confined catalytic entities.<sup>9-11</sup> Whilst the majority of work has been particularly focused on the use of covalent intramolecular interactions for the synthesis of robust SCNPs, it is increasing the number of approaches based on reversible intramolecular interactions for the development of stimuli-responsive SCNPs.<sup>6,12,13</sup> Reversibly bonded SCNPs synthesis was first achieved *via* non-covalent interactions through hydrogen-bonding.<sup>14</sup> Subsequently, many other folding/collapsing routes have been investigated, based on hydrogen-bonding,<sup>15-19</sup> host-guest interactions,<sup>20-22</sup> dynamic covalent bonds,<sup>6</sup> disulfide bridges,<sup>23</sup> redox/pH/UV-responsive SCNPs<sup>24-26</sup> or metal complexation.<sup>9,27-31</sup> All of these SCNPs can be disassembled by applying different stimuli (*e.g.* pH/temperature/redox change, solvent polarity variation, include host competitors). The formation of reversible SCNPs linkages that rely on dynamic configuration processes represent probably the most promising pathway towards enzyme biomimicry since the nature of these non-covalent bonds could determine the function and performance of synthetic SCNPs as it occurs in certain proteins.<sup>6</sup> As a new type of non-covalent bonding in SCNPs technology, ionic-liquids (ILs or PILs in the polymerized version) display a solvent-independent ionization state and have found unusually broad potential applications such as catalysis, due to their negligible vapor pressure, high thermal stability and powerful solvation capability.<sup>32-34</sup> Moreover, the freedom to choose the cation and anion and their tunable miscibility with numerous organic compounds/solvents make (P)ILs potential candidates as new type of non-covalent bond based SCNPs for catalysis. To this purpose, imidazolium-based (P)ILs have been found to serve as a latent source of catalytically active *N*-heterocyclic carbenes (NHCs), which are readily generated through a temperature-dependent acid-base equilibrium.<sup>35,36</sup> These masked-NHCs have been widely implemented in both molecular or supported macromolecular structures using a variety of different imidazolium precatalysts. Interestingly, supported imidazolium-based masked-NHCs were previously decorated in our

group with different basic counter anions in wide array of different polymeric structures such as with  $\text{HCO}_3^-$  (in linear polymers),<sup>37,38</sup> acetate (in both linear polymers and folded SCNP),<sup>39,40</sup> or sebacate (in gels),<sup>41</sup> by simple anion exchange. Inspired by such a concept, supporting on the one hand the imidazolium cationic moieties (NHC source) and on the other hand the basic counter anions (thermally latent trigger) on the same single polymeric chain should enable the creation of a confined SCNP pocket, based on electrostatic interactions. This would facilitate the creation of thermally latent NHC based catalytic centers, which could then potentially be utilized as catalytic nanoreactors. In this context, a new methodology for the collapse of a linear imidazolium-based coPIL precursor, into an ionically-crosslinked SCNP, using a simple anion exchange has been explored. The folding procedure has then been carried out under mild conditions, through deprotonation of carboxylic acid functionality. The resulting carboxylate then has the dual role of physically crosslinking the SCNPs, whilst generating the masked-NHC precatalyst. These SCNPs were further used as a thermally latent homogeneous catalyst for the benzoin condensation and could be easily recycled for a number of cycles without any significant loss of activity (**Scheme 3.1**). Functionalization of the SCNPs with carbon disulfide

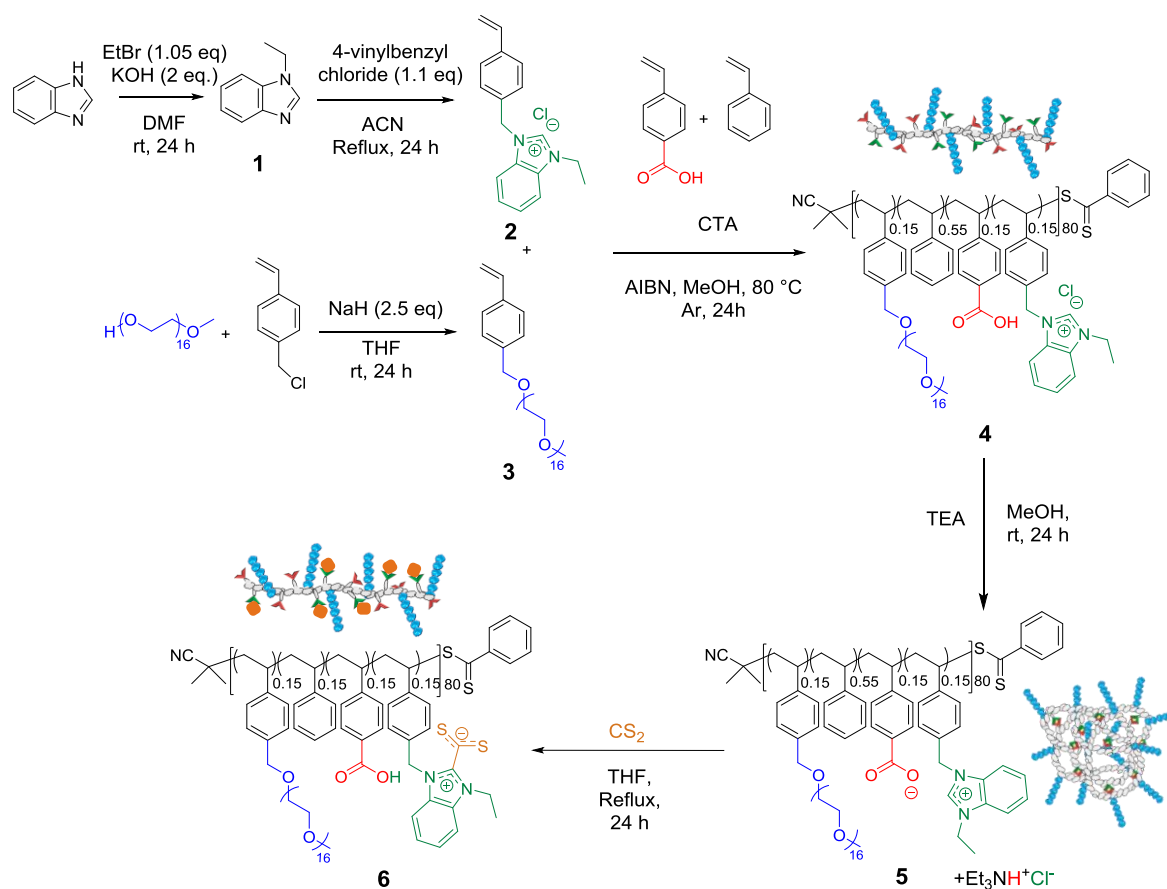
evidenced generation of the active NHC and resulted in unfolding of the ionically crosslinked SCNPs.



**Scheme 3.1.** Design of catalytically active SCNPs for benzoin condensation reaction.

### 3.3 Synthesis of catalytically active SCNPs

Amphiphilic copolymer **4** was synthesized by reversible addition fragmentation chain transfer (RAFT) polymerization in methanol at 80 °C, in the presence of 2-cyano-2-propyl benzodithioate as a chain transfer agent and AIBN as an initiator. Copolymers were prepared by randomly copolymerizing the commercially available monomers 4-vinyl benzoic acid and styrene as well as the synthesized vinyl ethyl benzimidazolium chloride (**2**) and PEG16-styrene (**3**). Note that monomer **2** was polymerized in its chloride form, which enabled the use of methanol as the copolymerization solvent (**Scheme 3.2**).



**Scheme 3.2.** Synthetic route to the parent linear copolymer **4** by RAFT copolymerization of **2**, **3**, 4-vinylbenzoic acid and styrene, followed by a folding step caused by anion-metathesis leading to the formation of SCNP **5**. Unfolded copolymer, **6** could be obtained by irreversibly post-functionalizing SCNP **5** with CS<sub>2</sub>.

To obtain SCNPs with comparable size and similar amphiphilic character to those reported in literature,<sup>28,41</sup> the total theoretical degree of copolymerization of different styrenic monomers

was kept around 80. The copolymerization was not carried out to full conversion (instead to ca. 40 %) to avoid side reactions which might have led to a loss of key functionality or to an increase in dispersity. Consequently, the molar mass distribution ( $D_M$ ) was narrow (1.2) for all of the copolymerizations. The conversion of the monomers was quantified via  $^1\text{H}$  NMR spectroscopy by both the disappearance of the vinyl peaks and the broadening of the C2- proton during copolymerization. The almost identical consumption of the four different styrenic monomers, together with the moderate conversion, indicated that a statistical copolymer distribution was achieved. The composition of benzoic acid, styrene, **2** and **3** in copolymer **4** was then found to be 0.15/0.55/0.15/0.15, respectively, as identified by  $^1\text{H}$  NMR spectroscopy (**Fig. 3.1A**).

In previous work from our group, SCNP-supported NHCs were generated upon heating to a temperature of 80 °C involving a post-functionalization approach to confer the thermally latent behavior to NHC precatalyst moieties.<sup>40,41</sup> As a more facile and scalable alternative, we apply here an anion-exchange method enabling to trigger the self-folding of the RAFT-derived copolymer precursor. This provides, on the one hand, a three-dimensional robust SCNPs structure and, on the other hand, a basic counter anion for the benzimidazolium moieties, hence enabling their utility as a latent NHC-source upon thermal triggering. Indeed, the ionic nature of the crosslinking requires only mild conditions for the triggering of SCNPs folding and also confers reversibility in this process. In detail, linear copolymer precursor **4** was subjected to an anion metathesis reaction under diluted conditions (1 mg/mL), replacing the chloride anions (present in benzimidazolium moieties) by carboxylate ones (present in benzoic acid moieties) in the presence of triethylamine (TEA) to afford SCNP **5**.

This folding process, in which a carboxylate counter anion ionically interacts with the benzimidazolium cation, was evidenced using a range of analysis methods, including  $^1\text{H}$ ,  $^{13}\text{C}$  NMR spectroscopy, diffusion ordered spectroscopy (DOSY), Fourier transform infrared spectroscopy (FTIR), size exclusion chromatography (SEC), dynamic light scattering (DLS), transmission electron microscopy (TEM), and small-angle X-ray scattering (SAXS). In particular, the  $^1\text{H}$  NMR spectroscopy revealed the disappearance of the acidic –OH proton signal, as well as the shift of the benzimidazolium C<sub>2</sub>-proton signal from 10.5 to 11.4 ppm (**Fig. 3.1**). The FTIR confirmed the disappearance of the acidic –OH vibration signal around 3300  $\text{cm}^{-1}$ , and the presence of the acetate symmetric and asymmetric vibrations in the 1500-1600  $\text{cm}^{-1}$  (specifically at 1590  $\text{cm}^{-1}$ ) region (**Fig. 3.2**).

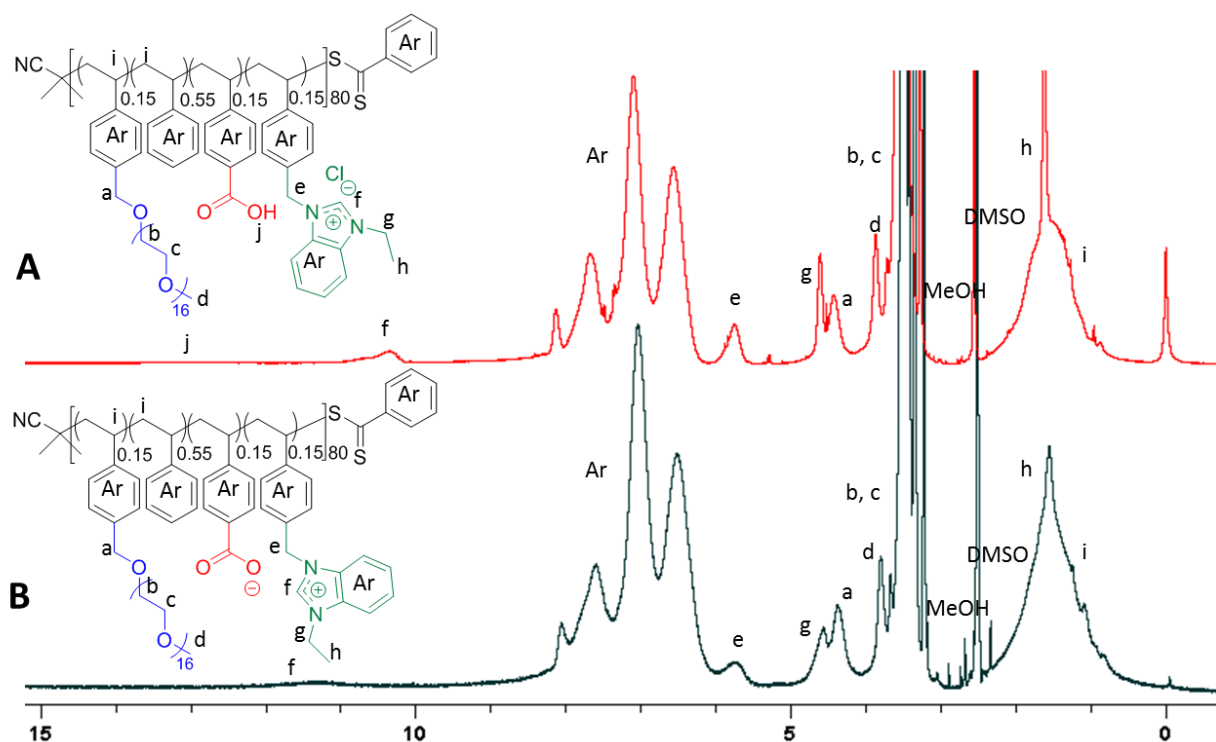


**Figure 3.1:** <sup>1</sup>H NMR spectrum in DMSO-*d*<sub>6</sub> of linear precursor **4** (A) and SCNP **5** (B) after folding.

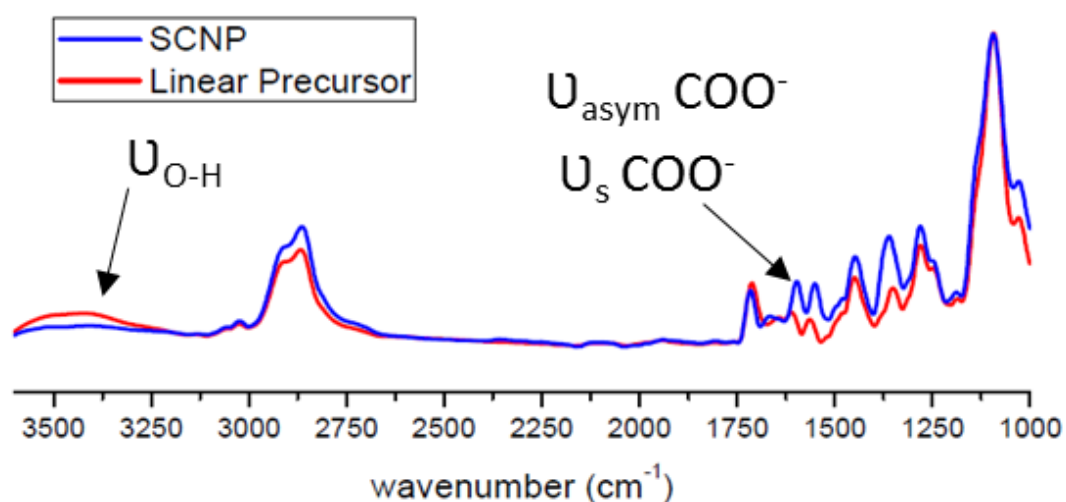


**Figure 3.2:** Attenuated total reflection Fourier transform infrared (ATR-FTIR) analysis for linear starting copolymeric precursor **4** (red) and folded SCNP **5** (blue).

It is known that PILs supporting polycations and polyanions in the same backbone are difficult to characterize by SEC analysis due to electrostatic interactions with the stationary phase.<sup>42,43</sup> Thus, after testing a number of different solvents, the use of DMF containing 10 mM ammonium tetrafluoroborate at 50 °C was found to be optimal. An increase in the retention

time for SCNP **5** compared to linear precursor **4** was observed, which was attributed to the decrease in hydrodynamic volume, confirming successful folding of the co(PILs) (**Fig. 3.3.A**).

Dynamic light scattering (DLS) experiments were performed to confirm the single chain folding of the prepared copolymers. The folded SCNP **5** was analyzed at a concentration of 5 mg/mL and showed a single peak around 12 nm for hydrodynamic diameter (distribution in volume) at room temperature. However, we were also interested in the particle size at catalysis temperature (*i.e.* 80 °C in THF) and hence variable temperature DLS analysis was performed, as summarized in **Fig. 3.3.B**. (see **Fig. 3.4** for 20-80 °C range). This analysis confirmed a relatively homogeneous diameter of the SCNPs from room temperature (rt) to catalytic conditions. Dry state TEM, stained with uranyl acetate, revealed particle diameters of 7-10 nm, confirming results obtained by DLS analysis (**Fig. 3.3.C**).

To further confirm the change in size upon folding, the linear and folded co(PILs) were characterized by DOSY NMR spectroscopy in DMSO-*d*<sub>6</sub>. This characterization technique confirmed the faster diffusion coefficient for the SCNP **5** ( $D = 3.14 \times 10^{-11} \text{ m}^2/\text{s}$ ) compared to the linear precursor **4** ( $D = 2.39 \times 10^{-11} \text{ m}^2/\text{s}$ ) and also allowed for the calculation of the hydrodynamic diameter of the SCNPs (of ~7 nm) using the Stokes-Einstein-equation (**Fig. S3.1**). Furthermore, despite the suggested presence of some larger aggregates, SAXS measurements (fitted to a compact particle model) unambiguously revealed a compaction from 9.4 nm to 5.3 nm calculated from the Porod region in the Kratky plot (**Fig. 3.1.D**). All of these characterization methods afforded similar values for SCNPs diameter (with variations attributable to the difference measurement conditions, solvents etc.) and confirmed successful folding of the linear coPIL **4** to form the SCNP **5**.

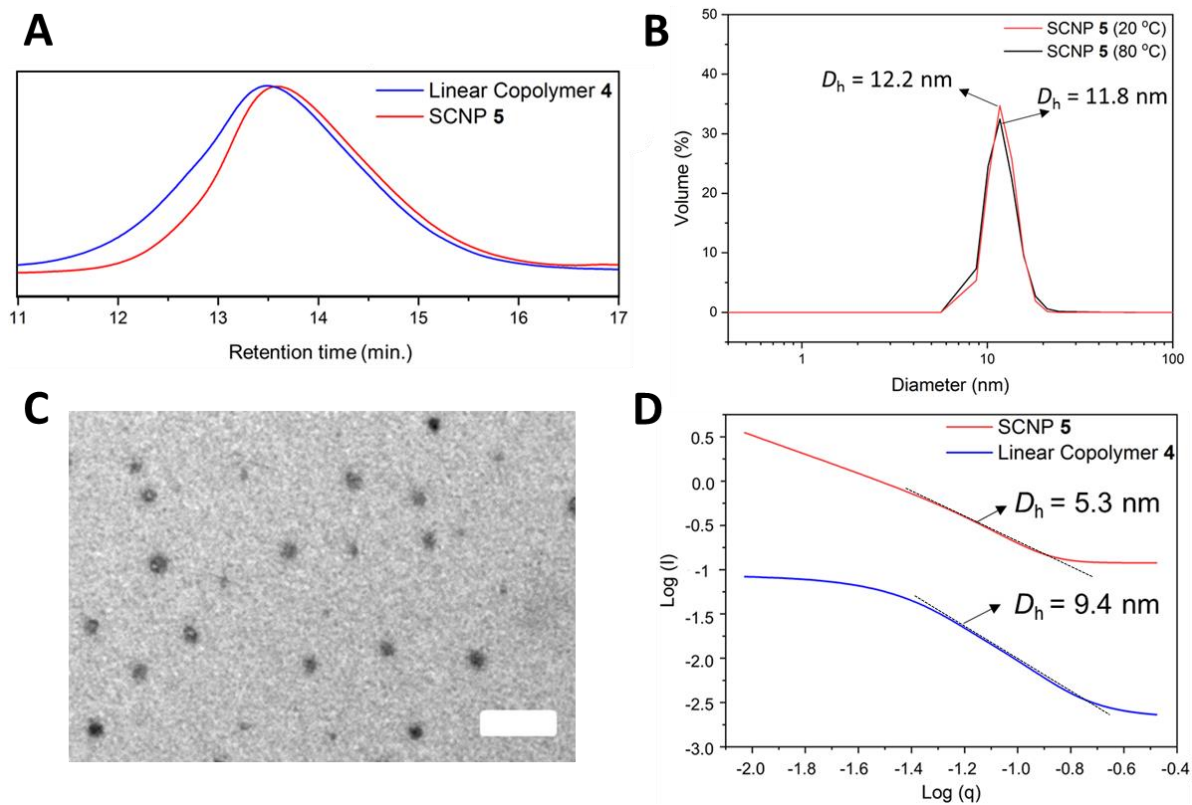


**Figure 3.3.** **A)** SEC responses (in DMF in presence of 10 mM  $\text{NH}_4\text{BF}_4$ ; RI detector) of SCNP **5** (red line) obtained *via* cross-linking of copolymer precursor **4** (blue line) by anion exchange. **B)** DLS analysis of SCNP **5** at rt (solid red line) and at catalysis temperature (solid black line) distributed by volume in THF (conc. = 5 mg/mL). **C)** TEM images of SCNP **5** (conc. = 1 mg/mL in methanol) stained with uranyl acetate; scale bar = 50 nm. **D)** Kratky Log-Log plot from SAXS analysis of precursor **4** (solid red line) and folded **5** (solid blue line) in THF (conc. = 1 mg/mL; fitted to compact particle model).



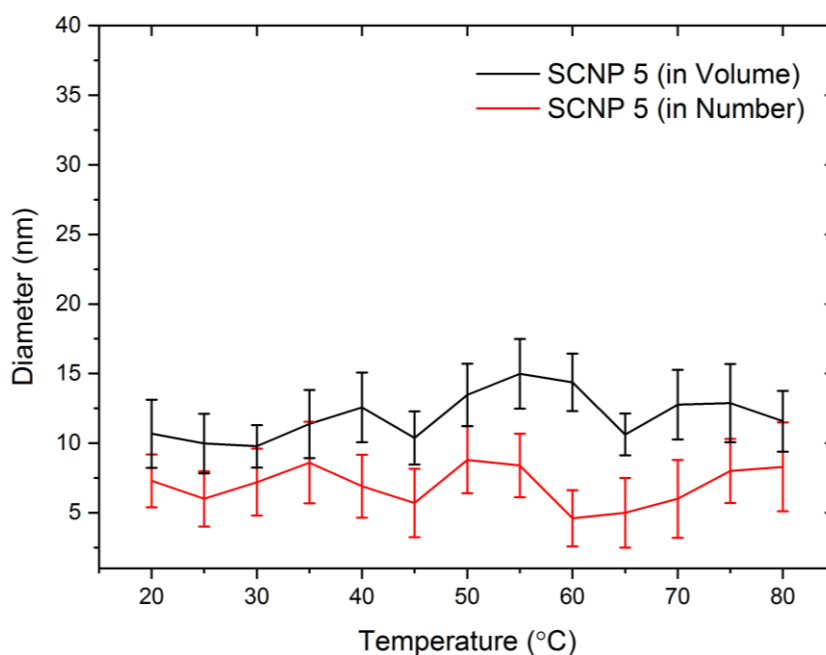


**Figure 3.4.** Multi-T DLS analysis of SCNP **5** from 20 to 80 °C in THF with volume (black line) and number (red line) distributions (Conc: 5 mg/mL).

### 3.4 Benzoin condensation catalysed by SCNP **5**

This particular folding technique was of interest as it provided a method for the generation of a thermally latent NHC-precatalyst, which could be activated upon thermal cleavage of the intrachain crosslinks. To prove that an active NHC species was generated upon heating SCNP **5**, an NHC-CS<sub>2</sub> adduct forming reaction was carried out (copolymer **6**; **Scheme 3.2**).<sup>40</sup> Upon addition of CS<sub>2</sub> irreversible and selective “trapping” of the generated active NHCs in the

SCNPs was expected. This was confirmed by identifying the characteristic signals of the NHC-CS<sub>2</sub> betaine (223.9 ppm, corresponding to the dithiolate group in <sup>13</sup>C NMR spectrum; **Fig. 3.5**).<sup>44</sup> Masked carbenes in their active form are known for their versatility and capability of acting as (organo)catalysts in a wide array of (macro)molecular reactions.<sup>35,36,45,46</sup> Since the folding step afforded a 3D conformational NHC-masked precatalyst, no further post-functionalization was required prior to catalysis. We hypothesized that the active NHC species could be generated upon heating as previously proven by NHC-CS<sub>2</sub> selective formation, resulting in the generation of a thermally latent catalyst, which could be utilized in an organic transformation.

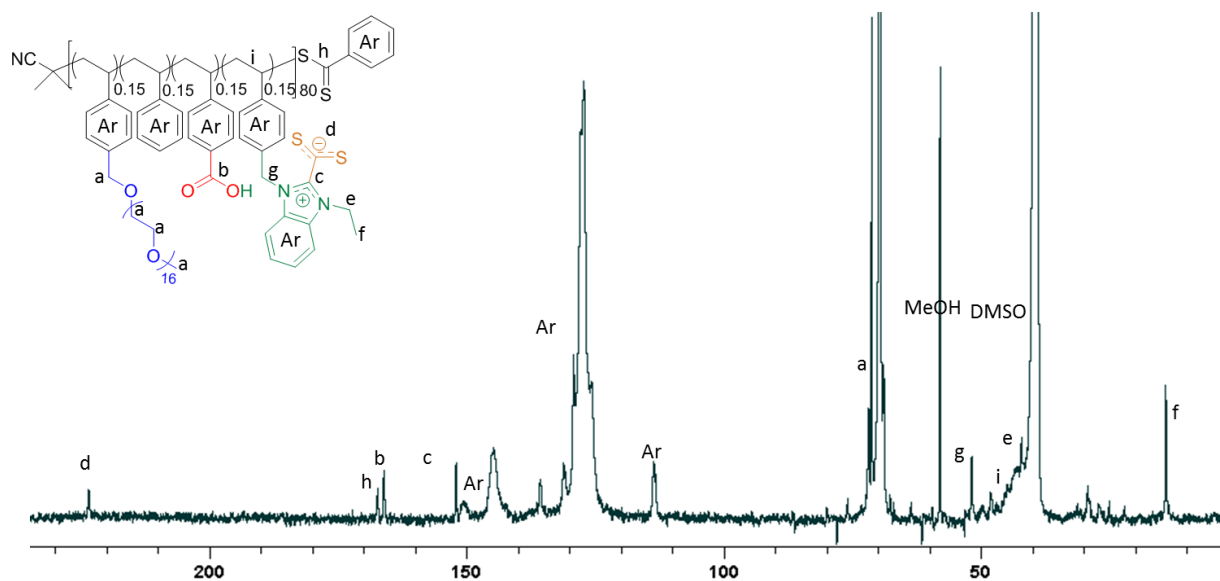


**Figure 3.5.**  $^1\text{H}$  NMR (A)  $^{13}\text{C}$  NMR (B) spectra of  $\text{CS}_2$  post-functionalization reaction in SCNP **6** in  $\text{DMSO-}d_6$ .

Benzoin condensation was chosen as model reaction because it is almost exclusively catalysed by carbenes,<sup>47</sup> and hence would permit to evaluate the catalytic performance of our system. Therefore, this reaction was first implemented in THF using benzaldehyde as the substrate and 10 mol.% of SCNP **5** (reference concentration: 20 mg/mL) relative to benzimidazolium moieties. In the first catalyst run using these conditions, 71% of benzaldehyde units were converted into benzoin after 24 h (Run 1; **Table 3.1**) and no higher conversions were observed when prolonging experiment time up to 48 h (Run 2). Interestingly, owing to both the incorporated side oligo-PEG in the polymeric structure and thermo-latent behavior of SCNPs, the increased solubility allowed polymer-supported catalyst recycling after catalyst deactivation, namely, by dialysis against methanol (see experimental). Conversions remained around 70% after 24 h reaction time, and after three consecutive catalytic cycles when SCNP **5** was applied. This highlights the robust and reversible nature of our latently crosslinking approach (Runs 3 and 4).

The role of confined space, where the reagents are able to efficiently interact with the thermally latent NHC, was then explored. The amount of SCNP **5** catalyst was thus decreased from 10 mol.% to 1 mol.%. Interestingly, conversions increased from 71% to 85%, passing upon reducing the mol.% of the SCNP **5** ten-fold (Runs 5 and 6). However, when the catalyst amount was dropped further to 0.1 mol.% (Run 7), the conversion did not increase, suggesting a product inhibition effect in the catalytic pocket of SCNP **5**, which has been observed before in similar

confined systems.<sup>48</sup> More specifically, we hypothesized that this inhibition effect could come from the generated –OH moieties in benzoin molecules that would inhibit the NHC catalyst as similarly occurred in other masked-NHC catalytic systems.<sup>37–39,49</sup>

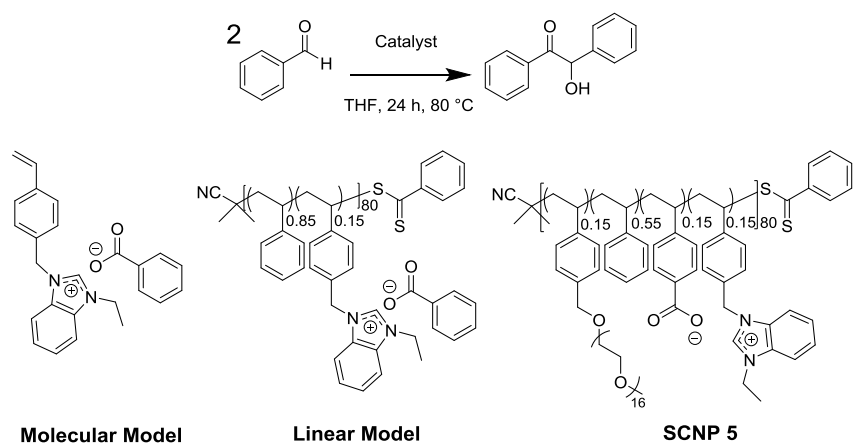
To examine the relationship between the confinement effect and inhibition provoked by the catalysed benzoin product, SCNP **5** was compared with a linear polymeric model, *i.e.* only bearing NHC precatalyst and spacer moieties, and a molecular model based on an active benzimidazolium monomer. Both molecular and macromolecular models were assessed for the benzoin condensation reaction under the same catalysis conditions as SCNP **5**. No appreciable confinement effect was found when the molecular model was used, showing a progressive decrease from 74% to 45% conversion when dropping the catalytic amount from 10 to 0.1 mol.% (Run 8-12). The lower catalytic performance of the molecular model compared to SCNP **5** could be due to the poor solubility of benzimidazolium benzoate and subsequent aggregation in the solvent used (*i.e.* THF). Conversely, the linear copolymeric model based on styrenic benzimidazolium benzoate moieties showed higher solubility compared to the molecular model, but led to a lower catalytic activity than both the molecular model and, more importantly, SCNP **5**. In fact, only 61% conversion was obtained when using 10 mol.% of the linear copolymer, which dropped up to 50% when decreased down to 0.1 mol.% catalyst loading (Runs 13-16). The observed plateau of 50% conversion when using either 1 and 0.1 mol.% catalyst (Runs 15 and 16, respectively), suggested that the inhibition effect was probably more apparent in the linear model, since the catalytic sites were more exposed to the obtained product (*i.e.* benzoin), and hence, more prone to inhibition than SCNP **5**. This is proposed to be due to the confinement effect on SCNP **5**, leading to an energy-free driven catalytic nanoreactor system based on the osmotic gradient between the SCNP pocket and the external solution.<sup>48,50–52</sup>

Otherwise, for comparison, the chlorine-containing monomer **2** and the linear parent coPIL **4** were also tested under the same conditions (Runs 17 and 18). However, no benzoin product was obtained, providing further evidence for the role of benzoate counter-anions to generate *in situ* catalytic SCNP-supported NHCs. Finally, control experiments were performed in order to successfully discard any catalytic activity of SCNP **5** in H<sub>2</sub>O (Run 19) or spontaneously generated benzoin without catalyst under previously used conditions (Run 20). It is also worth mentioning that no benzoin conversion was observed when the experiments were run at room

temperature, in good agreement with previously reported studies of our group reporting similar systems.<sup>39–41</sup>

This non-covalently crosslinked SCNPs approach illustrates the importance of having the normally ionic catalyst tethered to the SCNPs scaffold for efficient catalysis of generated soluble products which may entail inhibition in relatively apolar solvent conditions.

**Table 3.1.** Benzoin condensation reactions of benzaldehyde under different conditions using NHC-containing SCNPs and control experiments.



<b>Run</b>	<b>Catalyst</b>	<b>Cat. (mol%)</b>	<b>Cycle</b>	<b>Time (h)</b>	<b>Conv<sup>(a)</sup> (%)</b>
1	SCNP 5	10	1 <sup>st</sup>	24	71
2	SCNP 5	10	1 <sup>st</sup>	48	71
3	SCNP 5	10	2 <sup>nd</sup>	24	69
4	SCNP 5	10	3 <sup>rd</sup>	24	68
5	SCNP 5	5	1 <sup>st</sup>	24	76
6	SCNP 5	1	1 <sup>st</sup>	24	85
7	SCNP 5	0.1	1 <sup>st</sup>	24	80
8	<b>Molecular model<sup>(c)</sup></b>	10	1 <sup>st</sup>	24	74
10	<b>Molecular model</b>	5	1 <sup>st</sup>	24	62
11	<b>Molecular model</b>	1	1 <sup>st</sup>	24	61
12	<b>Molecular model</b>	0.1	1 <sup>st</sup>	24	45
13	<b>Linear model<sup>(d)</sup></b>	10	1 <sup>st</sup>	48	61
14	<b>Linear model</b>	5	1 <sup>st</sup>	24	61
15	<b>Linear model</b>	1	1 <sup>st</sup>	24	50
16	<b>Linear model</b>	0.1	1 <sup>st</sup>	24	50
17	<b>2</b>	10	1 <sup>st</sup>	24	0

<sup>a</sup> Conversions were calculated by <sup>1</sup>H NMR spectroscopy (**Fig. S3.8**); <sup>b</sup> THF was dried under Na/benzophenone prior to use in each catalytic run except from Run 19) <sup>c</sup> Active monomer based molecular model; <sup>d</sup> Linear model containing randomly ordered spacers and active monomer units. <sup>e</sup> Entry 19 the catalysis reaction was run in water. The reference catalyst concentration used was 20 mg/mL and temperature set at 80 °C. In all catalytic experiments, no enantiomeric selectivity was observed.

### 3.5 Conclusions

In summary, a novel type of non-covalently bonded SCNPs obtained by RAFT copolymerization is reported. Exploiting the PIL nature of the parent linear precursor, amphiphilic SCNPs folding was triggered by a mild anion-metathesis intramolecular reaction. The collapse was confirmed by different characterization methods ( $^1\text{H}/^{13}\text{C}$  NMR spectroscopy, SEC, DLS, SAXS, TEM and FTIR). These SCNPs contain latent NHC-type active species which could be thermally activated without the need for an exogenous reagent. The relatively high-conversions (~70%) in the benzoin condensation reactions could be maintained up to 3 catalytic cycles. Interestingly, the conversions could be enhanced up to 85% when 1 mol.% catalyst was used, as a result of the confinement in the catalytic environment in THF. The latter was further evidenced when comparing SCNPs to both molecular and polymeric models, showing higher catalytic efficiency, probably due to less catalyst inhibition effect in SCNPs catalytic pocket. Finally, post-modification of SCNPs by  $\text{CS}_2$  insertion confirms the NHC active species generation, as well as providing a simple SCNPs unfolding route. Although synthetically challenging, opening SCNPs chemistry to an entirely new terrain based on non-covalent interactions using PILs structures can answer to major organocatalysis challenges.

### 3.6 References

- 1 M. Ouchi, N. Badi, J.-F. Lutz and M. Sawamoto, *Nature Chemistry*, 2011, **3**, 917–924.
- 2 M. Gonzalez-Burgos, A. Latorre-Sanchez and J. A. Pomposo, *Chem. Soc. Rev.*, 2015, **44**, 6122–6142.
- 3 S. Mavila, O. Eivgi, I. Berkovich and N. G. Lemcoff, *Chemical Reviews*, 2016, **116**, 878–961.
- 4 A. M. Hanlon, C. K. Lyon and E. B. Berda, *Macromolecules*, 2016, **49**, 2–14.
- 5 O. Altintas and C. Barner-Kowollik, *Macromolecular Rapid Communications*, 2016, **37**, 29–46.

- 6 O. Altintas and C. Barner-Kowollik, *Macromolecular Rapid Communications*, 2012, **33**, 958–971.
- 7 A. Latorre-Sánchez and J. A. Pomposo, *Polymer International*, 2016, **65**, 855–860.
- 8 J. Rubio-Cervilla, E. González and J. Pomposo, *Nanomaterials*, 2017, **7**, 341.
- 9 H. Rothfuss, N. D. Knöfel, P. W. Roesky and C. Barner-Kowollik, *Journal of the American Chemical Society*, 2018, **140**, 5875–5881.
- 10 A. R. A. Palmans, in *Self-assembling Biomaterials*, Elsevier, 2018, pp. 563–583.
- 11 Y. Liu, S. Pujals, P. J. M. Stals, T. Paulöhr, S. I. Presolski, E. W. Meijer, L. Albertazzi and A. R. A. Palmans, *Journal of the American Chemical Society*, 2018, **140**, 3423–3433.
- 12 M. Artar, E. Huerta, E. W. Meijer and A. R. A. Palmans, in *Sequence-Controlled Polymers: Synthesis, Self-Assembly, and Properties*, eds. J.-F. Lutz, T. Y. Meyer, M. Ouchi and M. Sawamoto, American Chemical Society, Washington, DC, 2014, vol. 1170, pp. 313–325.
- 13 J. A. Pomposo, J. Rubio-Cervilla, A. J. Moreno, F. Lo Verso, P. Bacova, A. Arbe and J. Colmenero, *Macromolecules*, 2017, **50**, 1732–1739.
- 14 M. Seo, B. J. Beck, J. M. J. Paulusse, C. J. Hawker and S. Y. Kim, *Macromolecules*, 2008, **41**, 6413–6418.
- 15 E. J. Foster, E. B. Berda and E. W. Meijer, *Journal of the American Chemical Society*, 2009, **131**, 6964–6966.
- 16 T. Terashima, T. Mes, T. F. A. De Greef, M. A. J. Gillissen, P. Besenius, A. R. A. Palmans and E. W. Meijer, *Journal of the American Chemical Society*, 2011, **133**, 4742–4745.
- 17 T. Mes, R. van der Weegen, A. R. A. Palmans and E. W. Meijer, *Angewandte Chemie International Edition*, 2011, **50**, 5085–5089.
- 18 F. Wang, H. Pu, M. Jin, H. Pan, Z. Chang, D. Wan and J. Du, *Journal of Polymer Science Part A: Polymer Chemistry*, 2015, **53**, 1832–1840.
- 19 N. Hosono, A. M. Kushner, J. Chung, A. R. A. Palmans, Z. Guan and E. W. Meijer, *Journal of the American Chemical Society*, 2015, **137**, 6880–6888.

- 20 E. A. Appel, J. Dyson, J. del Barrio, Z. Walsh and O. A. Scherman, *Angewandte Chemie International Edition*, 2012, **51**, 4185–4189.
- 21 J. Willenbacher, B. V. K. J. Schmidt, D. Schulze-Suenninghausen, O. Altintas, B. Luy, G. Delaittre and C. Barner-Kowollik, *Chemical Communications*, 2014, **50**, 7056.
- 22 B. V. K. J. Schmidt and C. Barner-Kowollik, *Angewandte Chemie International Edition*, , DOI:10.1002/anie.201612150.
- 23 B. T. Tuten, D. Chao, C. K. Lyon and E. B. Berda, *Polymer Chemistry*, 2012, **3**, 3068.
- 24 A. Sanchez-Sanchez, D. A. Fulton and J. A. Pomposo, *Chemical Communications*, 2014, **50**, 1871–1874.
- 25 J. He, L. Tremblay, S. Lacelle and Y. Zhao, *Soft Matter*, 2011, **7**, 2380.
- 26 H. Frisch, J. P. Menzel, F. R. Bloesser, D. E. Marschner, K. Mundsinger and C. Barner-Kowollik, *Journal of the American Chemical Society*, 2018, **140**, 9551–9557.
- 27 R. Lambert, A.-L. Wirotius, S. Garmendia, P. Berto, J. Vignolle and D. Taton, *Polymer Chemistry*, 2018, **9**, 3199–3204.
- 28 K. Freytag, S. Säfken, K. Wolter, J. C. Namyslo and E. G. Hübner, *Polymer Chemistry*, 2017, **8**, 7546–7558.
- 29 A. Sanchez-Sanchez, A. Arbe, J. Kohlbrecher, J. Colmenero and J. A. Pomposo, *Macromolecular Rapid Communications*, 2015, **36**, 1592–1597.
- 30 N. D. Knöfel, H. Rothfuss, J. Willenbacher, C. Barner-Kowollik and P. W. Roesky, *Angewandte Chemie International Edition*, 2017, **56**, 4950–4954.
- 31 Y. Bai, X. Feng, H. Xing, Y. Xu, B. K. Kim, N. Baig, T. Zhou, A. A. Gewirth, Y. Lu, E. Oldfield and S. C. Zimmerman, *Journal of the American Chemical Society*, 2016, **138**, 11077–11080.
- 32 J. Yuan, D. Mecerreyes and M. Antonietti, *Progress in Polymer Science*, 2013, **38**, 1009–1036.
- 33 J. Yuan and M. Antonietti, *Polymer*, 2011, **52**, 1469–1482.



- 34 A. Eftekhari and T. Saito, *European Polymer Journal*, 2017, **90**, 245–272.
- 35 M. Fevre, J. Pinaud, Y. Gnanou, J. Vignolle and D. Taton, *Chemical Society Reviews*, 2013, **42**, 2142.
- 36 S. Naumann and M. R. Buchmeiser, *Catalysis Science & Technology*, 2014, **4**, 2466.
- 37 M. Fèvre, J. Pinaud, A. Leteneur, Y. Gnanou, J. Vignolle, D. Taton, K. Miqueu and J.-M. Sotiropoulos, *Journal of the American Chemical Society*, 2012, **134**, 6776–6784.
- 38 P. Coupillaud, J. Pinaud, N. Guidolin, J. Vignolle, M. Fevre, E. Veaudecenne, D. Mecerreyes and D. Taton, *Journal of Polymer Science Part A: Polymer Chemistry*, 2013, n/a-n/a.
- 39 R. Lambert, P. Coupillaud, A.-L. Wirotius, J. Vignolle and D. Taton, *Macromolecular Rapid Communications*, 2016, **37**, 1143–1149.
- 40 R. Lambert, A.-L. Wirotius and D. Taton, *ACS Macro Letters*, 2017, **6**, 489–494.
- 41 S. Garmendia, R. Lambert, A.-L. Wirotius, J. Vignolle, A. P. Dove, R. K. O'Reilly and D. Taton, *European Polymer Journal*, 2018, **107**, 82–88.
- 42 H. He, M. Zhong, B. Adzima, D. Luebke, H. Nulwala and K. Matyjaszewski, *Journal of the American Chemical Society*, 2013, **135**, 4227–4230.
- 43 E. Blasco, B. T. Tuten, H. Frisch, A. Lederer and C. Barner-Kowollik, *Polymer Chemistry*, 2017, **8**, 5845–5851.
- 44 P. Coupillaud, J. Vignolle, D. Mecerreyes and D. Taton, *Polymer*, 2014, **55**, 3404–3414.
- 45 D. M. Flanigan, F. Romanov-Michailidis, N. A. White and T. Rovis, *Chem. Rev.*, 2015, **115**, 9307–9387.
- 46 W. N. Ottou, H. Sardon, D. Mecerreyes, J. Vignolle and D. Taton, *Progress in Polymer Science*, 2016, **56**, 64–115.
- 47 R. S. Menon, A. T. Biju and V. Nair, *Beilstein Journal of Organic Chemistry*, 2016, **12**, 444–461.

- 48 A. Lu, D. Moatsou, D. A. Longbottom and R. K. O'Reilly, *Chem. Sci.*, 2013, **4**, 965–969.
- 49 D. Kuzmicz, P. Coupillaud, Y. Men, J. Vignolle, G. Vendraminetto, M. Ambrogi, D. Taton and J. Yuan, *Polymer*, 2014, **55**, 3423–3430.
- 50 A. D. Ievins, X. Wang, A. O. Moughton, J. Skey and R. K. O'Reilly, *Macromolecules*, 2008, **41**, 2998–3006.
- 51 P. Cotanda, N. Petzetakis and R. K. O'Reilly, *MRS Communications*, 2012, **2**, 119–126.
- 52 A. Lu, P. Cotanda, J. P. Patterson, D. A. Longbottom and R. K. O'Reilly, *Chemical Communications*, 2012, **48**, 9699.

### 3.7 Experimental Section

#### Synthesis of different monomers

**Synthesis of *N*-ethylbenzimidazole (1).** Benzimidazole (5 g, 42.32 mmol) was dissolved in DMF (20 mL) and 4.75 g of potassium hydroxide was added (2.5 eq., 106 mmol). The solution was stirred for 15 minutes and 3.45 mL (5.07 g, 46.55 mmol) of ethyl bromide was then added drop-wise. After stirring at room temperature for 24h, the solution was diluted with 50 mL of water and extracted with dichloromethane (4 x 25 mL). The organic phases were combined, dried over MgSO<sub>4</sub> and evaporated, yielding a yellow viscous oil (4.93 g, 33.8 mmol, yield = 80%) <sup>1</sup>H NMR (DMSO-*d*<sub>6</sub>): δ = 8.25 (s, 1H, N-CH-N), 7.69-7.20 (m, 4H, aromatics), 4.12 (t, 2H, N-CH<sub>2</sub>-CH<sub>3</sub>), 1.32 (t, 3H, -CH<sub>3</sub>). <sup>13</sup>C NMR (DMSO-*d*<sub>6</sub>): δ = 144.5, 143.7, 123, 119.8, 110.0, 43.1, 14.8.

**Synthesis of 4-vinylbenzylethylbenzimidazolium chloride ([ViEBIm]Cl) (2).** *N*-ethylbenzimidazole **1** (4.82 g, 33 mmol) was dissolved in 25 mL of acetonitrile and 4.65 mL (1 eq. 5.03 g) of 4-vinylbenzylchloride were added into a schlenk tube. After stirring 24 h at 80 °C, the monomer was precipitated in EtOAc and dried under vacuum to remove the solvent leading to a white powder (8.87 g, 42 mmol, yield = 91%). <sup>1</sup>H NMR (DMSO-*d*<sub>6</sub>): δ = 9.68 (s, 1H, N-CH-N), 8.12-7.14 (m, 8H, aromatics), 6.72 (dd, 1H, Ph-CH-CH<sub>2</sub>), 5.95 (s, 2H, Ph-CH<sub>2</sub>-N), 5.76 (d, 2H, CH=CH<sub>2</sub>), 5.25 (d, 1H, CH=CH<sub>2</sub>), 4.15 (dd, 2H, N-CH<sub>2</sub>-CH<sub>3</sub>), 1.31 (t, 3H, -CH<sub>2</sub>-CH<sub>3</sub>). <sup>13</sup>C NMR (DMSO-*d*<sub>6</sub>): δ = 142, 136.2, 135, 133.8, 131.5, 128.8, 128.7, 126.5, 126.3, 114.1, 113.5, 58.6, 44.5, 14.9.

**Synthesis of 4-vinylbenzyl-PEO<sub>16</sub> (3).** The hydroxy-containing polyoligo(ethylene oxide) monomethylester (CH<sub>3</sub>O-PEO<sub>16</sub>-OH, 750 g.mol<sup>-1</sup>) (11.87 g, 15.82 mmol) was dissolved in THF (40 mL) and an excess of NaH (0.8 g, 40 mmol) was added slowly. After 1 hour stirring, 2.9 mL (3.14 g, 23.73 mmol) of 4- vinylbenzylchloride were added drop-wise. The reaction was stirred at rt for 24h. The excess NaH was quenched with water. After filtration an extraction with chloroform was performed. The chloroform was then removed under vacuum and the monomer purified by precipitation in cold heptane. The pure product was recovered as a yellow viscous oil (7.3 g, 8.31 mmol, yield = 70%) . <sup>1</sup>H NMR (DMSO-*d*<sub>6</sub>): δ = 7.4 ( m, 4H, aromatics), 6.7 (dd, 1H, Ph-CH-CH<sub>2</sub>), 5.5 (d, 2H, CH=CH<sub>2</sub>), 4.5 (s, 2H, Ph-CH<sub>2</sub>-O), 3.5 (m, 64H, O-CH<sub>2</sub>-

*CH*<sub>2</sub>-O-), 3.22 (s, 3H, O-*CH*<sub>3</sub>). <sup>13</sup>C NMR (DMSO-*d*<sub>6</sub>): δ = 137.2, 137.0, 129.6, 128.2, 114.5, 73.1, 71.5, 70.3, 70, 59.1.

**Synthesis of linear copolymer 4** CTA (15 mg, 0.067 mmol), styrene (0.86 mL, 7.53 mmol), monomer **2** (570 mg, 1.89 mmol), 4-vinylbenzoic acid (280 mg, 1.89 mmol) and monomer **3** (1.8 g, 2.02 mmol) were placed in a 20 mL glass tube. Methanol (10 mL) was added into the tube and the solution was stirred. AIBN (11.1 mg, 0.067 mmol) was added under dry argon at room temperature. Immediately after mixing, the polymerization mixture was placed in an oil bath at 80 °C for 24 h. After reaching 40% conversion measured by <sup>1</sup>H NMR spectroscopy, the reaction was terminated by cooling the mixture to room temperature. The conversion was determined from the concentration of residual monomer detected by <sup>1</sup>H NMR spectroscopy. The quenched reaction solution was purified by dialysis against MeOH (1 L) using a 3.5 kDa dialysis membrane and finally evaporated to dryness and subsequently dried overnight under vacuum at room temperature. Yield = 33%. <sup>1</sup>H NMR (DMSO-*d*<sub>6</sub>): δ (ppm) = 13.2-12.1 (br, 1H, HOOC-Ar), 10.9-10.5 (br, 1H, N-*CH=N*), 8.3-6 (br, 34.3H, Ar-*H*), 5.9-5.5 (br, 2H, Ar-*CH*<sub>2</sub>-N), 4.7-4.1 (br, 4H, N-*CH*<sub>2</sub>-CH<sub>3</sub>, O-*CH*<sub>2</sub>-Ar), 4.1-3.1 (br, 67H, O-*CH*<sub>2</sub>-CH<sub>2</sub>, CH<sub>3</sub>-CH<sub>2</sub>-O), 2.3-0.9 (br, 13H, CH<sub>2</sub>-CH- (backbone), N-CH<sub>2</sub>-CH<sub>3</sub>) (**Fig. 3.1A**); <sup>13</sup>C NMR (DMSO-*d*<sub>6</sub>): 166.4, 164.9, 150.2, 145.5, 142.7, 141.3-126.2, 113.1, 72.1, 70.3, 68.7, 52.1, 50.9, 13.2 ppm (**Fig. S3.3A**); IR: ν 3422.7 (OH), 1719.6 (C=O), cm<sup>-1</sup> (**Fig. 3.2** in red).

**Synthesis of SCNP 5.** Linear copolymer **4** (1 g) was dissolved in 1 L of MeOH at a concentration of 1 mg/mL in a 1 L round bottom flask. A large excess of TEA (10 eq.) was added dropwise to the methanolic solution. The resulting mixture was stirred at room temperature for 24 h until the anion-exchange was complete, as evidenced by <sup>1</sup>H NMR spectroscopy. The SCNP **5** solution was concentrated *in vacuo* and dialyzed (3.5 kDa MWCO against MeOH (1 L) to remove the liberated salt and the excess TEA. The purified SCNP **5** was dried under reduced pressure to yield a viscous oil. Yield: 89% <sup>1</sup>H NMR (DMSO-*d*<sub>6</sub>): δ (ppm) = 11.6-10.9 (br, 1H, N-*CH=N*), 8.3-6.05 (br, 34.3, Ar-*H*), 6-5.55 (br, 2H, Ar-*CH*<sub>2</sub>-N), 4.83-4.05 (broad, 4H, N-*CH*<sub>2</sub>-CH<sub>3</sub>, Ar-*CH*<sub>2</sub>-O), 4.1-3.1 (br, 67H, O-CH<sub>2</sub>-CH<sub>2</sub>, CH<sub>3</sub>-CH<sub>2</sub>-O), 2.3-0.8 (br, 13H CH<sub>2</sub>-CH-(backbone), N-CH<sub>2</sub>-CH<sub>3</sub>) (**Fig. 3.1B**); <sup>13</sup>C NMR (DMSO-*d*<sub>6</sub>): 166.8, 150.4, 145.4, 132.4-127.3, 113.1, 72.1, 70.3, 51.9, 13.2 ppm (**Fig. S3.3B**); IR: ν 1715.6 (C=O), 1619.7, 1536.7 (COO<sup>-</sup>) cm<sup>-1</sup> (**Fig. 3.2** in blue).

**Synthesis of unfolded copolymer 6.** In a 10 mL glass tube, folded SCNP **5** (155 mg) was azeotropically dried using distilled THF. Then 2 mL of dry THF was added and the solution stirred. CS<sub>2</sub> (0.4 mL) was then added at room temperature under argon. The solution was stirred at 80 °C for 24 h and the color change from colorless to red was observed, this being indicative of NHC-CS<sub>2</sub> formation. After cooling, the excess of CS<sub>2</sub> and solvent were removed under reduced pressure. Yield = >95% <sup>1</sup>H NMR (DMSO-*d*<sub>6</sub>):  $\delta$  (ppm) = 13.2-12.9 (br, 1H, HOOC-Ar), 8.2-6 (br, 34.3H, Ar-*H*), 5.9-5.3 (br, 2H, Ar-CH<sub>2</sub>-N), 4.8-4.1 (br, 4H, N-CH<sub>2</sub>-CH<sub>3</sub>, O-CH<sub>2</sub>-Ar), 4.1-3.1 (br, 67H, O-CH<sub>2</sub>-CH<sub>2</sub>, CH<sub>3</sub>-CH<sub>2</sub>-O), 2.3-0.9 (br, 13H, CH<sub>2</sub>-CH-(backbone), N-CH<sub>2</sub>-CH<sub>3</sub>) (**Fig. S3**); <sup>13</sup>C NMR (DMSO-*d*<sub>6</sub>): 223.9, 167.2, 166.6, 152.7, 150.4, 145.2, 132.6-124.3, 113.1, 72.1, 69.7, 52.3, 43.2, 13.8 ppm (**Fig. 3.5**).

**Synthesis of molecular model.** Monomer **2** (0.5 g, 1.67 mmol) was solubilized in methanol (2 mL). Potassium acetate (0.18 g, 2 mmol) was added and the reaction carried out at rt under stirring for 16 h. The solution was filtered to remove the formed KCl and dried under reduced pressure. Yield > 95%. <sup>1</sup>H NMR (DMSO-*d*<sub>6</sub>):  $\delta$  (ppm) = 10.6 (s, 1H, N-CH=N), 8.15-7.4 (m, 8H, Ar-*H*), 6.78-6.6 (dd, 1H, CH<sub>2</sub>-CH-Ar), 5.85 (d, 2H, CH<sub>2</sub>-CH-), 5.79 (s, 2H, Ar-CH<sub>2</sub>-N), 5.3 (d, 2H, CH<sub>2</sub>-CH-), 4.5 (m, 2H, N-CH<sub>2</sub>-CH<sub>3</sub>), 1.6 (s, 3H, OOC-CH<sub>3</sub>), 1.5 (t, 3H, CH<sub>2</sub>-CH<sub>3</sub>) (**Fig. S3.4**).

**Synthesis of linear model polymer.** 2-cyano-2-propyl benzodithioate CTA (30 mg, 0.13 mmol), styrene (2.64 mL, 23 mmol) and monomer **2** (1.21 g, 4 mmol) were placed in a 20 mL glass tube. Methanol (10 mL) was added and the suspension allowed stirring for 5 min until a solution was obtained. AIBN (27 mg, 0.11 mmol) was then added to the methanolic solution under dry argon at room temperature. After mixing, the glass tube was placed at 80 °C in an oil bath for 17 h. 46% conversion was reached as evidenced by <sup>1</sup>H NMR spectroscopy. The reaction was quenched by cooling the solution to room temperature. The crude copolymer was then purified by dialysis against methanol (1 L x 2 every 24 h) using 3.5 kDa MWCO dialysis membranes. The obtained copolymer (1 g) was solubilized in methanol and subjected to anion-exchange by adding potassium acetate (0.7 g, 10 eq.) to the solution, this was then left overnight under stirring. The reaction was then cooled, filtered, and dried under reduced pressure. Yield= 39%. <sup>1</sup>H NMR (DMSO-*d*<sub>6</sub>):  $\delta$  (ppm) = 11.5-10.5 (br, 1H, N-CH=N), 8.2-6.05 (br, Ar-*H*), 6-5.55 (br, 2H, Ar-CH<sub>2</sub>-N), 4.6-4.4 (br, 2H, N-CH<sub>2</sub>-CH<sub>3</sub>), 2.3-0.9 (br, 9H, OOC-CH<sub>3</sub>, N-CH<sub>2</sub>-CH<sub>3</sub>, -CH<sub>2</sub>-CH- (backbone)) (**Fig. S3.5**). SEC analysis «*D*» = 1.18; M<sub>n</sub> = 14.8 kDa (**Fig. S3.6**).

**General procedure for benzoin condensation reaction.** In a 10 mL glass tube, different catalysts were first azeotropically dried using distilled THF. Then, dry THF was added keeping a reference catalyst concentration of 20 mg/mL. The solution was stirred, and previously distilled benzaldehyde (10 eq.) was added under argon. The resulting mixture was stirred under argon at 80 °C for 24 h. After cooling, an aliquot was immediately taken and analyzed by <sup>1</sup>H NMR spectroscopy to determine the conversion by comparing the integral value of the aldehyde signal of the benzaldehyde starting material (s, 1H, 10 ppm) with that of the -CH- benzoin product signal (s, 1H, 6 ppm) (**Fig. S3.7-9**).

### **General catalyst recycling procedure**

After the previous catalytic cycle was performed, the resulting mixture was cooled down, significantly diluted in methanol and purified by dialysis (3.5 kDa MWCO) against MeOH (1L x 2 every 24 h) in order to remove unconverted benzaldehyde, formed benzoin and THF. The catalyst was dried under vacuum and the azeotropically dried again once using THF before the next catalytic run.

### **Diffusion Ordered Spectroscopy**

Molecules are distinguished according to their diffusion, which correlates with their hydrodynamic radius. Samples of polymer **4** as well as the SCNP **5**, were analyzed in DMSO-*d*<sub>6</sub> employing the conditions displayed in experimental part. Calculation of the diameter, applying the Stokes-Einstein-Equation.

Stokes-Einstein-Equation:

$$D = \frac{kT}{6\pi\eta r}$$

$$k = 1.38 \times 10^{-23} \text{ J.K}^{-1}$$

$$D = 3.14 \cdot 10^{-11} \text{ m}^2/\text{s}$$

$$T = 298 \text{ K}$$

$$\eta \text{ DMSO viscosity} = 1.99 \cdot 10^{-3} \text{ Pa.s}$$

$$R = 3.5 \text{ nm } D = 7 \text{ nm (SCNP 5)}$$

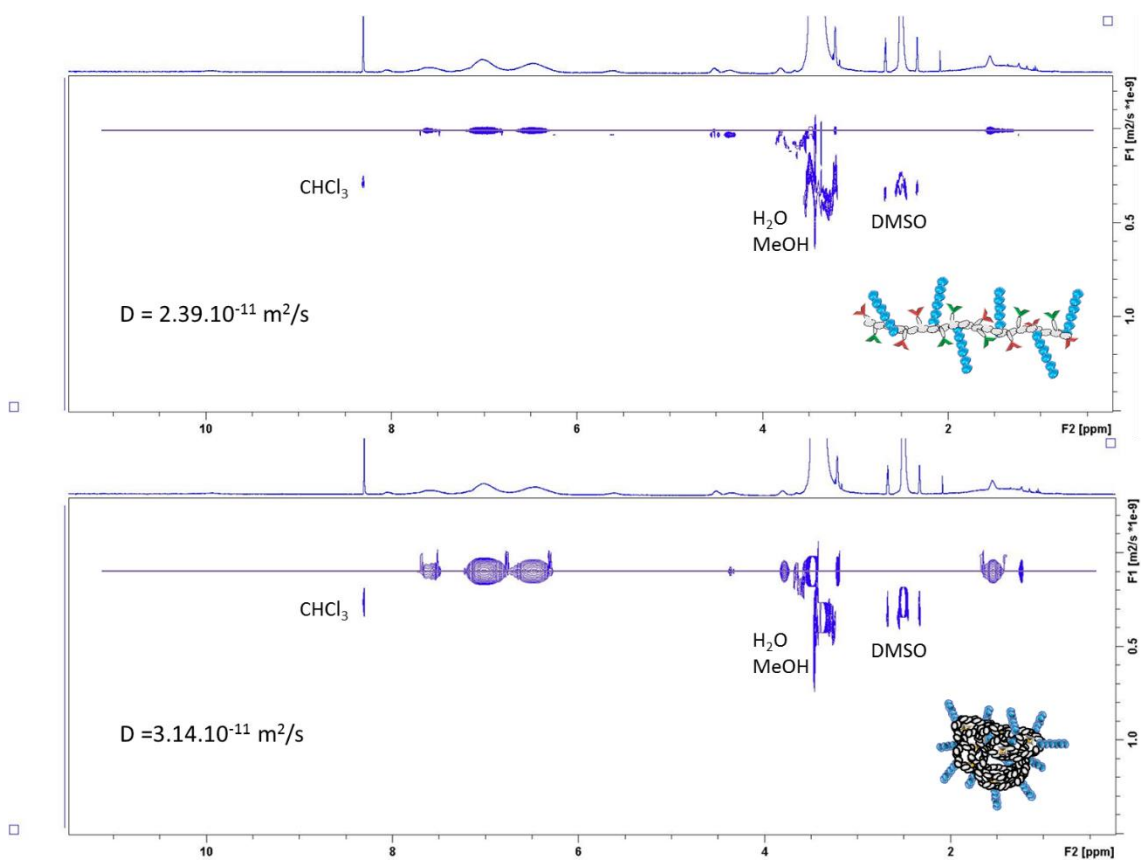


**Figure S3.1.** Original figure of DOSY measurements of the precursor copolymer **4** and SCNP **5**, recorded in  $\text{DMSO-}d_6$ .

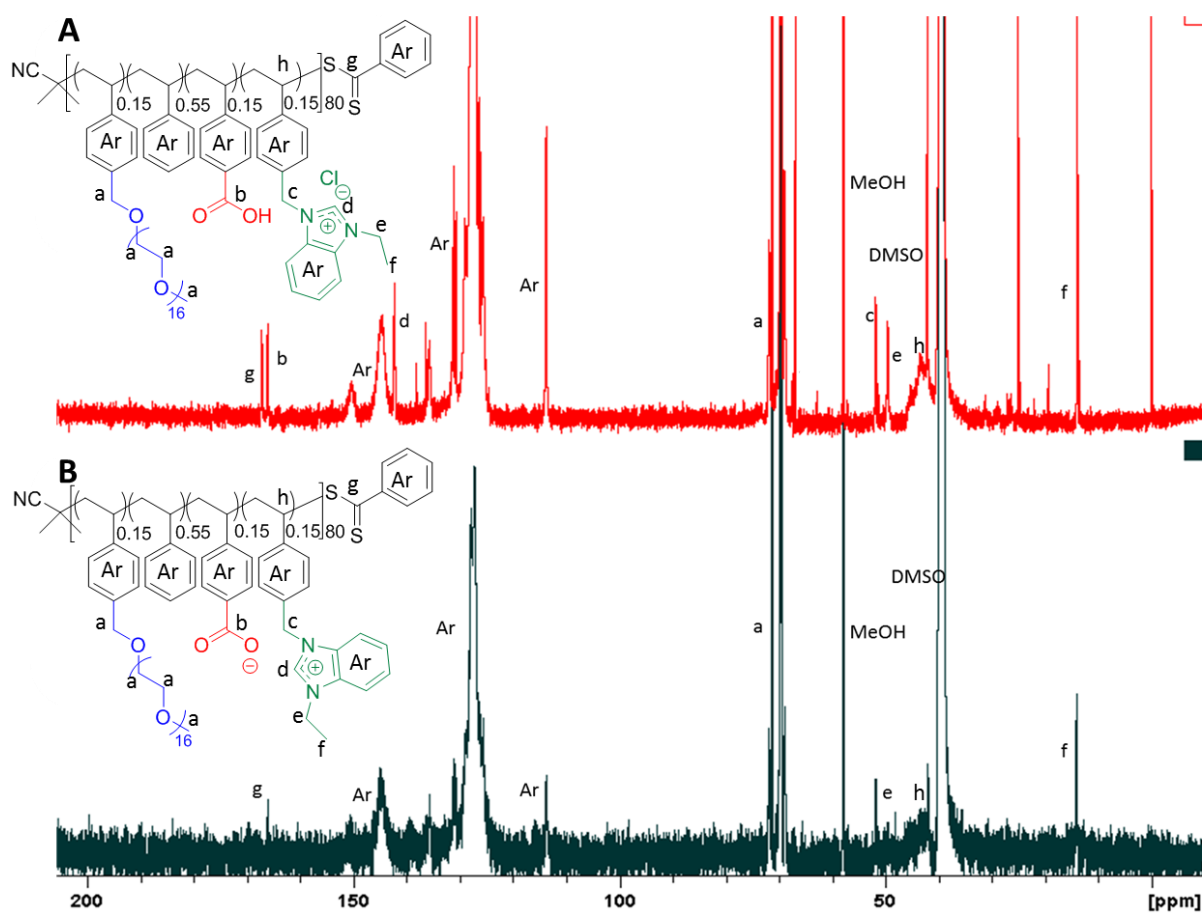
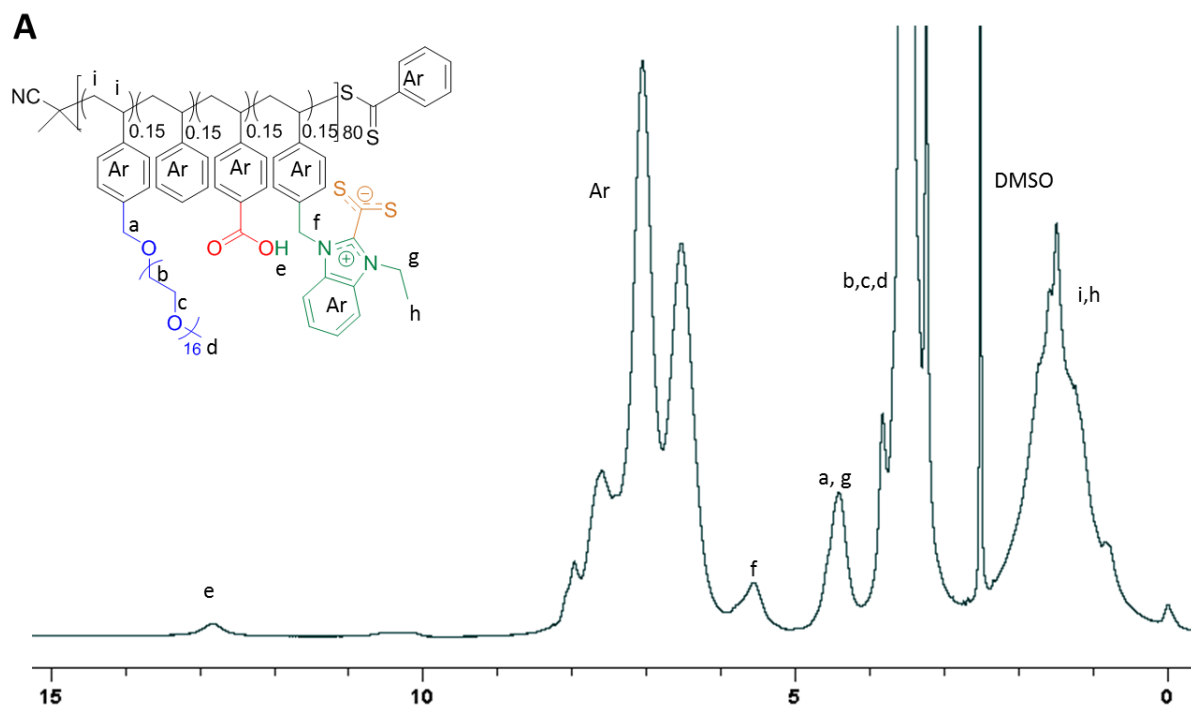


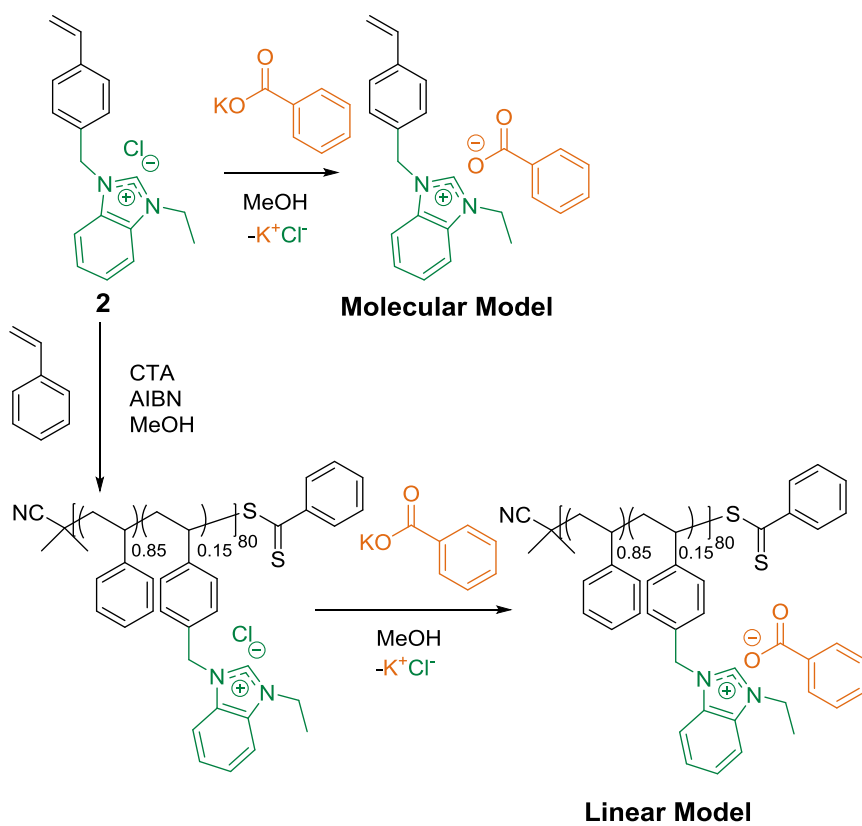
Figure S3.2:  $^{13}\text{C}$  NMR spectrum in  $\text{DMSO-}d_6$  of linear precursor 4 (A) and SCNP 5 (B) after folding.





**Figure S3.3:**  $^1\text{H}$  NMR (A)  $^{13}\text{C}$  NMR (B) spectra of CS<sub>2</sub> post-functionalization reaction in SCNP **6** in DMSO-*d*<sub>6</sub>.

### Synthesis of model catalysts



**Scheme S3.1.** Synthetic route to prepare molecular catalyst model based on the active monomer and linear catalyst model.

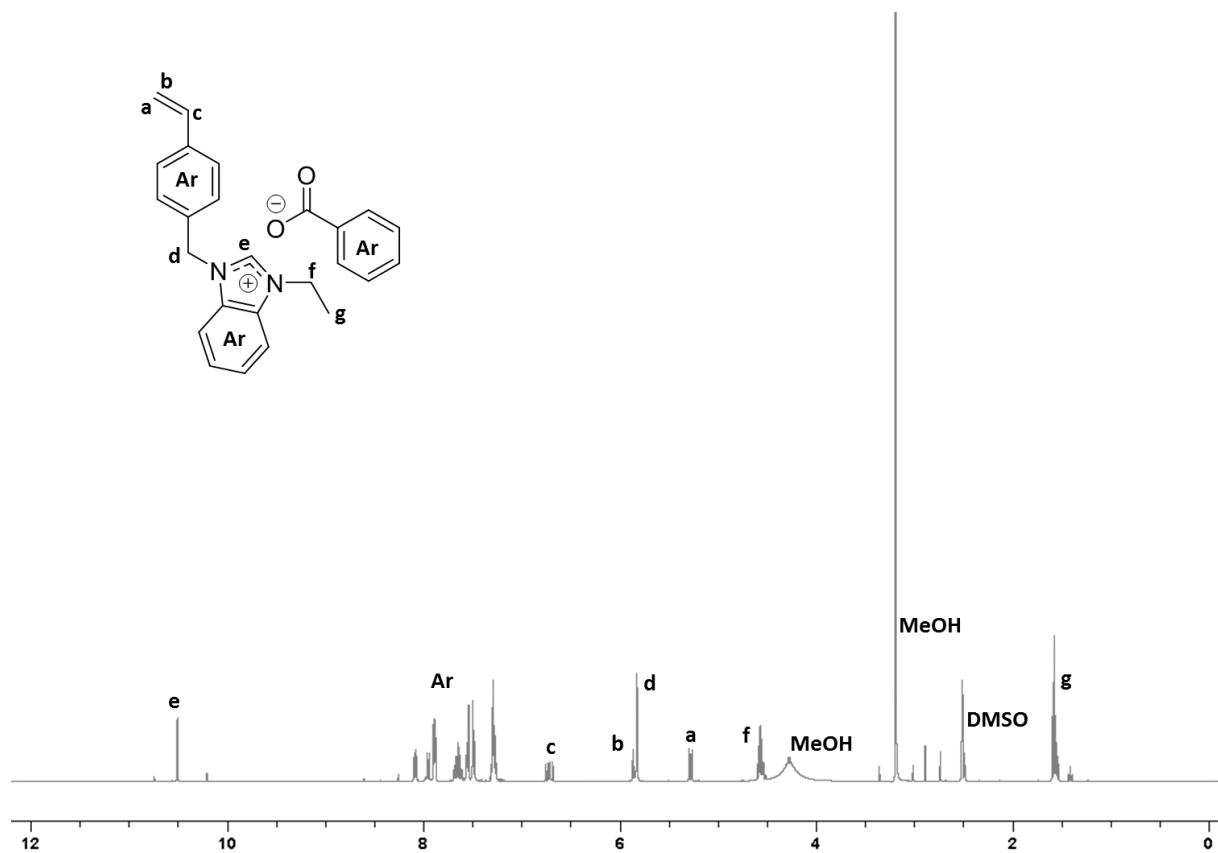


**Figure S3.4.**  $^1\text{H}$  NMR spectrum of molecular model catalyst in  $\text{DMSO-}d_6$ .

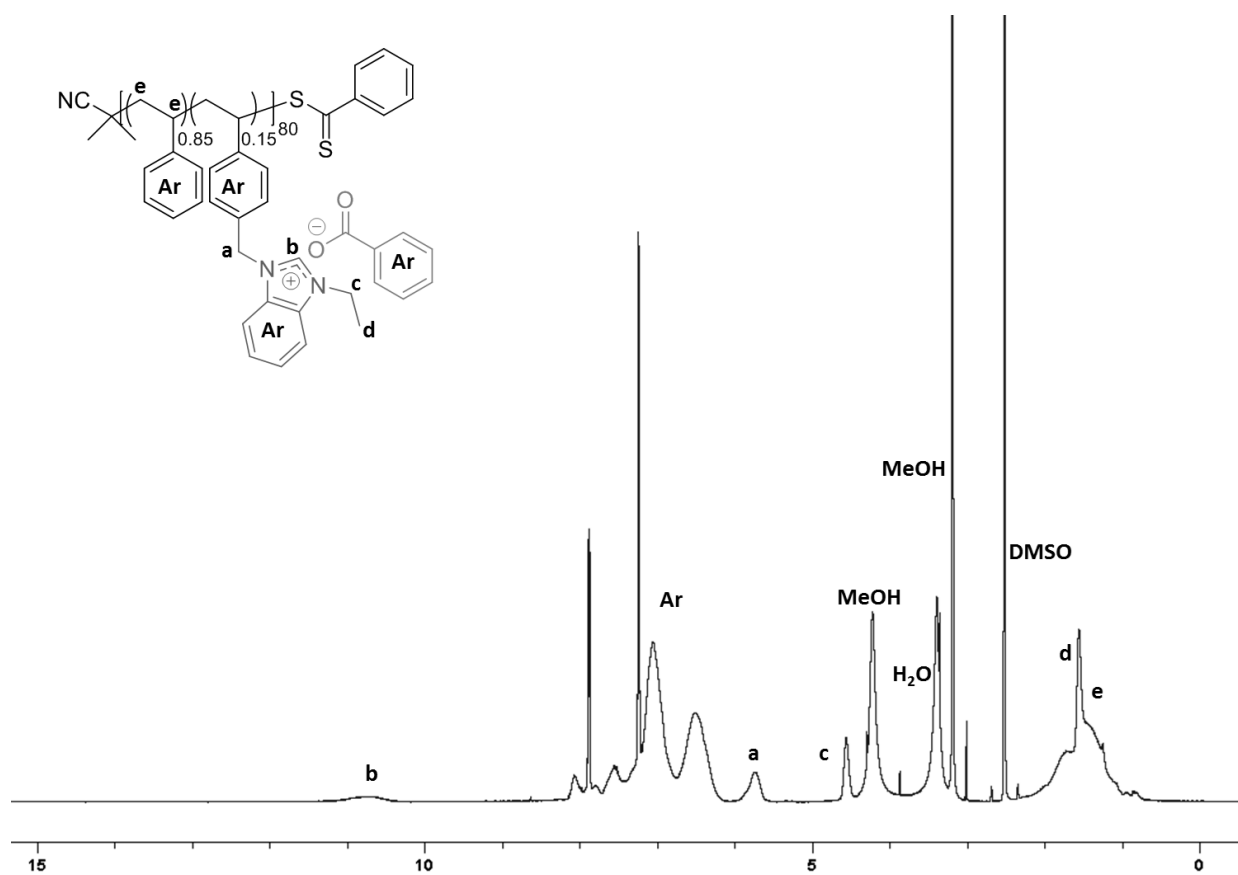


**Figure S3.5.**  $^1\text{H}$  NMR spectrum of catalyst linear copolymer model in  $\text{DMSO-}d_6$ .

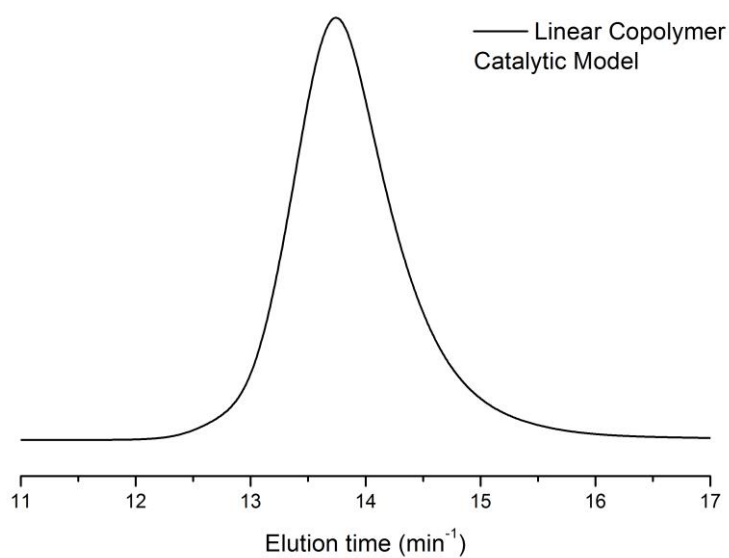


**Figure S3.6.** SEC traces of Linear Copolymer model (in  $\text{Cl}^-$  anion form) in DMF (10 mM ammonium tetrafluoroborate) with RI detector ( $\ll D = 1.18$ ;  $M_n = 14.8$  kDa; Universal calibration).

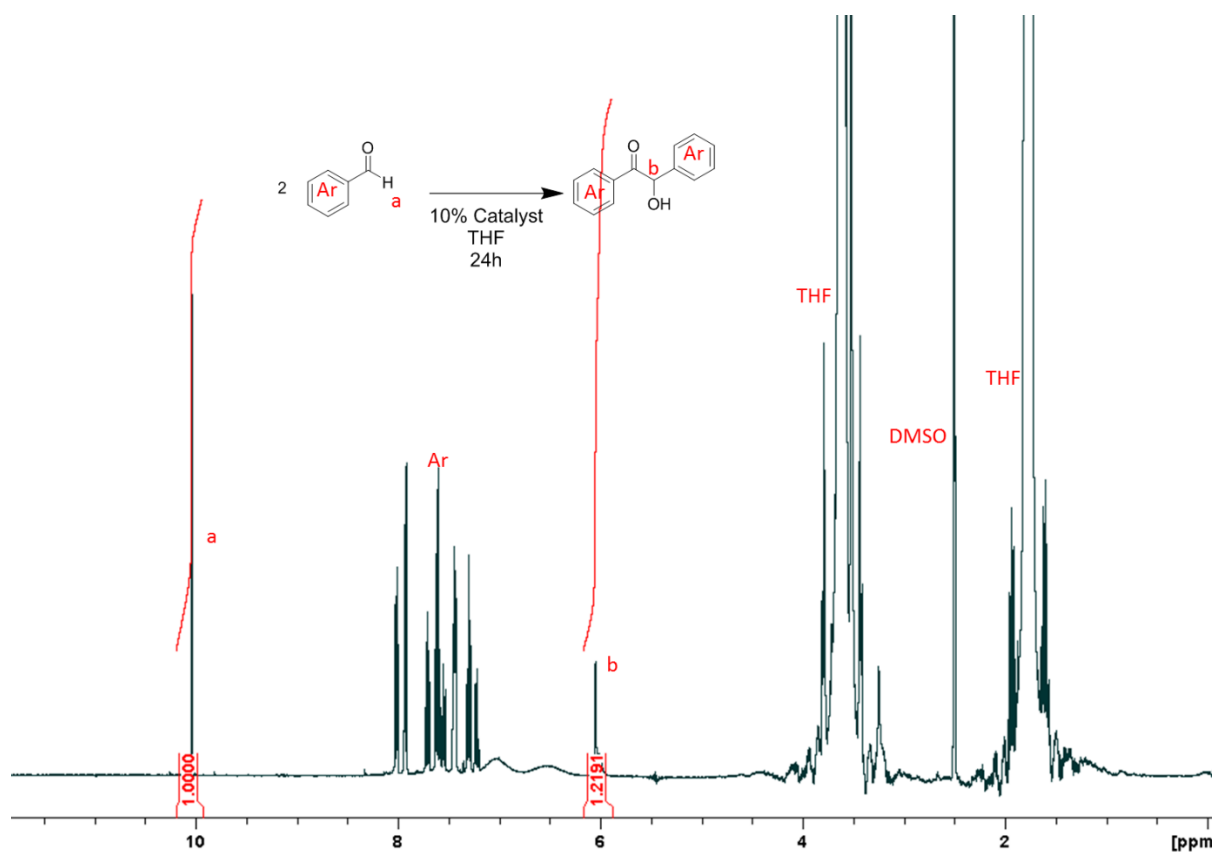


**Figure S3.7.** Reaction of benzoin condensation with benzaldehyde catalyzed by SCNP **5** and conversion obtained  $^1\text{H NMR}$  spectroscopy in DMSO- $d_6$ .

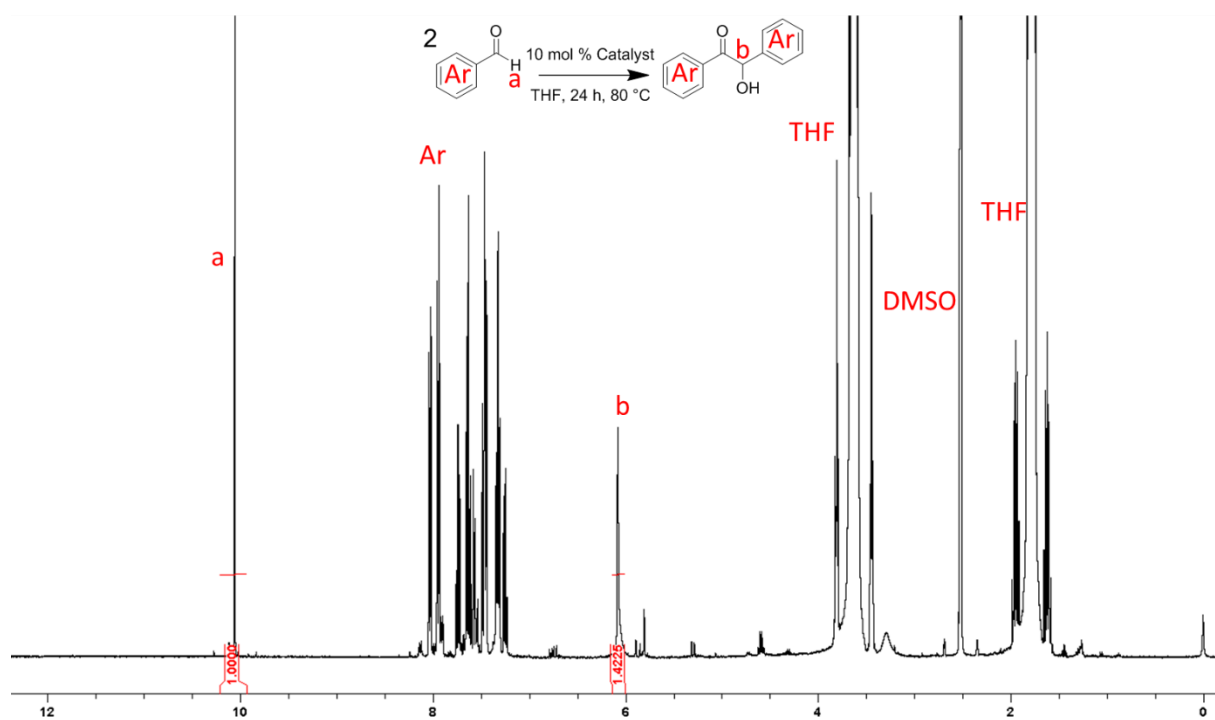


**Figure S3.8.** Reaction of benzoin condensation with benzaldehyde catalyzed by molecular model and conversion obtained  $^1\text{H}$  NMR spectroscopy in  $\text{DMSO-}d_6$ .

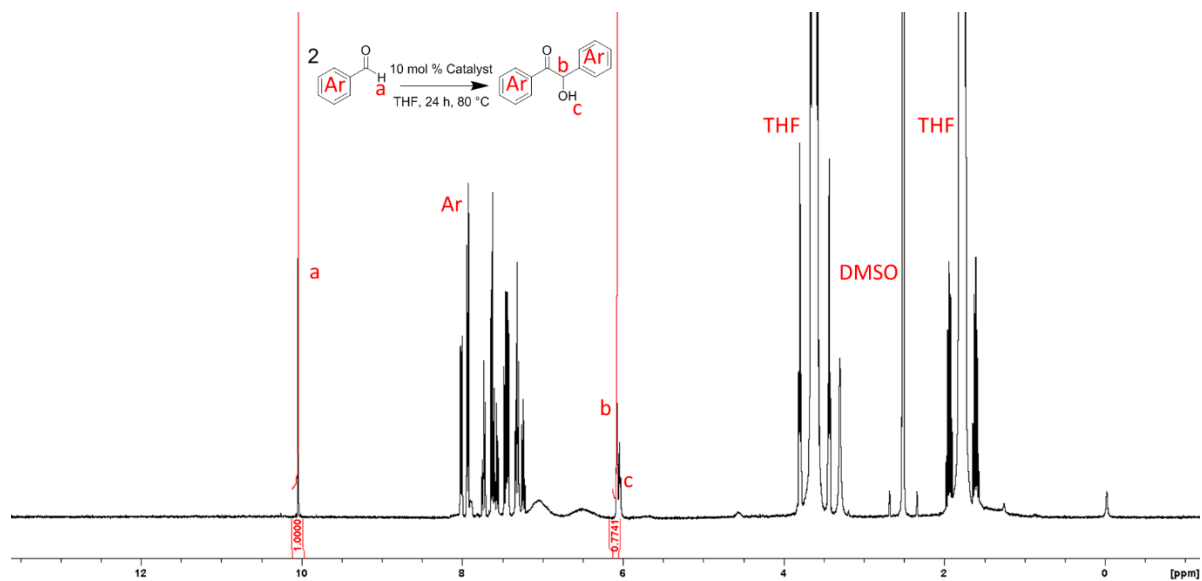


**Figure S3.9.** Reaction of benzoin condensation with benzaldehyde catalyzed by linear copolymer model and conversion obtained  $^1\text{H}$  NMR spectroscopy in  $\text{DMSO-}d_6$ .

### Waterborne catalysis conditions

PEG-based side-oligopolymers were incorporated along the (co)polymer chain to render this system soluble in water. When a  $^1\text{H}$  NMR analysis experiment was performed using  $\text{D}_2\text{O}$  as deuterated solvent, only the PEG side chains were observed due to the external conformation of the SCNP **5** (Fig. S10).

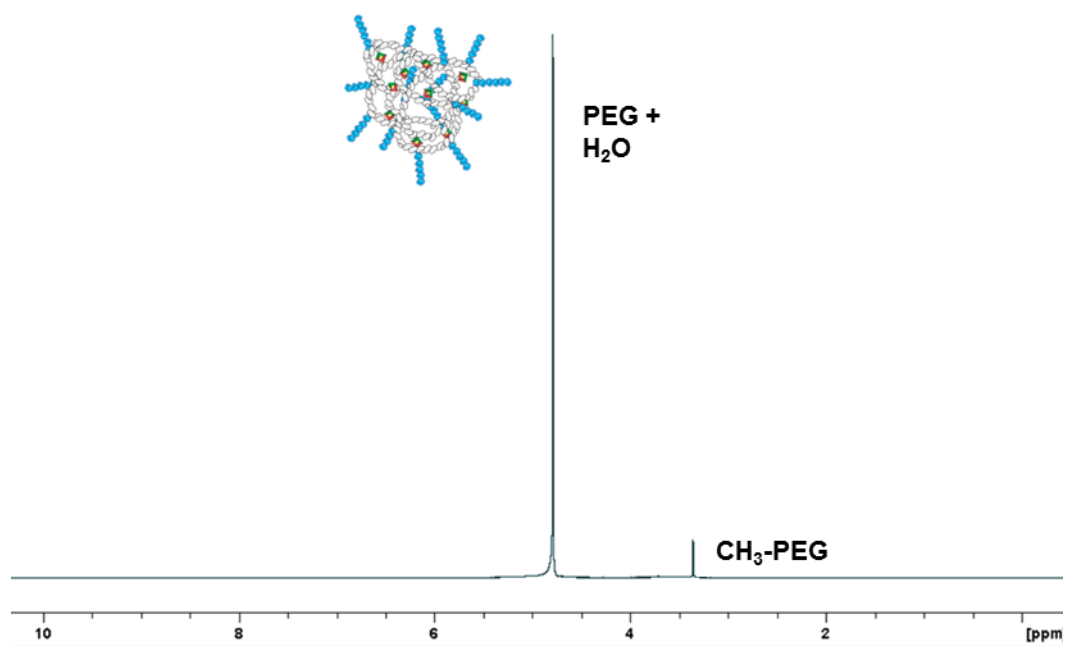


**Figure S3.10.**  $^1\text{H}$  NMR spectra of the SCNP 5 in  $\text{D}_2\text{O}$ .

**Chapter IV: Self-catalysed folding of single chain nanoparticles (SCNPs) by NHC-mediated intramolecular benzoin condensation**





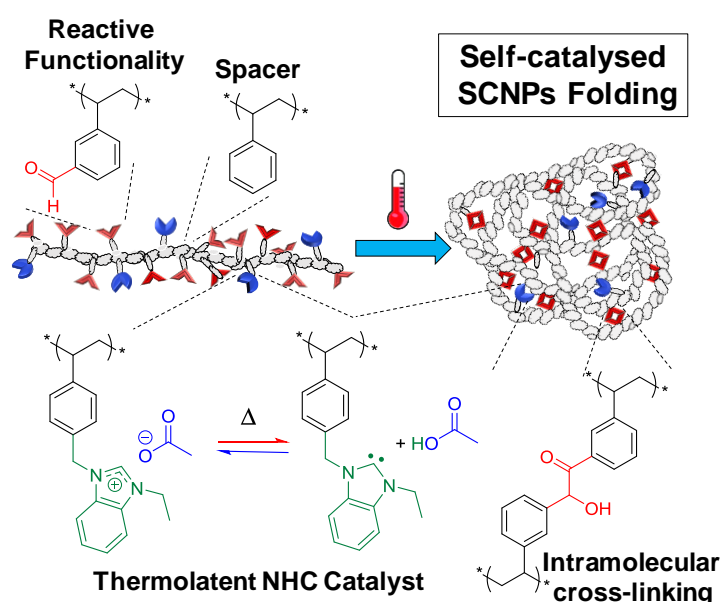
# Table of Contents

## **Chapter IV: Self-catalysed folding of single chain nanoparticles (SCNPs) by NHC-mediated intramolecular benzoin condensation**

4.1. Abstract.....	173
4.2. Introduction.....	174-176
4.3. Synthesis of catalytically active SCNPs.....	176-182
4.4. Transesterification reaction catalysed by SCNP 5.....	182-186
4.5 Conclusions.....	186-187
4.6. References.....	187-189
4.7. Experimental section.....	190-209

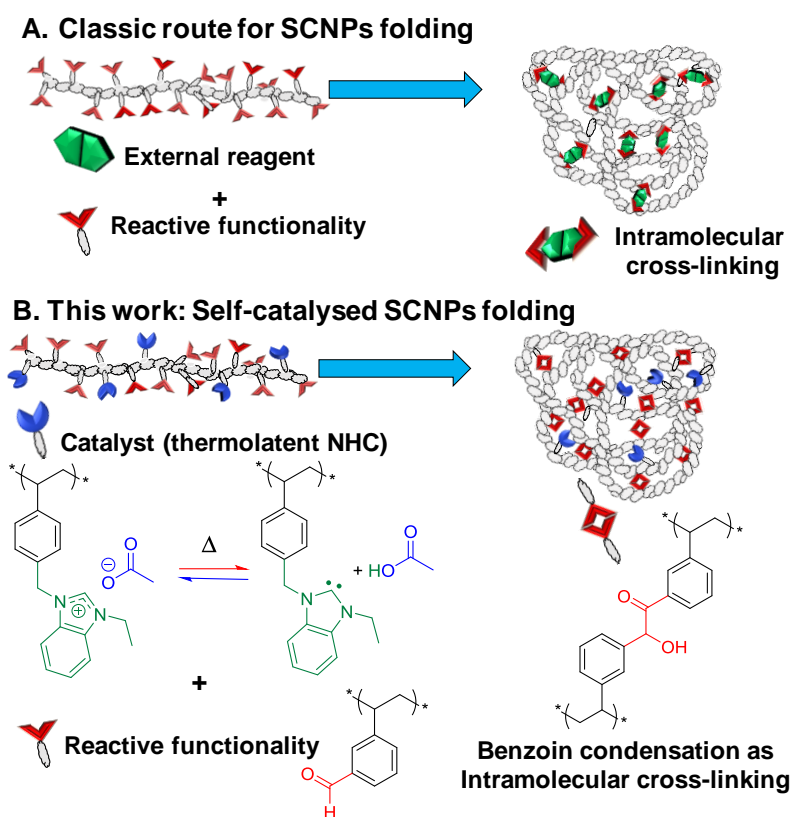
## 4.1 Abstract

A self-catalysed folding strategy to form single chain nanoparticles (SCNPs) was developed via an intramolecular *N*-heterocyclic carbene (NHC)-mediated benzoin condensation. Benzaldehyde, styrene and benzimidazolium chloride units were randomly incorporated into a poly(ionic liquid)-based (PIL) copolymer precursor by reversible addition–fragmentation chain transfer (RAFT) copolymerisation. Post-chemical modification of this linear precursor by insertion of a non-innocent acetate counter-anion into the benzimidazolium moieties conferred thermolabile catalytic behaviour owing to the equilibrium between benzimidazolium acetate units and corresponding NHC ones. Upon heating, catalytically active NHCs allowed the formation of benzoin-type intramolecular cross-links, thus folding linear chains into SCNPs. NHC moieties became deactivated after cooling to room temperature, which enabled easy isolation and purification of the covalently and intramolecularly cross-linked SCNPs. Importantly, the latent NHC moieties were proven to retain their catalytic activity when arranged into SCNPs as evidenced through their reactivation by simple heating. The catalytic activity of these SCNPs was further confirmed by implementing another NHC-organocatalysed reaction, namely, transesterification reaction between vinyl acetate and benzyl alcohol. This work represents the first example of catalysis by a parent linear precursor which drives its own folding and remains catalytically active.



## 4.2 Introduction

Single-chain nanoparticles (SCNPs) have recently emerged as versatile soft nano-objects with unique characteristics, that make them suitable in an array of applications, such as nanomedicine,<sup>1,2</sup> bioapplications (bioimaging, drug delivery),<sup>3,4</sup> or catalysis.<sup>5-7</sup> SCNPs consist of single polymer chains that are cross-linked through intramolecular bonding, in an attempt to mimic the unique properties of natural biomacromolecules (*e.g.* polypeptides, DNA, enzymes).<sup>8-13</sup> In this context, synthetic enzymatic mimics that utilise polymer backbones present a number of opportunities for preparing efficient catalysts, by controlling key properties such as polymer solubility,<sup>14</sup> increased accessibility to a larger library of substrates,<sup>15</sup> increased turnover frequency (TOF),<sup>16</sup> recycling,<sup>17-19</sup> or supporting organic/metallic catalysts on a soluble polymeric support.<sup>20-24</sup> The most common strategy to prepare SCNPs is based on the design of a linear single chain precursor that features pendant functionalities to facilitate folding through the formation of intramolecular cross-links following exposure to an external *stimuli* (*e.g.* temperature, solvent, UV-irradiation), or addition of external reagents.<sup>13,25-27</sup> After covalent and/or non-covalent cross-linking, the SCNPs may be used as nanoreactors. However, the catalytic ability of the parent linear precursor has not been so far exploited as a driving force for its own folding. Here, new insight is brought to this field through immobilisation of both the reactive functionality and the catalyst onto the same linear copolymer precursor, enabling triggering through a self-catalysed folding as a novel route to SCNPs (**Scheme 4.1**).



**Scheme 4.2.** Strategies to conduct SCNP synthesis for use as catalytic nanoreactors. **A)** Classic route involving the addition of external reagents to induce chain folding. **B)** Self-catalysed SCNPs folding mediated by supported thermally latent NHC precatalysts.

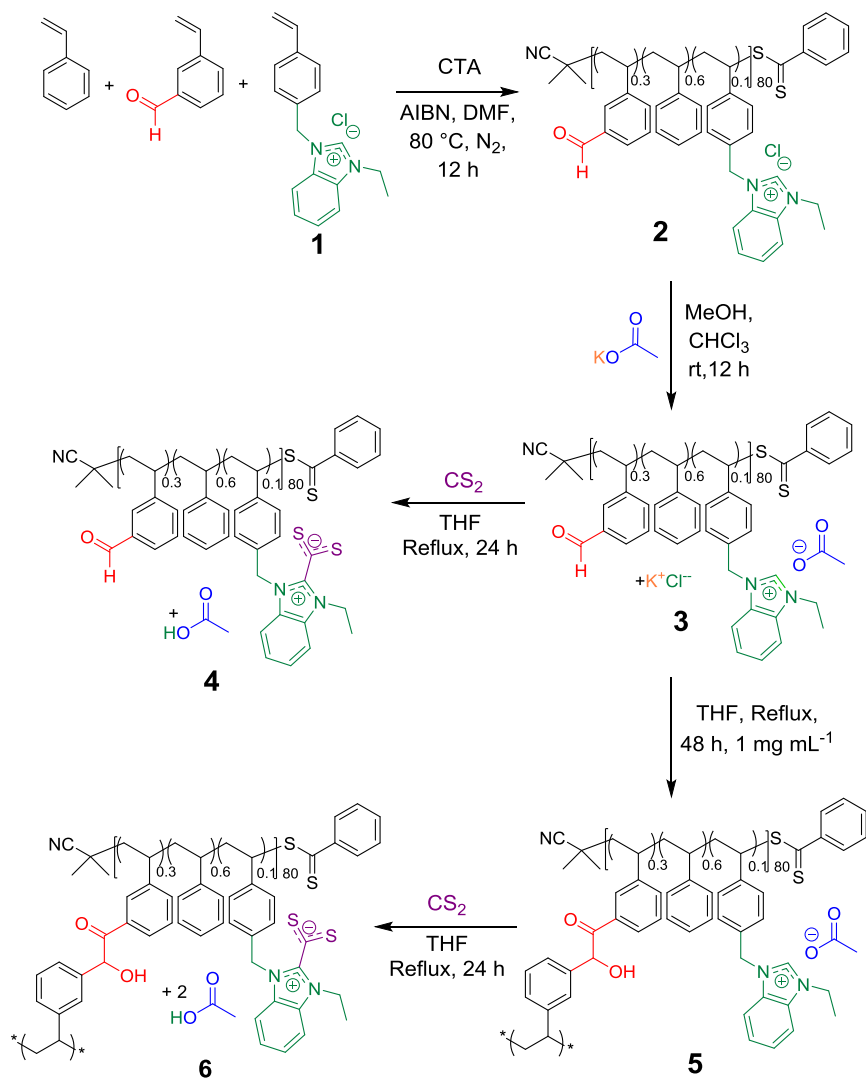
One possible obstacle to the folding process lies in the orthogonality between reactive functionalities and the catalyst. We therefore turned to the use of a copoly(ionic liquid) (coPIL) precursor, PILs representing modular polymeric platforms where different orthogonal functionalities can be introduced, thanks to the broad selection of monomeric ionic liquids.<sup>28–30</sup> In particular imidazolium-based ILs are known as versatile precursors of *N*-heterocyclic carbenes (NHCs), which can be activated *in situ* for instance by means of solvent change or upon heating among other triggers. More specifically, imidazolium-based precursors featuring a slightly basic counter-anion, *e.g.* hydrogen carbonate,<sup>31</sup> acetate,<sup>32</sup> sebacate<sup>33</sup> or benzoate,<sup>19</sup> can autonomously generate NHCs, *i.e.* without the need for any external reagent, owing to the deprotonation of the C2-position by the basic anion. Installation of the latter is straightforward

as it can be achieved one step by simple anion-metathesis (= anion exchange reaction). Synthesis of imidazolium-type coPILs bearing such anions provides a convenient strategy to immobilize latent NHCs onto a polymeric support, which can be catalytically turned on and off simply three decades, not only as ligands for transition metals, but also as true organocatalysts for numerous molecular and macromolecular transformations.<sup>34–37</sup> The so-called benzoin condensation is an emblematic NHC-catalysed carbon-carbon bond-forming reaction occurring by self-condensation of two aldehyde substrates forming a  $\beta$ -keto alcohol with no by-product.<sup>38,39</sup> By introducing both latent aldehyde-type units and benzimidazolium acetate units as site-isolated latent NHCs into the same copolymer chain, we reasoned that intramolecular benzoin condensation of supported benzaldehydes could be triggered by simple heating under dilute solution, causing the single copolymer chain to fold through the formation of benzoin-type crosslinks. This inherent thermal-latency would be further harnessed by cooling/deactivating the masked supported NHCs after folding, to isolate the resulting SCNPs. These could be further used as nanoreactors to mediate another NHC-catalysed reaction, namely, transesterification between benzyl alcohol and vinyl acetate. Herein, we thus report a novel self-catalysed folding strategy to SCNPs, forming intramolecular covalent cross-links of benzoin-type. Of particular interest, the resulting SCNPs remains catalytically active. By immobilizing for the first time both the catalytic species and the substrates onto the same single copolymer chain, the synthetic strategy we describe here further expands the scope of SCNPs.

### 4.3 Synthesis of catalytically active SCNPs

The linear statistical single chain precursor was devised to be constituted of three distinct monomer units, namely, deriving from benzaldehyde, benzimidazolium and styrene functionalities (**Scheme 4.2**). As emphasised above, benzimidazolium chloride moieties served as NHC precursors, benzaldehyde as reactive substrate both being immobilised onto the coPIL backbone, while styrene units would play the role as spacers to facilitate easier accessibility of the NHC catalyst to the reactive functionalities, also conferring some hydrophobicity to the copolymer backbone. As depicted in **Scheme 4.2**, the IL monomer, namely, 4-vinylbenzylethylbenzimidazolium chloride **1** was synthesised following an established procedure.<sup>14,19,33</sup> Copolymerisation of **1** with 3-vinylbenzaldehyde and styrene was achieved *via* the reversible addition fragmentation chain transfer (RAFT) process in DMF, using AIBN

as a radical source and 2-cyano-2-propyl benzodithioate as the RAFT agent. A [Monomer(s)]/[CTA]/[AIBN] ratio of 98/1/1 was targeted. The reaction was carried out for 12 h at 80 °C, reaching *ca.* 40% conversion. The structure of the resulting linear coPIL **2** was authenticated by <sup>1</sup>H NMR spectroscopy. In particular, the proportion of the different monomer units within the backbone structure could be determined by relative integration of the characteristic signals of each monomer obtained by <sup>1</sup>H NMR spectroscopy (**Fig. 4.1**). Briefly, the intensity of signals corresponding to the aldehyde proton was compared to the *N*-alkylated moieties of benzimidazolium chloride, *i.e.* benzyl-CH<sub>2</sub>-N at 5.4 ppm and br. N-CH<sub>2</sub>-CH<sub>3</sub> at 4.6 ppm, and the aromatic region at 6-8 ppm, corresponding to the number of styrene units. This calculation gave an average composition of 48 styrene units, 8 units of **1** and 24 units of benzaldehyde. Therefore, the calculated molecular weight for copolymer **2** was found equal to ~10.5 kg mol<sup>-1</sup>, that was, slightly smaller than the value delivered by SEC in DMF of 11.9 kg mol<sup>-1</sup>.



**Scheme 4.2.** Synthetic route to functional linear copolymer **3** and subsequent self-catalysed folding step leading to catalytically active SCNP **5**. The NHC-CS<sub>2</sub> functionalised versions of both linear precursor (**4**) and obtained SCNP (**6**) as well as corresponding active NHC intermediates are also represented.

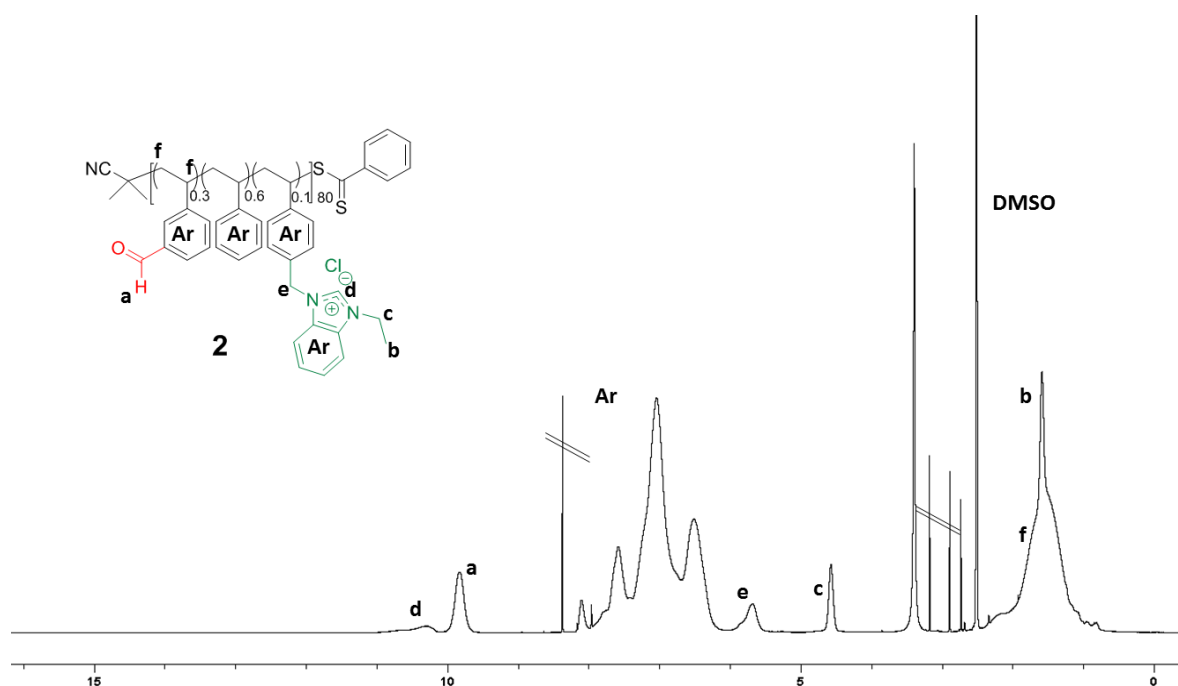


**Figure 4.1.**  $^1\text{H}$  NMR spectrum of copolymer **2** in  $\text{DMSO-}d_6$ .

The benzimidazolium chloride functionality was then subjected to an anion exchange, substituting the acetate anion for the chloride in one step and thus affording a latent NHC pre-catalyst.<sup>40</sup> This metathesis reaction was carried out at room temperature in dry methanol in presence of KOAc, yielding copolymer **3** (Fig.S4.2, S4.3). This was confirmed first by the appearance of a new signal corresponding to acetate  $-\text{CH}_3$  protons at *ca.* 1 ppm in  $^1\text{H}$  NMR analysis and the presence of the same acetate carbonyl signal at 176.6 ppm in  $^{13}\text{C}$  NMR spectroscopy. This strategy enables the easy handling and storage of the coPIL precursor **3** in an inactive state at low temperature.<sup>21,32,41,42</sup>

We first examined the latent NHC-like behaviour of coPIL **3** *via* a simple chemical postmodification consisting in the reaction between benzimidazolium acetate units with an excess of carbon disulfide ( $\text{CS}_2$ ). Upon heating in THF this reaction mixture for 24 h, polymer-supported NHCs thus released NHCs from **3** are trapped, forming a red solution characteristic of a NHC- $\text{CS}_2$  adduct (= copolybetaine **4**). This was evidenced by the appearance of diagnostic signals in the  $^{13}\text{C}$  NMR spectrum at 224.1 ppm and 153.1 ppm corresponding to  $\text{C}_{2\text{imi}}$  and  $\text{CS}_2^-$ , respectively (Fig. 4.2).<sup>31,43</sup>



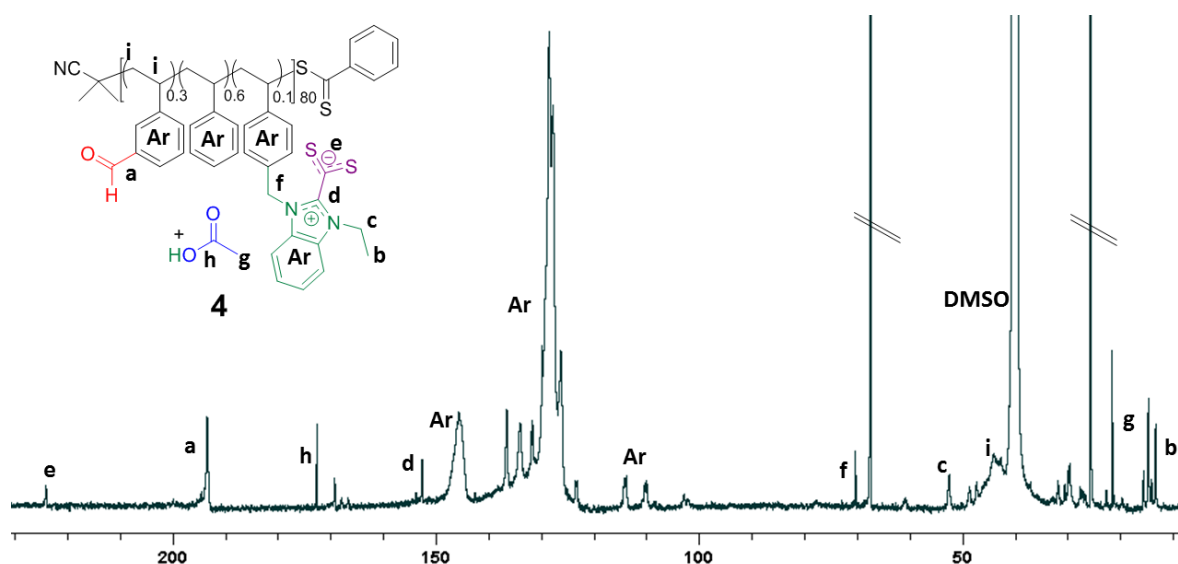


**Figure 4.2.**  $^{13}\text{C}$  NMR spectrum of copolymer **4** in  $\text{DMSO-}d_6$ .

This reaction test thus allowed us, to confirm the crucial role of acetate anion in supplying copoly(NHC)s from the linear coPIL precursor **3** upon heating. The self-catalysed folding based on the intramolecular benzoin condensation of benzaldehyde units could then be investigated. To this end, a solution of coPIL **3** was heated to  $80\text{ }^\circ\text{C}$  in THF at  $1\text{ mg mL}^{-1}$  concentration for 48 h. The folding process generating SCNP **5** constituted of benzoin covalent cross-links was evaluated by  $^1\text{H}$  and  $^{13}\text{C}$  NMR spectroscopy, size exclusion chromatography (SEC), dynamic light scattering (DLS), transmission electron microscopy (TEM), diffusion-ordered spectroscopy (DOSY) NMR and Fourier-transform infrared spectroscopy (FTIR). Characteristic signals corresponding to the newly formed benzoin moieties were clearly detected in the  $^1\text{H}$  NMR spectrum, namely, at 5.4 ppm (H from the chiral benzoin carbon) and at 4.2 ppm (-OH from the same chiral carbon; **Fig. S4.4**).  $^{13}\text{C}$  NMR analysis also revealed the presence of both a newly formed carbonyl signal at 179.3 ppm and the -CH- benzoin carbon at 80.7 ppm (**Fig. S4.5**). Formation of benzoin-type crosslinks was further evidenced by HSQC spectroscopy (**Fig. S4.6**) correlating the -CH- of benzoin moieties to the corresponding chiral carbon atom. Furthermore, FT-IR spectroscopy showed both the appearance of the benzoin -OH group at  $3300\text{ cm}^{-1}$ , as well as the broadening of the carbonyl vibration signal at  $1700\text{ cm}^{-1}$ , due to the presence of the acetate (counter-anion), ketone (benzoin) and residual aldehyde (**Fig. S4.7**). Self-folding was also demonstrated by a decrease in the hydrodynamic diameter of

the as-obtained SCNPs, according to different analytical techniques, as summarised in **Figure 4.3**. Firstly, a decrease in the apparent molecular weight was noted by SEC, compared to the linear precursor **2** (**Fig. 4.3A**) due to compaction by intramolecular crosslinking upon forming SCNP **5**. DLS performed in THF at 20 °C revealed a slight decrease in hydrodynamic diameter ( $D_H$ ), from 7.5 nm to 6.1 nm (**Fig. 4.3B**; see **Fig. 4.4** for the range 20-80 °C). In addition, dry-state TEM analysis confirmed the presence of spherical nanoparticles corresponding to SCNP **5** with an average diameter of *c.a.* 4.5 nm (**Fig. 4.3C**). Finally, DOSY NMR spectroscopy in DMSO- $d_6$  showed a reduction in diameter after the self-catalysed benzoin condensation step, with a diameter of 2.3 nm calculated for SCNP **5**, whilst a value of 6.6 nm was obtained for the linear precursor **2** (**Fig. S4.8**). All these results are consistent with a compaction due to self-catalysed folding step formation benzoin-type crosslinks.

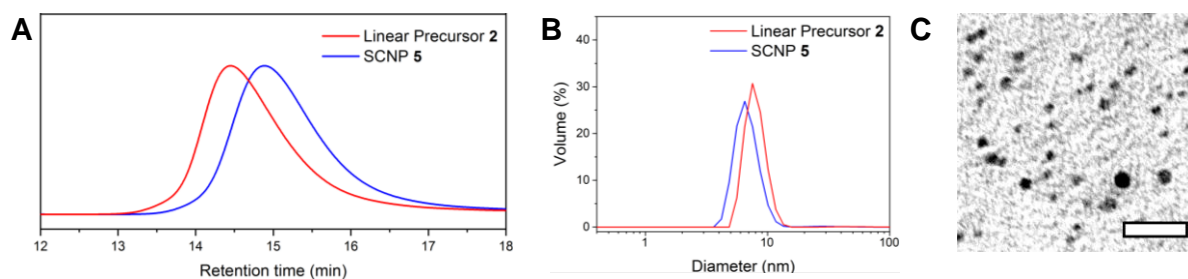


**Figure 4.3.** **A)** SEC traces (in DMF with 10 mM  $\text{NH}_4\text{BF}_4$ ) of SCNP **5** (blue line) obtained *via* intramolecular cross-linking of coPIL **2** (red line) by self-catalysis (UV detector). **B)** DLS analysis of coPIL **2** (red line) and SCNP **5** (blue line) diameters at 20 °C distributed by volume in THF (conc. 1 mg  $\text{mL}^{-1}$ ). **C)** TEM images of SCNP **5** (conc. 1 mg  $\text{mL}^{-1}$  in methanol) stained with uranyl acetate. Scale bar = 20 nm.

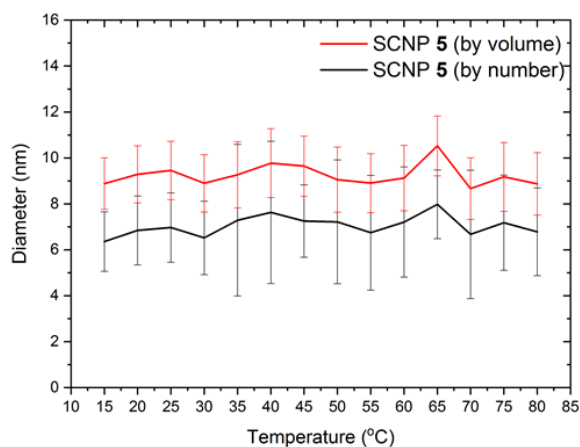


**Figure 4.4.** Hydrodynamic diameter-temperature correlation obtained for SCNP **5** by variable temperature dynamic light scattering (DLS) in THF (Conc.: 1 mg mL<sup>-1</sup>; 173° back-scattering detector; average value of 4 runs is reported along with the error corresponding to the standard deviation in the measurements; solid red line corresponds to values obtained for the volume distribution, whilst the solid black refers to the number distribution).

#### 4.4 Transesterification reaction catalysed by SCNP **5**

As SCNPs **5** thus formed still contains benzimidazolium acetate units, they were in turn evaluated as masked NHCs. This was first achieved through their post-functionalisation by insertion of CS<sub>2</sub>, generating polybetaine **6**. Thus, the reaction mixture in THF turned orange upon heating **5** in the presence of CS<sub>2</sub> after 24 h. The characteristic signal of functionalised C<sub>2</sub>imi at 153.1 ppm (**Fig. S4.9**) was again present in the <sup>13</sup>C NMR spectrum of **6**, although it was hardly detected likely because of the confined environment provided by SCNP **6**. In contrast, the COOH proton of the acetic acid by-product released during the functionalisation step was detected in the <sup>1</sup>H NMR spectrum, appearing at 12.5 ppm (**Fig. S4.10**). Formation of polybetaine **6** was further confirmed by FT-IR spectroscopy with the appearance of the asymmetric vibration of CS<sub>2</sub><sup>-</sup> at 1030 cm<sup>-1</sup> (**Fig. 4.5**). These results highlight that thermally latent NHC units remain active after the folding step.

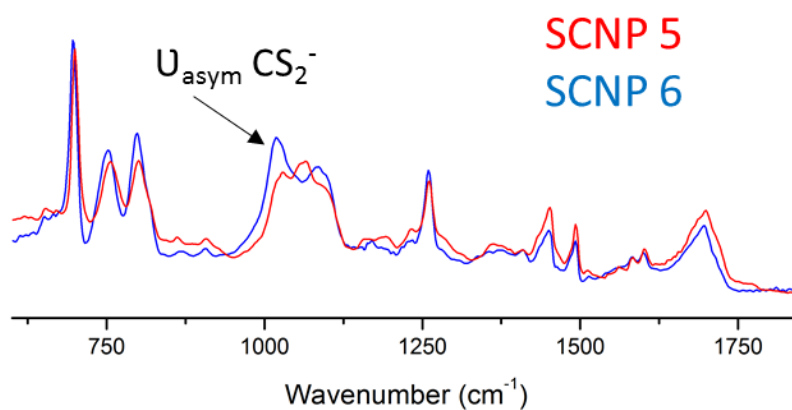
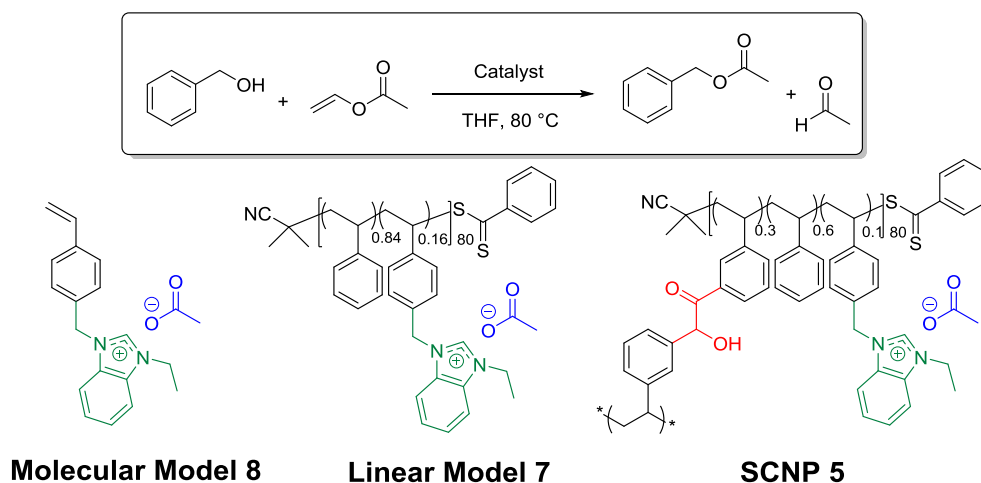


**Figure 4.5.** FTIR spectrum of SCNP **5** (in red) and NHC-CS<sub>2</sub> functionalised SCNP **6** (in blue) showing the appearance of the characteristic vibrational signal of CS<sub>2</sub><sup>-</sup> (at ~1030 cm<sup>-1</sup>) when forming the betaine.

The activity of SCNPs **5** was next tested in another NHC-mediated organocatalysis application, namely, the transesterification reaction between vinyl acetate and benzyl alcohol. This was first

achieved in THF using 1 eq. of benzyl alcohol and a slight excess of vinyl acetate (1.2 eq.) as, in presence of 1 mol.% of SCNP-supported masked NHCs **5**. Under such conditions, only 6% of benzyl alcohol was converted into benzyl acetate after 2 h (run 1; **Table 4.1**). Further optimisation using a loading of the catalytic SCNP **6** equal to 5 and 10 mol.%, whilst maintaining the concentration of reagents, allowed us to increase the conversion to 43% and up to 69% respectively (run 2 and 3). For a comparison purpose, SCNP **5** was compared to a linear statistical coPIL analogue **7** constituted of benzimidazolium acetate and styrene units, *i.e.* poly(styrene-*co*-4-vinylbenzylethylbenzimidazolium acetate) and to the 4-vinylbenzimidazole ethylimidazolium acetate monomer **8**, serving as molecular model. Both the molecular and macromolecular models were assessed for the transesterification reaction under the same catalysis conditions as SCNP **5**. Faster catalysis kinetics was observed from coPIL **7** compared to SCNP **5** (**Fig. 4.6B**), providing faster kinetics and higher conversions upon increasing the pre-catalyst loading (almost quantitative conversion was noted for 5 and 10 mol.% *vs.* 42% for 1 mol.% runs 5 and 6 and run 4, respectively). In comparison, almost quantitative conversions were obtained using 1, 5 and 10 mol.% catalyst loading of the molecular model after only 2 h (runs 7-9).

**Table 4.1.** Transesterification between benzyl alcohol and vinyl acetate under different reaction conditions using masked NHC-containing SCNPs and control experiments.



Run	Catalyst	Cat. (mol.%)	Conv <sup>(a)</sup> (%)
1	SCNP <b>5</b> <sup>(b)</sup>	1	6
2	SCNP <b>5</b>	5	43
3	SCNP <b>5</b>	10	69 <sup>(c)</sup>
4	<b>7</b> <sup>(d)</sup>	1	42
5	<b>7</b>	5	97
6	<b>7</b>	10	>99
7	<b>8</b> <sup>(e)</sup>	1	96
8	<b>8</b>	5	93
9	<b>8</b>	10	>99
10	SCNP <b>5</b> <sup>(f)</sup>	10	0
11	Copolymer <b>2</b>	10	0
12	Potassium Acetate	10	<2
13	-(g)	0	0

<sup>a</sup> The reaction was run for 2 h and conversions were calculated by <sup>1</sup>H NMR spectroscopy comparing conversion by comparing the integral value of the -CH<sub>2</sub>- benzyl alcohol signal (*d*, 2H, 4.5 ppm) to that of the -CH<sub>2</sub>- benzyl acetate signal (*d*, 2H, 5 ppm) by <sup>1</sup>H NMR spectroscopy in DMSO-*d*<sub>6</sub> (**Fig. S4.13-24**). <sup>b</sup> THF was used as solvent and dried under Na/benzophenone prior to use in each catalytic run being 0.015 mmol mL<sup>-1</sup> reference catalyst concentration referred to benzimidazolium at 10 mol.%. <sup>c</sup> The conversion barely increased duplicating the reaction time up to 4 h of reaction obtaining *ca.*70% conversion. <sup>d</sup> Linear model **7** containing randomly ordered spacers and active monomer units in a 84/16 ratio. <sup>e</sup> Active monomer based molecular model **8**. <sup>f</sup> The same conditions as in run 1 were used running the experiment at rt instead of 80 °C. <sup>g</sup> This reaction was performed only using benzyl alcohol (1 eq.) and vinyl acetate (1.2 eq.) for 2 h at 80 °C. The results correspond to the average value obtained after two different runs for each reaction.

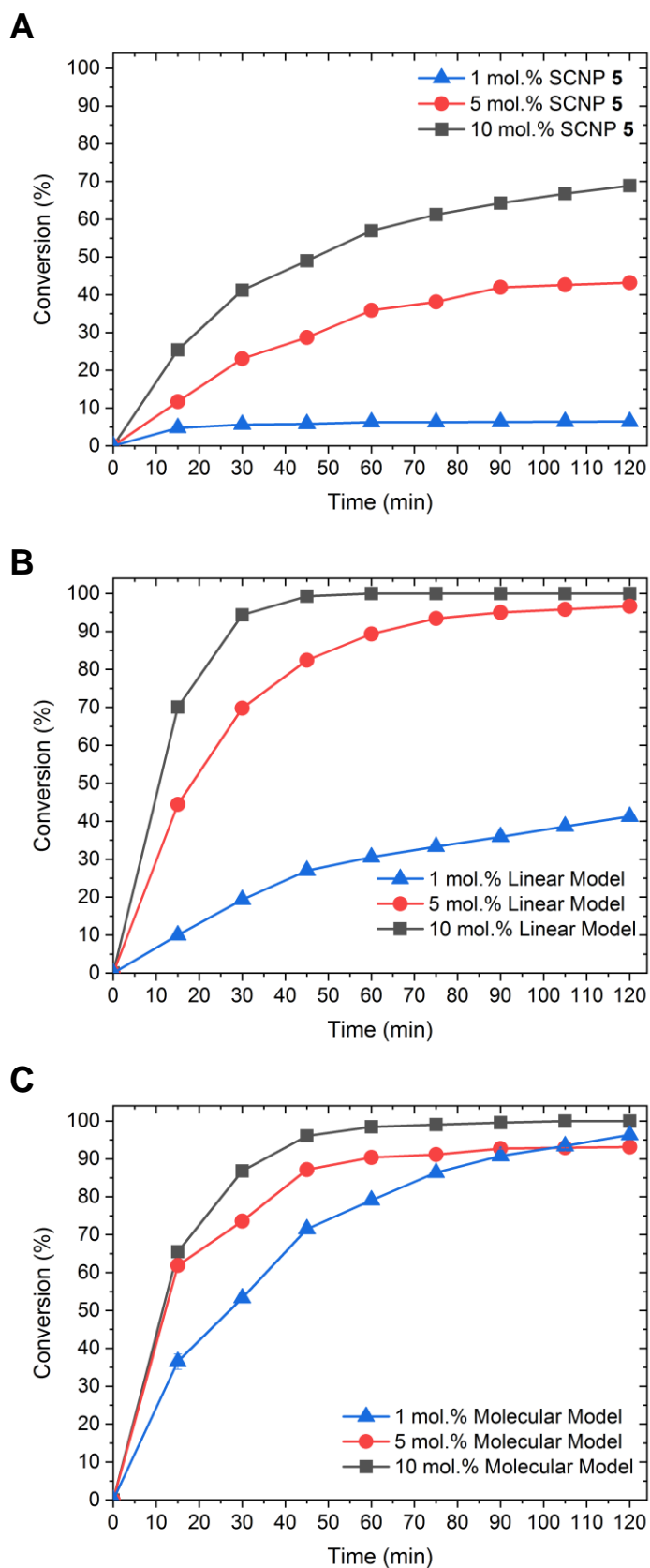


**Figure 4.6.** Kinetics for transesterification reaction at 1 mol.% (blue line), 5 mol.% (red line) and 10 mol.% (black line) using **A) SCNP 5**, **B) 7** and **C) 8** as catalysts.

In light of these comparative investigations of the three different catalytic systems (SCNP **5** vs. coPIL **7** and monomer **8**), higher conversions and faster rates observed with both the molecular and the linear coPIL models suggest that the microenvironment provided by SCNP **5** somehow restricts the catalytic activity of supported-NHCs relatively to both the linear and molecular models.<sup>5,44-47</sup> As expected, no organocatalytic activity was noted at room temperature, while the transesterified reaction product formed upon heating, demonstrating the thermal latency of SCNP **5** (run 3 vs. run 10). Despite the fact that SCNP **5** did not improve the catalytic performance of the transesterification reaction, it has been shown that the catalytic activity of the NHC is retained within the compact core of the 3D-SCNP.

#### 4.5 Conclusions

In this work, the modularity of PIL chemistry has been further exploited to design individual linear copolymer chains by RAFT, combining thermally latent and autonomous NHC behaviour, *i.e.* in absence of any external reagent, and the capability to self-catalyse some substrate units immobilized on these chains. These unique features can be exploited to achieve SCNPs by self-NHC-organocatalysed folding of the individual chains, as evidenced by different analytical techniques, including SEC, TEM, DLS and DOSY NMR. To this end, 3-vinylbenzaldehyde, styrene and 4-vinylbenzylethylbenzimidazolium chloride were randomly copolymerised using the RAFT process, resulting in a well-defined but catalytically inactive coPIL support. Installation of a slightly basic acetate counterion by anion metathesis imparts the catalytic activity and thermally latent behaviour to the coPIL precursor. The self-catalysed folding process lead to the formation of SCNPs occurs by the formation of covalent cross-links through the benzoin condensation of benzaldehyde moieties. The as-obtained SCNPs retain their NHC behaviour, as demonstrated not only through the trapping of CS<sub>2</sub>, but also by the possibility to further catalyse the transesterification reaction between vinyl acetate and benzyl alcohol. Comparison with both a molecular and a linear coPIL catalyst homologues show however that the confined environment provided by the SCNPs does not improve the organocatalytic performance. Efforts to tune the catalytic environment of the SCNPs, by varying the cross-linking density, is currently in progress. Overall, this study highlights the

versatility of thermally-latent NHC catalysts, demonstrating their use as a novel trigger for the folding of catalytically active SCNP nanoreactors.

#### 4.6 References

- 1 R. Gracia, M. Marradi, G. Salerno, R. Pérez-Nicado, A. Pérez-San Vicente, D. Dupin, J. Rodriguez, I. Loinaz, F. Chiodo and C. Nativi, *ACS Macro Letters*, 2018, **7**, 196–200.
- 2 T.-K. Nguyen, S. J. Lam, K. K. K. Ho, N. Kumar, G. G. Qiao, S. Egan, C. Boyer and E. H. H. Wong, *ACS Infectious Diseases*, 2017, **3**, 237–248.
- 3 Y. Liu, S. Pujals, P. J. M. Stals, T. Paulöhr, S. I. Presolski, E. W. Meijer, L. Albertazzi and A. R. A. Palmans, *Journal of the American Chemical Society*, 2018, **140**, 3423–3433.
- 4 I. Perez-Baena, I. Loinaz, D. Padro, I. García, H. J. Grande and I. Odriozola, *Journal of Materials Chemistry*, 2010, **20**, 6916.
- 5 H. Rothfuss, N. D. Knöfel, P. W. Roesky and C. Barner-Kowollik, *Journal of the American Chemical Society*, 2018, **140**, 5875–5881.
- 6 J. Rubio-Cervilla, E. González and J. Pomposo, *Nanomaterials*, 2017, **7**, 341.
- 7 J. Rubio-Cervilla, E. González and J. A. Pomposo, in *Single-Chain Polymer Nanoparticles*, ed. J. A. Pomposo, Wiley-VCH Verlag GmbH & Co. KGaA, Weinheim, Germany, 2017, pp. 341–388.
- 8 J. A. Pomposo, I. Perez-Baena, F. Lo Verso, A. J. Moreno, A. Arbe and J. Colmenero, *ACS Macro Letters*, 2014, **3**, 767–772.
- 9 A. Latorre-Sánchez and J. A. Pomposo, *Polymer International*, 2016, **65**, 855–860.
- 10 M. Ouchi, N. Badi, J.-F. Lutz and M. Sawamoto, *Nature Chemistry*, 2011, **3**, 917–924.
- 11 A. M. Hanlon, C. K. Lyon and E. B. Berda, *Macromolecules*, 2016, **49**, 2–14.
- 12 O. Altintas and C. Barner-Kowollik, *Macromolecular Rapid Communications*, 2016, **37**, 29–46.
- 13 S. Mavila, O. Eivgi, I. Berkovich and N. G. Lemcoff, *Chemical Reviews*, 2016, **116**, 878–961.
- 14 R. Lambert, A.-L. Wirotius, S. Garmendia, P. Berto, J. Vignolle and D. Taton, *Polymer Chemistry*, 2018, **9**, 3199–3204.



- 15 Y. Bai, X. Feng, H. Xing, Y. Xu, B. K. Kim, N. Baig, T. Zhou, A. A. Gewirth, Y. Lu, E. Oldfield and S. C. Zimmerman, *Journal of the American Chemical Society*, 2016, **138**, 11077–11080.
- 16 M. Artar, T. Terashima, M. Sawamoto, E. W. Meijer and A. R. A. Palmans, *Journal of Polymer Science Part A: Polymer Chemistry*, 2014, **52**, 12–20.
- 17 Y. Azuma, T. Terashima and M. Sawamoto, *ACS Macro Letters*, 2017, **6**, 830–835.
- 18 N. D. Knöfel, H. Rothfuss, J. Willenbacher, C. Barner-Kowollik and P. W. Roesky, *Angewandte Chemie International Edition*, 2017, **56**, 4950–4954.
- 19 S. Garmendia, A. P. Dove, D. Taton and R. K. O'Reilly, *Polymer Chemistry*, 2018, **9**, 5286–5294.
- 20 M. Artar, E. R. J. Souren, T. Terashima, E. W. Meijer and A. R. A. Palmans, *ACS Macro Letters*, 2015, **4**, 1099–1103.
- 21 R. Lambert, A.-L. Wirotius and D. Taton, *ACS Macro Letters*, 2017, **6**, 489–494.
- 22 J. Willenbacher, O. Altintas, V. Trouillet, N. Knöfel, M. J. Monteiro, P. W. Roesky and C. Barner-Kowollik, *Polym. Chem.*, 2015, **6**, 4358–4365.
- 23 A. Sanchez-Sanchez, A. Arbe, J. Colmenero and J. A. Pomposo, *ACS Macro Letters*, 2014, **3**, 439–443.
- 24 J. De-La-Cuesta, I. Asenjo-Sanz, A. Latorre-Sánchez, E. González, D. E. Martínez-Tong and J. A. Pomposo, *European Polymer Journal*, 2018, **109**, 447–452.
- 25 I. Berkovich, V. Kobernik, S. Guidone and N. G. Lemcoff, in *Single-Chain Polymer Nanoparticles*, ed. J. A. Pomposo, Wiley-VCH Verlag GmbH & Co. KGaA, Weinheim, Germany, 2017, pp. 217–257.
- 26 H. Frisch, J. P. Menzel, F. R. Bloesser, D. E. Marschner, K. Mundsinger and C. Barner-Kowollik, *Journal of the American Chemical Society*, 2018, **140**, 9551–9557.
- 27 S. Basasoro, M. Gonzalez-Burgos, A. J. Moreno, F. L. Verso, A. Arbe, J. Colmenero and J. A. Pomposo, *Macromolecular Rapid Communications*, 2016, **37**, 1060–1065.
- 28 D. Mecerreyes, Ed., *Applications of Ionic Liquids in Polymer Science and Technology*, Springer Berlin Heidelberg, Berlin, Heidelberg, 2015.
- 29 J. Yuan, D. Mecerreyes and M. Antonietti, *Progress in Polymer Science*, 2013, **38**, 1009–1036.
- 30 A. Eftekhari and T. Saito, *European Polymer Journal*, 2017, **90**, 245–272.
- 31 M. Fèvre, J. Pinaud, A. Leteneur, Y. Gnanou, J. Vignolle, D. Taton, K. Miqueu and J.-M. Sotiropoulos, *Journal of the American Chemical Society*, 2012, **134**, 6776–6784.

- 32 R. Lambert, P. Coupillaud, A.-L. Wirotius, J. Vignolle and D. Taton, *Macromolecular Rapid Communications*, 2016, **37**, 1143–1149.
- 33 S. Garmendia, R. Lambert, A.-L. Wirotius, J. Vignolle, A. P. Dove, R. K. O'Reilly and D. Taton, *European Polymer Journal*, 2018, **107**, 82–88.
- 34 M. Fevre, J. Pinaud, Y. Gnanou, J. Vignolle and D. Taton, *Chemical Society Reviews*, 2013, **42**, 2142.
- 35 S. Naumann and A. P. Dove, *Polym. Chem.*, 2015, **6**, 3185–3200.
- 36 D. M. Flanigan, F. Romanov-Michailidis, N. A. White and T. Rovis, *Chem. Rev*, 2015, **115**, 9307–9387.
- 37 W. N. Ottou, H. Sardon, D. Mecerreyes, J. Vignolle and D. Taton, *Progress in Polymer Science*, 2016, **56**, 64–115.
- 38 R. S. Menon, A. T. Biju and V. Nair, *Beilstein Journal of Organic Chemistry*, 2016, **12**, 444–461.
- 39 M. Alrayyani and O. Š. Miljanić, *Chemical Communications*, 2018, **54**, 11989–11997.
- 40 S. Naumann and M. R. Buchmeiser, *Catalysis Science & Technology*, 2014, **4**, 2466.
- 41 O. Holloczki, D. Gerhard, K. Massone, L. Szarvas, B. Nimeth, T. Veszprimi and L. Nyulaszi, *New Journal of Chemistry*, 2010, **34**, 3004.
- 42 G. Gurau, H. Rodriguez, S. P. Kelley, P. Janiczek, R. S. Kalb and R. D. Rogers, *Angewandte Chemie International Edition*, 2011, **50**, 12024–12026.
- 43 L. Delaude, *European Journal of Inorganic Chemistry*, 2009, **2009**, 1681–1699.
- 44 J. A. Pomposo, J. Rubio-Cervilla, A. J. Moreno, F. Lo Verso, P. Bacova, A. Arbe and J. Colmenero, *Macromolecules*, 2017, **50**, 1732–1739.
- 45 P. Cotanda, N. Petzetakis and R. K. O'Reilly, *MRS Communications*, 2012, **2**, 119–126.
- 46 A. D. Ievins, X. Wang, A. O. Moughton, J. Skey and R. K. O'Reilly, *Macromolecules*, 2008, **41**, 2998–3006.
- 47 A. Lu, P. Cotanda, J. P. Patterson, D. A. Longbottom and R. K. O'Reilly, *Chemical Communications*, 2012, **48**, 9699.

## 4.7 Experimental section

**Synthesis of monomer 1: Synthesis of 4-vinylbenzylethylbenzimidazolium chloride ([ViEBIm]Cl).** *N*-Ethylbenzimidazole was synthesised according to the previously reported procedure from Taton, O'Reilly *et al.*<sup>19,33</sup> Benzimidazole (5 g, 42.32 mmol, 1 eq.) was first dissolved in DMF (20 mL), potassium hydroxide was then added (4.75 g, 106 mmol, 2.5 eq.). The solution was stirred for 30 minutes before the drop-wise addition of ethyl bromide (3.45 mL, 46.55 mmol). After stirring at room temperature for 24 h, the reaction mixture was diluted using H<sub>2</sub>O (50 mL), the aqueous phase was then extracted with dichloromethane (4 x 25 mL). The organic phases were combined, dried over MgSO<sub>4</sub> and evaporated, yielding *N*-ethylbenzimidazole as a viscous yellow oil (4.93 g, 33.8 mmol, 80% yield) <sup>1</sup>H NMR (DMSO-*d*<sub>6</sub>):  $\delta$  = 8.25 (s, 1H, N-*CH*-N), 7.69-7.20 (m, 4H, aromatics), 4.12 (t, 2H, N-*CH*<sub>2</sub>-CH<sub>3</sub>), 1.32 (t, 3H, -CH<sub>3</sub>).

A portion of *N*-ethylbenzimidazole (4.65 mL, 31.8 mmol, 1 eq.) was then dissolved in acetonitrile (20 mL) within a Schlenk tube, this was immediately followed by the addition of 4-vinylbenzylchloride (4.82 g, 31.8 mmol, 1 eq.) After stirring for 24 h at 80 °C, the crude reaction mixture was precipitated into ethyl acetate (20 mL) and dried under vacuum to remove the solvent, yielding the target monomer 4-vinylbenzylethylbenzimidazolium chloride as a white powder (8.64 g, 28.9 mmol, yield = 91%). <sup>1</sup>H NMR (DMSO-*d*<sub>6</sub>):  $\delta$  = 9.7 (s, 1H, N-*CH*-N), 8.12-7.1 (m, 8H, aromatics), 6.7 (dd, 1H, Ph-*CH*-CH<sub>2</sub>), 5.9 (s, 2H, Ph-*CH*<sub>2</sub>-N), 5.8 (d, 1H, CH=CH<sub>2</sub>), 5.2 (d, 1H, CH=CH<sub>2</sub>), 4.2 (dd, 2H, N-*CH*<sub>2</sub>-CH<sub>3</sub>), 1.3 (t, 3H, -CH<sub>2</sub>-CH<sub>3</sub>). Characterisation matches that previously reported in the literature.<sup>19,33</sup>

**Synthesis of linear copolymer 2.** 2-Cyano-2-propyl benzodithioate (43 mg, 0.19 mmol) as a chain transfer agent (CTA), styrene (2.4 mL, 23.6 mmol), 4-vinylbenzylethylbenzimidazolium chloride (1.18 g, 3.93 mmol), 3-vinylbenzaldehyde (1.5 mL, 11.8 mmol) and AIBN (31 mg, 0.19 mmol) were dissolved in 12 mL of DMF. The solution was purged with nitrogen for 30 min and stirred for 12 h at 80 °C. The as-obtained copolymer was purified by dialysis against methanol (1 L x 2 every 24 h, MWCO 3.5 kDa membrane) and the solvent was removed under reduced pressure, yielding copolymer **2** as a pink powder (1.6 g, yield = 31%). <sup>1</sup>H NMR (DMSO-*d*<sub>6</sub>):  $\delta$  = 10.9-10.1 (br, 1H, N=CH-N), 9.9-9.6 (br, 3H, H-CO-), 8.2-6.1 (br, 53.1 H, Ar-), 5.9-5.5 (br, 2H, Ar-CH<sub>2</sub>-N), 4.7-4.5 (br, 2H, N-CH<sub>2</sub>-CH<sub>3</sub>), 2.2-0.9 (br, 30.2 H, backbone, CH<sub>2</sub>-

$CH_3$ ) (**Fig. 4.1**).  $^{13}C$  NMR (DMSO- $d_6$ ):  $\delta = 193.1, 147.6-143.9, 142.7, 136.6-124.8, 114.2, 80.1, 42.9, 14.4$  (**Fig. S4.1**). SEC analysis:  $D_M = 1.2$ ;  $M_n = 11.9$  kDa.

**Synthesis of linear copolymer 3.** Copolymer **2** (1 g, 0.095 mmol) was dissolved in 12 mL of methanol and 3 mL of chloroform in a round-bottom flask. Potassium acetate (0.15 g, 1.15 mmol) was added and the reaction mixture was stirred overnight at room temperature. The solution was filtered and purified by dialysis against methanol/ethanol (75:25, 1 L x 2 every 24 h, MWCO 3.5 kDa membrane). The solvent was removed under reduced pressure, yielding copolymer **3** as a yellow powder (0.93 g, yield = 92%).  $^1H$  NMR (DMSO- $d_6$ ):  $\delta = 10.5-9.6$  (br, 4H,  $H-CO-$ ,  $N=CH-N$ ), 8.2-6.1 (br, 53.1 H, Ar-), 5.8-5.5 (br, 2H, Ar- $CH_2-N$ ), 4.7-4.5 (br, 2H, N- $CH_2-CH_3$ ), 2.2-0.9 (br, 36.4 H, backbone,  $O=C-CH_3$ ,  $CH_2-CH_3$ ) (**Fig. S4.2**).  $^{13}C$  NMR (DMSO- $d_6$ ):  $\delta = 193.1, 176.6, 147.6-143.9, 143.7, 136.6-124.8, 114.2, 80.1, 59.8, 42.9, 24.4, 14.4$  (**Fig. S4.3**).

**Synthesis of linear copolymer 4.** Copolymer **3** (80 mg, 0.008 mmol) was first azeotropically dried in THF. The sample was then heated at 80 °C for 24 h in THF (3 mL) in presence of  $CS_2$  (0.6 mL). The solvent and excess of  $CS_2$  were removed under reduced pressure, yielding copolymer **4** as a red viscous oil. (Yield >95%).  $^1H$  NMR (DMSO- $d_6$ ):  $\delta = 12.2-12.0$  (br, 0.5 H,  $-COOH$ ), 10.5-9.6 (br, 1H,  $H-CO-$ ), 8.2-6.1 (br, 34.2 H, Ar- $H$ ), 5.8-5.4 (br, 2H, Ar- $CH_2-N$ ), 4.4-4.2 (br, 2H, N- $CH_2-CH_3$ ), 2.2-0.2 (br, 32.6 H, backbone,  $HOOC-CH_3$ ,  $-CH_2-CH_3$ ) (**Fig. S4.25**).  $^{13}C$  NMR (DMSO- $d_6$ ):  $\delta = 224.1, 193.1, 174.4, 153.1, 147.6-143.9, 141.3, 136.6-124.8, 114.2, 110.1, 71.1, 52.3, 24.4, 13.7$  (**Fig.4.2**).

**Synthesis of SCNP 5.** Copolymer **3** (150 mg, 0.015 mol) was dissolved in 150 mL of dry THF and heated to 80 °C in a 1 L Schlenk flask for 48 h. The solvent was removed under reduced pressure and the resulting material was dialysed against methanol (1 L x 2 every 24 h, MWCO 3.5 kDa membrane) producing SCNP **5** (130 mg, yield = 87%).  $^1H$  NMR (DMSO- $d_6$ ):  $\delta = 12.0-11.8$  (br, 1H,  $N=CH-N$ ), 10.1-9.7 (br, 1.2 H,  $O=C-H$ ), 8.3-5.8 (br, 47.5 H, Ar- $H$ ), 5.4 (s, 0.3 H,  $O=C-CHOH-Ar$ ), 4.2 (s, 0.25 H,  $O=C-CHOH-Ar$ ), 4.05 (s, 0.15 H, N- $CH_2-CH_3$ ), 2.2-0.2 (br, 50.2 H, backbone,  $O=C-CH_3$ ,  $-CH_2-CH_3$ ) (**Fig. S4.4**).  $^{13}C$  NMR (DMSO- $d_6$ ):  $\delta = 179.3, 172.6, 153.1, 147.6-143.9, 140.0, 132.1-122.6, 97.6, 80.7, 67.9, 53.3, 42.9, 24.4, 14.4$  (**Fig. S4.5**). SEC analysis:  $D_M = 1.2$ ;  $M_n = 10.8$  kDa.

**Synthesis of SCNP 6.** SCNP 5 (35 mg, 0.003 mmol) was dissolved in THF (2 mL) in presence of a large excess of CS<sub>2</sub> (0.4 mL) in a Schlenk tube for 24 h at 80 °C. Yield > 95%. <sup>1</sup>H NMR (DMSO-*d*<sub>6</sub>): δ = 12.9-12.3 (br, 0.4 H, -COOH), 10.4-9.6 (br, 1H, *H*-CO-), 8.3-5.9 (br, 40.8 H, Ar-*H*), 5.4 (s, 0.2 H, , O=C-*CHOH*-Ar), 5.2-5.0 (br, 0.5 H, Ar-*CH*<sub>2</sub>-N), 4.4-4.2 (br, 0.4 H, O=C-*CHOH*-Ar) 2.3-0.2 (br, 51.2 H, backbone, HOOC-*CH*<sub>3</sub>, -*CH*<sub>2</sub>-*CH*<sub>3</sub>) (**Fig. S4.10**). <sup>13</sup>C NMR (DMSO-*d*<sub>6</sub>): δ = 193.3, 168.8, 153.1, 152.0, 147.6-143.9, 139.9, 135.1-122.6, 109.6, 97.6, 80.7, 67.9, 42.9, 24.4, 19.4 (**Fig. S4.9**).

**Synthesis of the model polymer 7.** 2-Cyano-2-propyl benzodithioate CTA (30 mg, 0.13 mmol), styrene (2.34 mL, 20.4 mmol) and monomer 1 (0.68 g, 2.26 mmol) were added to a 20 mL glass tube. Methanol (12 mL) was added and the suspension was allowed to stir for 10 min until a homogenous solution was obtained. AIBN (27 mg, 0.11 mmol) was added to the methanolic solution under dry nitrogen at room temperature. After mixing and purging the solution with dry nitrogen, the glass tube was sealed and placed at 80 °C in an oil bath for 16 h. After this time, 52% conversion was reached, as evidenced by <sup>1</sup>H NMR spectroscopy. The reaction was then quenched by cooling the solution to room temperature. The crude copolymer was purified by dialysis against methanol (1 L x 2 every 24 h, MWCO 3.5 kDa membrane). The obtained copolymer (0.9 g) was solubilised in methanol and subjected to anion exchange by adding potassium acetate (0.65 g, 10 eq.) to the solution and then further dialysed against methanol (1 L x 2 every 24 h) using a 3.5 kDa MWCO dialysis membrane. Yield = 40%. <sup>1</sup>H NMR (DMSO-*d*<sub>6</sub>): δ = 11.5-10.2 (br, 1H, N=*CH*-N), 8.2-6.1 (br, 30.1 H, Ar-), 5.9-5.5 (br, 2H, Ar-*CH*<sub>2</sub>-N), 4.7-4.5 (br, 2H, N-*CH*<sub>2</sub>-*CH*<sub>3</sub>), 2.2-0.9 (br, 10.6 H, backbone, O=C-*CH*<sub>3</sub>, *CH*<sub>2</sub>-*CH*<sub>3</sub>) (**Fig. S4.11**). SEC analysis:  $D_M = 1.1$ ;  $M_n = 12.7$  kDa (**Fig. S4.12**).

**Synthesis of molecular model 8.** Monomer 1 (0.25 g, 0.83 mmol, 1 eq.) was first solubilised in methanol (2 mL). Potassium acetate (0.1 g, 1 mmol, 1.2 eq.) was then added and the reaction carried out at room temperature with stirring for 16 h. The solution was then filtered to remove the KCl side-product and the filtrate dried under reduced pressure. Yield >95%. <sup>1</sup>H NMR (DMSO-*d*<sub>6</sub>): δ = 10.9-10.1 (br, 1H, N=*CH*-N), 9.9-9.6 (br, 3H, *H*-CO-), 8.2-6.1 (br, 53.1 H, Ar-), 5.9-5.5 (br, 2H, Ar-*CH*<sub>2</sub>-N), 4.7-4.5 (br, 2H, N-*CH*<sub>2</sub>-*CH*<sub>3</sub>), 2.2-0.9 (br, 30.2 H, backbone, *CH*<sub>2</sub>-*CH*<sub>3</sub>). Characterisation matches that reported in the literature.<sup>3</sup>

**General procedure for the transesterification reaction.** In a 10 mL glass tube, different catalysts were first azeotropically dried using distilled THF. Dry THF was then added,

maintaining a reference catalyst concentration of  $0.015 \text{ mmol mL}^{-1}$  referred to benzimidazolium moieties. The solution was stirred, and previously distilled benzyl alcohol (1 eq.) and vinyl acetate (1.2 eq.) were added under nitrogen. The resulting mixture was stirred under nitrogen at  $80 \text{ }^\circ\text{C}$  for 2 h. The reaction kinetics were monitored by extracting aliquots every 15 min and calculating the conversion by comparing the integral value of the signal due to the  $-\text{CH}_2-$  group of benzyl alcohol ( $d$ , 2H, 4.5 ppm) to that of the  $-\text{CH}_2-$  benzyl acetate signal ( $d$ , 2H, 5 ppm) by  $^1\text{H}$  NMR spectroscopy in  $\text{DMSO-}d_6$  (Fig. S4.13-S4.24).

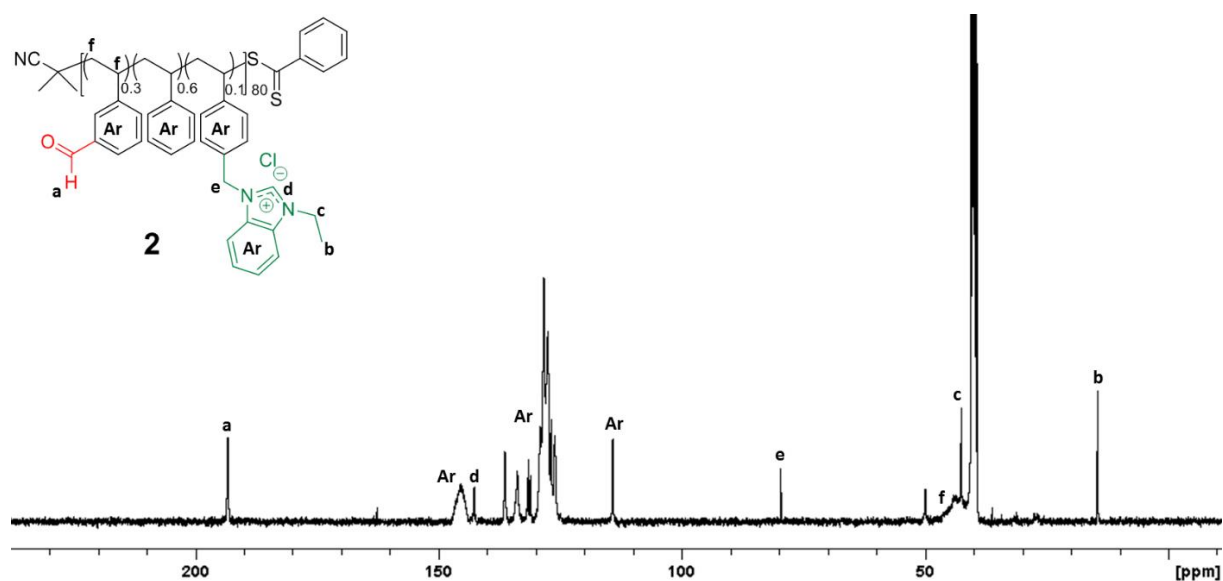


**Figure S4.1.**  $^{13}\text{C}$  NMR spectrum of copolymer **2** in  $\text{DMSO-}d_6$ .

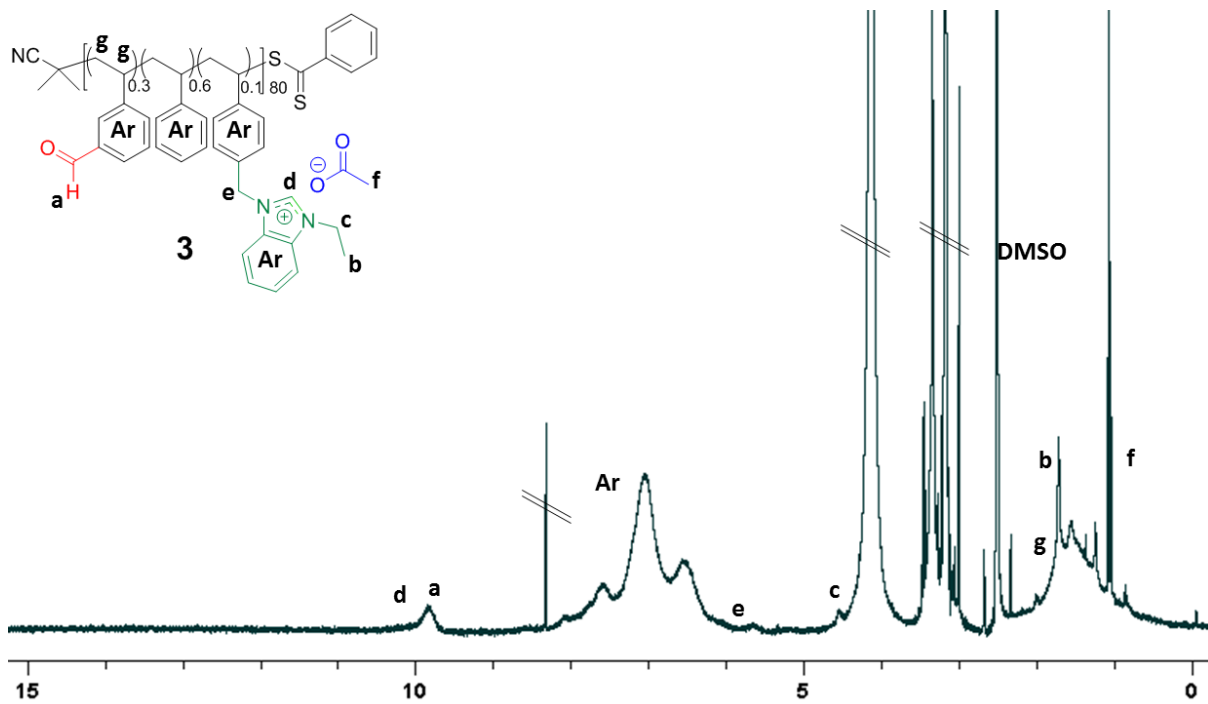


**Figure S4.2.**  $^1\text{H}$  NMR spectrum of copolymer **3** in  $\text{DMSO-}d_6$

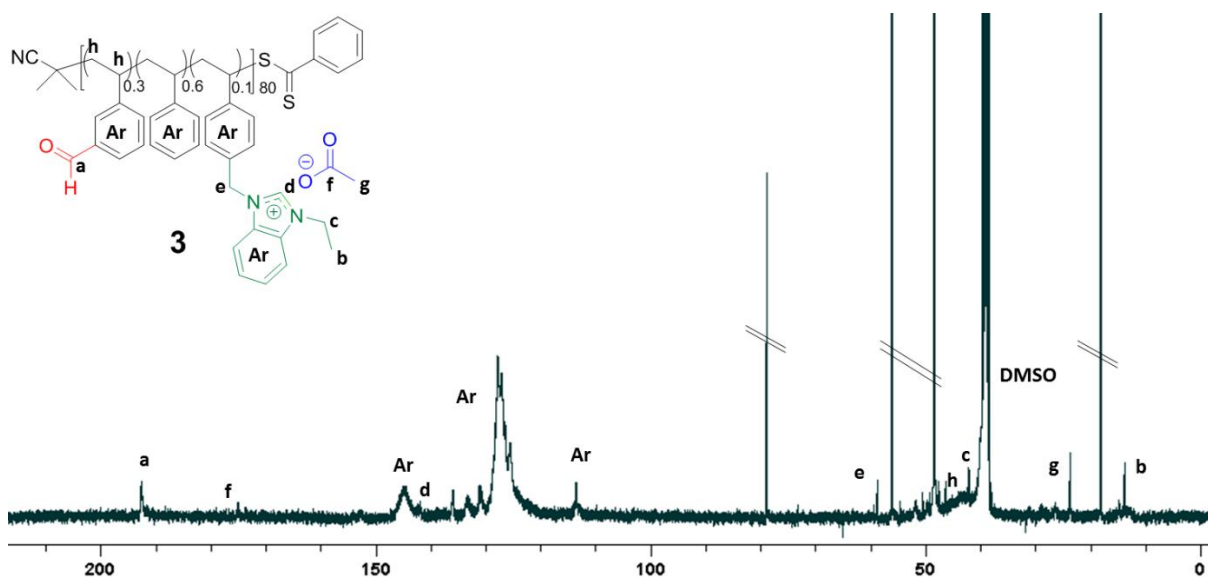


**Figure S4.3.**  $^{13}\text{C}$  NMR spectrum of copolymer **3** in  $\text{DMSO-}d_6$ .

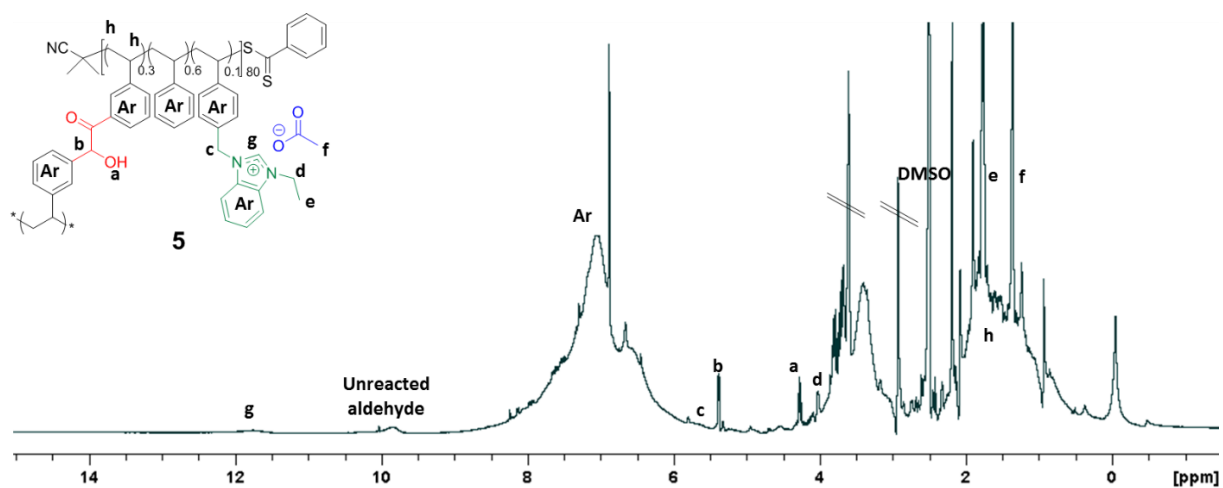


**Figure S4.4.**  $^1\text{H}$  NMR spectrum of SCNP **5** in  $\text{DMSO-}d_6$ .

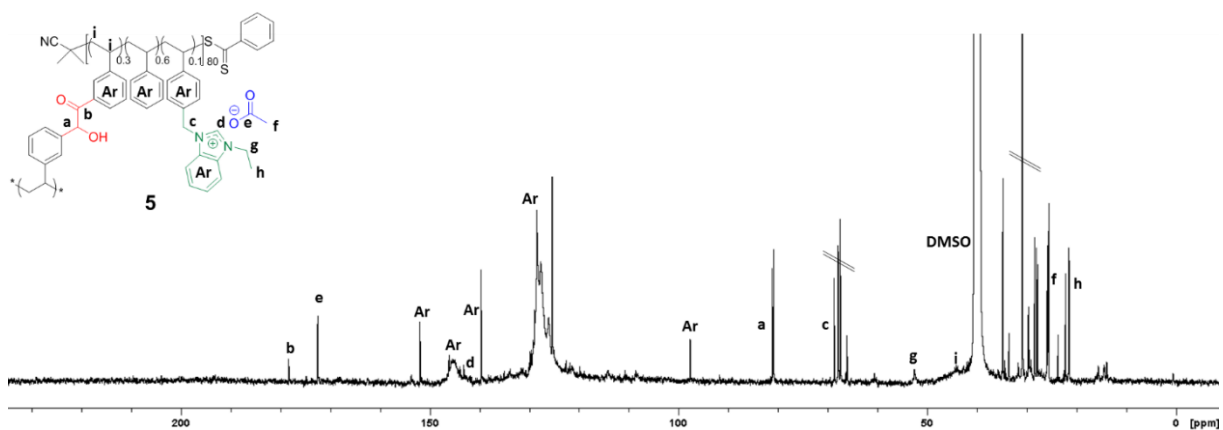


**Figure S4.5.**  $^{13}\text{C}$  NMR spectrum of copIL **5** in  $\text{DMSO-}d_6$ .

The multiplicity-edited HSQC NMR spectrum was used to confirm the incorporation of the benzoin moiety into SCNP **5**, with a clear coupling observed between the signal at  $\sim 5.4$  ppm and the tertiary carbon corresponding to the  $-\text{CH}-$  of the benzoin bridge.



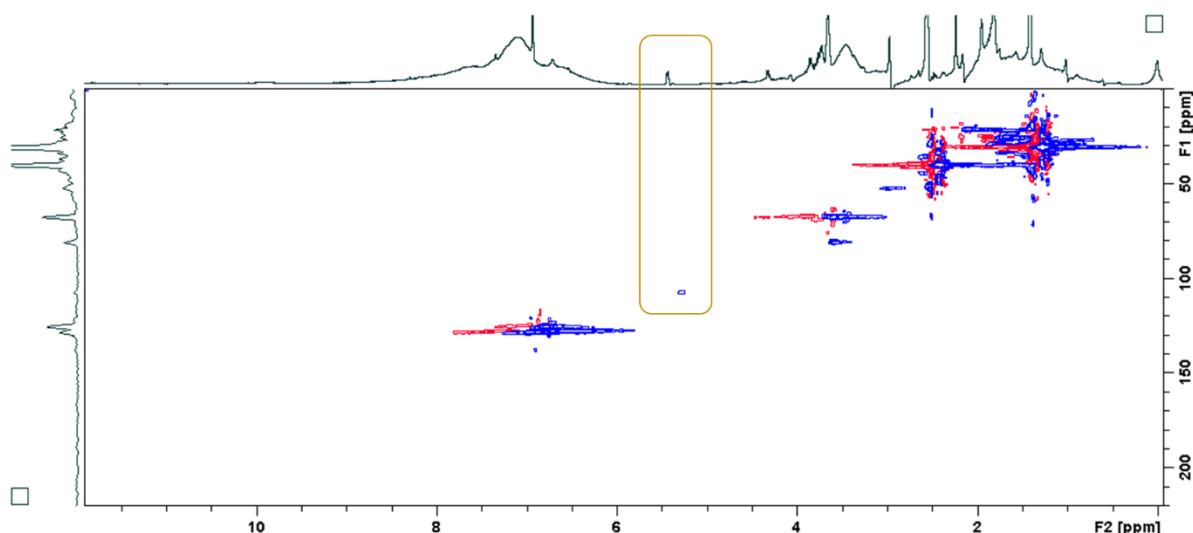


**Figure S4.6.** Representative multiplicity-edited HSQC spectrum of SCNP **5** in DMSO- $d_6$ , with tertiary and primary carbons identified in blue, and quaternary and secondary carbons identified in red.

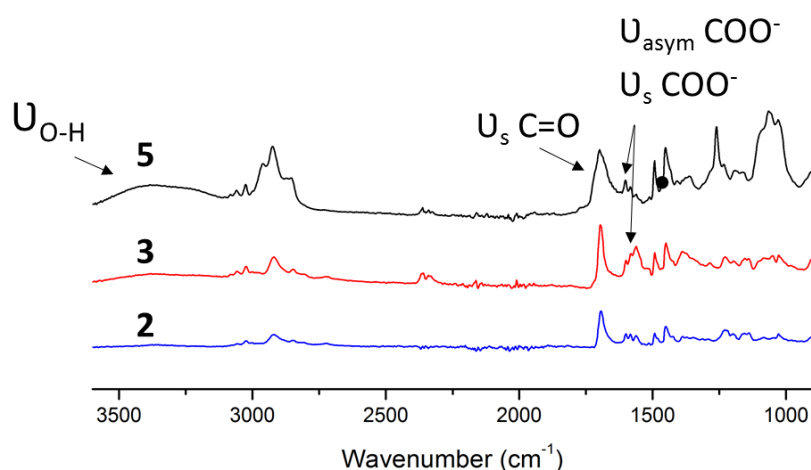


**Figure S4.7.** Representative FTIR spectrum of SCNP **5** (in black), linear polymer **3** (in red) and linear polymer **2** (in blue).

**Diffusion Ordered Spectroscopy (DOSY).** The folded SCNP and the linear copolymer were distinguished according to their diffusion coefficients as determined by DOSY NMR spectroscopy, which correlates their hydrodynamic radius to their relative rates of diffusion through DMSO- $d_6$ . Full details for the experimental conditions used for DOSY NMR spectroscopy can be found within the experimental of the main article. Calculation of the

hydrodynamic radius and therefore the diameter was done so by applying the Stokes-Einstein equation.

Stokes-Einstein equation:

$$D = \frac{kT}{6\pi\eta r}$$

$$k = 1.38 \cdot 10^{-23} \text{ J K}^{-1}$$

$$D = 3.14 \cdot 10^{-11} \text{ m}^2 \text{ s}^{-1}$$

$$T = 298 \text{ K}$$

$$\eta \text{ DMSO viscosity} = 1.99 \cdot 10^{-3} \text{ Pa s}$$

$$R \text{ (polymer 5)} = 1.15 \text{ nm}; D = 2.3 \text{ nm}$$

$$R \text{ (polymer 2)} = 3.3 \text{ nm}; D = 6.6 \text{ nm}$$

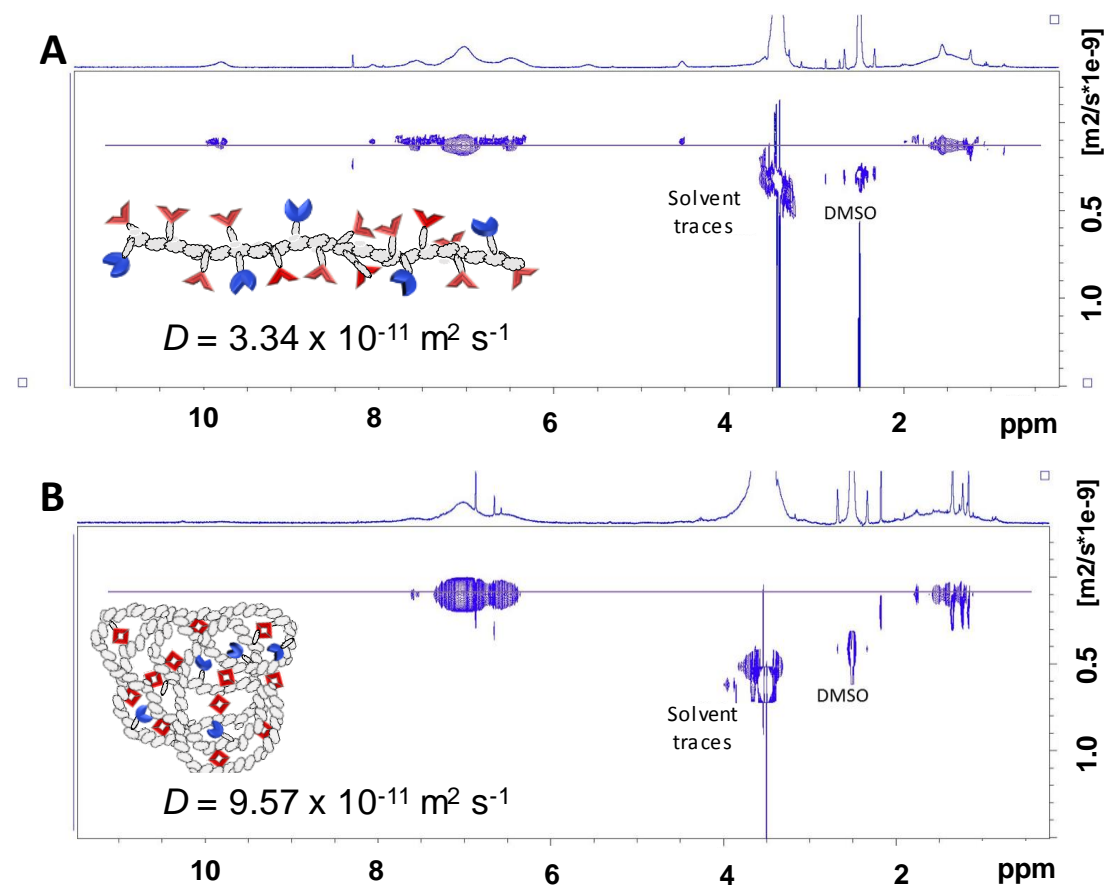


**Figure S4.8.** DOSY NMR spectroscopy in DMSO- $d_6$  for linear precursor **2** (A) and folded SCNP **5** (B).

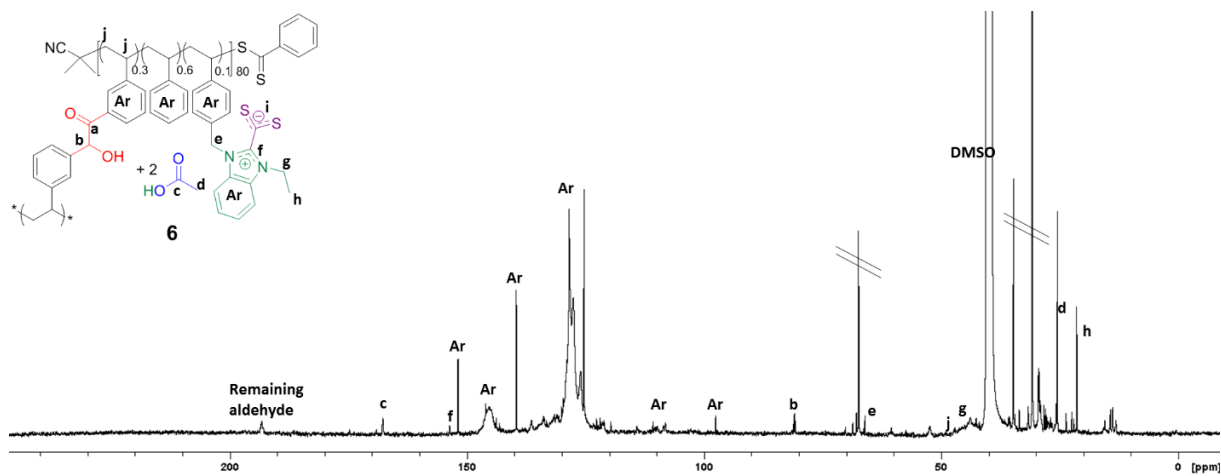


**Figure S4.9.**  $^{13}\text{C}$  NMR spectrum of SCNP **6** in DMSO- $d_6$ .

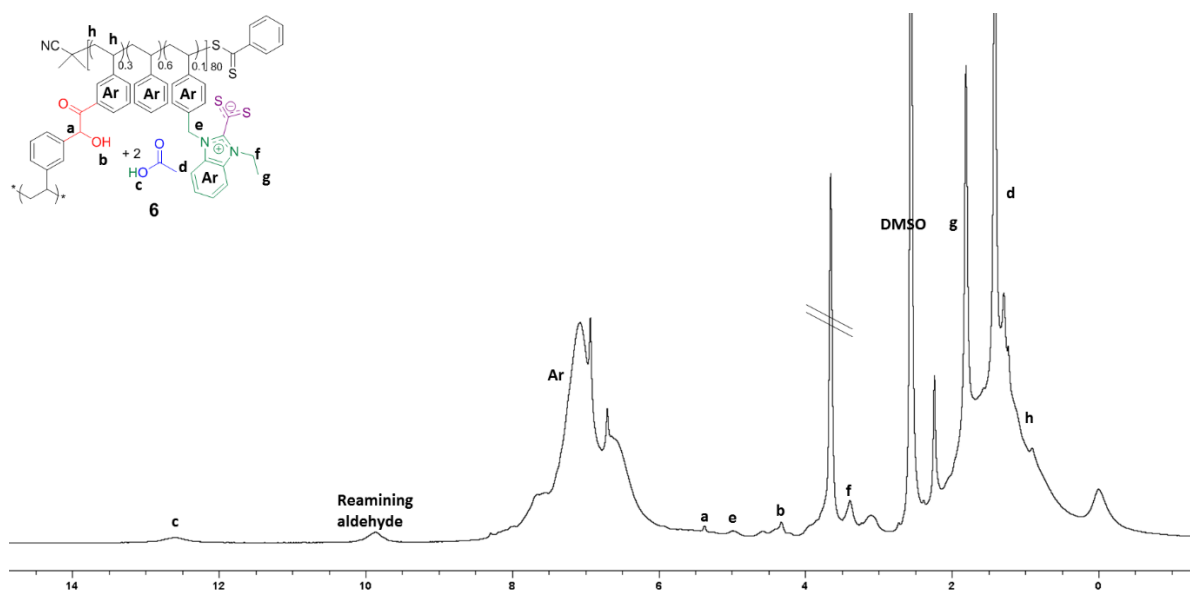


**Figure S4.10.**  $^1\text{H}$  NMR spectrum of SCNP **6** in DMSO- $d_6$ .

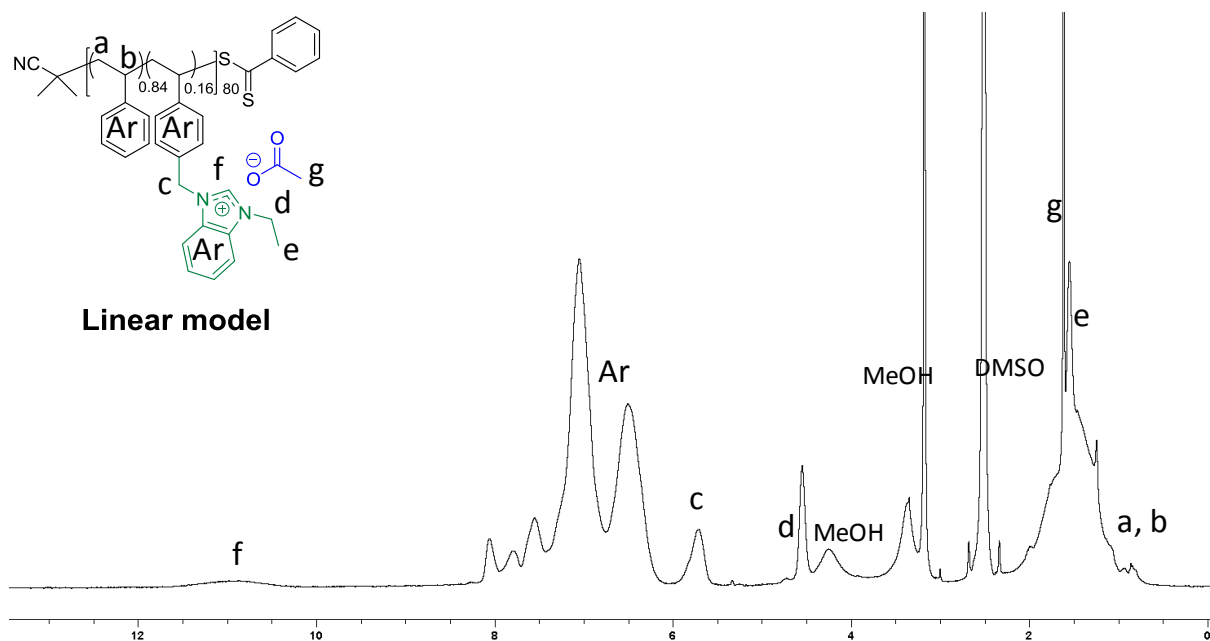


**Figure S4.11.**  $^1\text{H}$  NMR spectrum of linear model **7** in  $\text{DMSO-}d_6$ .

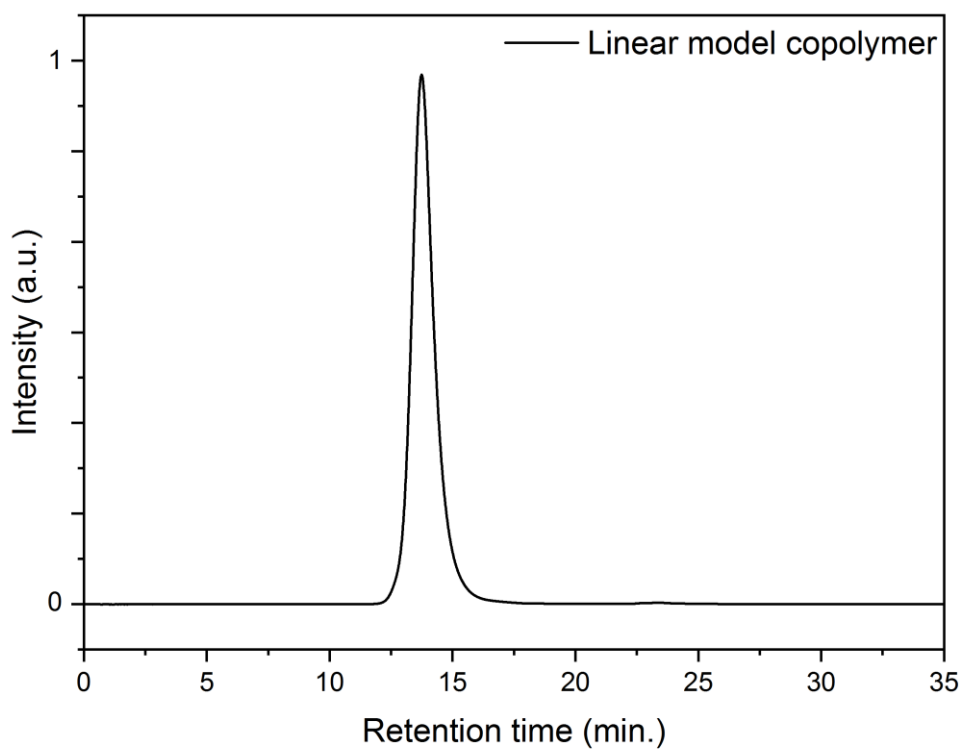


**Figure S4.12.** SEC trace corresponding to (bis(trifluoromethane)sulfonimide) TFSI-decorated linear model **7** in DMF (10 mM  $\text{NH}_4^+\text{BF}_4^-$ ; UV detector; SEC analysis:  $D_M = 1.1$ ;  $M_n = 12.7$  kDa).

## Transesterification reaction

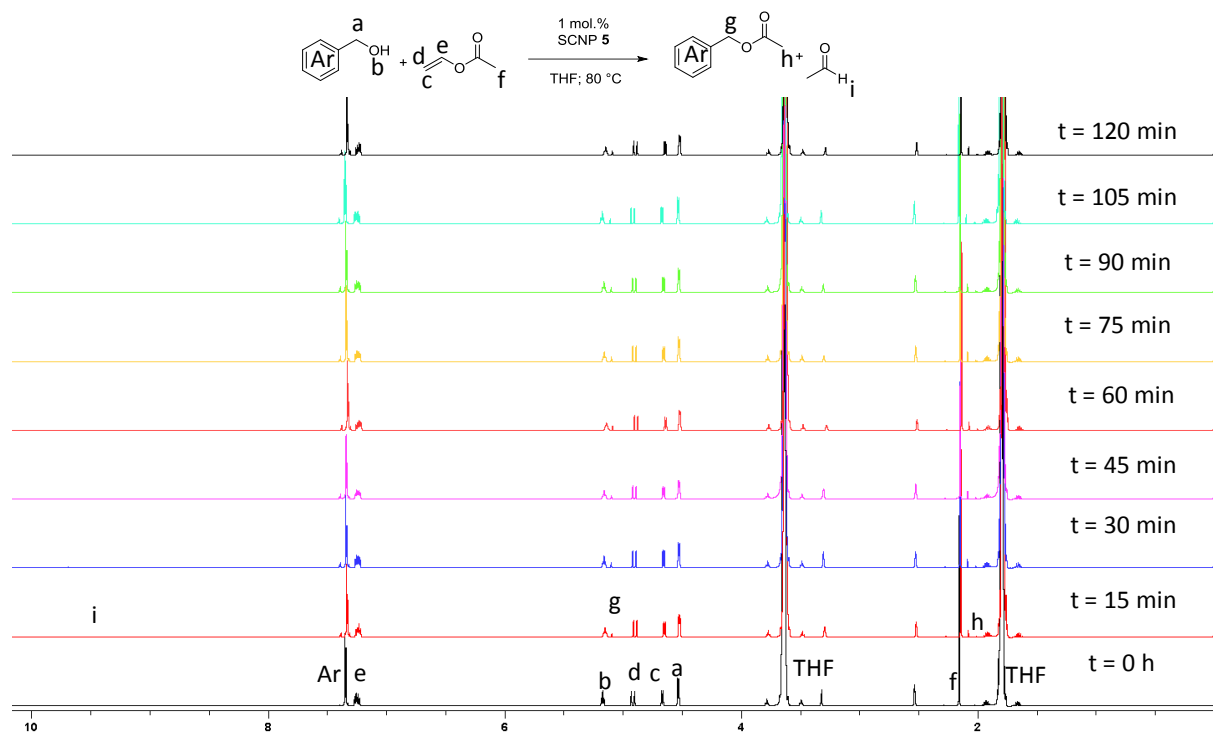


**Figure S4.13.** Reaction kinetics for run 1 (Table 4.1) monitored by  $^1\text{H}$  NMR spectroscopy in  $\text{DMSO-}d_6$ .

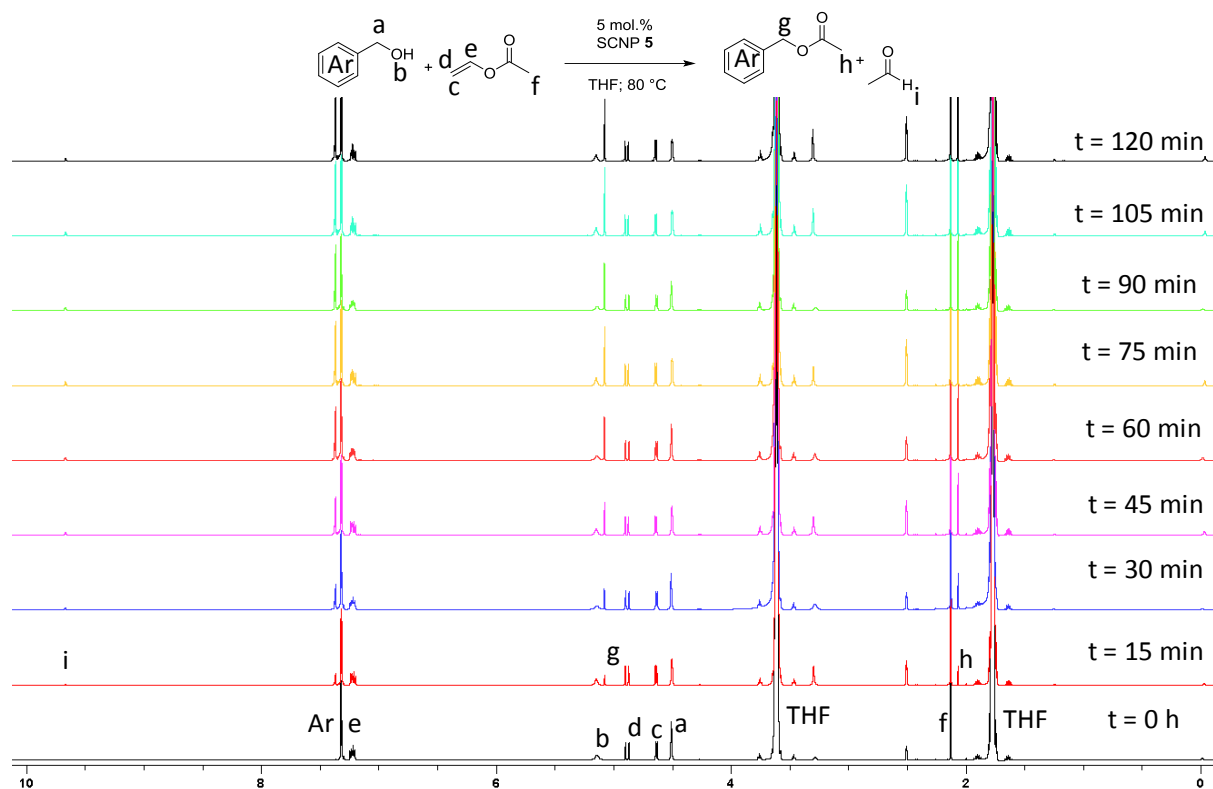


**Figure S4.14.** Reaction kinetics for run 2 (Table 4.1) monitored by  $^1\text{H}$  NMR spectroscopy in  $\text{DMSO-}d_6$ .

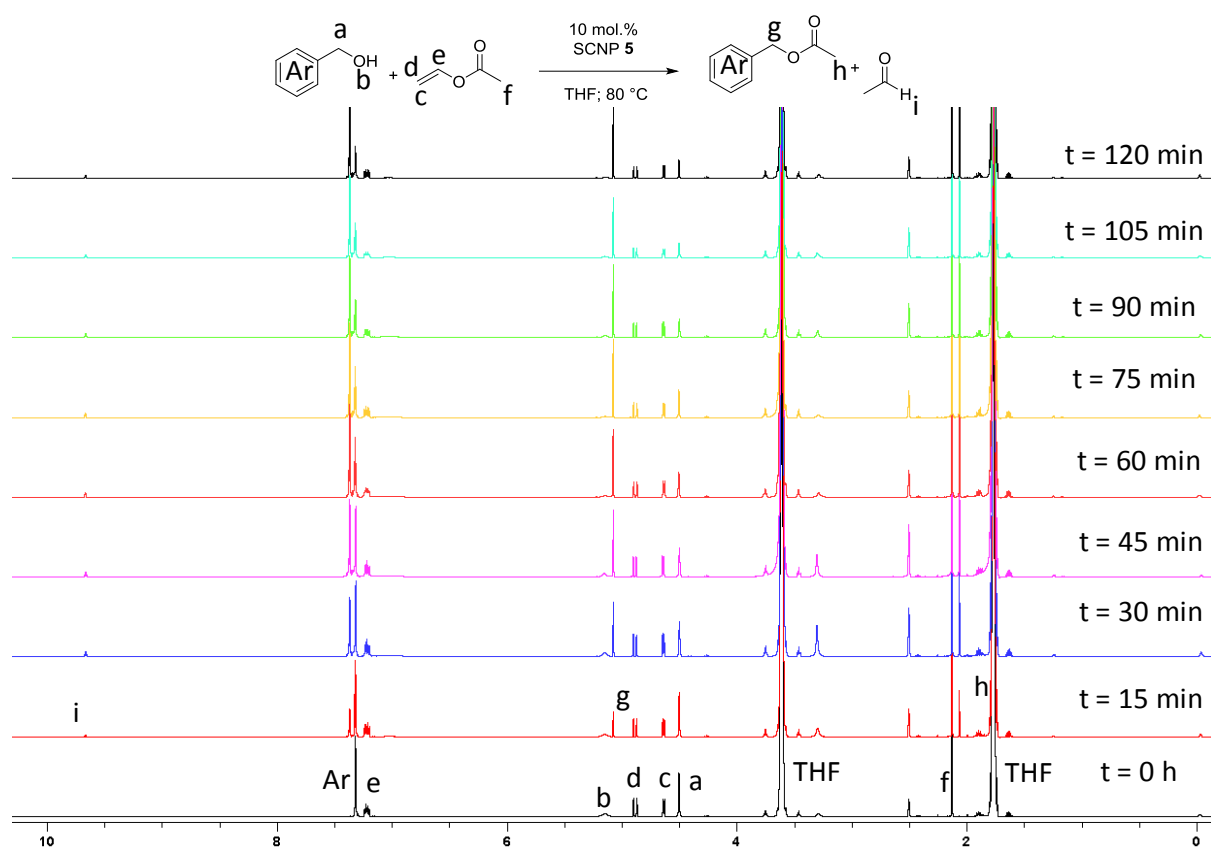


**Figure S4.15.** Reaction kinetics for run 3 (Table 4.1) monitored by  $^1\text{H}$  NMR spectroscopy in  $\text{DMSO-}d_6$ .

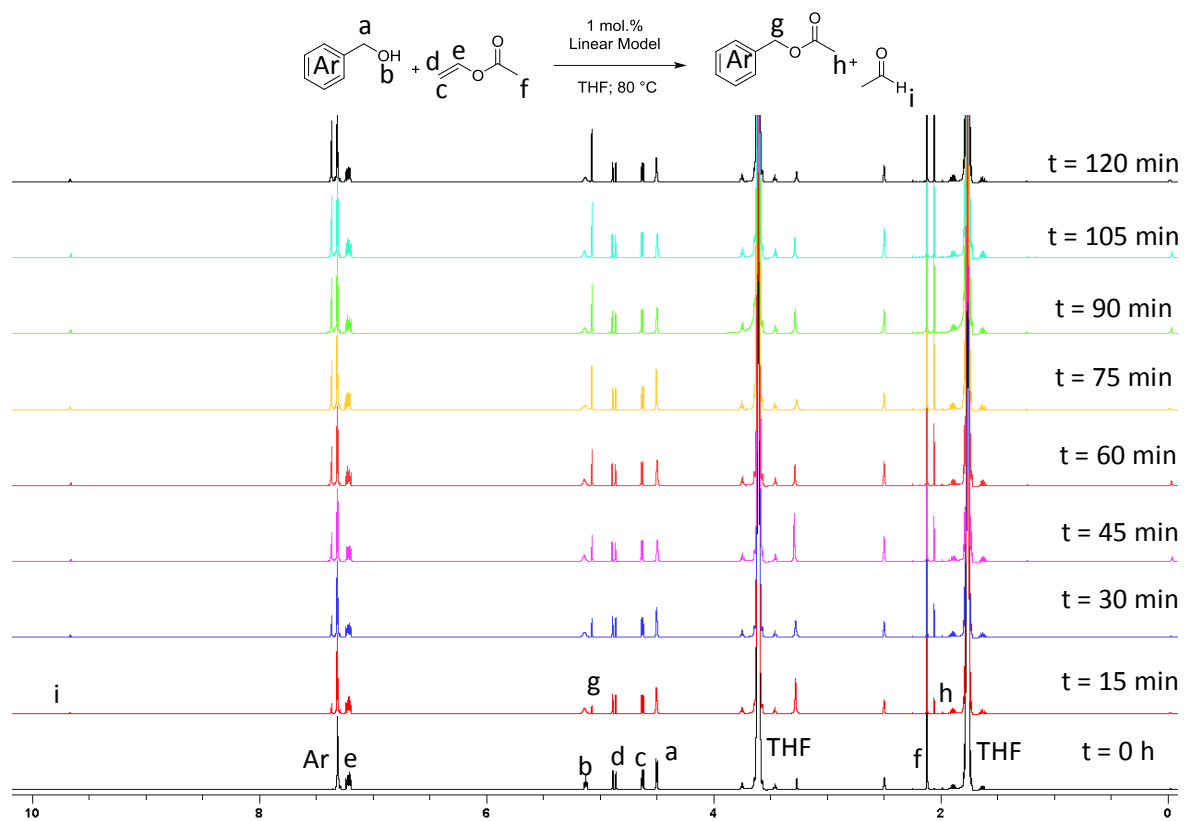


**Figure S4.16.** Reaction kinetics for run 4 (Table 4.1) monitored by  $^1\text{H}$  NMR spectroscopy in  $\text{DMSO-}d_6$ .

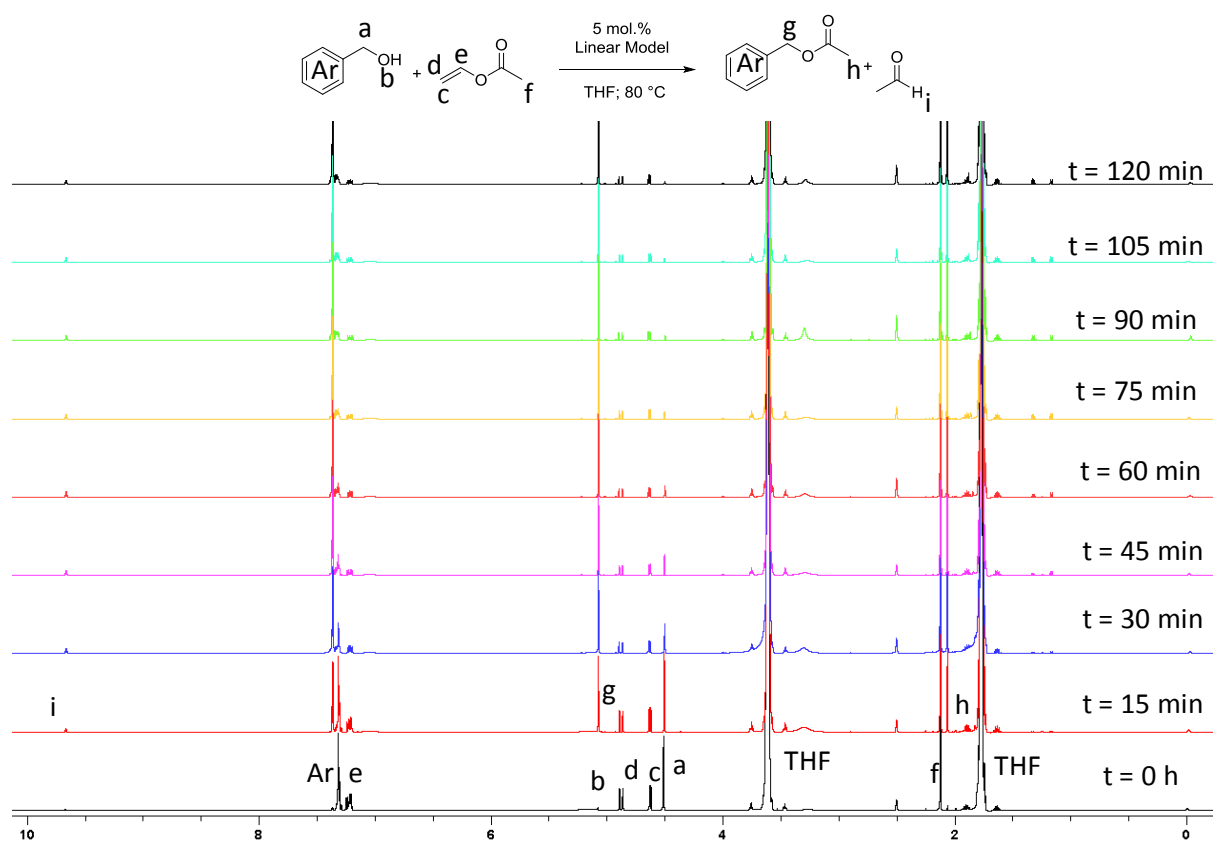


**Figure S4.17.** Reaction kinetics for run 5 (Table 4.1) monitored by  $^1\text{H}$  NMR spectroscopy in  $\text{DMSO-}d_6$ .



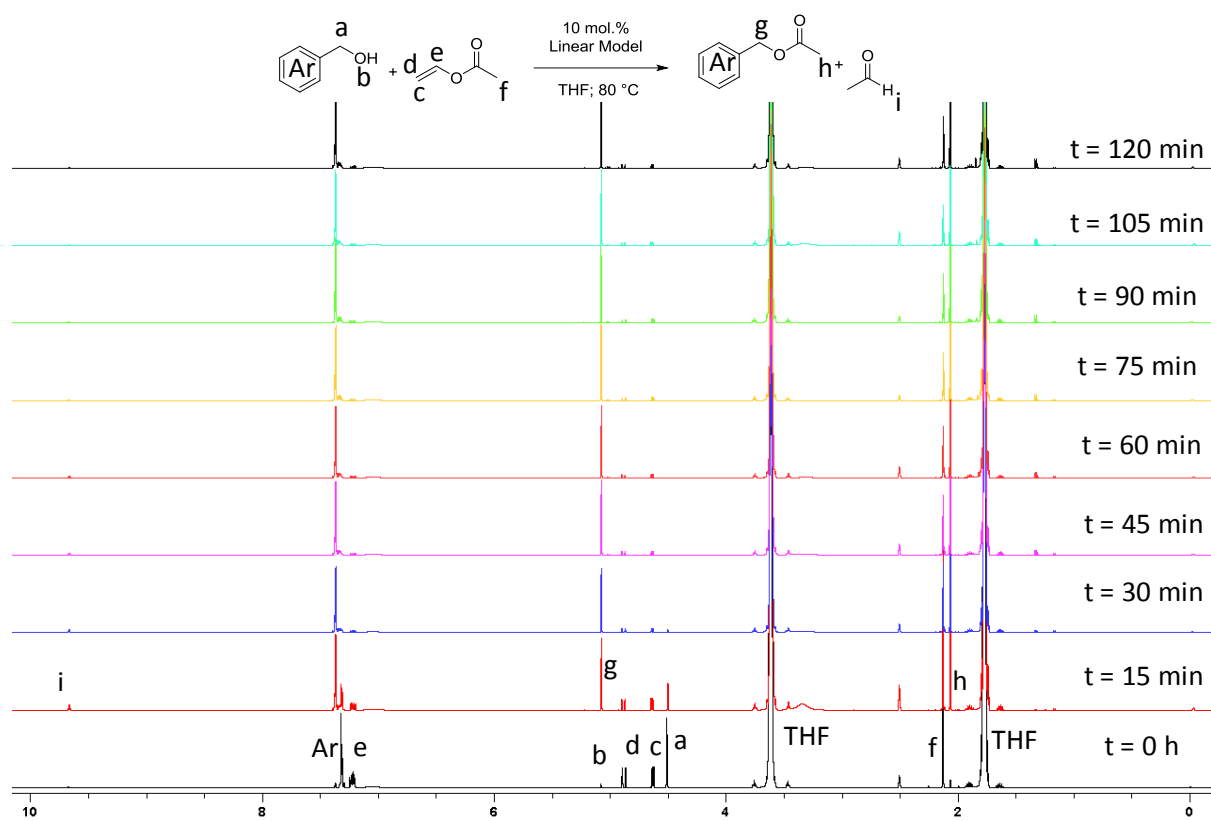


**Figure S4.18.** Reaction kinetics for run 6 (**Table 4.1**) monitored by  $^1\text{H}$  NMR spectroscopy in  $\text{DMSO-}d_6$ .

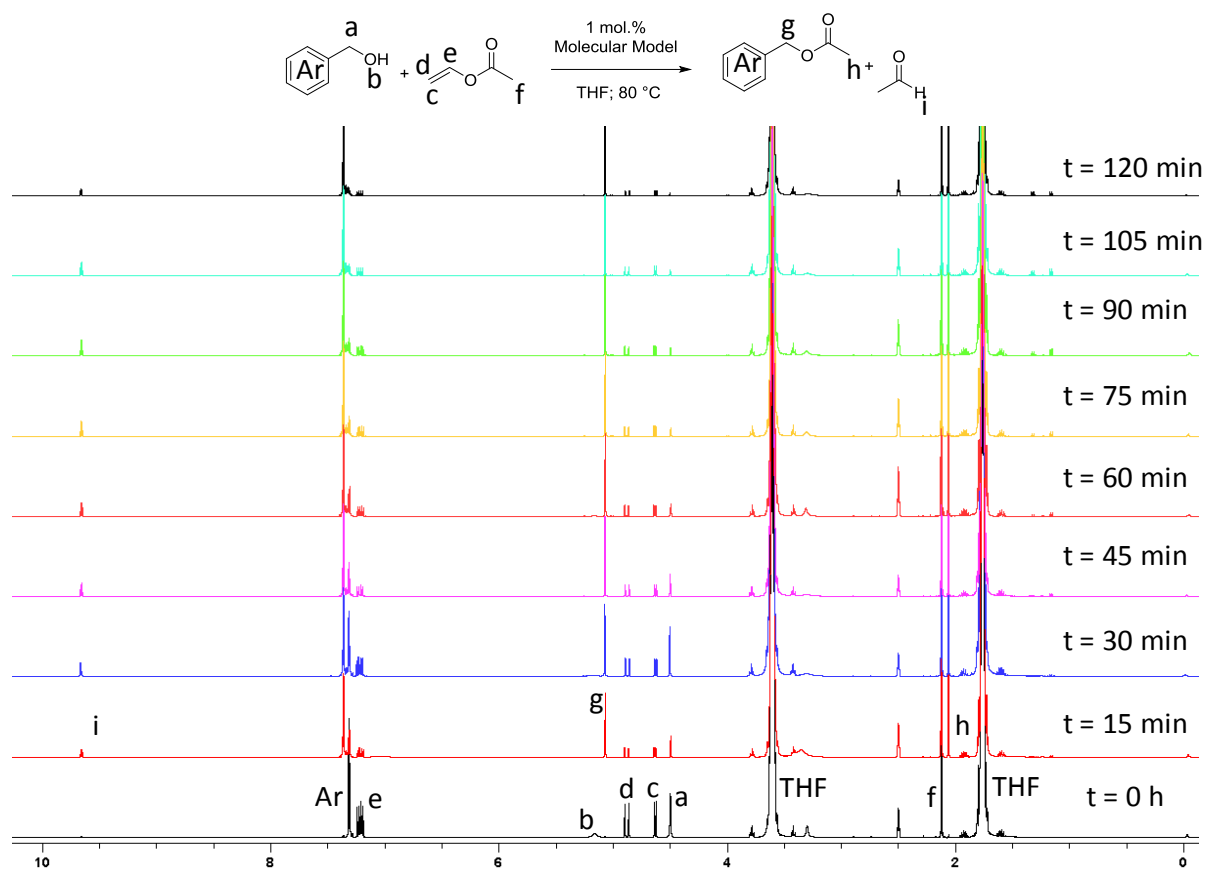


**Figure S4.19.** Reaction kinetics for run 7 (Table 4.1) monitored by  $^1\text{H}$  NMR spectroscopy in  $\text{DMSO-}d_6$ .

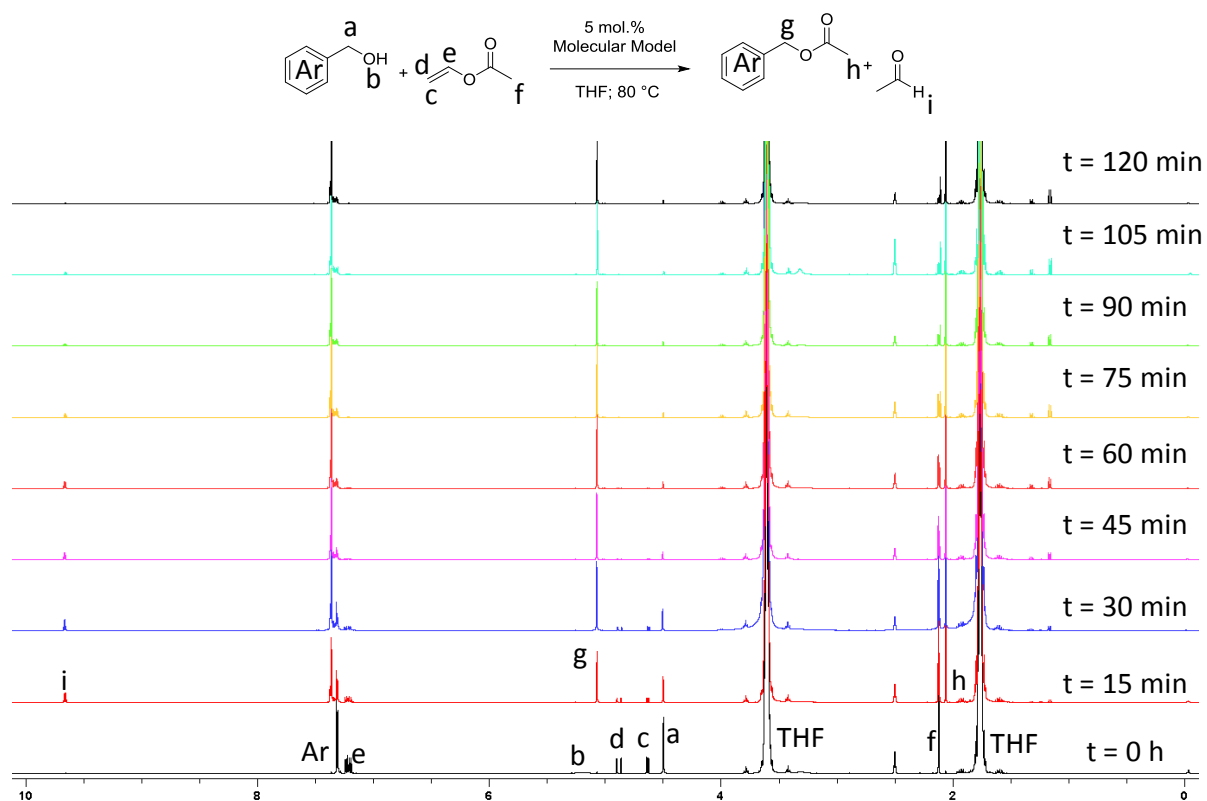


**Figure S4.20.** Reaction kinetics for run 8 (Table 4.1) monitored by  $^1\text{H}$  NMR spectroscopy in  $\text{DMSO}-d_6$ .

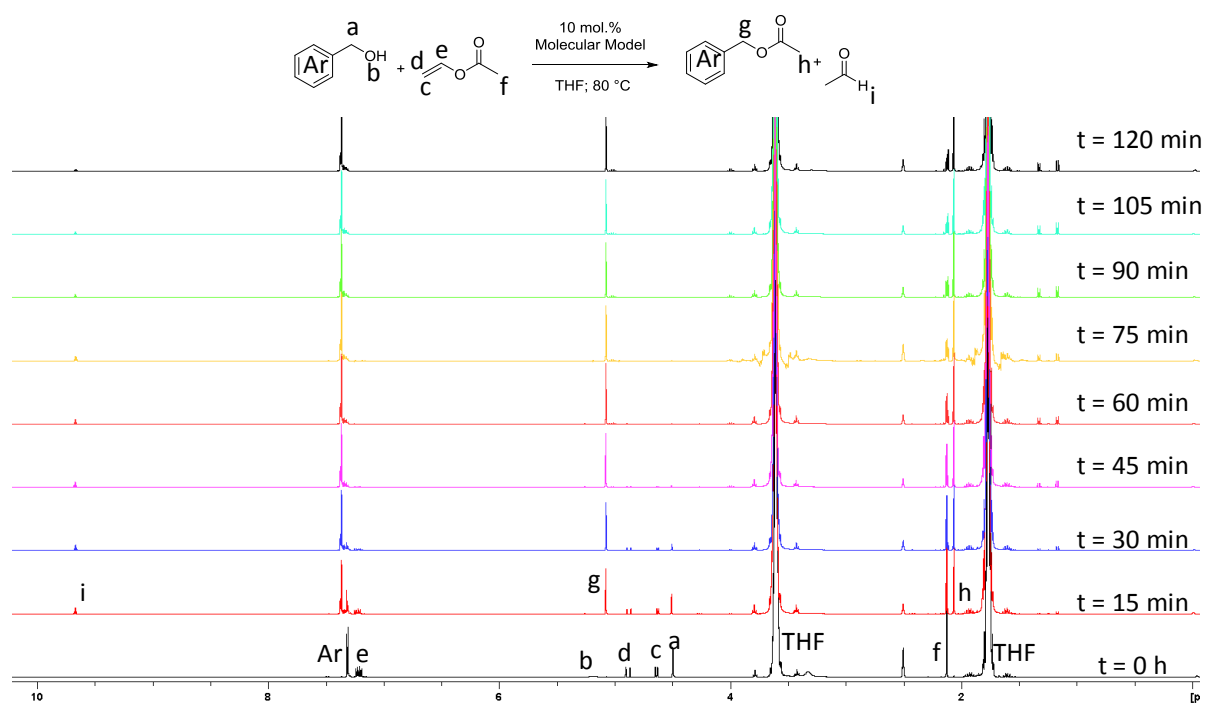


**Figure S4.21.** Reaction kinetics for run 9 (**Table 4.1**) monitored by  $^1\text{H}$  NMR spectroscopy in  $\text{DMSO-}d_6$ .

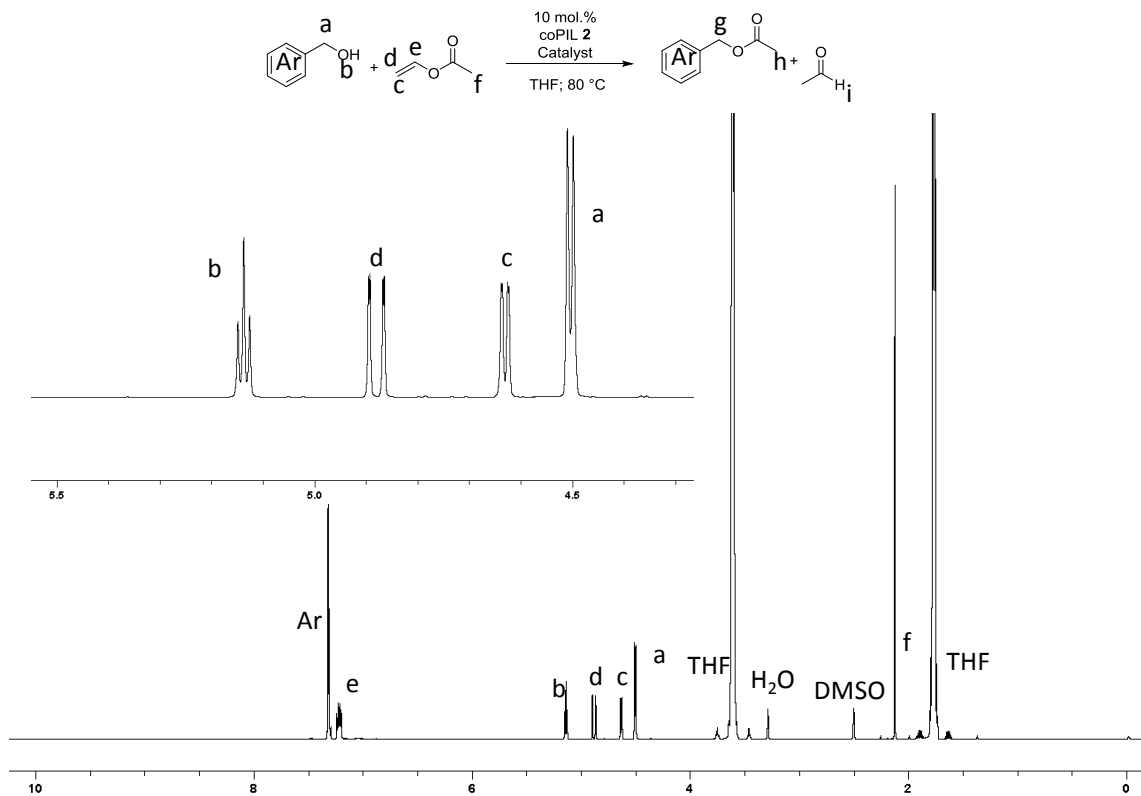


**Figure S4.22.** Reaction kinetics for run 11 (**Table 4.1**) monitored by  $^1\text{H}$  NMR spectroscopy in  $\text{DMSO-}d_6$ .

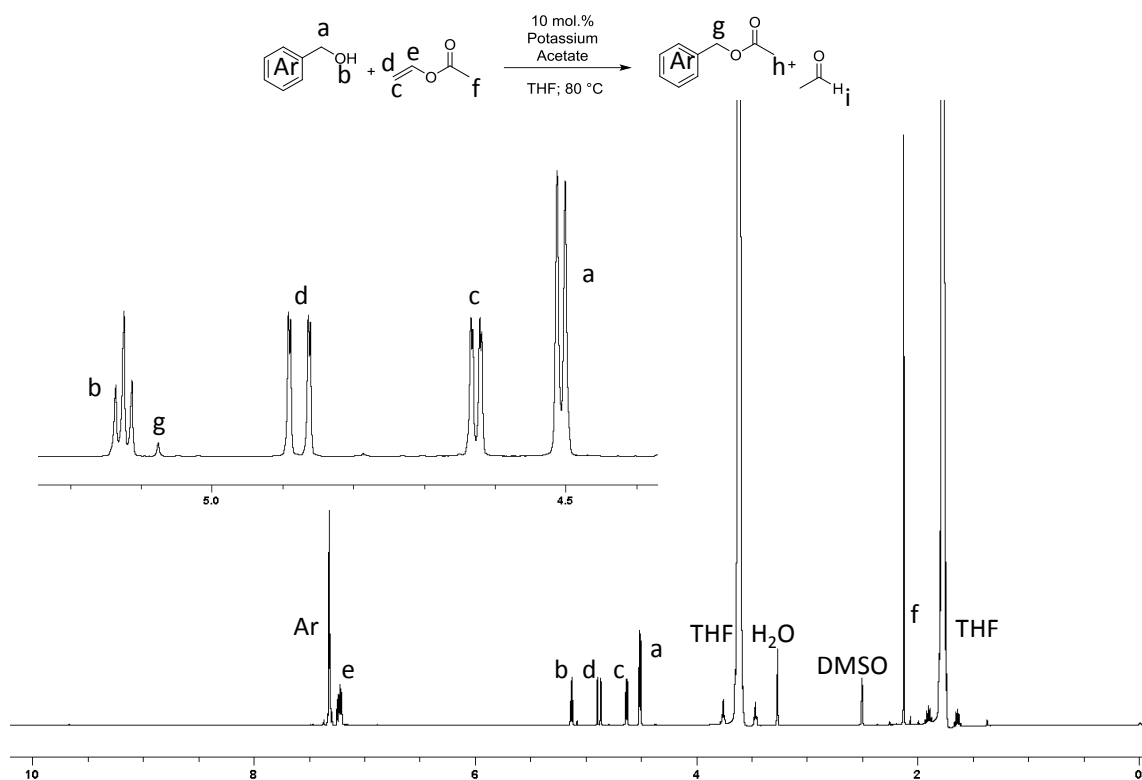


**Figure S4.23.** Reaction kinetics for run 12 (**Table 4.1**) monitored by  $^1\text{H}$  NMR spectroscopy in  $\text{DMSO-}d_6$ .

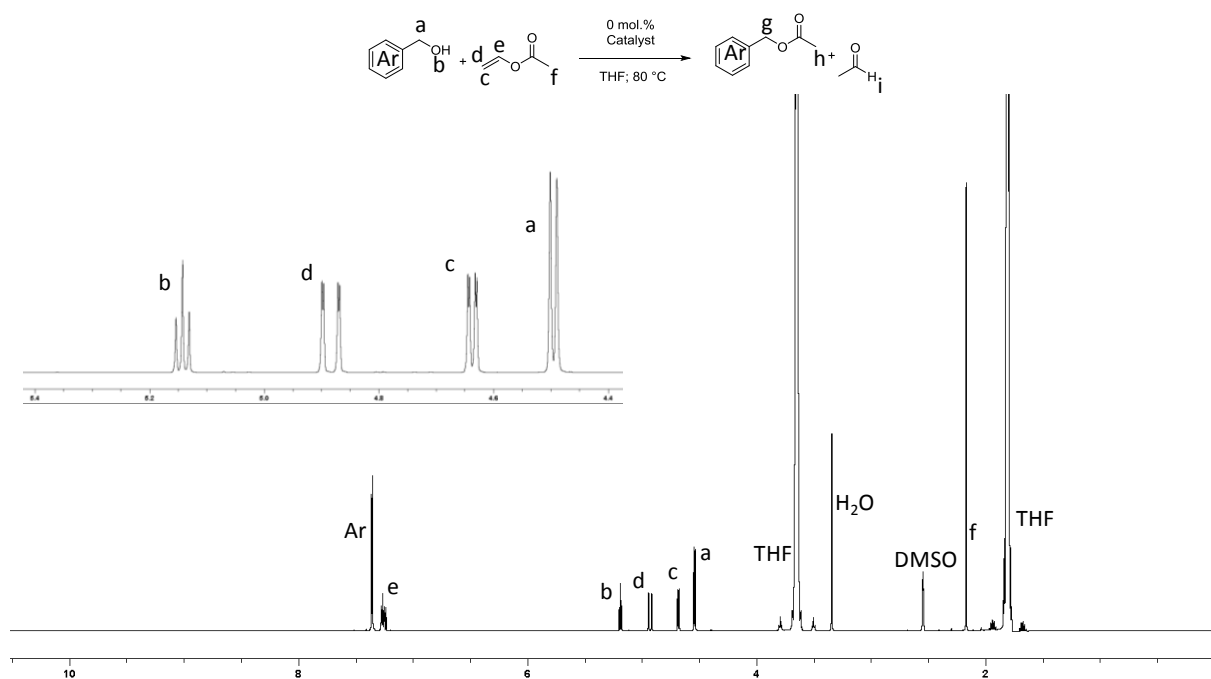


**Figure S4.24.** Reaction kinetics for run 13 (**Table 4.1**) monitored by  $^1\text{H}$  NMR spectroscopy in  $\text{DMSO-}d_6$ .

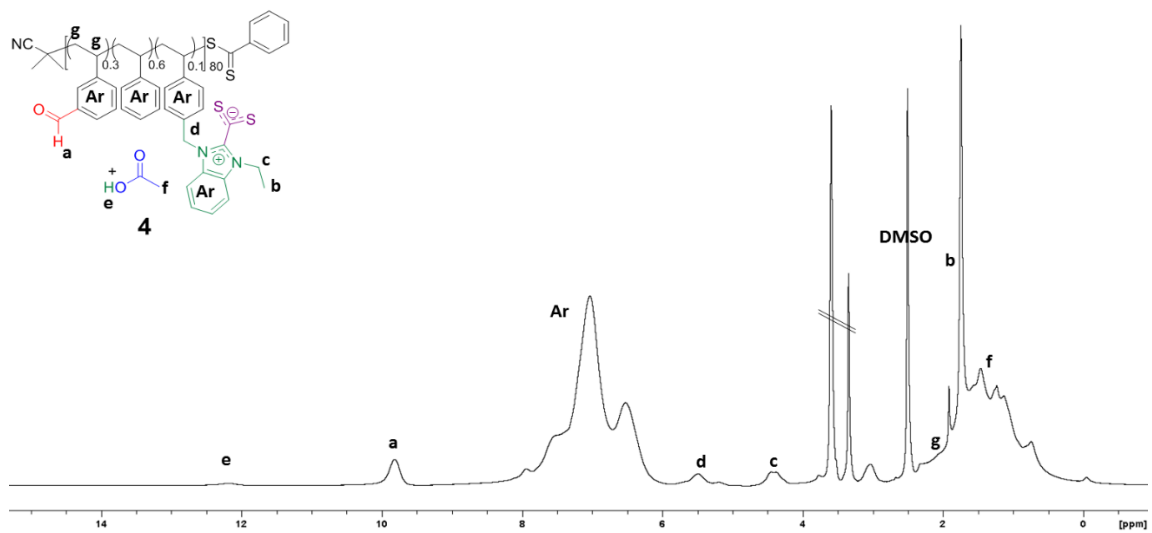


**Figure S4.25.**  $^1\text{H}$  NMR spectrum of copolymer **4** in  $\text{DMSO-}d_6$ .

**Chapter V: Catalytically Active *N*-Heterocyclic  
Carbene Release from Single-Chain Nanoparticles  
following a Thermolysis-driven Unfolding Strategy**





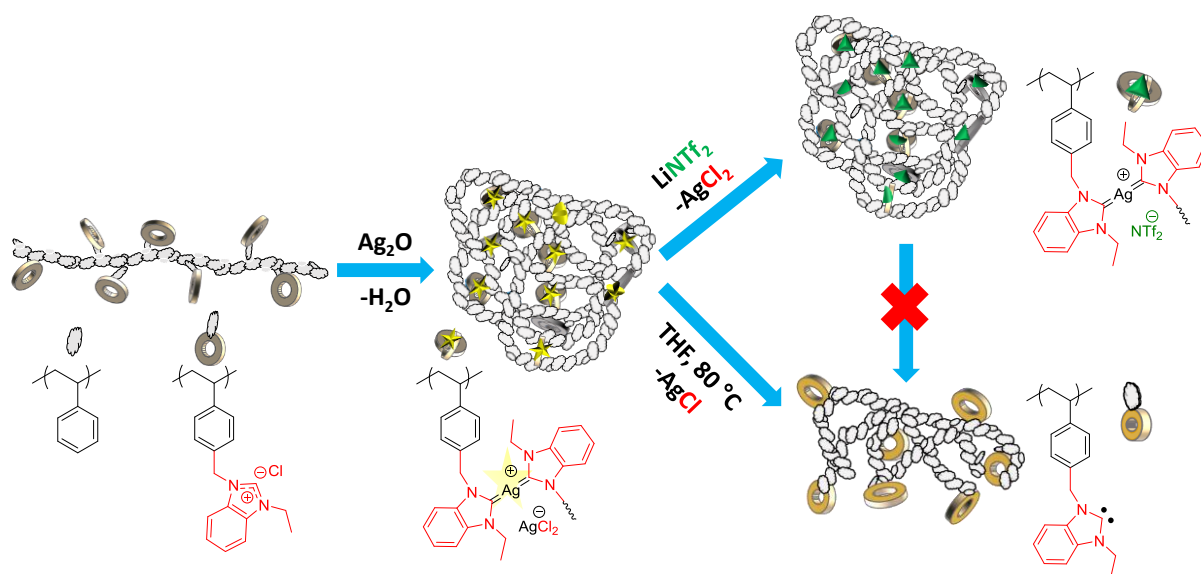
# Table of Contents

## **Chapter V: Catalytically Active *N*-Heterocyclic Carbene Release from Single-Chain Nanoparticles following a Thermolysis-driven Unfolding Strategy**

5.1. Abstract.....	213
5.2. Introduction.....	214-215
5.3. Synthesis of catalytically-active SCNPs.....	216-220
5.4. NHC-mediated benzoin condensation reaction.....	220-223
5.5. Conclusions.....	223
5.6 References.....	224-227
5.7. Experimental Section.....	228-239

## 5.1 Abstract

The need for efficient, tailor-made catalysts has inspired chemists to design synthetic macromolecular architectures for selective catalysis. To this purpose, we report herein the synthesis and in-depth characterization of Ag(I)-crosslinked single-chain nanoparticles (SCNPs) and demonstrate their application as catalysts. Specifically, a copolymer of styrenic benzimidazolium chloride was synthesized as a linear precursor *via* RAFT polymerisation. Metalation of the benzimidazolium moieties by Ag(I) resulted in the intramolecular cross-linking of single chains *via* the formation of Ag-NHC (silver-*N*-heterocyclic carbene) linkages under dilute conditions. The successful formation of well-defined, robust SCNPs was evidenced by size-exclusion chromatography, dynamic light scattering, nuclear magnetic resonance, and transmission electron microscopy. Finally, we demonstrate that our Ag-SCNPs can be used as NHC pre-catalysts, by firstly indirectly evidencing the formation of the corresponding unfolded NHC-CS<sub>2</sub> polybetaine and then organocatalysing a benzoin condensation reaction.



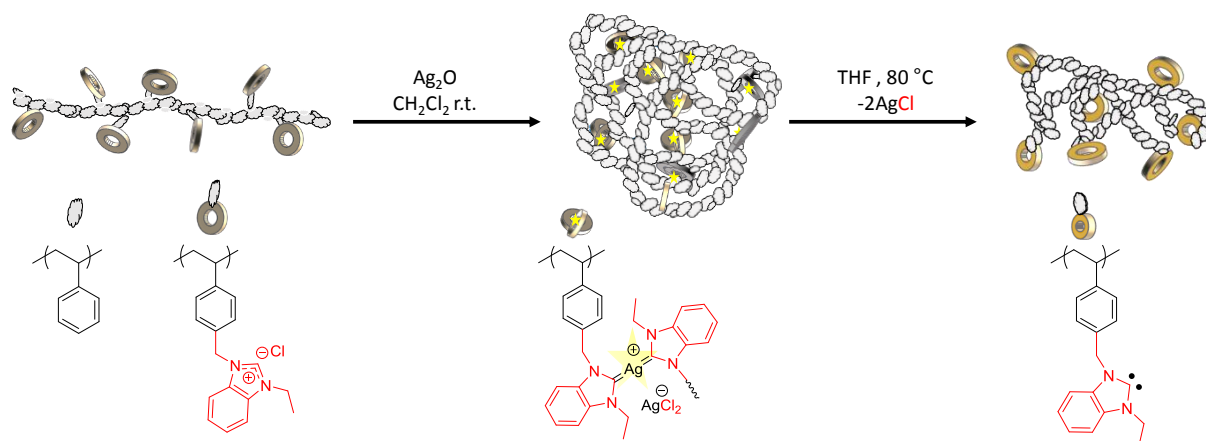
## 5.2 Introduction

Stable *N*-heterocyclic carbenes (NHCs) have become an fascinating area of research since their discovery by Arduengo in 1991.<sup>1</sup> Specifically, their peculiar electronic and steric properties make them powerful ligands of transition metals,<sup>2–6</sup> while their inherent nucleophilicity<sup>7</sup> and Brønsted-basicity<sup>8</sup> account for their efficient performance as organocatalysts for both molecular<sup>9</sup> and macromolecular transformations.<sup>10–12</sup> To overcome their air and moisture sensitivity, a variety of masked NHCs, including NHC-CO<sub>2</sub> adducts, NHC-2-alkoxy adducts or NHC-Ag have been developed.<sup>11–17</sup> Interestingly, silver complexes represent a versatile class of labile NHC metal complexes because of the relative weakness of the C<sub>2</sub>-Ag bond.<sup>18</sup> The most popular route to obtain Ag(I)-NHC compounds uses Ag<sub>2</sub>O, allowing the direct conversion of imidazolium salts (ionic liquids; ILs) into the corresponding metal complexes by transmetalation reaction. Thus, in comparison to the approaches used to produce Zn- and Sn-NHC complexes,<sup>19</sup> the free carbenes do not interfere with the synthesis of Ag(I)-NHC, allowing to achieve good yields using standard laboratory techniques.<sup>6,11,13,20,21</sup>

Moreover, thanks to the easy accessibility and high versatility of NHCs, several functionalized architectures can be achieved from Ag(I)-NHC complexes for different applications, such as antibacterial agents<sup>18,22</sup> or catalysis.<sup>23–26</sup> In particular, a promising synthetic strategy inspired by nature has emerged to prepare unimolecular versatile nano-objects referred to as single-chain nanoparticles (SCNPs).<sup>27–31</sup> Indeed, these folded/collapsed soft nanostructures have gained increasing attention for the development of functional materials in the fields of nanomedicine, protein mimicry, and catalysis.<sup>30–34</sup> In the catalysis field, the design of supported organometallic catalysts aims to emulate the unique features of (metallo)enzymes, such as structural complexity, compartmentalized functions, and site isolation.<sup>33,35–39</sup> Previous work in the area has typically focused on the formation of SCNPs by hydrogen or covalent bonding between supported orthogonal functions.<sup>34</sup> More recently, coordination chemistry, where metals act as cross-linkers inducing the single-chain particle formation, has been developed.<sup>33,40–44,44</sup> Surprisingly, the ability of Ag to trigger the single-chain folding of catalytically active SCNPs remains unexploited despite the potential of Ag(I)-NHC complexes to generate free NHCs and undergo transmetalation.<sup>30</sup>

Herein, we report for the first time the formation of Ag-SCNPs obtained by cross-linking benzimidazolium moieties using Ag(I) as metalation agent. Upon heating, the free carbene can

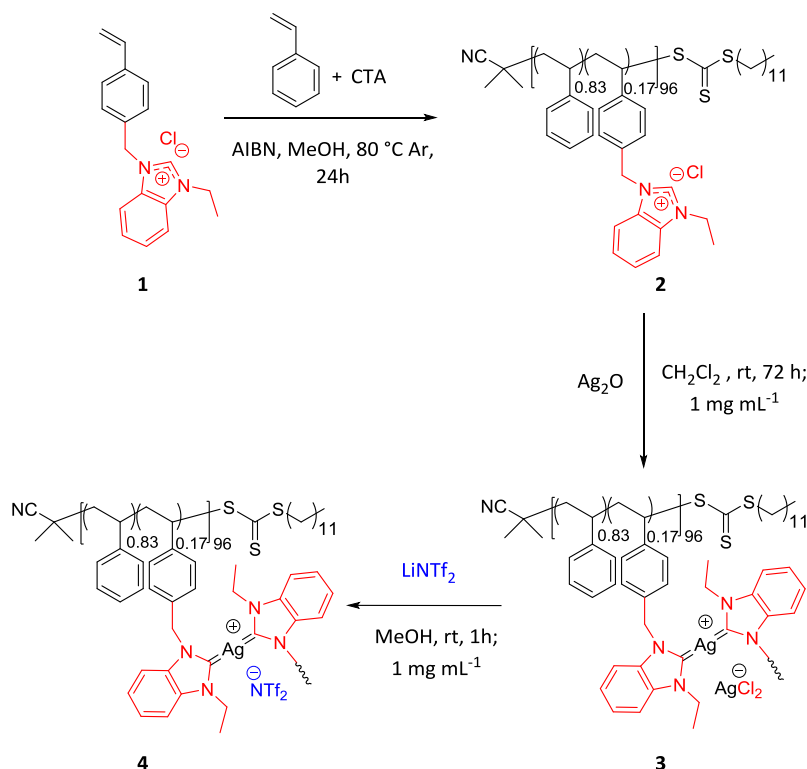
be released from the Ag-NHC precursors, thus enabling free NHC to catalyse the benzoin condensation in THF. The generation of NHC-CS<sub>2</sub> betaine resulting from the reaction between Ag-SCNPs and CS<sub>2</sub> provided indirect evidence of free NHC formation upon thermal-triggered unfolding of SCNPs. Therefore, our Ag-SCNPs combine the unique properties of Ag-NHC complexes with the SCNP technology to create versatile and functional nanoparticles for catalytic applications.



**Scheme 5.1.** Folding of a single-chain polymer into a nanoparticle structure *via* addition of a metal ion source (*i.e.*  $\text{Ag}_2\text{O}$ ). These SCNPs are then employed as sources of free NHC upon thermal decomposition of the organometallic Ag-NHC bond in the nanoreactor to form an active catalyst species.

### 5.3 Synthesis of catalytically-active SCNP

The 4-vinylbenzylethylbenzimidazolium chloride (**1**) ionic liquid monomer was prepared following a two-step synthesis (**Scheme 5.2**), as previously reported in the literature.<sup>45–48</sup> A random copolymer of monomer **1** and styrene units was then obtained *via* reversible addition-fragmentation chain-transfer (RAFT) polymerisation, using 2-cyano-2-propyl dodecyl trithiocarbonate as chain transfer agent (CTA) and azobisisobutyronitrile (AIBN) as radical source in methanol to yield copolymer **2**. The monomer conversion was quantified *via* <sup>1</sup>H NMR spectroscopy by following the disappearance of the C(H) signals of styrene and **1**, as well as the broadening of CH<sub>imi</sub> in the polymer. Moreover, the consumption of styrene and **1** in similar ratio indicates that the imidazolium functional groups were homogeneously distributed throughout the chains. The final structure of **2** corresponded to a styrene/benzimidazolium ratio of ~5, as confirmed by <sup>1</sup>H NMR spectroscopy (**Fig. S5.1**), which was selected to increase the solubility of **2** and its derivatives (*i.e.* **3**, **4** and **5**) in relatively apolar solvents, such as THF.



**Scheme 5.2.** Synthesis of copolymer **2** *via* RAFT polymerization of styrene and **1** in methanol. The subsequent addition of Ag<sub>2</sub>O results in the formation of **3** as SCNPs. Further anion exchange was performed by inserting a non-coordinating anion (NTf<sub>2</sub><sup>-</sup>) into **3** to confer less dynamic behavior (**4**).

In contrast to previous works where the preparation of imidazolium-based SCNPs involved harsh reaction conditions<sup>45</sup> and tedious purification steps,<sup>52</sup> our approach affords robust NHC-loaded SCNPs under relatively mild conditions. The controlled intramolecular formation of SCNPs (**4**) was achieved by simply adding Ag<sub>2</sub>O to a solution of copolymer **3** (1 mg.mL<sup>-1</sup>) in dichloromethane at rt. Trapping the produced H<sub>2</sub>O with molecular sieves (4 Å) afforded a better yield of **3**.<sup>26</sup> Interestingly, the insolubility of Ag<sub>2</sub>O in dichloromethane provided a means of monitoring the reaction progress by observing its gradual disappearance, as a consequence of its incorporation in the copolymer structure. The folding of **2** was thus monitored through the disappearance of the C<sub>2</sub>H signal corresponding to the benzimidazolium ( $\delta = 10.2$  ppm), as well as the broadening of the *N*-ethyl signals ( $\delta = 4.55$  ppm) by <sup>1</sup>H NMR spectroscopy (**Fig. 5.1A**). After 72 h, full conversion to the Ag-NHC moieties ( $\delta = 10.7$ - $10.1$ ) was also confirmed by <sup>13</sup>C NMR spectroscopy with the complete disappearance of the C<sub>2</sub>H signal from benzimidazolium at  $\delta = 146.7$  ppm, and the observation of a new signal at  $\delta = 188.8$  ppm corresponding to C-Ag (**Fig. 5.2 and S5.4**). In addition, SEC characterization was used to further confirm the folding of **2** into well-defined SCNPs (**3**). Specifically, in comparison to **2** ( $M_n = 18,000$  g mol<sup>-1</sup>,  $D_M = 1.2$ ), the SEC trace of **3** shifted towards a smaller apparent molecular weight (**Fig. 5.1B**,  $M_n = 17,600$  g mol<sup>-1</sup>,  $D_M = 1.2$ ), which is indicative of the formation of a more compact structure with a smaller hydrodynamic radius, compared to the linear polymer. As a consequence of the poor solubility of **2** in THF (with added salt for SEC analysis), it was not possible to directly compare the apparent molecular weight in the same solvent as catalysis is performed. Finally, mean hydrodynamic diameters of  $4.5 \pm 0.4$  nm (number-weighted size distribution) and  $4.8 \pm 0.7$  nm (volume-weighted size distribution at a concentration of 1 mg mL<sup>-1</sup> of polymer sample) were determined by DLS for **3** (**Fig. S5.11**), in excellent agreement with the size (*ca.*  $5 \pm 1.5$  nm) observed by transmission electron microscopy (TEM) (**Fig. 5.1C**).

In order to confirm the thermolability of the Ag-NHC crosslinking bridges present in **3**, the variation in size distribution of the SCNPs with temperature was monitored by DLS analysis. Interestingly, the size of SCNPs **3** increased notably, from 15 nm to 70 nm, at  $\sim 40$  °C (**Fig.5.1D**), likely as a consequence of intermolecular rearrangements into larger aggregates after disassembly.<sup>20</sup> In fact, the silver-carbene bond, which is the weakest among the noble metals (*i.e.* gold > copper > silver), is subjected to dynamic exchange, especially when the steric hindrance is less pronounced.<sup>6</sup> Furthermore, in Ag-NHC complexes, both the nature of the azolium anion and the solvent also play an important role in the bond strength, as coordinating

anions, such as halides (*e.g.* Cl<sup>-</sup>, Br<sup>-</sup>, I<sup>-</sup>), form stronger hydrogen bonds compared to non-coordinating anions (*e.g.* BF<sub>4</sub><sup>-</sup>, NTf<sub>2</sub><sup>-</sup>).<sup>53-55</sup> However, halides usually facilitate the dynamic exchange in the resulting complexes *via* their reversible binding to the silver center, whereas non-coordinating anions prevent such dynamic behavior, which leads exclusively to the formation of cationic bis(NHC) complexes, *i.e.* crosslinked SCNPs.<sup>6</sup> Hence, such dynamic exchange behavior allows halide Ag-NHC complexes to generate free NHCs by thermolysis. Conversely, the enhanced stability of Ag-NHC complexes with non-coordinating anions prevents such dynamic process.<sup>6,56</sup>

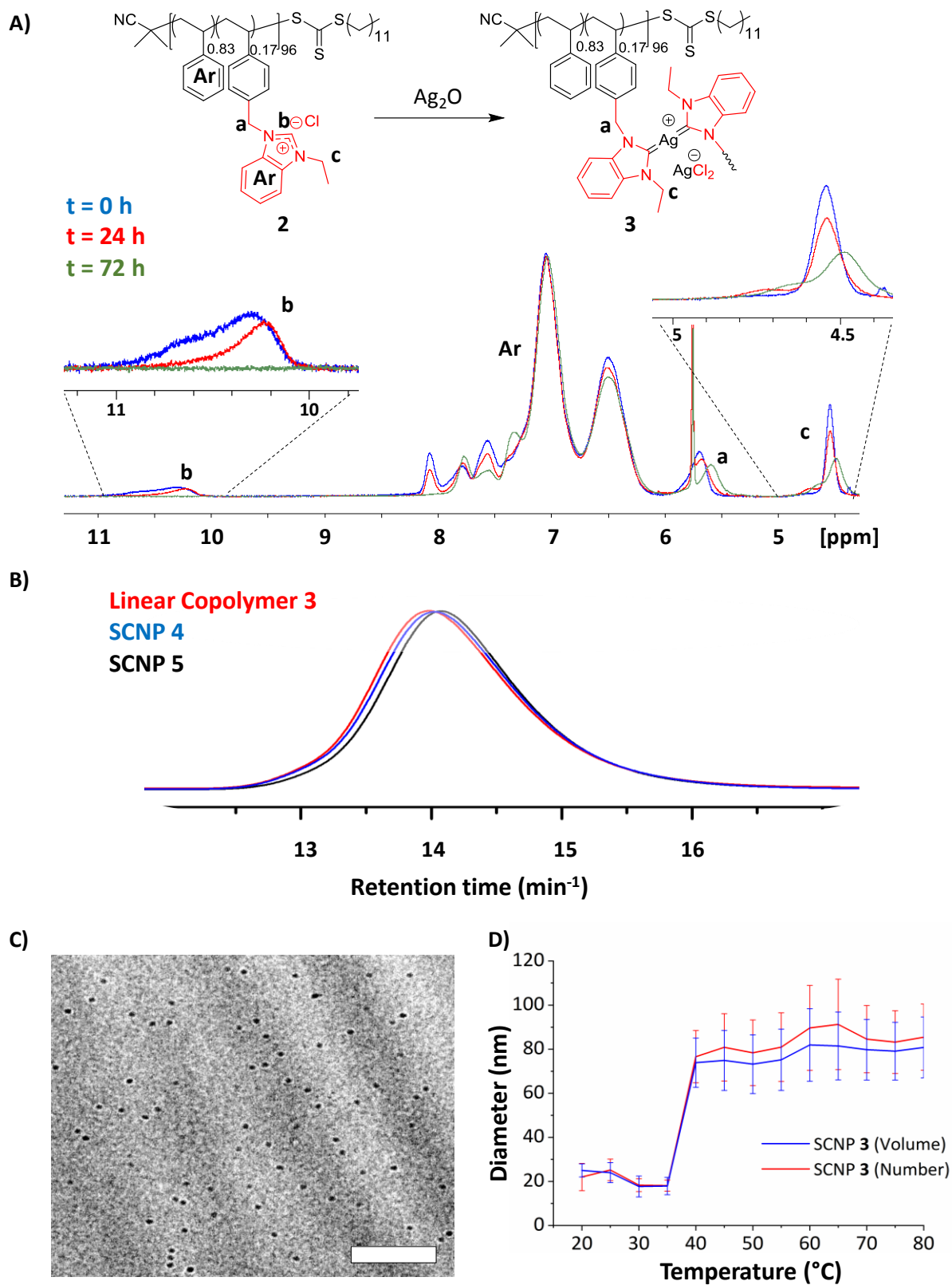


**Figure 5.1.** A) Ag-NHC complexation reaction monitored by  $^1\text{H}$  NMR spectroscopy (400 MHz; 298 K;  $\text{DMSO-}d_6$ ) at different time points ( $t_0$  = blue line, 24 h = red line, 72 h = green line). B) SEC curves (in

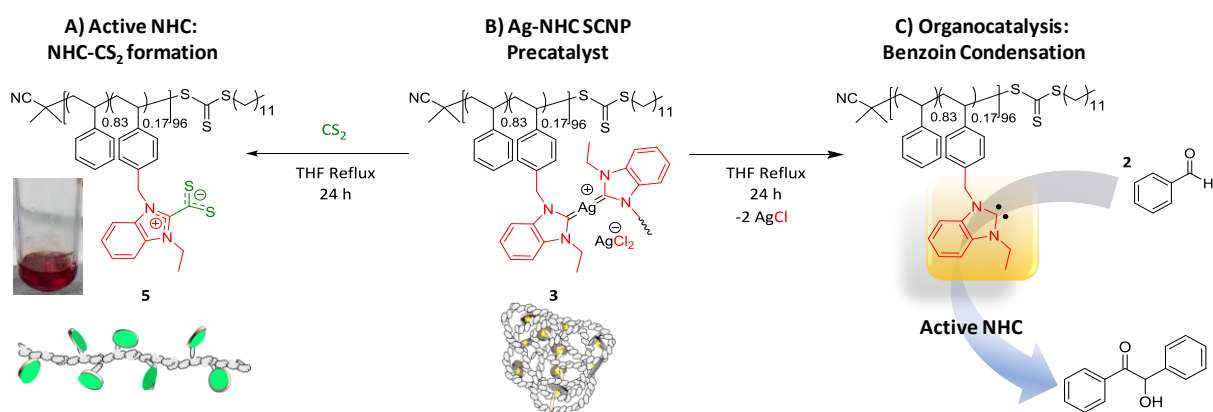


DMF with 10 mM  $\text{NH}_4\text{BF}_4$ ) of **2** (red line), **3** (blue line) and **4** (black line) using RI detector polystyrene standard. **C**) TEM micrograph of SCNPs **4** (scale bar = 50 nm). **D**) Hydrodynamic mean diameter of SCNPs **4** (blue line volume distribution; red line number distribution) using multi-temperature DLS analysis from 20 °C to 80 °C in THF (Conc. 5 mg mL<sup>-1</sup>).

In addition to **3** which is stabilized by coordinating  $\text{AgCl}_2^-$  anions, the more stable Ag-NHC complex **4** bearing non-coordinating  $\text{NTf}_2^-$  anions, was prepared by applying a mild anion-exchange to **3** using an excess of  $\text{LiNTf}_2$  salt that provided an efficient driving force to displace  $\text{Cl}^-$ , precipitating  $\text{AgCl}$  as a byproduct. SEC analysis of the resulting polymer showed a decrease in apparent molecular weight (**Fig. 5.1B**,  $M_n = 17,300 \text{ g mol}^{-1}$ ,  $D_M = 1.2$ ) which is most likely a consequence of the strong preference of the  $\text{NTf}_2^-$  containing SCNPs to be retained as a dimeric  $\text{NHC}_2\text{Ag}$  complex and hence presenting a more compact hydrodynamic volume during analysis.

#### 5.4 NHC-mediated benzoin condensation reaction

Before investigating **3** as a catalyst for the carbene-mediated benzoin condensation reaction,<sup>57,58</sup> we first examined whether active carbene species could be generated upon thermal decomposition of the poly(bis-NHC)-silver complex in **3**. For that purpose, **3** was heated at 80 °C in THF in the presence of carbon disulfide ( $\text{CS}_2$ ; **Scheme 5.3**). After 24 h, the solution turned red-brown, which was indicative of the formation of copolybetaine **5**, as it was further confirmed by <sup>13</sup>C NMR spectroscopy ( $\delta = 151.8$  and 219.9 ppm corresponding to  $\text{C}_{2(\text{imi})}$  and  $\text{CS}_2^-$  respectively; **Fig. 5.2**).<sup>20,21</sup>



**Scheme 5.3.** Application of SCNPs **3** as a catalytic platform (**B**) for the benzoin condensation reaction by exposing active NHC upon heating (**C**) Indirect evidence of the formation of active NHC intermediate (**A**).

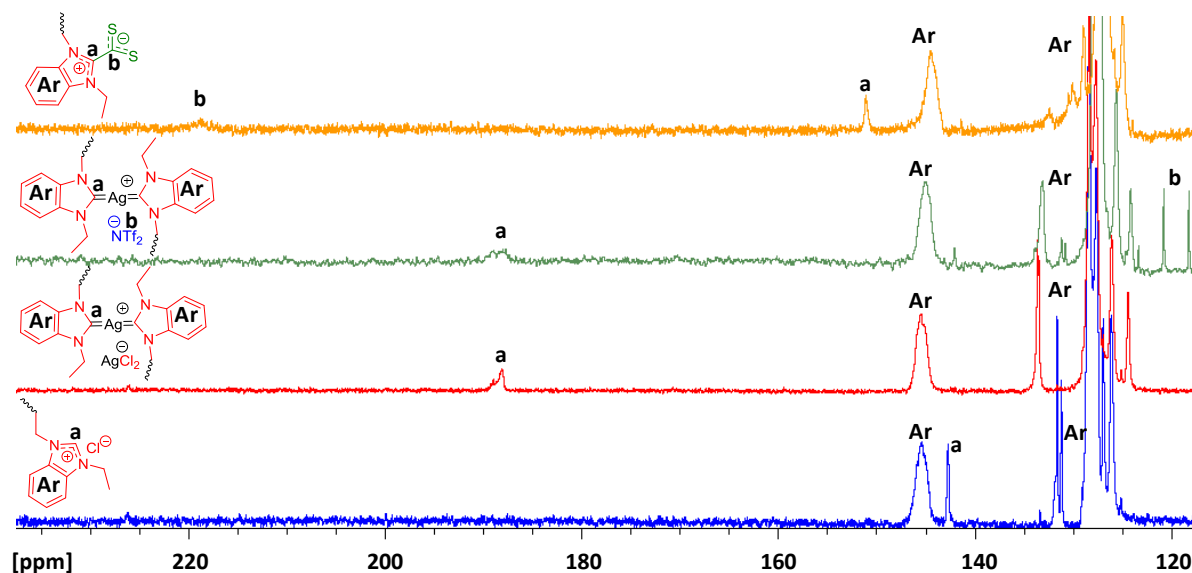


**Figure 5.2.**  $^{13}\text{C}$  NMR spectra (100.7 MHz; 298 K;  $\text{DMSO-}d_6$ ) of **2** (blue), SCNP **3** (red), SCNP **4** (green), and copolybetaine **5** (yellow).

Since the benzoin condensation is specifically catalyzed by carbenes,<sup>57,58</sup> **3** was evaluated as pre-catalyst for this reaction (**Scheme 5.3**). Firstly, we tested the catalyst system at ambient temperature which displayed no activity and hence confirms that no NHC catalyst (SCNP **3**) was delivered at room temperature (Run 1; **Table 5.1**). Therefore, although the thermolysis of Ag-bis(NHC) complexes can occur at temperatures as low as 40 °C,<sup>20</sup> the temperature was set at 80 °C to increase the release of free NHCs. As summarized in **Table 5.1**, the conversion increased from 13 to 32% by increasing the catalyst loading from 1 to 10 mol%, under otherwise identical conditions (*i.e.* THF at 80 °C for 24 h; Runs 2-4). However, increasing the reaction time up to 48 h (Run 5) did not afford any improvement, suggesting the likely decomposition of the catalyst at this temperature for longer than 24 h, as previously reported.<sup>6</sup> This premature deactivation also prevented the recycling of SCNP **3**, as no catalytic activity was observed in the subsequent run (6).

In order to introduce a control system, a small molecule model with benzylic *N*-substituents on the NHC moieties, **6**, (see ESI) was used to catalyze the benzoin condensation reaction under similar conditions (Runs 7-9). This experiment showed higher catalytic activity, reaching up to 51% conversion of benzaldehyde after 24 h, probably because of the easier access to the catalytic site (Run 7). Similarly, no further increase in conversion was observed after 48 h (Run 8), while the non-recyclability of the molecular model became further evident in the subsequent run (9). It has to be acknowledged however, that both Ag-(bis)NHC based molecular and macromolecular systems show lower catalytic performance for this reaction compared to our previously reported masked-NHC based SCNPs.<sup>47,52</sup>

Finally, in good agreement with our initial hypothesis, the presence of non-coordinating counteranions (*i.e.* NTf<sub>2</sub><sup>-</sup>) in **4** hindered the formation of active carbenes, precluding the formation of active catalytic species and thus preventing the synthesis of benzoin (Run 10). Hence, the nature of the counteranion significantly influences the robustness and thermolability of Ag-SCNPs to deliver catalytically active NHC in a suitable environment, hence highlighting the potential to employ the anion exchange reaction as a successful strategy to switch on and off the catalytic activity of this system.

**Table 5.1.** Condensation reaction of benzaldehyde under different conditions using Ag-NHC SCNPs and a small molecule model as catalysts.

Run	Catalyst	Loading mol (%) <sup>a</sup>	Cycle	Solvent	Temperature (°C)	Time (h)	Conv (%) <sup>b</sup>
1	SCNP 3	10	1	THF <sup>c</sup>	80	24	0
2	SCNP 3	1	1	THF	80	24	13
3	SCNP 3	5	1	THF	80	24	21
4	SCNP 3	10 <sup>d</sup>	1	THF	80	24	32
5	SCNP 3	10	1	THF	80	48	32
6	SCNP 3	10	2 <sup>e</sup>	THF	80	24	0
7	<b>6</b> <sup>f</sup>	10	1	THF	80	24	51
8	<b>6</b>	10	1	THF	80	48	51
9	<b>6</b>	10	2 <sup>g</sup>	THF	80	24	0

---

10	SCNP 4	10	1	THF	80	24	0
----	--------	----	---	-----	----	----	---

---

<sup>a</sup> Mol% calculated relative to the benzimidazolium moieties; <sup>b</sup> conversion was calculated by <sup>1</sup>H NMR spectroscopy (**Fig. S5.10**); <sup>c</sup> THF was dried over Na/Benzophenone before distillation; <sup>d</sup> a 20 mg mL<sup>-1</sup> concentration of catalyst was used as reference; <sup>e</sup> **3** purified by dialysis against MeOH; <sup>f</sup> synthesis and characterization of the molecular model used in this reaction is included in the ESI. ; <sup>g</sup> molecular catalyst was recovered by precipitation into cold MeOH.

## 5.5 Conclusion

The formation of SCNPs crosslinked by Ag-NHC bridges has been achieved for the first time. Ag was used as metalation agent to trigger the folding of a linear styrene-benzimidazolium copolymer into 5 nm SCNPs under relatively mild conditions. These nanoreactors were able to respond to external increase in temperature and unfold to release free NHC, which was then able to catalyse the benzoin condensation reaction in the same pot, although in modest yield. Furthermore, by simply changing the counterion, the catalytic activity can be switched off. In conclusion, Ag-NHC SCNPs can be envisaged as a valuable nanoplatform for transmetalation reactions.

## 5.6 References

- 1 A. J. Arduengo III, R. L. Harlow and M. Kline, *Journal of the American Chemical Society*, 1991, **113**, 361–363.
- 2 D. Bourissou, O. Guerret, F. P. Gabba and G. Bertrand, *Chemical Reviews*, 2000, **100**, 39–92.
- 3 M. N. Hopkinson, C. Richter, M. Schedler and F. Glorius, *Nature*, 2014, **510**, 485–496.
- 4 P. de Frémont, N. Marion and S. P. Nolan, *Coordination Chemistry Reviews*, 2009, **253**, 862–892.
- 5 S. Díez-González, N. Marion and S. P. Nolan, *Chemical Reviews*, 2009, **109**, 3612–3676.
- 6 Han Vinh Huynh, *The Organometallic Chemistry of N-heterocyclic Carbenes*, John Wiley & Sons Ltd., 2017.
- 7 B. Maji, M. Breugst and H. Mayr, *Angewandte Chemie International Edition*, 2011, **50**, 6915–6919.
- 8 E. M. Higgins, J. A. Sherwood, A. G. Lindsay, J. Armstrong, R. S. Massey, R. W. Alder and A. C. O'Donoghue, *Chem. Commun.*, 2011, **47**, 1559–1561.
- 9 D. M. Flanigan, F. Romanov-Michailidis, N. A. White and T. Rovis, *Chem. Rev.*, 2015, **115**, 9307–9387.
- 10 S. Naumann and A. P. Dove, *Polym. Chem.*, 2015, **6**, 3185–3200.
- 11 M. Fevre, J. Pinaud, Y. Gnanou, J. Vignolle and D. Taton, *Chemical Society Reviews*, 2013, **42**, 2142.
- 12 W. N. Ottou, H. Sardon, D. Mecerreyes, J. Vignolle and D. Taton, *Progress in Polymer Science*, 2016, **56**, 64–115.
- 13 S. Naumann and M. R. Buchmeiser, *Catalysis Science & Technology*, 2014, **4**, 2466.
- 14 Y. An, J. Yu and Y. Han, *Chinese Journal of Chemistry*, 2019, **37**, 76–87.

- 15 A. Melaiye, Z. Sun, K. Hindi, A. Milsted, D. Ely, D. H. Reneker, C. A. Tessier and W. J. Youngs, *Journal of the American Chemical Society*, 2005, **127**, 2285–2291.
- 16 C. K. Lee, C. S. Vasam, T. W. Huang, H. M. J. Wang, R. Y. Yang, C. S. Lee and I. J. B. Lin, *Organometallics*, 2006, **25**, 3768–3775.
- 17 D. Yu, M. X. Tan and Y. Zhang, *Advanced Synthesis & Catalysis*, 2012, **354**, 969–974.
- 18 A. Kascatan-Nebioglu, M. J. Panzner, C. A. Tessier, C. L. Cannon and W. J. Youngs, *Coordination Chemistry Reviews*, 2007, **251**, 884–895.
- 19 V. Nesterov, D. Reiter, P. Bag, P. Frisch, R. Holzner, A. Porzelt and S. Inoue, *Chemical Reviews*, 2018, **118**, 9678–9842.
- 20 A. C. Sentman, S. Csihony, R. M. Waymouth and J. L. Hedrick, *The Journal of Organic Chemistry*, 2005, **70**, 2391–2393.
- 21 P. Coupillaud, J. Vignolle, D. Mecerreyes and D. Taton, *Polymer*, 2014, **55**, 3404–3414.
- 22 N. A. Johnson, M. R. Southerland and W. J. Youngs, *Molecules*, 2017, **22**, 1263.
- 23 I. J. B. Lin and C. S. Vasam, *Comments on Inorganic Chemistry*, 2004, **25**, 75–129.
- 24 H. M. Wang and I. J. Lin, *Organometallics*, 1998, **17**, 972–975.
- 25 C. A. Citadelle, E. L. Nouy, F. Bisaro, A. M. Z. Slawin and C. S. J. Cazin, *Dalton Transactions*, 2010, **39**, 4489.
- 26 A. A. Tulloch, A. A. Danopoulos, S. Winston, S. Kleinhenz and G. Eastham, *Journal of the Chemical Society, Dalton Transactions*, 2000, 4499–4506.
- 27 M. Gonzalez-Burgos, A. Latorre-Sanchez and J. A. Pomposo, *Chem. Soc. Rev.*, 2015, **44**, 6122–6142.
- 28 O. Altintas and C. Barner-Kowollik, *Macromolecular Rapid Communications*, 2016, **37**, 29–46.
- 29 M. Ouchi, N. Badi, J.-F. Lutz and M. Sawamoto, *Nature Chemistry*, 2011, **3**, 917–924.
- 30 A. M. Hanlon, C. K. Lyon and E. B. Berda, *Macromolecules*, 2016, **49**, 2–14.

- 31 S. Mavila, O. Eivgi, I. Berkovich and N. G. Lemcoff, *Chemical Reviews*, 2016, **116**, 878–961.
- 32 J. Rubio-Cervilla, E. González and J. Pomposo, *Nanomaterials*, 2017, **7**, 341.
- 33 H. Rothfuss, N. D. Knöfel, P. W. Roesky and C. Barner-Kowollik, *Journal of the American Chemical Society*, , DOI:10.1021/jacs.8b02135.
- 34 O. Altintas, T. S. Fischer and C. Barner-Kowollik, in *Single-Chain Polymer Nanoparticles*, ed. J. A. Pomposo, Wiley-VCH Verlag GmbH & Co. KGaA, Weinheim, Germany, 2017, pp. 1–45.
- 35 A. Sanchez-Sanchez, A. Arbe, J. Colmenero and J. A. Pomposo, *ACS Macro Letters*, 2014, **3**, 439–443.
- 36 S. Thanneeru, S. S. Duay, L. Jin, Y. Fu, A. M. Angeles-Boza and J. He, *ACS Macro Letters*, 2017, 652–656.
- 37 S. Mavila, C. E. Diesendruck, S. Linde, L. Amir, R. Shikler and N. G. Lemcoff, *Angewandte Chemie International Edition*, 2013, **52**, 5767–5770.
- 38 Y. Bai, X. Feng, H. Xing, Y. Xu, B. K. Kim, N. Baig, T. Zhou, A. A. Gewirth, Y. Lu, E. Oldfield and S. C. Zimmerman, *Journal of the American Chemical Society*, 2016, **138**, 11077–11080.
- 39 J. Chen, J. Wang, Y. Bai, K. Li, E. S. Garcia, A. L. Ferguson and S. C. Zimmerman, *Journal of the American Chemical Society*, 2018, **140**, 13695–13702.
- 40 Y. Azuma, T. Terashima and M. Sawamoto, *ACS Macro Letters*, 2017, **6**, 830–835.
- 41 N. D. Knöfel, H. Rothfuss, J. Willenbacher, C. Barner-Kowollik and P. W. Roesky, *Angewandte Chemie International Edition*, 2017, **56**, 4950–4954.
- 42 S. Mavila, I. Rozenberg and N. G. Lemcoff, *Chemical Science*, 2014, **5**, 4196–4203.
- 43 I. Berkovich, V. Kobernik, S. Guidone and N. G. Lemcoff, in *Single-Chain Polymer Nanoparticles*, ed. J. A. Pomposo, Wiley-VCH Verlag GmbH & Co. KGaA, Weinheim, Germany, 2017, pp. 217–257.
- 44 K. Freytag, S. Säfken, K. Wolter, J. C. Namyslo and E. G. Hübner, *Polymer Chemistry*, 2017, **8**, 7546–7558.

- 45 R. Lambert, A.-L. Wirotius, S. Garmendia, P. Berto, J. Vignolle and D. Taton, *Polymer Chemistry*, 2018, **9**, 3199–3204.
- 46 S. Garmendia, R. Lambert, A.-L. Wirotius, J. Vignolle, A. P. Dove, R. K. O'Reilly and D. Taton, *European Polymer Journal*, 2018, **107**, 82–88.
- 47 S. Garmendia, A. P. Dove, D. Taton and R. K. O'Reilly, *Polymer Chemistry*, 2018, **9**, 5286–5294.
- 48 R. Lambert, A.-L. Wirotius, J. Vignolle and D. Taton, *Polymer Chemistry*, 2019, **10**, 460–466.
- 49 H. M. Lima and C. J. Lovely, *Organic Letters*, 2011, **13**, 5736–5739.
- 50 P. O. Asekunowo, R. A. Haque, Mohd. R. Razali, S. W. Avicor and M. F. F. Wajidi, *Applied Organometallic Chemistry*, 2017, **31**, e3655.
- 51 M. W. P. van de Put, J. P. Patterson, P. H. H. Bomans, N. R. Wilson, H. Friedrich, R. A. T. M. van Benthem, G. de With, R. K. O'Reilly and N. A. J. M. Sommerdijk, *Soft Matter*, 2015, **11**, 1265–1270.
- 52 R. Lambert, A.-L. Wirotius and D. Taton, *ACS Macro Letters*, 2017, **6**, 489–494.
- 53 S. Kuwata and F. E. Hahn, *Chemical Reviews*, 2018, **118**, 9642–9677.
- 54 M.-M. Gan, J.-Q. Liu, L. Zhang, Y.-Y. Wang, F. E. Hahn and Y.-F. Han, *Chemical Reviews*, 2018, **118**, 9587–9641.
- 55 Á. Vivancos, C. Segarra and M. Albrecht, *Chemical Reviews*, 2018, **118**, 9493–9586.
- 56 H.-L. Su, L. M. Pérez, S.-J. Lee, J. H. Reibenspies, H. S. Bazzi and D. E. Bergbreiter, *Organometallics*, 2012, **31**, 4063–4071.
- 57 R. S. Menon, A. T. Biju and V. Nair, *Beilstein Journal of Organic Chemistry*, 2016, **12**, 444–461.
- 58 M. Alrayyani and O. Š. Miljanić, *Chemical Communications*, 2018, **54**, 11989–11997.



## 5.7 Experimental section

### Materials

Methanol, benzimidazole (>95%), 4-vinylbenzyl chloride (90%), ethyl bromide (99%), 2-cyano-2-propyl benzodithioate (>97%), potassium hydroxide (pellets), and benzyl chloride (97%) were obtained from Aldrich and used as received. Dichloromethane (99.7%), carbon disulfide (CS<sub>2</sub>), 2-Cyano-2-propyl dodecyl trithiocarbonate and (CTA) lithium bis(trifluoromethane)sulfonylimide (LiTFSI) were obtained from Aldrich and used as received. Azobis(2-methylpropionitrile) (AIBN, 99%) was received from Aldrich and was purified by recrystallization (2x) from methanol. The synthesis of 4-vinylbenzylethylbenzimidazolium chloride (**1**) was performed as previously described.<sup>45-48</sup> The synthesis of 1,3-dibenzyl-1H-benzimidazol-3-ium chloride was performed as described elsewhere.<sup>49,50</sup> Tetrahydrofuran (THF) was distilled over Na/benzophenone. Styrene and benzaldehyde were dried over CaH<sub>2</sub> and distilled prior to use. All synthesized polymers were purified by dialysis against methanol using “Standard Grade Regenerated Cellulose Dialysis Membranes (Spectra/Por6) Pre-wetted RC tubing” (SpectrumLab) with a molecular weight cut off (MWCO) of 3.5 kDa. All polymers were azeotropically dried using previously distilled THF before performing catalysis. Polymerization, catalyst loadings, and catalysis experiments were carried out by the syringe technique under dry argon in baked glass tubes equipped with a two-way stopcock.

### Characterisation

<sup>1</sup>H, <sup>13</sup>C and <sup>19</sup>F NMR spectra were recorded on a Bruker AC-400 spectrometer in appropriate deuterated solvents. All <sup>13</sup>C measurements were performed at 298 K on a Bruker Avance III 400 spectrometer operating at 400, 376.5 and 100 MHz and equipped with a 5 mm Bruker multinuclear direct cryo-probe. Dimethyl formamide (10 mM ammonium tetrafluoroborate) soluble polymers were first solubilized in concentrations of 1 mg mL<sup>-1</sup>, and their masses were determined by size exclusion chromatography (SEC) in DMF at 20 °C using refractometric (RI) detector (Varian) and polystyrene calibration as standards. Analyses were performed using a three-column set of TSK gel TOSOH (G4000, G3000, G2000 with pore sizes 20, 75, and 200 Å, respectively, connected in series). Hydrodynamic diameters (*D<sub>h</sub>*) and size distributions of SCNPs were determined by dynamic light scattering (DLS) on a Malvern Zetasizer Nano ZS operating at 20 °C with a 4 Mw He-Ne 633 nm laser module. Samples were filtered through a 0.22 µm PTFE filter prior to measurement, and quartz cuvettes were used. Measurements were

made at a detection angle of  $173^\circ$  (back scattering), and the data were analysed with Malvern DTS 6.20 software, using the multiple narrow modes setting. All measurements were performed in triplicate, with 10 runs per measurement. TEM analyses were performed on a JEOL 2011 (LaB<sub>6</sub>) microscope operating at 200 KeV, equipped with a GATAN UltraScan 1000 digital camera. Conventional bright field conditions were lacey carbon-coated copper grids (Agar Scientific, 400 mesh, S116-4). SCNP solutions were diluted to  $1 \text{ mg mL}^{-1}$  in MeOH before  $4 \mu\text{L}$  of each sample were drop-deposited onto the graphene oxide coated grids and allowed to air dry. Subsequent staining was applied using uranyl acetate ( $1 \text{ mg mL}^{-1}$ ,  $7 \mu\text{L}$ ) to enhance the contrast.<sup>51</sup> Images were analyzed using Image J software, and 50 particles were measured to produce a mean and standard deviation for the particle size ( $D_{av}$ ).

## Synthesis

### Synthesis of 4-vinylbenzylethylbenzimidazolium chloride ([ViEBIm]Cl) (1)

Benzimidazole (5 g, 42 mmol, 1 eq.) was first dissolved in *N,N*-dimethylformamide (20 mL). Potassium hydroxide (4.75 g, 106 mmol, 2.5 eq.) was then added and the solution stirred for 15 minutes before the drop-wise addition of ethyl bromide (3.45 mL, 46 mmol, 1.1 eq.). After stirring at room temperature for 24 hours, the solution was diluted with water (50 mL) and extracted with dichloromethane ( $4 \times 25 \text{ mL}$ ). The organic phases were then combined, dried over magnesium sulfate, and concentrated under reduced pressure, yielding *N*-ethylbenzimidazole as a yellow viscous oil (yield: 80%, 4.93 g). <sup>1</sup>H NMR (400 MHz; 298 K; DMSO-*d*<sub>6</sub>):  $\delta = 8.25$  (s, 1H, N-*CH*-N), 7.69–7.20 (m, 4H, aromatics), 4.12 (t, 2H, N-*CH*<sub>2</sub>-CH<sub>3</sub>), 1.32 (t, 3H, -CH<sub>3</sub>).

A portion of *N*-ethylbenzimidazole (4.82 g, 33 mmol) was first dissolved in acetonitrile (25 mL) in a Schlenk tube, this was then followed by the addition of 4-vinylbenzylchloride (4.65 mL, 33 mmol, 1 eq.). After stirring for 24 hours at 80 °C, the crude reaction mixture was precipitated into ethyl acetate and the resulting solid dried under reduced pressure, yielding the monomer **1** (4-vinylbenzylethylbenzimidazolium chloride) as a white powder (yield: 91%, 8.87 g). <sup>1</sup>H NMR (400 MHz; 298 K; DMSO-*d*<sub>6</sub>):  $\delta = 9.68$  (s, 1H, N-*CH*-N), 8.12–7.14 (m, 8H, aromatics), 6.72 (dd, 1H, Ph-*CH*-CH<sub>2</sub>), 5.95 (s, 2H, Ph-*CH*<sub>2</sub>-N), 5.76 (d, 1H, *CH*=CH<sub>2</sub>), 5.25 (d, 2H, *CH*=CH<sub>2</sub>), 4.15 (dd, 2H, N-*CH*<sub>2</sub>-CH<sub>3</sub>), 1.31 (t, 3H, -CH<sub>2</sub>-CH<sub>3</sub>). Characterisation is consistent with that previously reported within the literature.<sup>45–48</sup>

### Synthesis of copolymeric linear precursor 2.

2-Cyano-2-propyl dodecyl trithiocarbonate (60 mg, 0.17 mmol), styrene (3.1 mL, 30 mmol) 4-vinylbenzylethylbenzimidazolium chloride **1** (1.57 g, 5.21 mmol), AIBN (27 mg, 0.17 mmol) were dissolved in dry methanol in a 10 mL glass tube. The solution was degassed by five successive freeze-pump cycles and stirred for 16 h at 80 °C. The as-obtained copolymer (**2**) was purified by dialysis against methanol (3.5 kDa MWCO) and obtained as a pink powder (yield: 51%, 2.05 g). <sup>1</sup>H NMR (400MHz; 298 K; DMSO-*d*<sub>6</sub>): 10.7-10.1 (br, 1H, N-CH=N), 8.2-6.1 (br, 32.8H, Ar-*H*), 5.9-5.5 (br, 2H, Ar-CH<sub>2</sub>-N), 4.6-4.4 (br, 2H, N-CH<sub>2</sub>-CH<sub>3</sub>), 2.1-0.9 (br, 27.5H, backbone: CH and CH<sub>2</sub>, CH<sub>2</sub>-CH<sub>3</sub>) (**Fig. S5.1**); <sup>13</sup>C NMR (100.7 MHz; 298 K; DMSO-*d*<sub>6</sub>): 146.7, 142.3, 132.9, 129.1-126.6, 114.1, 62.9, 50.8, 42.6, 14.3 (**Fig. S5.2**). SEC analysis:  $M_n = 18,000 \text{ g mol}^{-1}$ ,  $M_w = 21,600 \text{ g mol}^{-1}$ ,  $D_M = 1.2$

### Synthesis of SCNP 3

Linear copolymer **2** (350 mg; 0.44 mmol referred to benzimidazolium) was dissolved in 350 mL of dry dichloromethane at a concentration of 1 mg mL<sup>-1</sup> in a 1 L round bottom flask. Then, Ag<sub>2</sub>O (60 mg; 0.26 mmol) was added by previously preparing a dispersion in dichloromethane in order to ease the dropwise addition into the flask. Molecular sieves (4 Å) were added in order to trap the generated water, shifting the equilibrium towards the bis-NHC-Ag moiety. The red colored solution was stirred for 72 h, during which time the solution turned transparent, and filtered twice to remove the excess of Ag<sub>2</sub>O. The solvent was finally removed under reduced pressure, and **3** was obtained as a viscous liquid (yield: 82%, 322.1 mg). <sup>1</sup>H NMR (400 MHz; 298 K; DMSO-*d*<sub>6</sub>) = 8.2-6.0 (br, 34.1, Ar-*H*), 5.9-5.4 (br, 2H, Ar-CH<sub>2</sub>-N), 4.6-4.3 (br, 2H, N-CH<sub>2</sub>-CH<sub>3</sub>), 2.2-0.9 (br, backbone: CH and CH<sub>2</sub>, CH<sub>2</sub>-CH<sub>3</sub>) (**Fig. S5.3**); <sup>13</sup>C NMR (100.7 MHz; 298 K; DMSO-*d*<sub>6</sub>): 188.8, 147.3, 134.0, 129.9-123.7, 113.5, 52.8, 47.7, 44.1, 17.9 (**Fig. S5.4**). SEC analysis:  $M_n = 17,600 \text{ g mol}^{-1}$ ,  $M_w = 21,100 \text{ g mol}^{-1}$ ,  $D_M = 1.2$

### Synthesis of SCNP 4

SCNP **3** (150 mg; 0.19 mmol) was solubilized in a glass flask containing 35 mL of methanol and 80 mg (0.29 mmol) of LiTFSI previously dissolved in 35 mL methanol. The solution was stirred at rt (room temperature) until SCNP **4** precipitated. The precipitate was then washed with methanol (5 mL x 2) (yield: 48%, 77.8 mg). <sup>1</sup>H NMR (400 MHz; 298 K; DMSO-*d*<sub>6</sub>) = 8.3-6.0 (m, broad, Ar-*H*), 6.0-5.5 (s, broad, Ar-CH<sub>2</sub>-N), 4.9-4.4 (d, broad, N-CH<sub>2</sub>-CH<sub>3</sub>), 2.3-0.9 (m, broad, backbone: CH and CH<sub>2</sub>, CH<sub>2</sub>-CH<sub>3</sub>) (**Fig. S5.5**); <sup>13</sup>C NMR (100.7 MHz; 298 K; DMSO-*d*<sub>6</sub>): 179.8, 145.5, 132.3, 129.9-123.7, 121.5, 119.1, 112.4, 51.9, 43.8, 41.2, 17.8 (**Fig. S5.6**);

$^{19}\text{F}$  NMR (376.5 MHz; 298 K; DMSO- $d_6$ ): -79.9 (**Fig. S5.7**). SEC analysis:  $M_n = 17,300 \text{ g mol}^{-1}$ ,  $M_w = 20,700 \text{ g mol}^{-1}$ ,  $D_M = 1.2$

### Synthesis of copolymer 5

SCNP **3** (30 mg; 0.04 mmol) was solubilized in dry THF (1 mL) in a glass tube and CS<sub>2</sub> (0.3 mL; 2.6 mmol) was added at rt under argon. The colorless solution was stirred at 80 °C for 24 h, during which time a color change to red was observed, indicative of NHC-CS<sub>2</sub> formation. After cooling, the excess of CS<sub>2</sub> and solvent were removed under reduced pressure, obtaining **5** as a viscous liquid (yield: >95%, 27.3 mg).  $^1\text{H}$  NMR (400 MHz; 298 K; DMSO- $d_6$ ) = 8.2-6.1 (m, broad, Ar-*H*), 5.9-5.5 (s, broad, Ar-*CH*<sub>2</sub>-N), 4.8-4.4 (d, broad, N-*CH*<sub>2</sub>-CH<sub>3</sub>), 2.5-0.9 (m, broad, backbone: CH and CH<sub>2</sub>, CH<sub>2</sub>-CH<sub>3</sub>) (**Fig. S5.8**);  $^{13}\text{C}$  NMR (100.7 MHz; 298 K; DMSO- $d_6$ ): 219.9, 151.8, 145.4, 131.3-124.6, 112.8, 48.2, 43.2, 14.8 (**Fig. S5.9**).

### Synthesis of molecular model 6

Benzimidazole (1 g, 8.5 mmol, 1 eq.) was first dissolved in *N,N*-dimethylformamide (5 mL). Potassium hydroxide (1.19 g, 21 mmol, 2.5 eq.) was then added and the solution allowed to stir for 30 minutes before the drop-wise addition of benzyl chloride (1.1 mL, 9.4 mmol, [Add] eq.). After stirring for 18 hours at room temperature, the solution was diluted with water (2 × 10 mL) and extracted with dichloromethane (3 × 20 mL). The organic phases were combined, dried over magnesium sulfate, and the solvent removed under reduced pressure, yielding *N*-benzylbenzimidazole as yellow viscous oil (yield: 82%, 1.45 g).  $^1\text{H}$  NMR (400 MHz; 298 K; DMSO- $d_6$ ):  $\delta = 8.2$  (s, 1H, N=*CH*-N), 8.7–7.14 (m, 9H, aromatics), 5.5 (s, 2H, Ph-*CH*<sub>2</sub>-N)

A portion of *N*-benzylbenzimidazole (1 g, 4.8 mmol, 1 eq.) was first dissolved acetonitrile (5 mL) in a Schlenk tube, this was then followed by the addition of benzyl chloride (0.66 mL, 5.8 mmol, 1.2 eq.). After stirring for 24 hours at reflux, the crude reaction mixture was precipitated into cold diethyl ether and the resulting solid dried under reduced pressure, yielding *N,N*-bisbenzylbenzimidazolium chloride as a white crystals (yield: 94%, 1.45 g).  $^1\text{H}$  NMR (400 MHz; 298 K; DMSO- $d_6$ ):  $\delta = 9.8$  (s, 1H, N=*CH*-N), 7.9–7.14 (m, 14H, aromatics), 5.6 (s, 4H, Ph-*CH*<sub>2</sub>-N).  $^{13}\text{C}$  NMR (100.7 MHz; 298 K; DMSO- $d_6$ ): 138.4, 136.7, 134.3, 131.5, 129.5, 128.1, 125.6, 114.2, 52.7.

*N,N*-Bisbenzylbenzimidazolium chloride (0.25 g, 0.75 mmol, 1 eq.) and silver(I) oxide (20 mg, 0.8 mmol, 1 eq.) were dissolved in dichloromethane (3 mL) and allowed to stir at room temperature for 24 hours. The solution was cooled down and filtered, yielding the molecular

model as an insoluble white powder (yield: 40%, 0.13 g).  $^1\text{H}$  NMR (400 MHz; 298 K;  $\text{DMSO-}d_6$ ):  $\delta = 7.9\text{--}7.14$  (m, 14H, aromatics), 5.6 (s, 4H,  $\text{Ph-CH}_2\text{-N}$ ).  $^{13}\text{C}$  NMR (100.7 MHz; 298 K;  $\text{DMSO-}d_6$ ): 136.7, 134.3, 131.5, 129.5, 128.1, 125.6, 114.2, 52.7. Characterisation is consistent with that previously reported within the literature.<sup>49,50</sup>

### General procedure for benzoin condensation reaction

In a typical experiment, 10 mol% of catalyst (61 mg; 0.07 mmol) was suspended in dry THF (3 mL; catalyst concentration 20  $\text{mg mL}^{-1}$ ) in a 10 mL Schlenk tube, to which 0.07 mL of benzaldehyde (0.7 mmol) was added under argon. The reaction mixture was stirred for 24 h at 80 °C. The mixture was allowed to cool down to rt, and an aliquot was withdrawn for  $^1\text{H}$  NMR spectroscopy characterization. Benzoin conversion was determined by  $^1\text{H}$  NMR spectroscopy in  $\text{DMSO-}d_6$  by comparing the integral value of the aldehyde signal of benzaldehyde (s, 1 H, 10 ppm) with the one of the  $\text{-CH-}$  benzoin signal (s, 1H, 6 ppm) (**Fig. S5.10**). For the experiments with variable quantity of catalyst, the volume of solvent and substrate were kept constant.

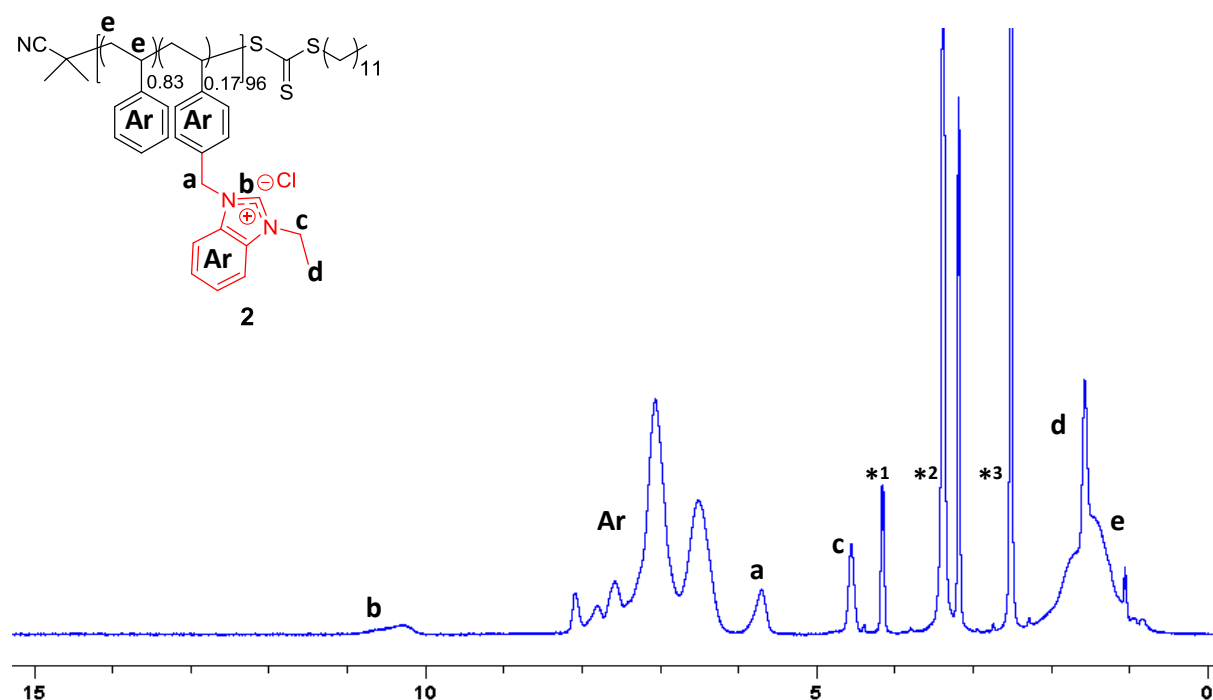


**Fig. S5.1.**  $^1\text{H}$  NMR spectrum of linear precursor **2** (400 MHz; 298 K;  $\text{DMSO-}d_6$ ; \*<sup>1</sup> methanol; \*<sup>2</sup> water and \*<sup>3</sup> DMSO)

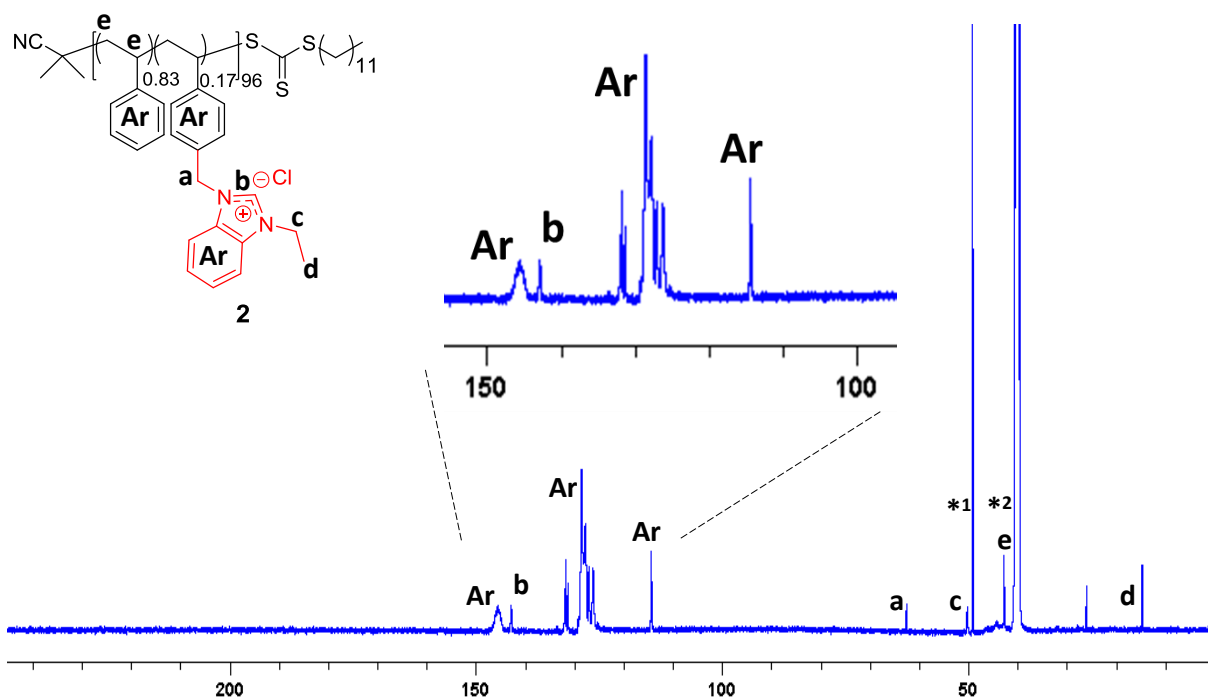


**Fig.S5.2.**  $^{13}\text{C}$  NMR spectrum of linear precursor **2** (100.7 MHz; 298 K;  $\text{DMSO-}d_6$ ; \*<sup>1</sup> methanol and \*<sup>2</sup> DMSO).

### Analysis of folded SCNP **3**

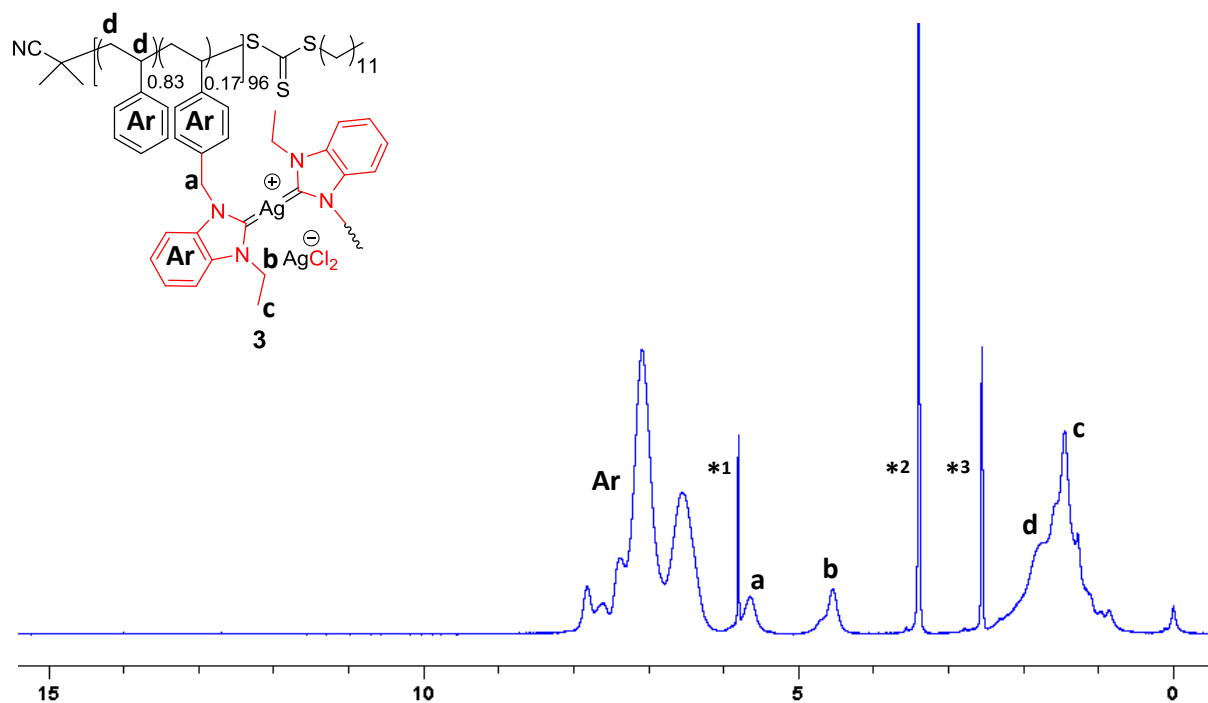


**Fig. S5.3.**  $^1\text{H}$  NMR spectrum of SCNP **3** (400 MHz; 298 K;  $\text{DMSO-}d_6$ ; \*<sup>1</sup> dichloromethane; \*<sup>2</sup> water and \*<sup>3</sup> DMSO).

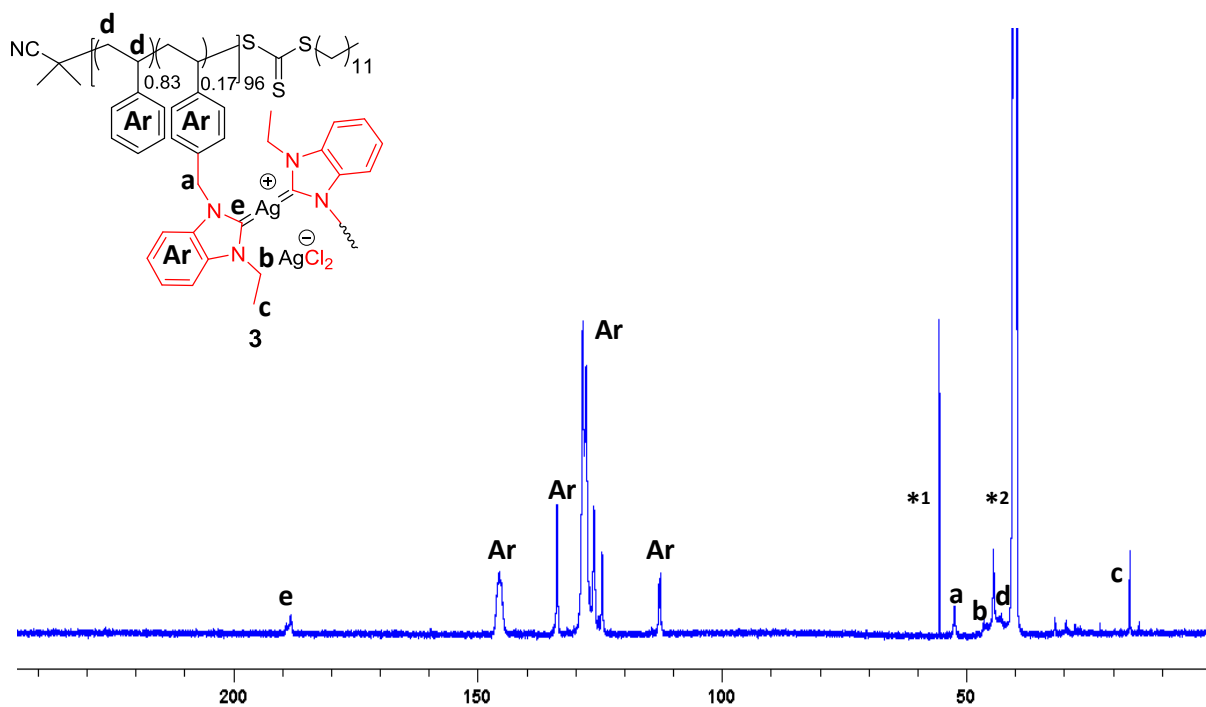


**Fig. S5.4.**  $^{13}\text{C}$  NMR spectrum of SCNP 3 (100.7 MHz; 298 K;  $\text{DMSO-}d_6$ ; \* $^1$  dichloromethane and \* $^2$  DMSO).

#### Analysis of modified SCNP 4

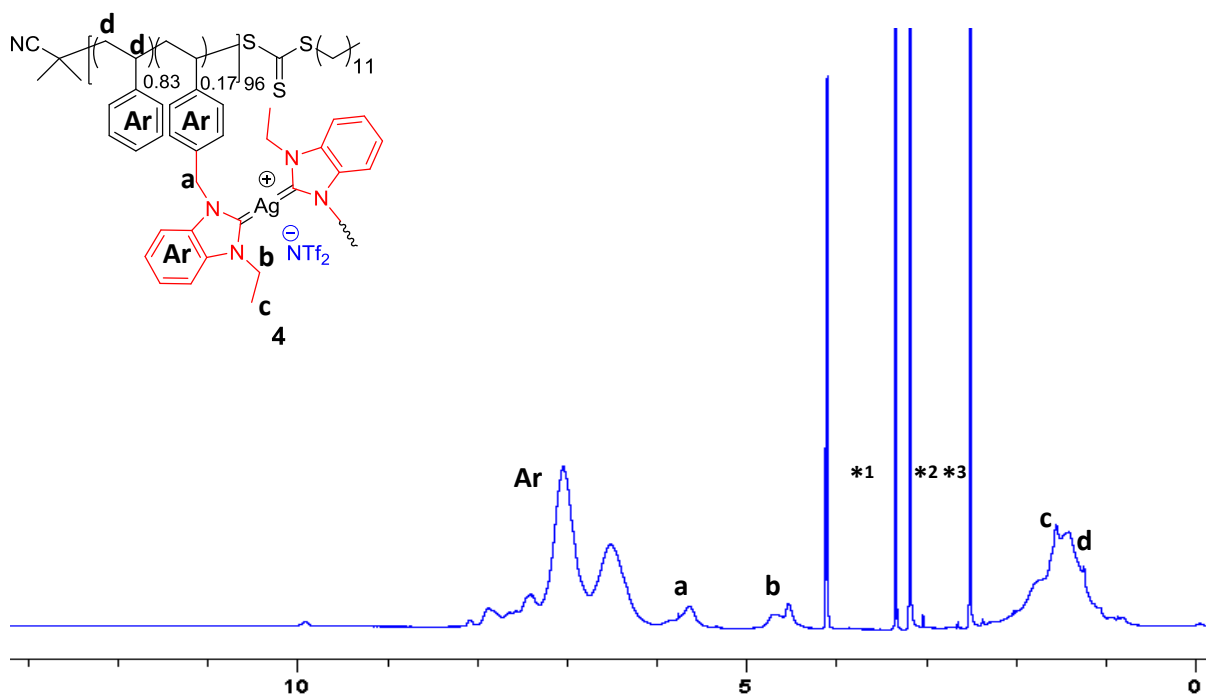


**Fig. S5.5.**  $^1\text{H}$  NMR spectrum of SCNP 4 (400 MHz; 298 K;  $\text{DMSO-}d_6$ ; \* $^1$  methanol; \* $^2$  water and \* $^3$  DMSO).

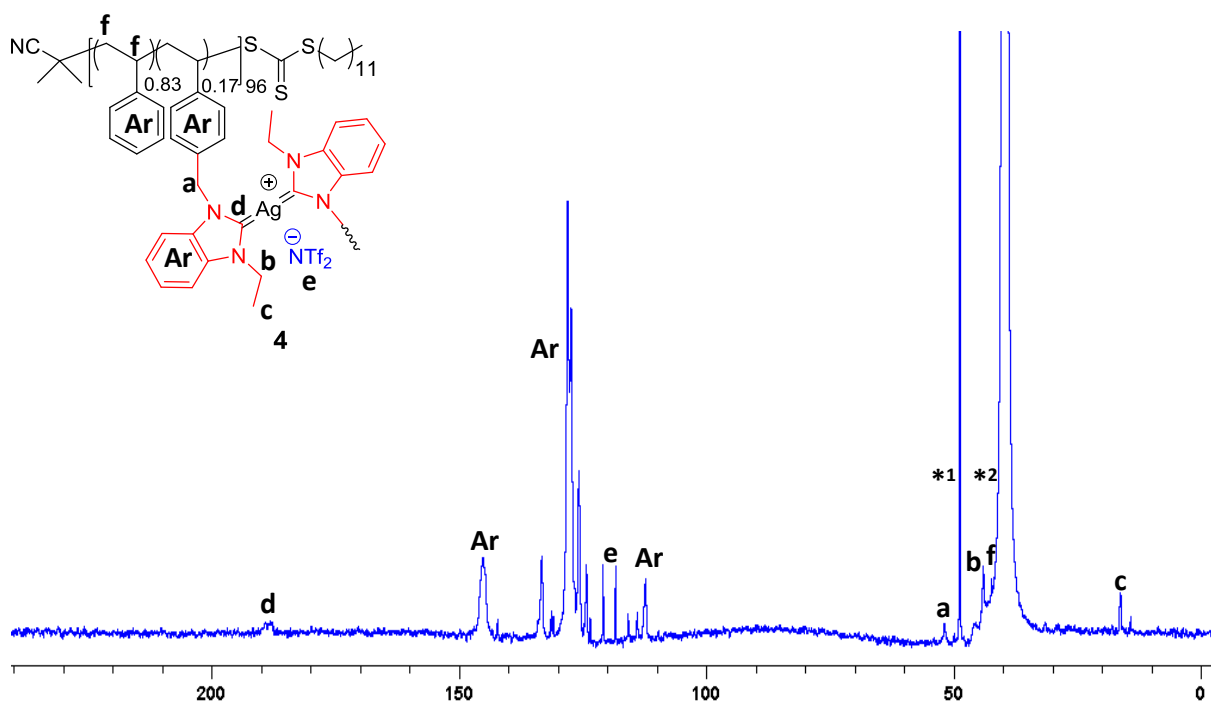


**Fig. S5.6.**  $^{13}\text{C}$  NMR spectrum of SCNPs **4** (100.7 MHz; 298 K;  $\text{DMSO-}d_6$ ; \*<sup>1</sup> methanol and \*<sup>2</sup> DMSO).

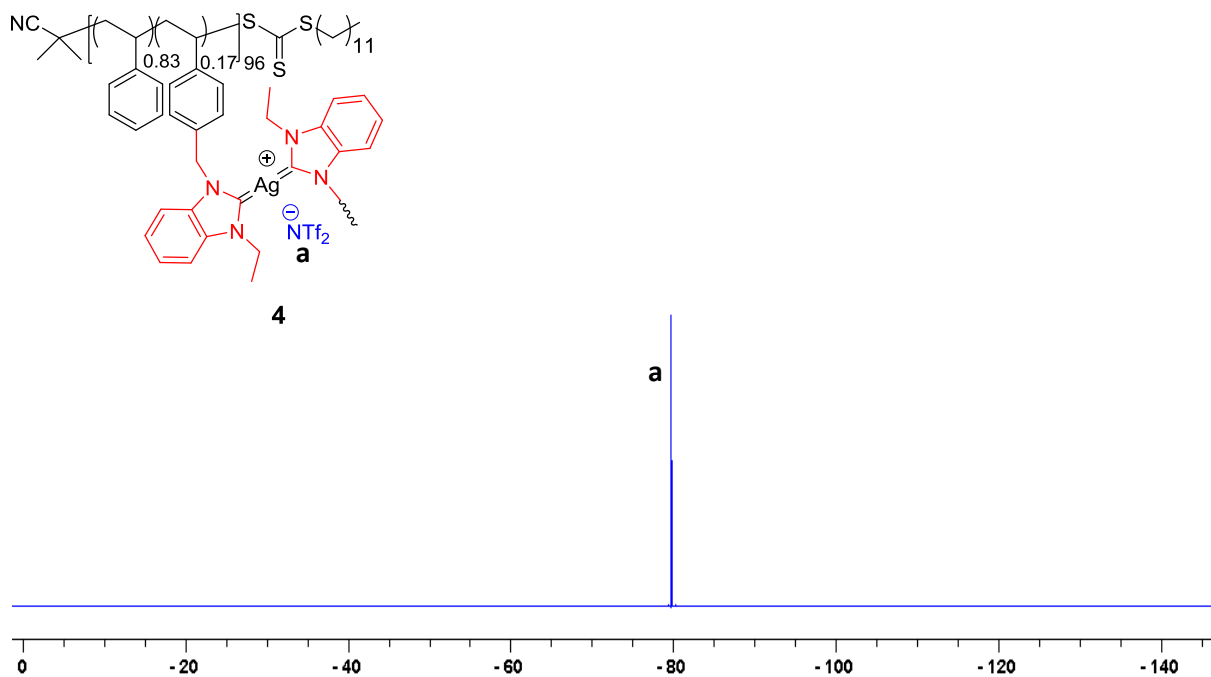


**Fig. S5.7.**  $^{19}\text{F}$  NMR spectrum of SCNPs **4** (376.5 MHz; 298 K;  $\text{DMSO-}d_6$ ).



## Analysis of polybetaine 5

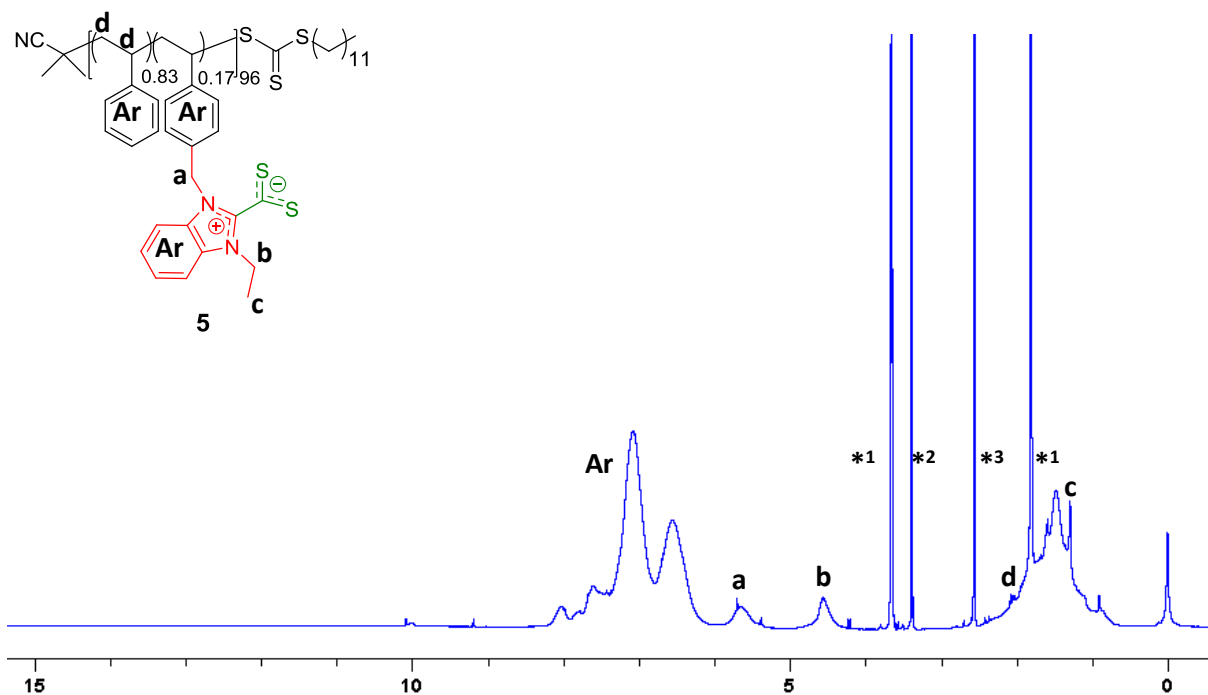


**Fig. S5.8.**  $^1\text{H}$  NMR spectrum of SCNP 5 (400 MHz; 298 K;  $\text{DMSO-}d_6$ ; \* $^1$  tetrahydrofuran; \* $^2$  water and \* $^3$  DMSO):

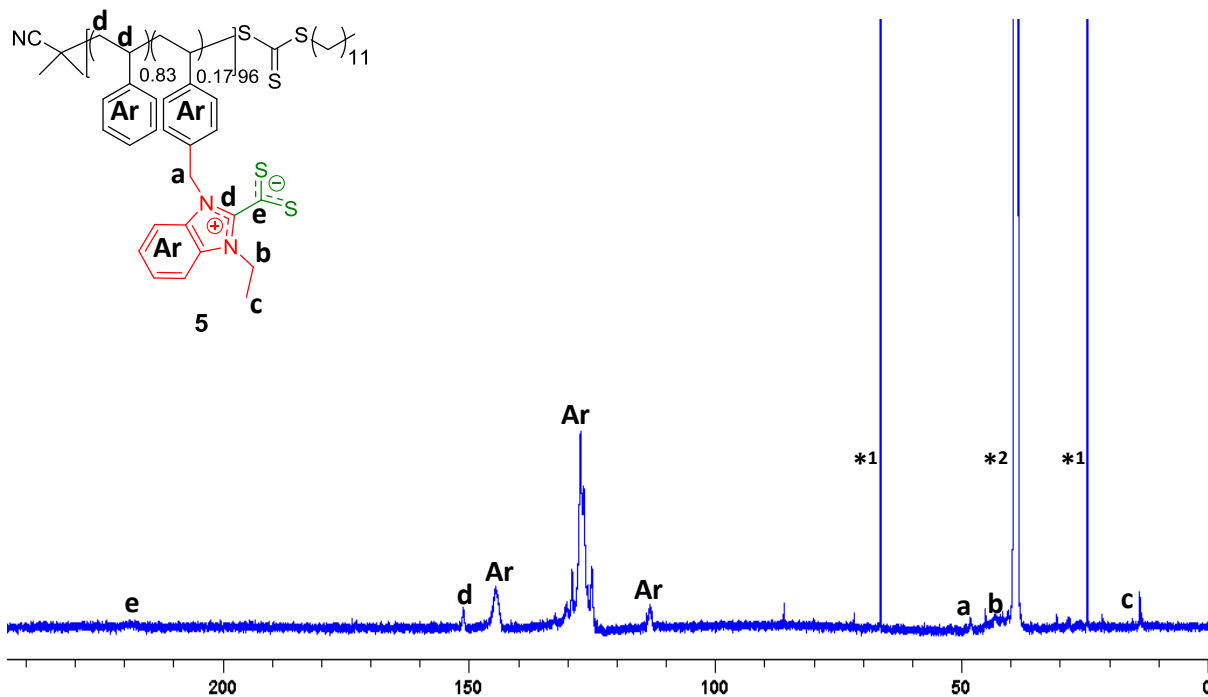


**Fig. S5.9.**  $^{13}\text{C}$  NMR spectrum of SCNP **5** (100.7 MHz; 298 K;  $\text{DMSO-}d_6$ ; \* $^1$  tetrahydrofuran and \* $^2$  DMSO).

### Catalysis using SCNPs

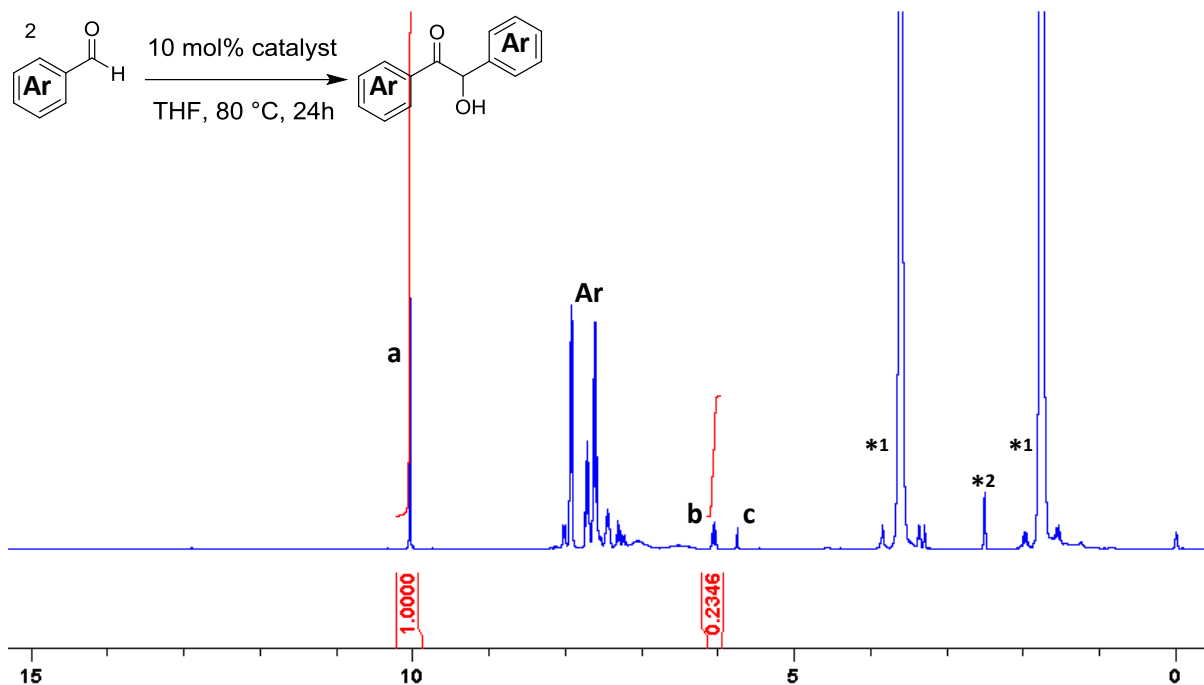


**Fig. S5.10.**  $^1\text{H}$  NMR spectrum of benzoin condensation catalysis using 10 mol% of catalyst **2** (400 MHz; 298 K;  $\text{DMSO-}d_6$ ; \* $^1$  tetrahydrofuran; \* $^2$  DMSO).

### Particle Characterisation

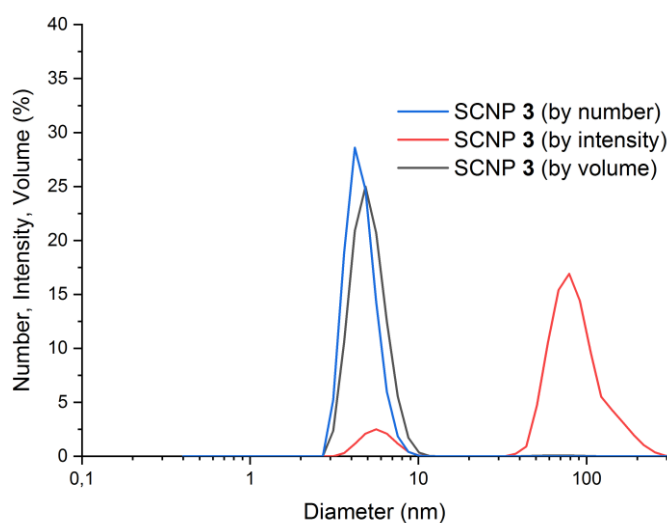


**Fig. S5.11.** Mean hydrodynamic diameter of SCNP 3 by volume (black line), number distribution (blue line) and by intensity (red line) obtained by DLS in THF. Concentration 1 mg mL<sup>-1</sup> analysis was performed at room temperature.

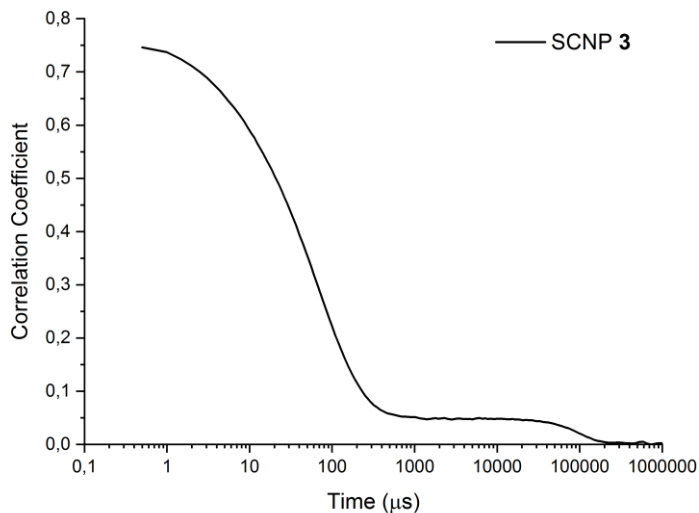


**Fig. S5.12.** Correlation function of SCNP 3 obtained by DLS in THF. Concentration 1 mg mL<sup>-1</sup> analysis was performed at room temperature.

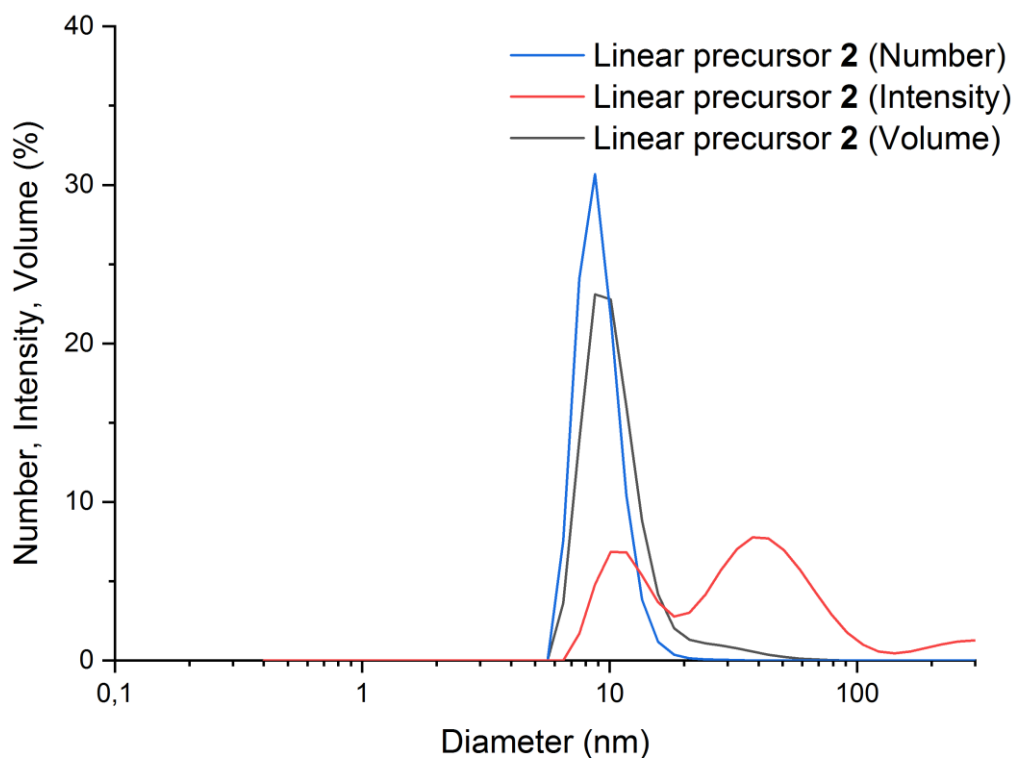


**Fig. S5.13.** Mean hydrodynamic diameter of linear precursor **2** by volume (black line), number distribution (blue line) and by intensity (red line) obtained by DLS in THF. Concentration 1 mg mL<sup>-1</sup> analysis was performed at room temperature.

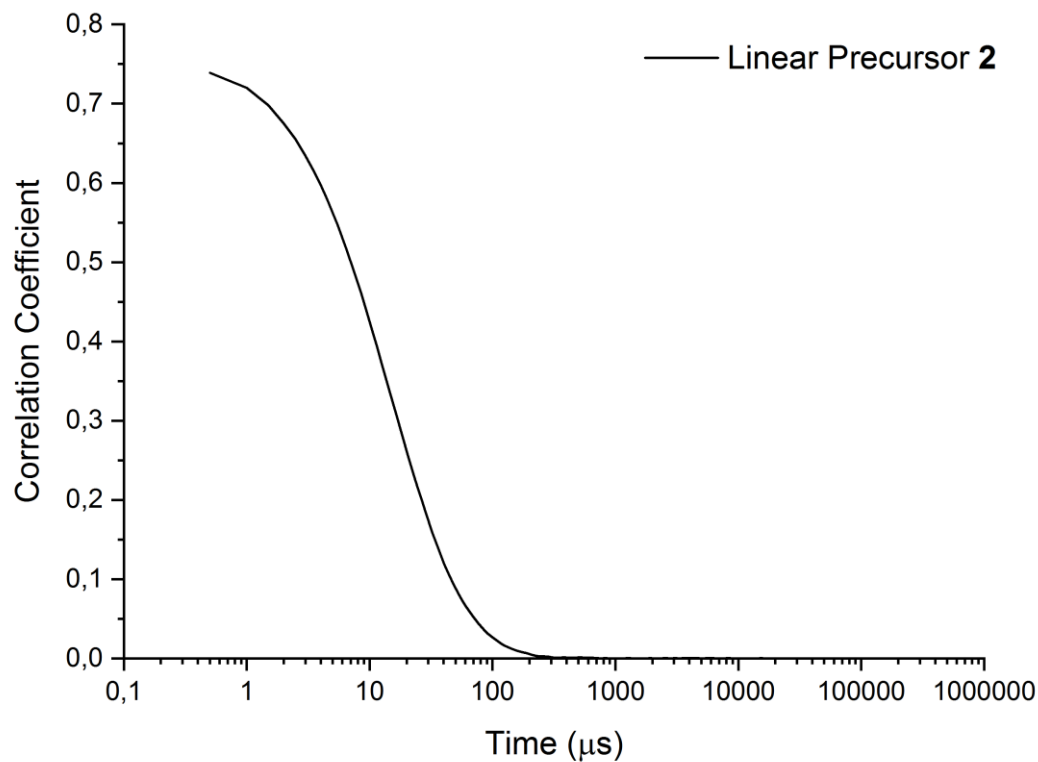


**Fig. S5.14.** Correlation function of linear precursor **2** obtained by DLS in THF. Concentration 1mg mL<sup>-1</sup> analysis was performed at room temperature.

## **Chapter VI: Summary and outlook**



# Table of Contents

## Chapter VI: Summary, principal conclusions and outlook

6.1. Summary.....	243
6.2. Principal conclusions.....	243
6.2.1. Importing PILs to SCNPs technology.....	243-244
6.2.2. Different SCNPs folding techniques.....	244-245
6.2.3 SCNPs as catalytically active nanoreactors.....	245-246
6.3. Outlook.....	246-247

## 6.1 Summary

The main focus of this thesis has been the applicability of poly(ionic liquid)s (PILs) in single chain nanoparticles as catalytically active nanoreactors. In particular, interest has been placed on the development of a range of thermolabile *N*-heterocyclic carbenes derived from ionic liquids in confined polymeric environments. Both the preparation of these SCNPs supported catalysts of controlled dimensions and their application as catalytically active nanostructures has been investigated, showing the ease of use and versatility of the folding linear precursors into SCNPs and the potential utility as synthetic enzymes.

## 6.2 Principal conclusions

### 6.2.1 Importing PILs to SCNPs technology

The theme of poly(ionic liquids) (PILs) is prevalent throughout this work and is utilised repeatedly to develop supported *N*-heterocyclic carbenes (NHC) (pre)catalysts. Largely, this is due to the discovery of the formation of active NHC from imidazolium carboxylate derivatives by applying heat. This work has demonstrated not only the ease of preparing such materials, but the tunability of different parts of PILs structures to thermally promote the generation of NHCs.

The large variety of different **modulability** options present in PILs technology allowed first to tune the solubility of a macrogel by inserting a biscarboxylate which ionically cross-linked the polymeric support and served as basic counter anion to *in situ* deprotonate the benzimidazolium moiety affording active NHCs.

Having developed the expertise in **ionically cross-linked** PILs, they were first imported to SCNPs domain by supporting polycations and polyanions in the same linear polymeric precursor which was subsequently folded into a nanoparticle *via* anion-exchange. This not only provided a NHC catalyst precursor, but also proved that PILs could adopt more sophisticated architectures/morphologies.

Interestingly, the particular ability of imidazolium-based PILs to act as metal ions poly(ligands) was further exploited using silver (I) as cross-linker. Similarly to previous examples, this organometallic bridges represent labile cross-linking points which could be broken delivering organic poly(NHC)s catalysts upon heating.



More commonly, PILs structures are usually based on (co)polymers which present ionic moieties and other non-ionic monomers. The capability of **combining different monomers** was harnessed by supporting benzoin cross-linker moieties and NHC-precursor (benzimidazolium acetate) into the same polymeric structure.

The **versatility** of PILs to act as NHC precursors by different means and based on **different architectures** permitted transitioning from less sophisticated linear or macroscopic gels to SCNPs based catalytically active nanoreactors.

### 6.2.2. Different SCNPs folding techniques

A wide variety of different synthetic approaches have been implemented for the formation of SCNPs. The most common utilised route is based on the post-functionalisation of linear copolymers under dilute conditions to favour intra-chain over inter-chain cross-linking. Many of the followed approaches are **inspired by biomacromolecules** in nature exploiting different orthogonal non-covalent interactions (*e.g.* hydrogen bonding or van der Waals), covalent interactions (*e.g.* disulfides) or dynamic covalent interactions (*e.g.* reversible acetal formation). In fact, the cross-linking nature is crucial not only in determining the SCNPs functionality and performance but also to establish a criterion for classification. Namely, SCNPs are commonly classified depending on the reversible or irreversible nature of cross-linkings present in the structure.

Inspired by such phenomena, PILs afforded new answers to the existing challenges in different SCNPs folding techniques. In fact, exploiting ionic nature intrinsic to IL moieties allowed the development of an unexplored and **reversible** folding technique based on ionically cross-linked SCNPs. More interestingly, these types of ionic interactions could be triggered by a simple anion exchange under mild conditions. The ease of preparation and lack of hazardous conditions permits an **easy scale up** which represents one of the major challenges to circumvent in SCNPs technology.

The use of PILs in SCNPs technology does not necessarily mean that they must be ionically cross-linked. Interestingly, PILs could be **combined with covalently cross-linked** different moieties. In this manner, ILs could have certain mobility and accessibility in a covalently -

hence more robustly- cross-linked SCNPs. These types of systems are known for presenting enhanced properties such as stability comparing to their purely non-covalently cross-linked SCNPs counterparts, in catalysis for instance.

Imidazolium based ILs are known for being used as ligands for wide array of different metal ions. These **versatile proligands** can be polymerised in a controlled fashion into linear polymers without side reactions and subsequently post-functionalised by inserting metal ions (*e.g.* Ag(I)) which cross-link SCNPs. Particularly, in the case of NHC precursors, the metal ion has to be bound at least to two ligands to promote the intramolecular folding. Therefore, imidazolium based PILs can act as poly(NHC)s ligands affording large number of possibilities depending on the inserted metal ion.

Imidazolium-type linear polymeric precursors have been found to be versatile starting platforms to trigger the intramolecular folding into SCNPs following different routes based on the attractive properties almost exclusive to imidazolium ILs.

### 6.2.3. SCNPs as catalytically active nanoreactors

With the ultimate goal of mimicking the natural occurring enzymatic catalysis reactions, SCNPs arise as the synthetic alternative to emulate this phenomenon. Few of the most important motivations for emulating enzymes as catalytic reactors are reaching their high specificity, selectivity, rate and/or tolerance to different environments. Following the bioinspired approach, the **organocatalyst** used throughout this thesis was the NHC, which finds its biological analogue in the vitamin B<sub>1</sub> in its thiazole form.

Indeed, all the NHC-based SCNPs used in this study were activated upon heating. This **thermolatency** permitted to easily handle and store these nanoreactors

The presence of the catalytic moieties in the SCNPs pocket was found to have a dramatic impact in the catalytic performance due to a favourable effect of the **confinement effect** avoiding product inhibition. Moreover, the incorporation of side PEG-stabilisers enabled an easy recyclability without any loss of activity.

The **versatility** of NHCs to mediate different organic reactions was proved by organocatalysing first the intramolecular benzoin condensation to promote the SCNPs folding and then use the obtained nanoreactors to organocatalyse transesterification reactions.

Metalloenzymes were also used as source of bioinspiration by developing an **organometallic SCNPs** cross-linked by Ag-NHC bridges. Although, Ag-NHC can act as a metal catalytic center, or even as transmetallation agent, in this study the organometallic bridges were thermolysed delivering active poly(NHC)s.

### 6.3 Outlook

As the most prominent theme of this work, poly(ionic liquid) based single chain nanoparticles have been investigated for the formation of catalytically active nanoreactors. In particular, given the high interest in the sophisticated supported organocatalysts, the ability to readily access and control the assembly of polymers into SCNPs through intramolecular cross-linking process provides a platform to develop a range of new nanomaterials.

Further research, especially for imidazolium-based PILs copolymers, will investigate the incorporation of functional counter-anions which have multiple roles. This approach should allow for the thermololent generation of active NHCs but also incorporating cocatalysts, chiral information, stabilisers or even polymerisation control agents.

It is also expected that future work in the area of SCNPs will target the catalytic activity in the nanoscale, allowing for intramolecular folding of linear polymer nanostructures to create even more complex catalytically active functional materials. Such an approach will not only allow to use imidazolium ILs moieties as genuine organocatalysts but also as ligands for the incorporation of wide array of metal centers. Potential research in this area may seek to exploit the ability of imidazolium ILs to act as ligands which can bind metal ions to form different metal-NHC complexes. It is predicted that mild conditions or intermediate transmetallation complexes (*e.g.* Ag-NHC) could be used to easily scale up the production of organometallic nanoreactors.

Finally, the underlying theme of this work is providing a transition from molecular or less sophisticated supported NHC-based catalyst to more optimised and functional NHC containing SCNPs-based nanoreactors. To this purpose, these nanoreactors could mediate molecular but

also macromolecular reactions as their molecular homologues for instance. In this manner, SCNPs could act as synthetic polymerases but also as hydrolases for depolymerisation processes in confined environments. However, the ultimate challenge for approaching natural enzyme performance, in the case of NHC-based SCNPs as nanoreactors, is retaining catalytic activity in biological conditions (*i.e.* water).

## 7.1 Sommaire

L'objectif principal de cette thèse a été l'applicabilité des poly (liquides ioniques) (PILs) dans des nanoparticules à chaîne unique en tant que nanoréacteurs catalytiquement actifs. En particulier, un intérêt a été porté au développement d'une gamme de carbènes *N*-hétérocycliques thermolatents dérivés de liquides ioniques dans des environnements polymériques confinés. La préparation de ces catalyseurs SCNP supportés de dimensions contrôlées et leur application en tant que nanostructures catalytiquement actives ont été étudiées, montrant la facilité d'utilisation et la polyvalence des précurseurs linéaires repliables en SCNP et l'utilité potentielle en tant qu'enzymes synthétiques.

## 7.2 Conclusions principales

### 7.2.1 Importation de PILs dans la technologie SCNPs

Le thème des poly (liquides ioniques) (PILs) est répandu tout au long de ce travail et est utilisé à plusieurs reprises pour développer des catalyseurs (pré) catalyseurs *N*-hétérocycliques (NHC) supportés. Cela est dû en grande partie à la découverte de la formation de NHC actif à partir de dérivés de carboxylate d'imidazolium par application de chaleur. Ce travail a démontré non seulement la facilité de préparation de tels matériaux, mais aussi l'accordabilité de différentes parties des structures de PILs pour favoriser thermiquement la génération de NHC.

La grande variété d'options de modulabilité différentes présentes dans la technologie PILs a permis d'abord de régler la solubilité d'un macrogel en insérant un biscarboxylate qui a réticulé ioniquement le support polymère et a servi de contre-anion de base pour déprotoner in situ la fraction benzimidazolium offrant des NHC actifs.

Ayant développé l'expertise dans les PILs réticulés ioniquement, ils ont d'abord été importés dans le domaine SCNPs en supportant des polycations et des polyanions dans le même précurseur polymère linéaire qui a ensuite été plié en une nanoparticule *via* un échange d'anions. Cela a non seulement fourni un précurseur de catalyseur NHC, mais a également prouvé que les PILs pouvaient adopter des architectures / morphologies plus sophistiquées.

Fait intéressant, la capacité particulière des PILs à base d'imidazolium à agir comme poly (ligands) d'ions métalliques a été davantage exploitée en utilisant de l'argent (I) comme agent

de réticulation. De la même manière que dans les exemples précédents, ces ponts organométalliques représentent des points de réticulation labiles qui pourraient être rompus en délivrant des catalyseurs organiques poly (NHC) lors du chauffage.

Plus communément, les structures PILs sont généralement basées sur des (co) polymères qui présentent des fragments ioniques et d'autres monomères non ioniques. La capacité de combiner différents monomères a été exploitée en soutenant des fragments de réticulant de benjoin et un précurseur de NHC (acétate de benzimidazolium) dans la même structure polymère.

La polyvalence des PIL pour agir en tant que précurseurs de NHC par différents moyens et sur la base de différentes architectures a permis de passer de gels linéaires ou macroscopiques moins sophistiqués à des nanoréacteurs catalytiquement actifs à base de SCNPs.

### **7.2.2. Différentes techniques de pliage SCNPs**

Une grande variété d'approches synthétiques différentes a été mises en œuvre pour la formation de SCNPs. La voie utilisée la plus courante est basée sur la post-fonctionnalisation des copolymères linéaires dans des conditions diluées pour favoriser la réticulation intra-chaîne plutôt qu'inter-chaîne. Bon nombre des approches suivies sont inspirées par des biomacromolécules dans la nature exploitant différentes interactions orthogonales non covalentes (par exemple, liaison hydrogène ou van der Waals), des interactions covalentes (par exemple disulfures) ou des interactions covalentes dynamiques (par exemple formation acétal réversible). En fait, la nature de la réticulation est cruciale non seulement pour déterminer la fonctionnalité et les performances des SCNPs, mais aussi pour établir un critère de classification. À savoir, les SCNPs sont généralement classés en fonction de la nature réversible ou irréversible des réticulations présentes dans la structure.

Inspirés par de tels phénomènes, les PILs ont apporté de nouvelles réponses aux défis existants dans les différentes techniques de pliage des SCNPs. En fait, l'exploitation de la nature ionique intrinsèque aux fractions IL a permis le développement d'une technique de repliement inexplorée et réversible basée sur des SCNP réticulés ioniquement. Plus intéressant, ces types d'interactions ioniques pourraient être déclenchés par un simple échange d'anions dans des conditions douces. La facilité de préparation et l'absence de conditions dangereuses permettent

une mise à l'échelle facile qui représente l'un des principaux défis à contourner dans la technologie SCNPs.

L'utilisation de PILs dans la technologie SCNPs ne signifie pas nécessairement qu'ils doivent être réticulés ioniquement. Fait intéressant, les PIL pourraient être combinés avec des fragments différents réticulés de manière covalente. De cette manière, les ILs pourraient avoir une certaine mobilité et accessibilité dans un SCNPs réticulé de manière covalente-donc plus robuste. Ces types de systèmes sont connus pour présenter des propriétés améliorées telles que la stabilité par rapport à leurs homologues SCNPs réticulés de manière non covalente, en catalyse par exemple.

Les ILs à base d'imidazolium sont connus pour être utilisés comme ligands pour un large éventail d'ions métalliques différents. Ces proligands polyvalents peuvent être polymérisés de manière contrôlée en polymères linéaires sans réactions secondaires et post-fonctionnalisés par la suite en insérant des ions métalliques (par exemple Ag (I)) qui réticulent les SCNPs. En particulier, dans le cas des précurseurs de NHC, l'ion métallique doit être lié au moins à deux ligands pour favoriser le repliement intramoléculaire. Par conséquent, les PILs à base d'imidazolium peuvent agir comme des ligands poly (NHC) offrant un grand nombre de possibilités en fonction de l'ion métallique inséré.

Les précurseurs polymères linéaires de type imidazolium se sont avérés être des plates-formes de départ polyvalentes pour déclencher le pliage intramoléculaire en SCNPs en suivant différentes voies en fonction des propriétés attrayantes presque exclusives aux ILs d'imidazolium.

### **7.2.3. SCNPs en tant que nanoréacteurs catalytiquement actifs**

Dans le but ultime d'imiter les réactions naturelles de catalyse enzymatique, les SCNPs se présentent comme l'alternative synthétique pour émuler ce phénomène. Peu des motivations les plus importantes pour émuler des enzymes en tant que réacteurs catalytiques atteignent leur haute spécificité, sélectivité, vitesse et / ou tolérance à différents environnements. Suivant l'approche bioinspirée, l'organocatalyseur utilisé tout au long de cette thèse était le NHC, qui trouve son analogue biologique dans la vitamine B1 sous sa forme thiazole.

En effet, tous les SCNPs à base de NHC utilisés dans cette étude ont été activés lors du chauffage. Cette thermolatence a permis de manipuler et de stocker facilement ces nanoréacteurs.

La présence des fractions catalytiques dans la poche SCNPs s'est avérée avoir un impact dramatique sur les performances catalytiques en raison d'un effet favorable de l'effet de confinement évitant l'inhibition du produit. De plus, l'incorporation de stabilisateurs PEG latéraux a permis une recyclabilité aisée sans aucune perte d'activité.

La polyvalence des NHC pour médier différentes réactions organiques a été prouvée en organocatalysant d'abord la condensation de benjoin intramoléculaire pour favoriser le repliement des SCNP, puis en utilisant les nanoréacteurs obtenus pour organocatalyser les réactions de transestérification.

Les métalloenzymes ont également été utilisées comme source de bioinspiration en développant un SCNP organométallique réticulé par des ponts Ag-NHC. Bien que l'Ag-NHC puisse agir comme un centre catalytique métallique, ou même comme un agent de transmétallation, dans cette étude, les ponts organométalliques ont été thermolysés délivrant des poly (NHC) actifs.

### 7.3. Perspectives

En tant que thème le plus important de ce travail, les nanoparticules à chaîne unique à base de poly (liquide ionique) ont été étudiées pour la formation de nanoréacteurs catalytiquement actifs. En particulier, étant donné le grand intérêt pour les organocatalyseurs pris en charge sophistiqués, la capacité d'accéder et de contrôler facilement l'assemblage des polymères dans les SCNPs *via* un processus de réticulation intramoléculaire fournit une plate-forme pour développer une gamme de nouveaux nanomatériaux.

D'autres recherches, en particulier pour les copolymères de PILs à base d'imidazolium, étudieront l'incorporation de contre-anions fonctionnels qui ont de multiples rôles. Cette approche devrait permettre la génération thermolatente de NHC actifs mais également l'incorporation de cocatalyseurs, d'informations chirales, de stabilisants ou même d'agents de contrôle de la polymérisation.

Il est également prévu que les futurs travaux dans le domaine des SCNPs cibleront l'activité catalytique à l'échelle nanométrique, permettant le pliage intramoléculaire de nanostructures de polymère linéaire pour créer des matériaux fonctionnels catalytiquement actifs encore plus complexes. Une telle approche permettra non seulement d'utiliser des fragments d'imidazolium



ILs comme de véritables organocatalyseurs mais également comme ligands pour l'incorporation d'un large éventail de centres métalliques. Les recherches potentielles dans ce domaine pourraient chercher à exploiter la capacité des IL d'imidazolium à agir comme des ligands qui peuvent se lier aux ions métalliques pour former différents complexes métal-NHC. Il est prévu que des conditions douces ou des complexes de transmétallation intermédiaires (par exemple Ag-NHC) pourraient être utilisés pour augmenter facilement la production de nanoréacteurs organométalliques.

Enfin, le thème sous-jacent de ce travail est de fournir une transition d'un catalyseur à base de NHC supporté moléculaire ou moins sophistiqué à un NHC plus optimisé et fonctionnel contenant des nanoréacteurs basés sur SCNPs. A cet effet, ces nanoréacteurs pourraient médier des réactions moléculaires mais aussi macromoléculaires comme leurs homologues moléculaires par exemple. De cette manière, les SCNP pourraient agir comme des polymérases synthétiques mais également comme des hydrolases pour les processus de dépolymérisation dans des environnements confinés. Cependant, le défi ultime pour l'approche des performances des enzymes naturelles, dans le cas des SCNP à base de NHC en tant que nanoréacteurs, est de conserver l'activité catalytique dans des conditions biologiques (c'est-à-dire l'eau).

**Titre: Synthèse de nouvelles nanoparticules composées de chaînes uniques basé sur de carbènes *N*-hétérocycliques comme de nanoréacteurs catalytiquement actifs.**

**Résumé:** Des poly(liquides ioniques) (PILs) arrangés sous la forme de copolymères aléatoires ont été développés avec des architectures telle que ce des nanoparticules à chaîne unique ou bien sous la forme de (macro)gels. Ces différents systèmes ont été employés comme précurseurs de carbènes *N*-hétérocycliques (NHC)s à des fins de catalyses organiques. L'introduction d'anions relativement basiques dans des unités PIL dérivées d'imidazolium permet la génération *in situ* des NHCs actifs pour la catalyse. D'abord, le développement de (macro)gel basé sur des unités PIL réactives représente l'étude préliminaire pour la compréhension et analyse de performance catalytique à l'échelle macroscopique. Cette étude a permis cibler des réactions modèles ainsi que des conditions et des standards pour établir un système de référence tout au long de cette thèse. Ensuite, ce gel a servi comme base pour développer des nanogels connus comme nanoparticules composées d'une chaîne unique polymère repliée sur elle-même (SCNP en anglais). Ces SCNPs ont été spécialement conçues basées sur la mouillabilité des PILs et ont été obtenues par polymérisation contrôlée (méthode RAFT). Dans le premier cas, la nature ionique des pré-catalyseurs NHC a été exploitée en favorisant l'interaction entre les dérivés d'imidazolium avec des anions basiques supportés dans le polymère en formant un SCNP ioniquement réticulé. Deuxièmement, les propriétés thermolatentes des précurseurs de NHC ont été mises en valeur en compatibilisant des substrats et pré-catalyseurs sur la même chaîne du polymère en favorisant le repliement des chaînes en condensant les substrats sous l'application de chaleur. Finalement, la capacité intrinsèque des poly(NHC)s pour agir comme poly-ligands a été démontrée de manière novatrice en formant des SCNPs par une réaction de complexation organométallique à l'aide d'un sel d'argent. Dans tous les différents supports polymériques, des aspects liés aux performances catalytiques ont été mis en avant comme le recyclage du catalyseur, des effets de confinement, la facilité pour augmenter l'échelle de synthèse des nanoréacteurs, la versatilité des NHC catalyseurs et l'adaptation de différents systèmes pour manipuler ces espèces polycarbeniques de manière simple et efficace.

**Mots clés:** Poly(liquides ioniques), imidazolium, *N*-hétérocyclique carbènes, NHC, carbènes masqués, catalyse supportée, organocatalyse, confinement, catalyse biomimétique, nanoréacteurs, mimétique enzymatique, nanoparticules, SCNPs, SNCsPs.

**Title : Synthesis of new *N*-Heterocyclic Carbene (NHC)-based Single Chain Nanoparticles (SNCsPs) as catalytically active nanoreactors**

**Abstract:** Random copolymers based on poly(ionic liquids) have been developed under different architectures such as single chain nanoparticles (SCNPs) or as (macro)gels. Those different systems have been employed as *N*-heterocyclic carbenes (NHCs) precursors to be used as organocatalysts. The incorporation of relatively basic counteranions in PIL units derived from imidazolium moieties allows the *in situ* generation of active NHC species for catalysis. Firstly, a reactive PIL based (macro)gel represents the preliminary study to better understand and analyse the catalytic performance in the macroscale. This study has permitted the identification of suitable model reactions as well as conditions and standards, becoming a reference system all along this thesis. Moreover, this (macro)gel has served as a base for the further development of more sophisticated nanogels known as single chain nanoparticles (aka SCNPs). These SCNPs have specially been designed based on their PIL tunability and synthesised by reversible addition fragmentation chain transfer (RAFT) polymerisation. In first place, the ionic nature of the NHC precatalyst was exploited by triggering the interaction between imidazolium derivatives and basic anions supported in the polymer leading to an ionically cross-linked SCNP. Secondly, the thermolabile properties of NHC precursors were harnessed by proving the compatibility of both substrates and precatalyst supported on the same polymer chain and triggering the folding by condensing the substrates by the simple application of heat. Finally, the intrinsic capacity of poly(NHC)s to act as poly-ligands was innovatively demonstrated by forming SCNPs after organometallic complexation using a silver salt. Overall, the different polymeric supports have served to highlight different aspects related to the catalytic performance of supported catalysts such as recycling, confinement effect, nanoreactor scaling up processes, NHC catalysts versatility as well as the adaptability of these systems for enabling and easy and efficient handling and storage.

**Keywords:** poly(ionic liquids), imidazolium, *N*-heterocyclic carbene, NHC, masked carbenes, supported catalysis, organocatalysis, confinement, biomimetic catalysis, nanoreactors, enzyme mimicry, nanoparticles, SCNPs, SNCsPs.

**Laboratoire de Chimie des Polymères Organique UMR5629 | 16 avenue Pey-Berland | F-33607 Pessac**